Implanted muon studies in condensed matter science

1987 J. Phys. C: Solid State Phys. 20 3187

(http://iopscience.iop.org/0022-3719/20/22/005)

J. Phys. C: Solid State Phys. **20** (1987) 3187–3319. Printed in the UK

REVIEW ARTICLE

Implanted muon studies in condensed matter science

S F J Cox
Rutherford Appleton Laboratory, Chilton, Oxfordshire OX11 0QX, UK

Received 28 April 1986

Abstract. The positive muon is a unique microscopic probe. When it is implanted in condensed matter, the evolution of its spin polarisation may be readily monitored to give information on the crystallographic or molecular sites it occupies, the local fields it experiences and the time dependence of these fields. This article describes the experimental techniques in current use, and the manner in which the muon behaviour is characterised. The implications for solid state and chemical physics are discussed. The comparison between muon and proton behaviour in similar circumstances is emphasised. For chemical aspects, the equivalent comparison is between muonium and hydrogen, with muonium considered as a radioactive light isotope. Examples of studies are reviewed for magnetic materials, for metals and metal hydrides, for semiconductors and ionic crystals, and for certain organic materials and liquids. Novel information is obtained on topics including spin dynamics, dynamic correlations and critical phenomena, the localisation and quantum mobility of light interstitial particles, charge screening, the local electronic structure of hydrogen-like defect centres, hyperfine interactions, various kinetic and dynamic isotope effects and the role of vibrational effects, including zero-point motion, in determining molecular structure. Comparisons are drawn with studies by other techniques, notably magnetic resonance. Techniques and applications appropriate to pulsed muon sources are considered. The major achievements to date and the potential for future developments and new science are identified.

Contents

1. Introduction

In the list of elementary particles used extensively in materials research and condensed matter science, the positive muon is fast establishing itself alongside the electron, the positron and the neutron—and deservedly so. It would perhaps be an exaggeration to describe the muon as a universal microscopic probe, but comparatively few restrictions exist as to the suitability of the host material. Research involving muons provides a wealth of structural and dynamical information on the atomic scale on metallic systems, on magnetic materials, on semiconductors and on insulators, including organic and molecular materials.

1.1. A lightweight proton and a light isotope of hydrogen

Beams of spin-polarised muons are available at certain large accelerator laboratories, especialy the so-called meson factories, and these may be used to *implant* muons in the material of a sample. Once stopped or thermalised in a material in this manner, positive muons play the role of lightweight protons. They have close to one ninth the proton mass. Thus in problems that involve the motion of particles within or between potential wells for instance (and this deceptively simple example is far from trivial when coupling to phonons or electrons is involved) comparison of the behaviour of protons and muons provides a severe test of theoretical models. Also the use of a lighter particle favours observation of specifically quantum motion.

These comparative studies are possible because muons invariably adopt similar sites for localisation to protons, whether in metal lattices, other crystalline solids or molecular materials. Like protons, muons are too reactive to remain as the bare particles when thermalised (or nearly thermalised) in a medium, but seek to lower their energy through the acquisition of electrons. In metals, they attract a screening charge of conduction electrons and occupy interstitial sites in the lattice. In dielectrics they may be stabilised by reacting with molecules of even weak basicity, sticking to lone electron pairs on polar molecules for instance, or reducing multiple bonds in organic materials (in these processes, analogous to protonation, diamagnetic cation states are formed in the first instance). Particularly important, muons will also accept and bind single excess electrons to form hydrogen-like atoms known as *muonium*, $\mathrm{Mu}^{\cdot} = \mu^+e^-$. These are stable in sufficiently inert media and may be detected in a variety of gases and liquids, and as neutral paramagnetic defect centres in certain solids. Muonium (or the muonic cation, whichever is formed initially) may also subsequently react with suitable solvents, solutes or substrates to become incorporated in a variety of chemical species, diamagnetic and paramagnetic, so it is fascinating to compare these with the 'normal' species incorporating hydrogen, i.e. to examine the physical and chemical consequences of replacing hydrogen by muonium in a molecule. The concept of muonium as a genuine light isotope of hydrogen emerges clearly from all investigations, so it is helpful to compare muonium substitution with deuteration or tritiation—the more familiar isotopic substitutions commonly exploited in dynamical and chemical studies. The unprecedented mass ratio, $m_{\mathrm{Mu}}/m_{\mathrm{H}} \simeq \frac{1}{9}$, provides a particularly sensitive probe of isotope effects, with the lighter isotope again facilitating observation of specifically quantum effects, notably the role of zero-point energy in the chemical bond.

1.2. *Nomenclature*

The chemical symbol Mu has been universally adopted to denote this isotope. In the following, $\mathrm{Mu}^{\cdot}$ is used to denote *atomic* muonium, the dot emphasising the presence of an unpaired electron, as for other paramagnetic species. Mu^+ is adopted for any equilibrium cationic state (emphasising, like the use of H^+, that some chemical association with the host is always implied). The usual symbol μ^+ for the positive muon is reserved for the free particle, e.g. in its pre-thermalised state on entry into the sample.

The muon–proton analogy is perhaps one that would worry a nuclear physicist, who would more properly regard the positive muon as a 'heavy positron', and its anti-particle the negative muon as a 'heavy electron'. These two charge states occur as intermediates in the decay of positive and negative pions to positrons and electrons. The negative muon does indeed play the expected role of a heavy electron in condensed matter, substituting for orbital electrons in 'exotic' atoms and molecules; but the fundamental differences between the proton and the positive muon that are important at much higher energies, notably that the muon does not experience the strong interaction, are not relevant to phenomena in solid state or chemical physics, where the characteristic energies are typically less than 1 eV. Of importance here is the similarity between positive muons and protons, namely that both are fermions carrying spin $\frac{1}{2}$ and having unit positive charge, and that they have comparable magnetic moments.

1.3. μSR

The electrostatic and magnetic interactions of muons with their environment are therefore very similar to those of protons in the same positions. Whilst it is of course primarily the electrostatic interaction that determines the choice of crystallographic or molecular site, and the dynamical or chemical behaviour, the information that is available on these stems chiefly from the magnetic interaction, via the evolution of spin polarisation. This may be displayed in a particularly direct manner by the experimental technique that has become known as μSR. The initials stand for muon spin rotation, relaxation or resonance, depending on the precise variant of the technique used—or for muon spin research, to cover all possibilities!†

Muons are of course unstable particles, disintegrating spontaneously by β-decay with a lifetime of about 2.2 μs. If this seems to make them a somewhat exotic probe for use in solid state or chemical physics it is exactly the special characteristics of this decay that allow their polarisation to be so conveniently monitored. The β-emission (positrons from positive muons, electrons from negative muons) is most intense in the direction of the instantaneous polarisation. The degree of anisotropy measures the magnitude of the polarisation. Like the mechanism by which the muons themselves become spin-polarised (via the decay of pions), this is an expression of non-conservation of parity, established for these decays by Garwin *et al* (1957). These authors were well aware of the implications. Their article concludes: . . . 'it seems possible that polarized positive and negative muons will become a powerful tool for exploring magnetic fields in nuclei, atoms and interatomic regions.' The present review is concerned (almost exclusively) with how their prediction has been realised for *positive* muons‡, exploring fields especially in the muonium atom, in the related paramagnetic defect centres and in muonated molecules, and in 'inter-atomic regions'. It is relevant here that the radioactive lifetime τ_μ of the positive muon (unlike the effective lifetime of the negative muon which may be captured prematurely by atomic nuclei) is independent of its chemical state. It sets the limit of observation time (this does not exceed about $10\,\tau_\mu \simeq 20\,\mu$s in state-of-the-art experiments; $5\,\tau_\mu \simeq 10\,\mu$s is more typical) and determines the timescale for the dynamical and chemical processes that may be studied.

1.4. *The plan of the article*

Despite the very different detection technique, notably the use of single-particle counting, there is a close analogy between μSR and magnetic resonance spectroscopy. The similarity of the acronym to 'ESR' was presumably contrived to emphasise this. For muons in diamagnetic molecules and for interstitial muons in metals, the closest parallel is in fact with proton NMR. Thus in muon spin *rotation*, precession signals are obtained that are exactly analogous to free induction decays, with similar characteristic frequencies and relaxation functions. This is explained in § 2. The frequency of these signals provides a direct measure of the magnetic field that the muon experiences. (The magnetic moment of the muon is about three times that of the proton so its precession frequencies in a given field are larger by the same factor.) The relaxation functions characterise the variation of these local fields (spatial or temporal). They may be interpreted in terms of the distribution of local fields, of fluctuation of these fields, or sometimes of the motion of the muons themselves. Studies of internal fields and spin dynamics in magnetic systems are the subject of § 3.

---

† cf. μSR Newsletter series, ed. K M Crowe, A Portis and T Yamazaki (Lawrence Berkeley Laboratory, California and University of Tokyo).

‡ Applications of μSR using *negative* muons are reviewed for instance by Yamazaki (1984a); a bibliography including studies of exotic atoms has been compiled by Horvàth and Lambrecht (1984).

For paramagnetic states, of which atomic muonium itself is the archetypal example, the analogy with ESR and related techniques is valid. The various methods of muonium spectroscopy, and the nature of the muonium-related centres which are observed in a great variety of non-metallic solids, are the subject of § 4. In crystals of oxides and halides, for instance, μSR measurements can be compared with ESR measurements on the various hydrogen defect centres. However, in the elemental (group IV) and compound (III–V) semiconductors the μSR results are unique—a real scoop for this spectroscopy—since the analogous hydrogen defect centres in these materials have not (yet) been observed by conventional magnetic resonance. A proper understanding of these fascinating centres has proved somewhat elusive, although the framework for comparison with results from other crystalline solids which is introduced in § 4 gives a strong clue to their chemical identity.

Muonium loses its on-site moment in a metallic environment. Muons implanted in metals, alloys, intermetallics and metal hydrides reach a diamagnetic state which is closely analogous to the 'screened proton', familiar in studies of hydrogen in metals. Hyperfine interaction (where important) is then with the ensemble of conduction electrons. It is fortunate for the comparative studies that, although bound somewhat less strongly by virtue of their greater zero-point energy, muons adopt the same interstitial sites in metallic lattices as do protons. Studies of this localisation, and of the mechanism of diffusion between neighbouring sites, are the main subject of § 5. Details of the charge screening and local electronic structure in metals, i.e. of the perturbation to the interstitial charge and spin densities that the muon produces, are of crucial importance in dynamical and magnetic studies respectively. These are touched on as appropriate in §§ 3 and 5.

The incorporation of muonium in organic modules is described in § 6. Structural and dynamical studies, the main subject of this section, are restricted to paramagnetic species, i.e. radicals, muon–electron hyperfine coupling being the principal source of information here. A variety of such species is formed following muon implantation in unsaturated organic materials. Muonium is covalently bonded in the product molecules via spin-paired σ-electrons, in a position 'normally' occupied by hydrogen. Hyperfine coupling is with an unpaired electron nominally localised on a more distant atom, and may be compared with ESR measurements of analogous proton couplings. The use of the muon as a radioactive label for chemical and kinetic studies is also mentioned: in contrast to the use of tritium, chemical processes may be followed and transient species detected on a microsecond and sub-microsecond timescale.

Muon spin *rotation* implies the detection of precession in a field that is transverse to the initial muon polarisation, whether this field is applied externally or generated internally to the sample. Muon spin *relaxation* is usually taken to denote studies of the evolution of polarisation parallel to its initial direction. Various situations are described in § 7, including studies performed in zero field. Although no longer unique to μSR, these benefit from the defined initial muon polarisation and the sensitivity of the detection technique in a unique fashion. They are able to distinguish static and slowly fluctuating environments in a manner that is not otherwise possible. Particularly noteworthy is the application to spin glasses. Also noteworthy is the use of a longitudinal field tuned so that energy level separations in the host systems may be precisely determined via cross-relaxation to the muon spins. Preliminary measurements include quadrupole and hyperfine couplings to other nuclei. These are undoubtedly the prelude to a variety of developments, e.g. the mapping of charge and spin density in the neighbourhood of the muon site. The precise characterisation of species, formed too slowly to be detected by muon spin *rotation*, is anticipated, as well as the measurement of other quantities such as tunnel splittings.

Most μSR experiments, including all early work, have been performed using 'continuous' muon sources. Muons arrive in the sample one at a time, more or less at random. The techniques of single-particle counting allow the accumulation of spectra in this manner and account for the remarkable sensitivity, in terms of signal-to-noise ratio per spin, compared with conventional magnetic resonance. By the same token, however, it is usually necessary to identify individual muon–positron decays. This requires that no more than one muon be present in the sample at a time and the rate at which data may be accumulated is limited accordingly. This restriction is lifted for certain experiments where 'integral counting' may be employed, and also for pulsed sources, where muons are implanted in intense sharp bursts. The pros and cons of pulsed and continuous sources, and the areas of research that they each favour, are identified in § 8. With the advent of pulsed sources, and of continuous sources that are so intense that a modulation of the beam to simulate the pulsed mode might be beneficial, such a discussion seems timely. Finally the RF techniques of muon spin *resonance*, in which the efficiency with which the RF power may be used is greatly enhanced in the pulsed mode, are also described briefly in this section, together with some suggestions for future developments.

1.5. Context

A number of reviews, monographs and edited volumes have already been devoted to μSR. These deal in depth with particular aspects, for instance the fundamental properties of the muon, the original experiments and the early development of the technique. Some are devoted to particular applications. Muonium chemistry, for instance, is a huge field which is only touched on here. Reference to these works as appropriate allows a briefer treatment of these aspects here than would otherwise be permissible. The recent development of the spectroscopy, covering the last decade, is well documented by the proceedings of three specialist conferences (Gygax *et al* 1979, Brewer and Percival 1981, Yamazaki and Nagamine 1984a). These give a particularly good indication of the dramatic increase in activity over this period, and likewise of a notable improvement in the definition of the aims and objectives of experiments, and of an increasing certainty in their interpretation.

The present article is intended to serve as a popular introduction to the specialist literature, concentrating on experimental studies, and to give an indication of the scope of present applications. Problems, paradoxes and outstanding puzzles are not overlooked. The references are chosen to illustrate particular points and topics and by no means constitute a comprehensive survey. They are selected from work published up until early 1986, when this review was completed. A more formal exposition of theoretical aspects, and a more extensive bibliography of work completed by early 1985, are given by Schenck (1985a). Progress has been lively during the intervening year, notable developments including the detection of 'critical' dynamic spin correlations well above the Curie temperature in certain intermetallics (§ 3.2.4), the extension of the spectroscopy of muonium defect centres to a great variety of more or less ionic crystals and the development of molecular orbital models for these centres (§§ 4.4–4.6), a new theoretical model for the quantum mobility of screened muons at very low temperatures (§ 5.6) and the emergence of 'level crossing resonance' as a μSR technique of major importance (§ 7.3)—these will figure prominently in the forthcoming proceedings of the μSR '86, the fourth international conference[†]. Reference to these proceedings will also reveal the extent of the international activity in muon spin *research*. Groups commute and collaborate worldwide to perform experiments, as is inevitable for any research that requries central facilities. However, it is also apparent that the activity is favoured where such a facility is within easy reach. With the construction now in progress of a major new European muon source—a particularly intense pulsed source based on the ISIS spallation neutron source in the UK and dedicated to condensed matter science—this seems an appropriate moment for a new overview of the achievements to date and the potential for the future[‡].

2. Muon spin rotation

The success of the μSR techniques relies on two circumstances. These are: the intrinsic polarisation of the muons during their production from pions (2.1)[§]; and the anisotropy of the positron emission in their subsequent decay (2.2)—both are expressions of the violation of parity conservation in processes where particles susceptible to the weak interaction are involved (Garwin *et al* 1957):

$$\pi^+ \rightarrow \mu^+ + \nu_\mu \qquad (\tau_\pi = 26\,\mathrm{ns}) \tag{2.1}$$

$$\mu^+ \rightarrow \mathrm{e}^+ + \bar{\nu}_\mathrm{e} + \nu_\mu \qquad (\tau_\mu = 2.2\,\mu\mathrm{s}). \tag{2.2}$$

The production process is illustrated in figure 1(*a*). Given that the neutrino has a defined helicity, conservation of angular momentum ensures that the muon is longitudinally polarised in the pion rest frame. The initial polarisation can be substantially preserved throughout the transport of the beam and usually also in the actual process of implantation and thermalisation. The subsequent evolution of the muon polarisation, within the sample, may then be monitored because the muon indicates its spin direction at the instant of its decay. This it does, very fortunately, by emitting a positron preferentially in this direction. Illustrated in figure 1, (*b*) and (*c*), the origin of this preference may be readily understood for the highest-energy positrons. In the three-body decay, the positron has maximum energy when it is ejected in line with the two neutrinos, and therefore in line with the instantaneous spin orientation of the parent nuon. The highest-energy positrons exhibit an anisotropy of close to 100%, i.e. they have the maximum 'analysing power'. (The lowest-energy positrons in fact have the opposite, i.e. negative, analysing power so it is sometimes advantageous to reject them.) Averaged over all possible positron energies, the anisotropy is about 30%, as in figure 1(*d*) (see, for instance, Brewer *et al* 1975a, Chappert 1984).

[†] *Note added in proof.* Hartmann *et al* (1986).

[‡] The new source and experimental facilities were commissioned early in 1987 (see note added in proof). This is quite an appropriate date. As well as being the 30th anniversary of the demonstration of parity non-conservation, Webster (1987) points out that 1987 is the 50th anniversary of the discovery of the muon, and the 40th anniversary of its 'correct' identification.

[§] A common means of production is to bombard a light target, e.g. graphite, with 500–800 MeV protons. Pions are liberated in the proton–nucleon collisions and subsequently decay rapidly to muons, as described by (2.1).

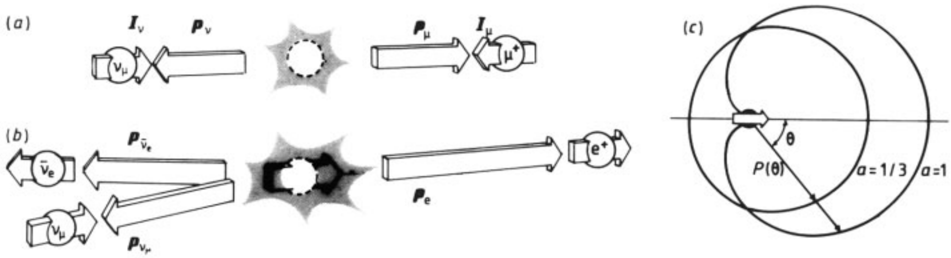

Figure 1. Production of a muon from the decay of a pion (a), and the subsequent decay of the muon (b). Momentum vectors $\boldsymbol{p}$ of the product particles are depicted in the rest frame of the parent particles. The vectors $\boldsymbol{I}$ denote particle spin or neutrino helicity. (If the pion decays in flight, $\boldsymbol{I}_\mu$ may be parallel or antiparallel to $\boldsymbol{p}_\mu$, depending on the value of muon momentum selected.) The angular distribution $P(\theta) = 1 + a\cos\theta$ of the positron intensity (from a bunch of muons or, equivalently, the emission probability from a single muon) is sketched in (c) for the positrons of the highest energy (asymmetry parameter $a = 1$), and averaged over all positron energies ($a = \frac{1}{3}$).

2.1. Implantation

Muon spin *rotation*, up to now the most common of the μSR methods, is illustrated in cartoon form in figure 2. Implantation is depicted in the first frame of the cartoon, figure 2(a). Two types of muon beam are in common use. In those known as decay channels, muons are collected from the decay of pions in flight. A beamline tuned to the momentum range 60–120 MeV/c collects 'backward-decay' muons with an average polarisation of typically 80%, which is parallel to their flight direction. The corresponding particle energy is about 40 MeV, and the stopping range in matter about 1 g cm^{-2}. A beamline tuned to the higher momentum range 140–180 MeV/c collects 'forward decays', with a similar polarisation but aligned in this case antiparallel to the beam. The corresponding particle energy is about 100 MeV, and the stopping range 3–4 g cm^{-2}. These are very modest energies by modern accelerator standards, of course; experiments in high-energy physics commonly use muons capable of penetrating several kilometres of material. Some 'moderation' or 'degrading' of these beams is normally employed, nonetheless, to reduce the incident energy on the sample, and to permit more or less uniform implantation in samples with dimensions of a few centimetres. The distribution of stopping range is about 10% of the above nominal values. The degrader is depicted in figure 2(a) and is typically of graphite, polythene or water (material containing heavier atoms tending to spread the slowed beam excessively). Its thickness is adjusted to maximise the stop rate in the sample, or to optimise it with respect to stops of unwanted particles, notably pions and positrons, which fortunately have different characteristic penetration depths (contamination from unwanted particles is generally somewhat worse in 'forward-decay' than in 'backward-decay' beams). With beams of these energies, bulk samples of at least 20 g total mass are required to secure a reasonable data rate, and so that the background μSR signal from muons stopped in neighbouring materials (e.g. sample mounts or cryostat walls) is not excessive.

Smaller samples may be used, or even several samples studied simultaneously, in a spectrometer that identifies the spatial coordinates of each recorded muon decay. Such an instrument is described by Podini and Tedeschi (1984). The scintillation detectors are supplemented by multi-wire proportional chambers, able to reconstruct the trajectories

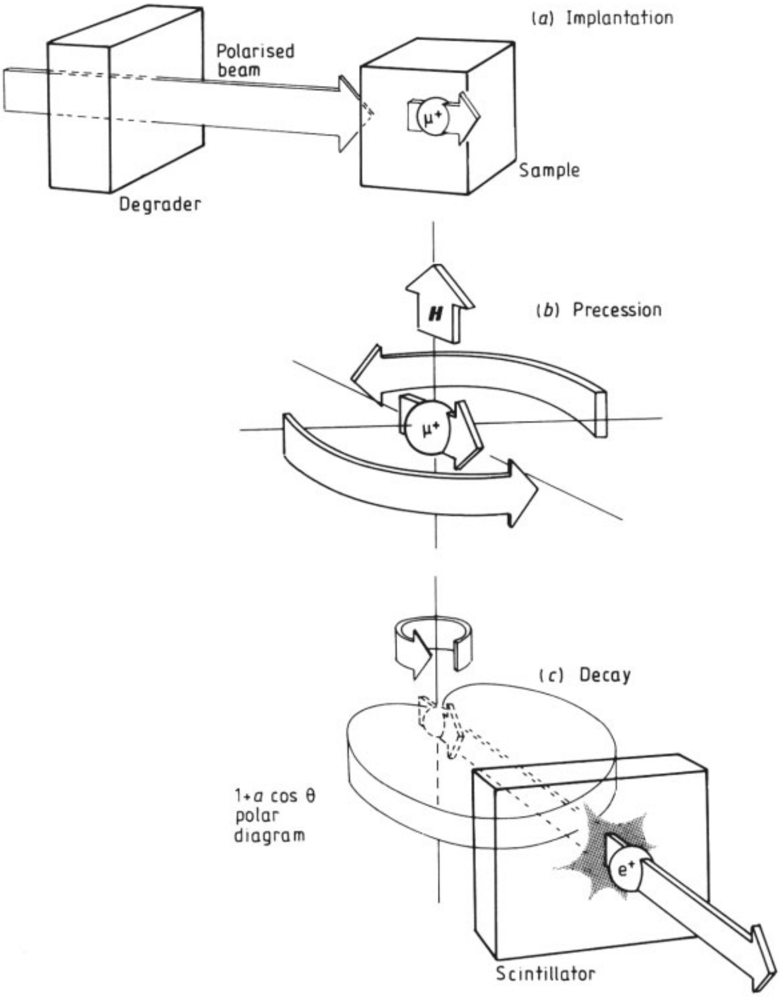

Figure 2. Representations of (*a*) muon implantation, (*b*) muon spin rotation (i.e. Larmor precession in a transverse magnetic field) and (*c*) disintegration of the muons and detection of the emitted positrons. The polar diagram of figure 1(*c*) rotates with the muon spin.

of both incoming muons and outgoing positrons. This spectrometer is likewise able to eliminate the unpolarised background signal arising from false muon-positron correlations (see § 8).

Alternatively, the beamline may be tuned to the particular momentum, 28 MeV/*c*, which selects muons coming only from the decay of pions that are at rest near the surface of the production target. Such a 'surface muon' beam (also known, in recognition of its developers, as an 'Arizona' beam) has a polarisation very close to 100% (Piper *et al* 1976). The muon energy is 4 MeV, and the stopping range correspondingly low and well defined. This is 0.15 ± 0.01 g cm^{-2}, which corresponds a penetration depth of about 0.2 mm in copper, for instance, 1.5 mm in water, or 1 m in He gas at STP. 'Surface muons' are therefore suitable for samples that are only available in small quantities, for metallic foils and for gas-phase studies. Thin windows in the beamline and cryostat are required to allow the muons to reach the sample. No additional degrader is necessary for bulk samples, which readily stop all incident muons; a few sheets of Mylar are sufficient to optimise the stop rate in thin-film specimens. In the future, beams tuned to lower energy still, i.e. to 'sub-surface' muons (Badertscher *et al* 1985) or 'cooled' by the special techniques of phase-space compression (Taqqu 1986), may be used for genuine surface-layer implantation†.

Since comparisons are frequently drawn in the following sections between data obtained from μSR experiments and from neutron scattering, it is perhaps worthwhile emphasising here that μSR is *not* a scattering technique. The muons are actually stopped, or at least thermalised, in the sample.

The muon bombardment is relatively gentle, but the incident energy is nevertheless in excess of the ionisation threshold for all beams in current use. Some damage to the sample lattice and the generation of certain radiolysis products are therefore to be expected. The various processes by which the muons lose their initial kinetic energy are fast; also the primary processes bring into play only electrostatic interactions, which are not spin-dependent. So there is rarely any loss of polarisation during thermalisation (Ford and Mullin 1957, Brewer *et al* 1975a). If one imagines a bunch of muons implanted at time zero (as would be the case for a pulsed muon source), the bunch has a well defined initial polarisation equal to that of the beam. At least this is true in metallic samples, where it also appears that the muons finally thermalise well away from any lattice damage that may be generated initially: separations of the order of 1 μm have been estimated (Brice 1978). The situation is less clear-cut in insulators, molecular materials and liquids. Here a certain discrepancy is not uncommon between the known beam polarisation and the starting polarisation as determined within the sample. This is referred to as the 'missing fraction', and has been the cause of some puzzlement and speculation. Especially where muonium formation is involved, or is suspected of being involved, this 'prompt' depolarisation is now commonly attributed to spin-flip encounters with other paramagnetic radiolysis products, which can occur in the brief interval of time before these species disperse by diffusion or recombination (§ 4.1.1).

2.2. *Precession frequencies and depolarisation functions*

For the present purposes, imagine a bunch of muons implanted at time zero (as would be the case for a pulsed muon source) and with an initial polarisation close to 100%. If now the implanted muons experience any magnetic field that is not parallel with their initial polarisation they will begin to precess about it at the corresponding Larmor frequency, given by the muon magnetogyric ratio

$$\gamma_\mu/2\pi = 136\ \mathrm{kHz\ mT^{-1}}. \tag{2.3}$$

This is illustrated in the second frame of the cartoon, figure 2(*b*). This description remains valid whether the field is externally applied or generated internally within the material. If the muons adopt equivalent sites within the lattice, or within the molecules of the sample, and experience there identical fields, they will precess in phase and the magnitude of their initial polarisation will be preserved during the rotation. Any variation of the local field between different occupied sites, on the other hand, will result in the muons dephasing as they precess, with a corresponding gradual loss of polarisation.

---

† Low-energy muons may in principle also be obtained from a decay channel tuned to the 'magic' pion momentum, 40 MeV/c; the resulting muon spectrum then extends to zero energy for backward decays (see, e.g., Tschalär 1977).

Unlike the prompt loss of the 'missing fraction', this progressive depolarisation can be monitored, and described by a relaxation function.

As in magnetic resonance, it is these characteristic frequencies and relaxation functions that constitute the spectroscopy of the system—the material plus the implanted muon.

The decay positrons, carrying this information, are sufficiently energetic to escape from the sample (through any surrounding cryostat etc, if this is not too heavily engineered) and are readily detected in simple scintillation counters arrayed about it. Following implantation of a burst of muons, at time zero, the positron count rate monitored in a particular direction is therefore modulated as the muons precess: the positron emission is most intense along the instantaneous orientation of the ensemble polarisation. One can almost imagine a somewhat diffuse 'lighthouse beam' of positrons sweeping around, periodically illuminating the detector. More accurately, the Larmor precession of the muon spin is accompanied by a precession of the polar diagram describing the probability of positron emission. Since the polarisation is well defined at time zero, its subsequent precession and evolution may be monitored with remarkable sensitivity. This is somewhat analogous to the situation in perturbed angular correlation (PAC) studies, where the polar diagram for γ-ray emission precesses with the magnetic moment of the radioactive nucleus. (In PAC, however, the initial *alignment* only of the nucleus is defined, rather less precisely, by observation of the first γ-ray of the cascade.)

Raw data typical of those recorded in many μSR experiments are shown in figure 3. This is the muon radioactive decay curve, modulated by the precession signal of interest. The depth of modulation may be seen to correspond to the expected average asymmetry of about 30%; in this example all the muons are in the same state, precessing at nearly

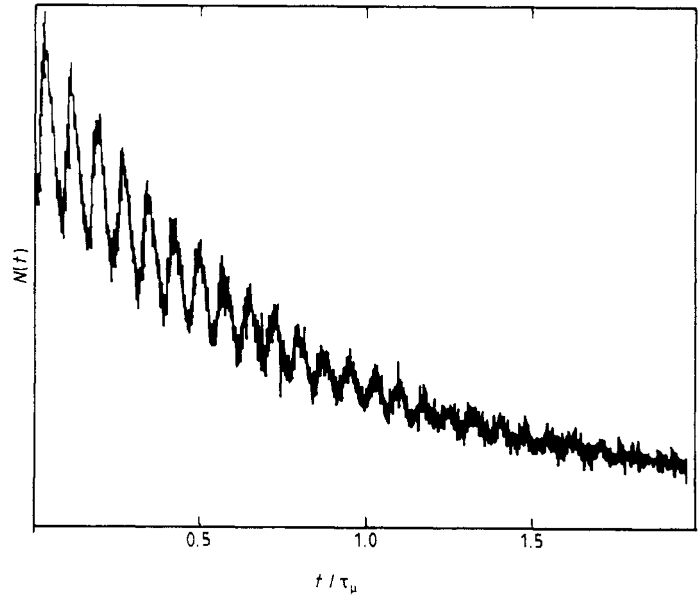

Figure 3. A μSR histrogram. This is the positron count rate following muon implantation (pulsed-beam technique) or, equivalently, a histogram of positron counts $N(t)$ as a function of parent-muon lifetime t (continuous-beam technique) (the photograph is courtesy of CERN). The different modes of data acquisition are described in § 8.

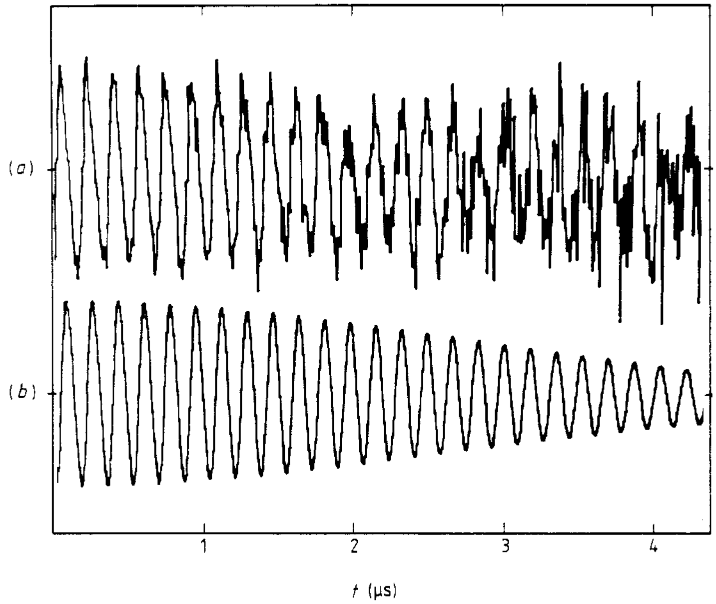

Figure 4. A μSR precession signal (*a*), together with its 'on-line' fit (*b*). These show the same data as in figure 3, compensated for a time-independent background and for the radioactive decay curve. In order to illustrate the curve-fitting procedure, somewhat noisy data corresponding to less than half a million recorded muon decays are shown (photograph courtesy of CERN). Higher statistics are usual, especially when a good fit to the relaxation function is required. Otherwise the signal is typical of muons rotating at their Larmor frequency in metals or metal hydride samples. Note the resemblance to free induction decays.

identical frequencies, and there is no loss of initial polarisation (i.e. no missing fraction). This single-component signal is typical of metallic samples. Subtraction of the small horizontal background (see §§ 2.4 and 8), and compensation for the known muon radioactive lifetime (i.e. multiplication of the data by the inverse exponential), reveal the pure precession signal (figure 4(*a*)). These are the same data as in figure 3, manipulated on-line in the minicomputer dedicated to data acquisition. Figure 4(*b*) represents a preliminary fit to the precession signal, also performed on-line, i.e. simultaneously with the accumulation of data. Such a fit provides approximate values for frequency, depolarisation rate, initial amplitude and phase. These values are adequate to allow the progress of the experiment to be controlled (e.g. for the succeeding experimental conditions to be chosen); they may be determined more precisely in a subsequent off-line analysis.

The similarity of these signals to free induction decays, familiar in pulsed NMR experiments, is to be emphasised. Since the exponential envelope representing the radioactive decay curve has already been compensated, the decreasing amplitude of the precession signal in figure 4(*a*) represents depolarisation of the muon ensemble by other processes. These are most commonly the magnetic interactions of the muons with the surrounding spins, i.e. the effective distribution of local fields.

Thus in figure 4(*b*), a gaussian depolarisation function has been fitted, appropriate to the distribution of static dipolar fields from spins on a regular lattice. Such a distribution may be effectively narrowed by fluctuation of the host spins, or by motion of the muon probe itself. In these cases the appropriate function tends to an exponential. Examples are common in the following sections. Unless nuclear or atomic magnetism is very weak or absent in the host material, an undamped precession signal is indicative of extreme 'motional narrowing'. The intrinsic distribution may also be effectively broadened, i.e. the depolarisation enhanced, if the muon changes its environment in a chemical reaction. This is lifetime broadening, i.e. a loss of coherence due to a large sudden change of precession frequency for individual muons. The appropriate function is again exponential, with a time constant equal to the chemical lifetime. The chemical reaction of muonium is shown as an example in figure 5 (Roduner 1979).

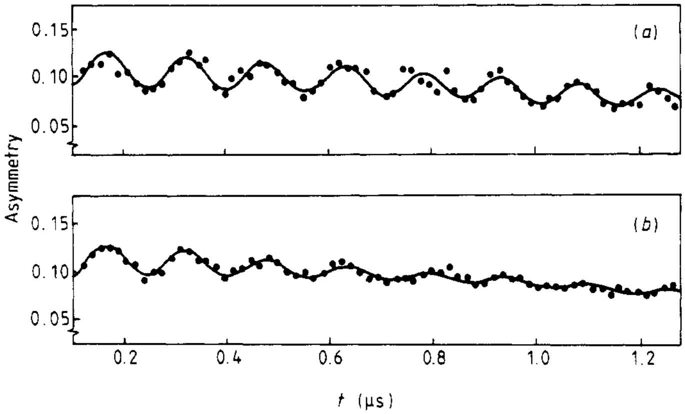

Figure 5. The precession signal of muonium showing its intrinsic depolarisation rate in pure water (*a*), and its enhanced depolarisation rate in the presence of reactive solute (*b*) (courtesy of E Roduner).

The presence of several characteristic frequencies may be revealed by a Fourier transform of the precession signal (see, for instance, Brewer *et al* 1982). It is usual to identify the different components present in this manner, prior to the fitting of frequency, damping rate (equivalent to linewidth), initial amplitude and phase to each component separately. Multiple frequencies are common in magnetic materials where more than one site may be available to the muon. In paramagnetic states, the muon–electron hyperfine interaction invariably generates several lines in the μSR spectrum (the hyperfine field adding to or subtracting from the applied field according to whether the muon and electron spins are parallel or antiparallel). There may also be more than one such state generated by muon implantation, as for the muonium centres in semiconductors (§ 4) and in certain organic compounds (§ 6). Figure 6, as an illustration, is the μSR spectrum of an organic liquid in which the muons both create and label free radicals.

2.3. *Amplitudes and phases*

The initial amplitude of a precession signal is a measure of the decay anisotropy. Referring to figures 1 and 2, it is commonly characterised by the effective asymmetry parameter *a*. After suitable calibration it yields the proportion of muons observed in a particular state. The amplitudes of different components in a multi-line spectrum are therefore a measure of the distribution of muon polarisation between the corresponding states. To within the uncertainty represented by any 'missing fraction', they represent the probability, per muon implanted, that the respective state is formed.

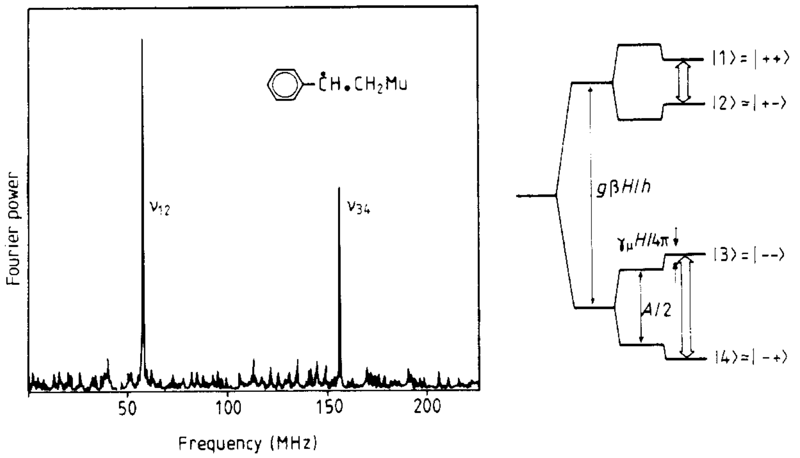

Figure 6. The μSR spectrum of a muonated radical (*a*) and its interpretation (*b*), illustrating the analogy with ENDOR spectra. A is the muon–electron hyperfine coupling (here equal to the sum of the two precession frequencies), $g\beta H/h$ is the electronic Zeeman splitting (in frequency units) and $\gamma_\mu H/2\pi$ is the muon or 'nuclear' Zeeman splitting. The two-line spectrum is characteristic in high fields, $g\beta H/h \gg A$, when the electron and muon spins are decoupled, i.e. the transitions observed correspond essentially to flips of the muon spin alone. The spectrum is of the radical CHPh.CH$_2$Mu, generated by muon implantation in styrene (Hill *et al* 1982), recorded at room temperature and 0.3 T.

A word is necessary about the counter geometries required to detect the precession signals. In this version of μSR, the field experienced by the muon—or a component of it at least—must be transverse to the initial polarisation. The frequency of the recorded signal reflects the *magnitude* of the field but the signal amplitude or effective asymmetry is reduced in proportion to the appropriate *component* or projection of the field that is transverse to the initial direction of polarisation. For the usual case of a longitudinally polarised beam, and an external field applied perpendicular to this direction (as in figure 2) the full asymmetry is observed by positron 'telescopes' placed anywhere in a plane perpendicular to this field, as in figure 2(*c*) and 7(*b*). Signals such as those of figure 3 are accumulated in each of several such telescopes, thereby maximising the information that is obtained in a single experiment, by maximising the total coverage of solid angle; they differ only in initial phase, by virtue of their respective angular positions (and in number of recorded events, by virtue of their individual solid angles subtended at the sample).

For the case of precession that is not about an externally applied field but about the internal fields of an antiferromagnet, or of a demagnetised ferromagnet, the full asymmetry may only be observed in counters in the forward or backward direction, i.e. at $\theta = 0°$ and $180°$ with respect to the initial polarisation. Here the signal amplitude varies as $\cos\theta$; in the perpendicular direction ($\theta = 90°$) there is a cancellation of the signals from ensembles of muons precessing in opposite senses (i.e. those in different domains of the ferromagnet, or dominated by different sublattices of the antiferromagnet; see § 3). Likewise the hyperfine signals of muonium or paramagnetic states in zero field (see § 4) are only observable in longitudinal geometry. These are not strictly precession or rotation signals, but rather an oscillation between the singlet and triplet states. Positron counters happily make no distinction between 'precession', 'oscillation' or 'modulation' of the muon polarisation!

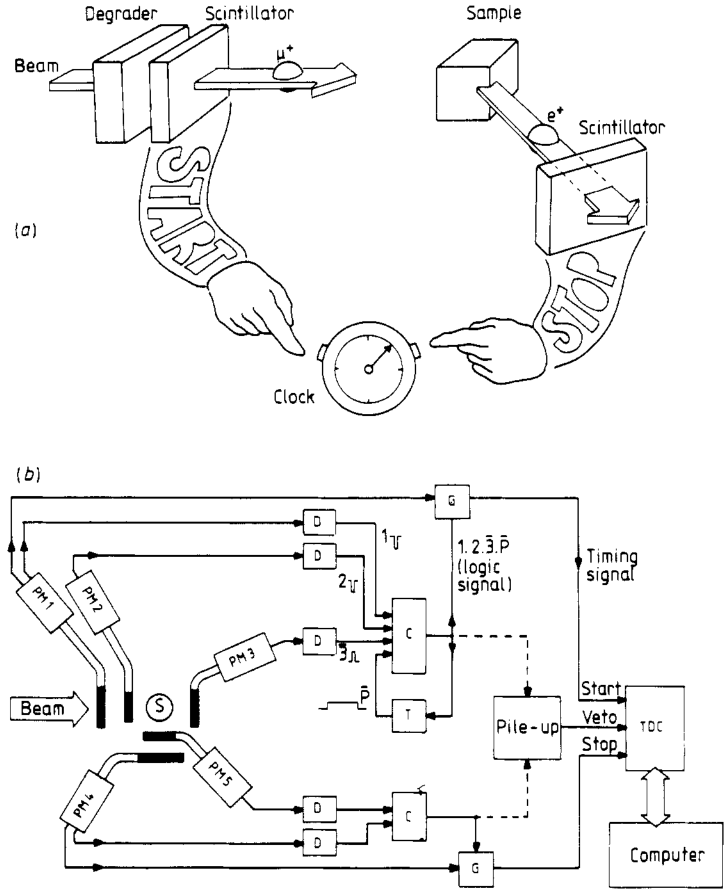

Figure 7. Cartoon (*a*) and schematic (*b*) representations of a 'time-differential' μSR spectrometer for use with a continuous muon source (S = sample, PM = photomultiplier, D = signal height discriminator, G = gated discriminator, T = timer (10–20 μs) and TDC = time-to-digital converter; appropriate delay lines are not shown and the logic for the selection of good events is greatly simplified). A single positron telescope comprising detectors 4 and 5 is shown transverse to the beam. Several such positron telescopes, transverse and longitudinal, would be included to improve the coverage of solid angle, and a histogram of events established for each telescope. Certain types of experiment *require* telescopes that are longitudinal, i.e. parallel to the beam polarisation, as explained in the text.

The initial phase of a precession signal can determine whether the muons reach the observed state promptly on implantation. If they do, the phase is determined simply by the angular position of the positron telescope relative to the incident beam. Any departure from this geometrical value indicates that the muon has spent a brief interval in a different state, characterised by a different precession frequency. The nature and lifetime of this chemical precursor state may be determined from careful phase measurements in favourable cases (see, e.g., Fleming *et al* 1979). The specific application to organic radicals is described in § 6.

For the relatively low-momentum surface muon beams, it is possible to manipulate the beam polarisation. For instance it may be rotated transverse to the beam direction by applying crossed magnetic and electrostatic fields in devices, known as separators, which are also used to eliminate positron contamination of the beam. This permits the observation of muon spin rotation signals in much higher external fields than are otherwise accessible, by applying the field *longitudinally* to the beam direction (i.e. still perpendicular to the initial polarisation). Muons will always penetrate a field that is axial to the beam direction, whereas the implantation of muons in fields *transverse* to the beam direction is restricted by the curvature of the beam in such a field, the practical upper limit (i.e. without substantial realignment of the apparatus) being about 0.1 T for surface beams, 0.5 T for decay channels. The similar spiralling of the decay positrons does not begin to limit the effective asymmetry seriously until much higher fields are reached. (It can even enhance it by suppressing detection of the lowest-energy positrons, which, as noted above, reduce the average asymmetry parameter. Some care is therefore required in the calibration of signal amplitudes, especially the field dependence of amplitude.)

Longitudinal counter geometry has a much more extensive use in the variant of the μSR technique known as muon spin *relaxation*. This includes the determination of the muon relaxation functions in longitudinal fields (i.e. fields *parallel* to the initial polarisation), as well as in zero field, and is the subject of § 7. Beam polarisation is assumed to be longitudinal, unless otherwise stated, in the remainder of this article.

2.4. *Data acquisition and sensitivity*

The spectra shown for illustration above were in fact recorded not with a pulsed source but with a continuous one, where muons are delivered more or less at random. Thus figure 3 represents a histogram complied from individual 'events'. This latter term is borrowed from nuclear methods and may be taken here to mean detection of a delayed muon–positron coincidence, i.e. a measurement of the time elapsed between a muon arriving and positron departing. The arrival of an individual muon is detected and starts a clock, which is stopped by detection of its decay positron. This is illustrated in figure 7(*a*), which is a delightful version of the cartoon, due to De Renzi, and more seriously in figure 7(*b*), which is a much simplified version of data acquisition schemes in common use by the μSR Collaboration working at CERN†.

The particle detectors comprise scintillators, lightguides and photomultiplier tubes. These may be used singly, but more commonly pairs of detectors are used in coincidence, as shown, to eliminate electronic noise and to obtain some telescopic effect. In this scheme the time-to-digital converter receives a start signal from an incoming muon when the coincidence $1.2.\bar{3}.\bar{P}$ is satisfied and a stop signal from an outgoing positron when a coincidence 4.5 is satisfied. The anti-coincidence signal $\bar{3}$ ensures that the muon has not passed through the sample. Additional anti-coincidence logic (not shown) further safeguards against stray or scattered particles whose trajectories do not intersect the sample; muons and positrons may also be distinguished by the inclusion of Čerenkov counters. In order to avoid serious ambiguity about the origin of each positron in such a scheme, only one muon should be present in the sample at any one time. The signal P in figure 7(*b*) ensures a sufficient lapse of time since detection of the previous muon, before a new start signal is accepted. This is the simplest part of the 'pile-up' logic which safeguards against false muon–positron correlations, by rejecting events where a second muon or positron arrives too soon.

---

† European Laboratory for Particle Physics (Geneva). Research groups from France, Germany, Italy, Sweden, Switzerland and the United Kingdom collaborate in μSR experiments.

With a pulsed source, it is neither necessary nor possible to correlate individual positrons with their parent muons. Muons are implanted in intense sharp bursts, so that there is now a common start signal. In principle a histogram may be established at each burst. The implications for the rate at which data may be collected, and the other advantages and limitations of this mode, are discussed in § 8.

The powerful 'nuclear techniques' of single-particle counting make the μSR technique enormously sensitive compared with conventional NMR. The muon spin transition is detected at the very much higher energy corresponding to the muon's radioactive decay. This corresponds to an enormous amplification of the signal. Figures 3(*a*) and (*b*) represent just 5×10^5 recorded muon decays—a precession signal from half a million spins! From this point of view the term used for free induction decay in the French NMR literature, which translates as 'free precession signal', is more appropriate since the μSR method does not rely on the detection of induced RF fields. Neither is a '90° pulse' of RF field required to induce the transverse polarisation (although in certain pulsed μSR experiments this would have some advantage; see § 8): in the geometry depicted in the cartoon (figure 2) the muons are implanted in a non-stationary state, with their initial polarisation perpendicular to the applied field. It is noteworthy that this initial transverse polarisation may be close to 100% irrespective of the temperature or magnetic field at which the experiment is performed. This also contributes substantially to the sensitivity of the μSR technique, and is to be contrasted with the situation in conventional nuclear magnetic resonance, where the initial polarisation is limited by Curie's Law, usually to a very small value. (Thermal equilibrium proton polarisation in 10 mT at room temperature, for instance is about 4×10^{-8}!) μSR experiments, on the other hand, give comparable signals from ovens and cryostats, in superconducting solenoids and in zero field. This feature has been put to good use in muonium studies at high temperature (§ 4). It has also been exploited in the study of magnetic fluctuations where a combination of excessive broadening and low polarisation renders NMR signals undetectable (§ 3): this advantage could be pushed to much higher temperatures still, for instance in systems with large exchange interactions (Baker and Owen 1984).

'Trigger detection, absence of interactions between the very few μ-mesons† existing in the sample at a given time, differences of population due to the non-conservation of parity, and magnetic dipole transition are the standard features of this experiment'. These observations by Abragam (1961) on the determination by Garwin *et al* (1957) of the muon's magnetic moment, remain true of all subsequent μSR studies.

3. Magnetism

μSR is first and foremost the use of the muon as a local magnetic probe. It is able to provide results on the local fields at the sites adopted by the muons within a lattice or molecule, via the μSR frequencies, as well as on the spatial or temporal variation of these fields, via the depolarisation rates or the shape of the relaxation functions. Thus it is no surprise that the study of magnetic systems is an important and successful application of this spectroscopy (see, e.g., Bucci 1981, Meier 1984). Information is obtained on the interplay between spin structure and dynamics in a wide range of systems: metallic and

---

† The name *muon* has been universally adopted since the late 1960s, the term 'meson' now being reserved for strongly interacting integer-spin particles. The history of the discovery and identification of the particle is nicely summarised by Wu and Hughes (1977).

insulating, dense and dilute, crystalline and disordered. Topics illustrated in this section are:

(i) the determination of the nature of the field experienced by the muons, e.g. 'dipolar' or 'hyperfine';
(ii) the measurement of spontaneous internal fields in ordered phases;
(iii) the interpretation of contact hyperfine fields in terms of local electronic structure (bonding in non-metals and screening in metals);
(iv) the investigation of spin dynamics, especially in the critical region close to an ordering transition; and
(v) the measurement of susceptibility in paramagnetic and diamagnetic systems.

The question arises here as to whether the muon is a passive or 'innocent' probe for these purposes. To what extent does it disturb the local structure and properties by its presence? It is in this application of μSR especially, where one might hope to probe the *intrinsic* magnetic properties of materials, that these questions are most relevant. They can only be answered by detailed μSR studies of particular materials, and by careful comparisons of the data with the results of established conventional techniques. The answers depend on whether the material is insulating or metallic, crystalline or disordered. These different classes are considered separately. Systems with a regular magnetic lattice are the principal subject of this section, although the extension to random and amorphous magnets is touched on where appropriate. (Dilute systems—especially the spin glasses—are treated in § 7, where the appropriate zero-field technique of muon spin *relaxation* is introduced.) The antiferromagnetic insulators (fluorides and oxides: § 3.1), the ferromagnetic elemental metals (§ 3.2) and a variety of magnetic alloys (rare earth and transition metal: §§ 3.2 and 7) have all received considerable attention. Present studies also include mixed-valence and heavy-fermion systems. The particular sensitivity of an interstitial probe to the local spin arrangement is illustrated by the unmistakable changes in the μSR signals that occur at ordering and at spin-flip transitions. Spin structures may generally be determined by other means, certainly, although one could imagine that the measurement of internal field from an interstitial position, which is not readily obtained otherwise, could provide a useful check on the ordered structure in certain instances. In metallic systems, where the spin structure is usually already well known, it is the value of the conduction electron spin density, as measured by a charged interstitial probe, that is of especial interest. The muon screening charge, and its spin polarisation, are of crucial importance here. (There may also be a contact hyperfine interaction from electrons whose wavefunctions vanish at the regular lattice sites and that therefore do not contribute directly to the contact hyperfine field as measured by a substitutional nuclear probe, as in NMR, PAC or Mössbauer spectroscopy).

This study of local electronic structure, and especially of the electronic response to the introduction of an interstitial test charge, extends to the paramagnetic and diamagnetic metals and alloys, via measurements of the muonic Knight shifts. These are amply reviewed elsewhere (see e.g., Schenck 1981, 1985) and so are dealt with only briefly, in § 3.3.

Once the nature of the field experienced by the muon has been established in a particular material, it is perhaps especially in spin dynamics that novel information may be obtained. The ability of μSR to determine spin correlation times over a wide dynamic range, bridging the gap betwen the nuclear probe techniques and neutron scattering, can be illustrated here for insulating and metallic systems and for 'soft' and 'hard' magnets (§§ 3.1 and 3.2). Again, the interstitial position of the muon is advantageous.

Thus whereas measurements on the nuclei of the magnetic atoms themselves can generally only give the self-correlation term in the spin fluctuations above the critical region (the hyperfine field at such a nucleus being dominated by the individual atom), the interstitial muon may often be well placed to report on pair correlation terms (§ 3.2).

3.1. *Magnetic insulators*

3.1.1. Metal fluorides. A particularly good illustration of the above topics, appropriate to insulators, is the μSR study of MnF_2 and CoF_2 by De Renzi *et al* (1984a, b). These materials exemplify the two classic models of antiferromagnetism: CoF_2 is Ising-like; MnF_2 shows a much weaker anisotropy (the magnetic ion being in the S state) and is one of the closest known approximations to the Heisenberg model. Their characteristics are well known from magnetic resonance studies, which were made in great detail on these materials in the 1960s (interst now being renewed by the study of random-field effects in the magnetically diluted materials). The μSR experiments are sketched in figure 8. In the antiferromagnetic phase, a precession signal is detectable (with a suitable counter geometry—see § 2) in zero applied field; its frequency is therefore a measure of the spontaneous internal field (figure 8(*a*)). In the paramagnetic phase an external field must be applied in order to generate a precession signal. The linewidth of this signal is found to diverge in the critical region as T_N is approached from above; this must represent the critical slowing down of the antiferromagnetic spin fluctuations (figure 8(*b*)).

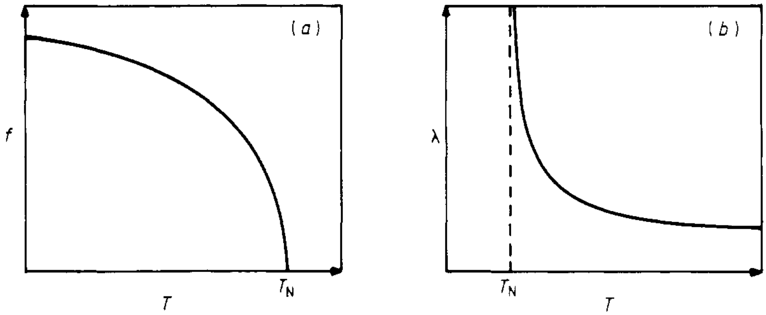

Figure 8. Temperature dependences of (*a*) the μSR frequency in zero field in the antiferromagnetic phase and (*b*) the μSR linewidth in an applied field in the paramagnetic phase.

In order to interpret these data in terms of the magnetic properties of interest, the sites adopted by the implanted muons in the crystal lattice and the nature of the field they experience there must first be established. This is the subject of a careful localisation study (De Renzi *et al* 1984a). The observation of a single, well defined μSR frequency in the ordered phase is already a good indication that the muons stop in crystallographically equivalent sites, and that these are intrinsic sites, not related to impurities or defects. Also, since (*a*) the internal field experienced below T_N is non-zero, and (*b*) critical behaviour is observed above T_N, these sites must be asymmetrically placed with respect to the two sublattices.

Measurements of the paramagnetic shift of the Larmor frequency above T_N, and of its orientational dependence (figure 9(*a*)), determine the muon site unambiguously (figure 9(*b*)). Measurements of the spontaneous field below T_N, and of its vector addition

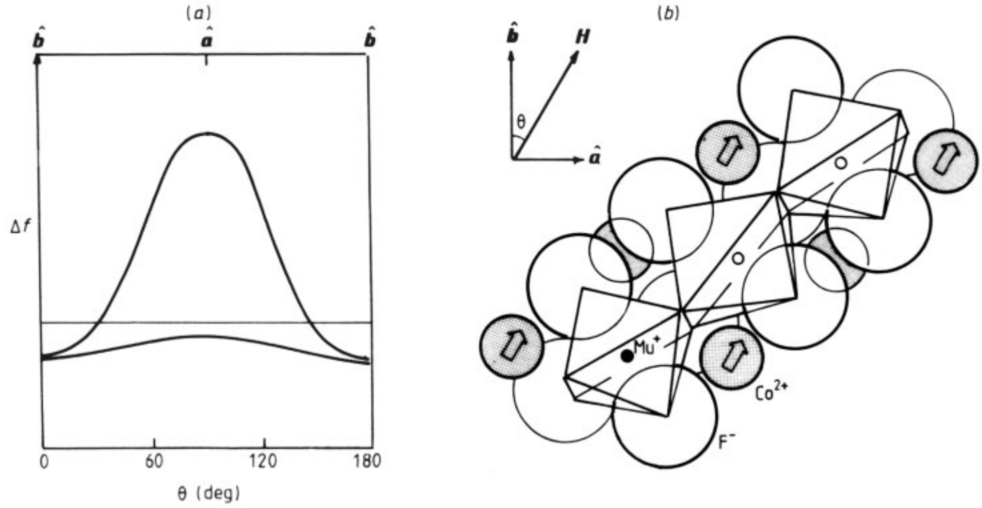

Figure 9. The orientational dependence of the paramagnetic shift in CoF_2 (*a*) (note the twofold splitting) and the interstitial muon sites deduced to be at the centres of octahedrons of F^- ions (*b*).

with an applied field, confirm that the same site is occupied in both phases, over the whole temperature range investigated. All these measurements indicate that the field experienced by the muon is uniquely dipolar, determined by the distant local moments of the Co^{2+} or Mn^{2+} ions. (At least, this is an adequate description for the fluorides—see § 3.1.4.) Crystallographically equivalent sites are not all magnetically equivalent, however. This is evident in figure 9(*b*) and accounts for the small but resolved splitting of the μSR line that is found in both the antiferromagnetic and paramagnetic phases. The precise angular variation of the splitting reflects how the susceptibility varies with the orientation of the applied field in the *a*–*b* plane. This is isotropic in MnF_2 but not in CoF_2, where the polarisability is greater when the field is applied along the direction of the Co–F bonds—the super-exchange path—than when perpendicular. Figure 9(*a*) shows a novel manifestation of the 'microscopic' tensor susceptibility (the orthogonal tensors of adjacent crystalline layers average to give an isotropic 'macroscopic' or bulk susceptibility) and constitutes a nice bonus to the site determination.

3.1.2. Linewidths. There are three spin systems to consider in these materials: atomic (i.e. electronic), nuclear and 'muonic'. It is the nature of the ordering of the metal-ion moments, Mn^{2+} or Co^{2+}, i.e. the interplay between dynamics and structure in the electronic spin system, that is of principal interest. Then there are the ^{19}F nuclear spins, and the muon spins. The nuclear spins constitute a thermodynamic system in their own right, but their behaviour is entirely dominated in these materials by that of the electronic spins, whence the use of ^{19}F NMR as a probe of the electronic magnetism (see, e.g., Shulman and Jaccarino 1957, Heller and Benedek 1962). In the present μSR experiments, the muons are implanted one by one and so cannot constitute a spin system in the usual sense. They are like the extreme limit of a 'rare' or 'dilute' nuclear spin species, and may also be used as a probe of the electronic magnetism. Far above T_N in the paramagnetic phase, reorientation of the atomic spins via their strong exchange interaction results in rapid fluctuation of the magnetic environment of the muons, as of the ^{19}F nuclei.

The μSR precession signal decays exponentially, as in (3.1), where the quantity $\langle\delta H^2\rangle$ characterises the intensity of the fluctuations and τ_c their correlation time.

$$P(t) \propto \exp(-\lambda t) \qquad \text{with } \lambda = \gamma_\mu^2\langle\delta H^2\rangle\tau_c \tag{3.1}$$

$$\gamma_\mu^2\langle\delta H^2\rangle^{1/2}\tau_c \ll 1. \tag{3.2}$$

At sufficiently high temperatures, τ_c is given by the (inverse) exchange interaction between nearest-neighbour Co^{2+} or Mn^{2+} spins, and the inequality (3.2) holds, corresponding to rapid fluctuation of the magnetic environment. The μSR (like the NMR) lines are then exchange-narrowed, the formalism being similar to that for motional narrowing (Abragam 1961; see also § 5). Although the inequality fails in the critical region, a lorentzian form remains appropriate for both NMR and μSR lines (Moriya 1962, De Renzi *et al* 1984b)†. Here the atomic spin dynamics is characterised by the onset of short-range order, i.e. of transient local configurations having antiferromagnetic character. The critical region is clearly recognisable in the NMR and μSR linewidths, which diverge as the antiferromagnetic mode fluctuations become more pronounced (relative to other wavelengths) and more sustained. The μSR linewidths measured in different crystallographic directions also show a distinct 'crossover', a convenient indication of the onset of critical behaviour, as the anisotropy of the fluctuations (which are polarised along the eventual ordering directions) dominates the anisotropy of their coupling to the muon probe. Since this coupling is predominantly dipolar (i.e. long-range, whereas the transferred hyperfine coupling to the ^{19}F nuclei is short-range), the spatial extent of the short-range order is also of importance. The divergence of the correlation length in the critical region facilitates interpretation of the μSR results, since it then exceeds the convergence radius for the dipolar sums, and allows the μSR and NMR data to be directly compared.

3.1.3. Comparison with other techniques. *(a) Sublattice magnetisation.* With the site and coupling of the muon probe both established, the μSR data can be analysed and confronted with the results of conventional techniques (De Renzi *et al* 1984b). In MnF_2 and CoF_2 it happens that the orientation of the atomic moments remains the same throughout the antiferromagnetic phase (i.e. there is no 'spin-flip' transition). The μSR measurement of the interstitial dipolar field is therefore a particularly direct and reliable measurement of sublattice polarisation—more so, indeed, than the analogous NMR measurement in CoF_2. Here the coupling to the probe, the ^{19}F nuclei, is the transferred hyperfine interaction, which changes in strength as the population of the electronic states alters with temperature. This variation has to be accurately compensated if it is not to falsify the measurement of magnetisation‡.

Accordingly, the measurements for CoF_2 show the expected overall variation with temperature, as sketched in figure 8(*a*) (somewhat flatter than in MnF_2, consistent with the greater anisotropy). In particular they show a low-temperature variation that includes the spin wave reduction (i.e. the muons respond to the local time-averaged polarisation of the host spins); the μSR measurements scale with those of neutron

---

† These authors use the conventional theory of critical phenomena. In the light of more modern theories this can only be regarded as a guide, but these (e.g. coupled mode theory: Kawasaki 1978, Lovesey 1986) have not yet been applied to the interpretation of μSR data.

‡ The absence of a significant transferred hyperfine interaction to the muon is discussed in § 3.1.4 below. In similar measurements for antiferromagnetic $CoCl_2.2H_2O$, a substantial difference between the temperature dependences of the internal field as measured by NMR and μSR is noted by Brewer *et al* (1981b).

scattering in this regime. In the critical region, the μSR measurements follow the predicted power law for the collapse of magnetisation as T_N is approached; here it is noteworthy that neutron scattering has so far proved unable to give a reliable value for the critical exponent for this compound (probably as a result of extinction).

(*b*) *Spin dynamics*. The μSR and NMR linewidths show the same critical divergence as T_N is approached from above: they scale with each other, so the temperature-dependent correlation time that may be extracted for the electronic spins is the same referred to the muon probes as to the ^{19}F nuclear probes. Unfortunately the critical exponent that may be extracted here is not precise enough to distinguish Ising and Heisenberg predictions, from either the NMR or μSR data. However, whereas the NMR observations are at their limit (broader lines would be impossible to detect) the μSR linewidth measurements could in principle be followed much closer to the transition (the present limitation is cryogenic stability only).

The ease with which precession signals may be observed over a wide frequency range (no 'retuning' being necessary, as in NMR) allows the μSR linewidth to be determined even in the critical antiferromagnetic region, where the sublattice magnetisation is collapsing. These results are added to those of figure 8(*b*) in figure 10. They show an asymmetry in the critical behaviour as T_N is approached from above and from below. The exponent of $|T - T_N|$ is the same, but the magnitude of the damping is different—slower at a certain distance below T_N than at the same distance above it. This indicates that the fluctuations are somehow sustained by the existing magnetism and is a novel result from μSR (the current position with regard to neutron scattering data is reviewed by Böni and Shirane 1986; the implication is that the scattering function should be systematically narrower below T_N than above it).

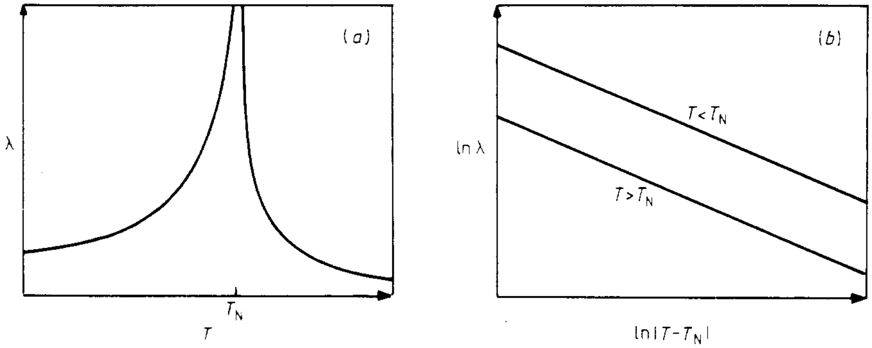

Figure 10. Sketches of the μSR linewidth measurements in the antiferromagnetic and paramagnetic phases, plotted on linear (*a*) and double-logarithmic (*b*) scales (from De Renzi *et al* 1984b).

μSR is unable to offer any spatial or wave-vector-dependent information, e.g. to comment on the size of the blocks of short-range order that exist above T_N, or to comment on the possible evolution from diffusive to propagating behaviour within these blocks. It is noteworthy that the muon probe is either static in the lattice or moving incoherently between equivalent sites (see § 5). In common with other nuclear probe techniques (NMR, PAC or Mössbauer spectroscopy), it therefore records a broad average over any variation of a property with wave-vector (except that wave-vectors near the Brillouin zone (in antiferromagnets) or near the origin (in ferromagnets) dominate the behaviour of λ in the critical region). With regard to spin waves as originally conceived, i.e. as describing the deviation from long-range order well below T_N, the question is how the μSR scales of time and range relate to these excitations. The μSR frequency data presented above evidently relate to the average local magnetisation, and include its decrease by magnon contributions, in addition to the mean-field variation.

3.1.4. Chemical binding of the muon. Since a consistent interpretation of the μSR frequencies is achieved in MnF_2 and CoF_2 on the basis of purely dipolar coupling to the muon probe, it is not necessary in this instance to consider further the chemical state of the implanted muons. Implicitly they are treated as 'bare' particles, their sites being determined by a purely electrostatic potential (De Renzi *et al* 1984a). A degree of covalency is in general to be expected, however. This appears to be the case in most of the magnetic oxides for instance, where it is necessary to invoke a small hyperfine field—a contact term—in addition to the distant-dipole coupling (Boekema (1984) and references therein). By analogy with the proton, which does not remain as the bare particle in any condensed medium, the muon is certainly expected to lower its energy by 'acquiring' electrons. The formation (and subsequent reaction) of muonium is the subject of § 4; the acquisition of a screening charge in metals is considered in § 5. Direct fixation of the muon (on a diffusion-limited timescale) should also be considered: for instance the reaction (3.3) in fluorides, or (3.4) in oxides, would in each case result in the formation of a two electron bond to the muon:

$$\mu^+ + F^- \rightarrow \mathrm{Mu{:}F} \tag{3.3}$$

$$\mu^+ + O^{2-} \rightarrow (\mathrm{O{:}Mu})^-. \tag{3.4}$$

The muon may be seen here as competing for bonding to the anion. The competition is presumably successful in the fluorides, i.e. the metal–ligand bond is broken, since there is no significant delocalisation of spin via fluorine onto the muon. The competition must be less successful in the oxides, since there is some transfer of spin density onto the muon in these materials, i.e. a conjugation of the metal–oxygen and oxygen–muon bonds. The overlap of wavefunctions envisaged is sketched in figure 11. It is noteworthy that an order of increasing metal–ligand bond strength can be written for the following four ligands:

$$\mathrm{HF} < F^- < (\mathrm{OH})^- < O^{2-}.$$

This general rule may be deduced from ESR studies (Symons 1985). The chemical properties of H and Mu can therefore be regarded as very similar for these purposes.

There is strong evidence that the muon is bonded in this manner in the magnetic oxides, since the muon sites compatible with the data are all found to be about 1 Å from an oxygen atom (Boekema *et al* 1981, Boekema 1984). This is just the separation expected for a hydroxyl ion. The multiple values of the zero-field μSR frequencies that are found in several antiferromagnetic oxides at low temperatures (§ 3.1.5.) most probably represent localisation of the muons at such sites within the unit cell that are chemically equivalent but magnetically inequivalent. If the muon bridges between two or more anions, then the separation of the anions will determine whether two or more potential minima are available to the muon or whether, in a tight geometry, the muon is constrained to the central position (figure 11(*c*,) (*d*)). (Chemical 'precedents' such as the existence of the $(\mathrm{FHF})^-$ ion may be cited here—likewise the analogy with hydrogen bonding; see also § 7.4 and figure 59(*b*).)

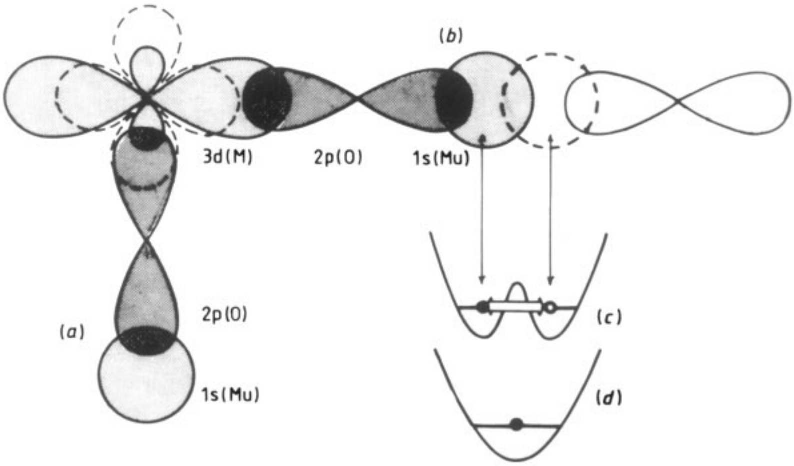

Figure 11. The schematic overlap, (*a*), (*b*), of metal, ligand and muonium ionic orbitals (various possibilities). In the absence of the muon, the bonding orbitals are full and magnetic behaviour is associated with unpaired electrons in the anti-bonding orbitals, which have mainly d character. On introduction of the muon, formation of a muoxyl bond (*a*) or bridge (*b*) tends to weaken or break the metal–ligand bond. Rapid hopping or tunnelling of the muon between two asymmetric positions, (*b*), (*c*), would be indistinguishable from central localisation (*d*).

The fate of atomic muonium should also be considered here, as its formation and trapping is known in various non-magnetic oxides and halides (§ 4). An on-site moment is involved (as opposed to a transferred hyperfine interaction) if the muonium retains its atomic identity or is otherwise localised as a paramagnetic centre. The double μSR signal observed in antiferromagnetic $CoCl_2 \cdot 2H_2O$, for instance, has been tentatively attributed to muonium, rather than Mu^+ at inequivalent sites (Brewer *et al* 1981b). This suggestion is probably unfounded, however: applied to the other antiferromagnets where multiple signals are observed, this would necessitate a quite different interpretation of the muon sites and values of the internal field experienced. More probably, muonium is rapidly depolarised in magnetic materials. This could indeed explain the substantial 'missing fraction', i.e. the proportion of the initial muon polarisation that is unaccounted for in many magnetic materials. Symons (1984b) suggests that muonium will form a two-electron bond to the anion, with simultaneous transfer of the excess electron to the cation. Likewise direct bonding of muonium to the cation can be envisaged so it is impossible to make general predictions. Stoneham (1984b) has suggested that in MnO, for instance, muonium may be *generated* by electron transfer to the positive muon from the cation: $Mn^{2+} + \mu^+ \rightarrow Mn^{3+} + Mu$ (see also § 4.7). The local magnetic character would be profoundly changed in any of these situations where the valence state of the cation is altered.

3.1.5. Metal oxides. Selected examples of the internal-field measurements in antiferromagnetic oxides are sketched in figure 12. Multiple values of the zero-field μSR frequency are not uncommon at low temperatures and probably represent localisation of the muon at inequivalent sites in the unit cell, as mentioned above. Figure 12(*a*) shows the results for Fe_2O_3 (Ruegg *et al* 1979, 1981). The collapse to a single frequency at about 110 K appears to indicate the onset of some local motion of the muon, effectively

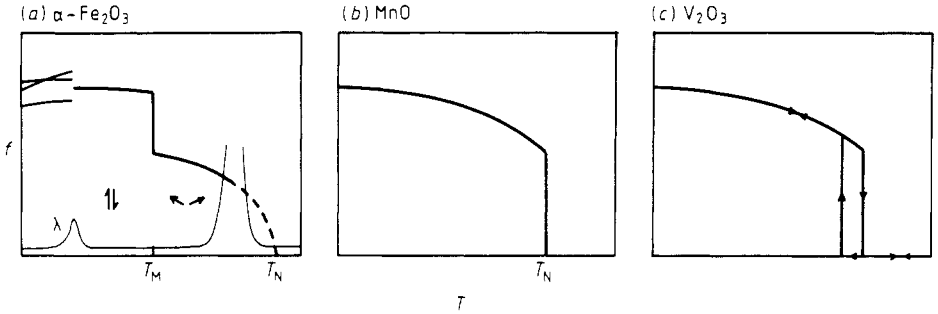

Figure 12. Internal-field measurements in the magnetic oxides. The zero-field μSR frequency f records the total field experienced by the interstitial muon. For Fe_2O_3 (*a*) it exhibits the following features (sketched from Ruegg *et al* 1981): (i) multiple values at low temperatures, indicating occupation of several muon sites; (ii) sensitivity to the change of the dipolar component at T_M; and (iii) peaks in the linewidth λ (fine line) suggesting the onset of local motion of the muon below T_M and long-range diffusion between T_M and T_N. For MnO (*b*) and V_2O_3 (*c*) the muon remains localised up to T_N (at least) so the collapse of the internal field can be monitored (sketched from Uemura *et al* 1984b); the discontinuity indicates a first-order transition associated with a lattice deformation (and for V_2O_3, which also shows some hysteresis, a metal–insulator transition). Apart from a split frequency at low temperatures, results for Cr_2O_3 resemble the simpler curve of figure 8(*a*) (Ruegg *et al* 1979).

averaging the different fields at the sites visited. This is readily envisaged for the situation depicted in figure 11(*c*)†.

The signal is lost altogether at the onset of long-range diffusion, at about 500 K; this is below T_N, so the collapse of sublattice magnetisation cannot be monitored in this material. The particularly striking feature of the results for Fe_2O_3, however, is the abrupt change of the μSR frequency at the Morin transition, $T_M = 250$ K. This demonstrates the sensitivity of an interstitial probe to the host spin structure (see also figure 13(*c*) and (*d*)). The dipolar component of the interstitial field drops by a factor of about 2 as the Fe spins reorient through 90° to the weakly ferromagnetic 'spin-flop' phase, although there is little change in the *magnitude* of the sublattice magnetisations at this point.

Similar features, namely multiple frequencies and changes with the spin structure, are found for various members of the rare-earth orthoferrite series, $REFeO_2$ (RE = Sm, Eu, Dy, Ho, Er, Yb) (Holzschuh *et al* 1983). The collapse to a single frequency coincides with the spin reorientation in $ErFeO_2$, but otherwise is taken to represent the conversion from metastable muon states (possibly delocalised) to single stable sites. The stable muon sites again suggest formation of hydroxyl-type bonds, although apparently with oxygen liganded to the rare-earth ions rather than with Fe, since no significant contact term is found in these materials. Conversion to a single stable site is also assumed in Cr_2O_3 (Ruegg *et al* 1981, Boekema *et al* 1981). The preferred site may in this case be impurity-related. The dominant μSR frequency can be followed right up to the Néel temperature in this material. Since there is no spin reorientation in Cr_2O_3, the measurements show a simpler temperature dependence, resembling that of figure 8(*a*).

Of the other magnetic oxides investigated, the behaviour of MnO and V_2O_3 is noteworthy, and is sketched for a comparison in figure 12(*b*), (*c*) (Uemura *et al* 1984b).

---

† This motion must be thermally activated, i.e. incoherent hopping. It is surprising that there is as yet no clear example of coherent local tunnelling of muons (as there is for protons, e.g. Wipf *et al* (1984); see also § 5).

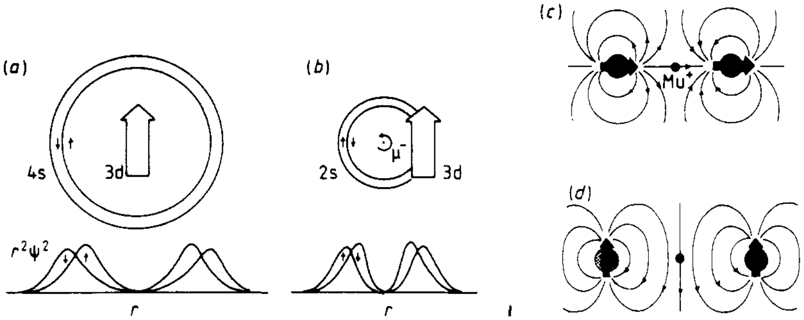

Figure 13. Hyperfine and dipolar fields. The distinction is made between the contact interaction with spin-polarised conduction electrons, and the distant-dipole interaction with remote localised moments. Exchange polaristion of the outer and inner electrons is depicted in (*a*) and (*b*). The large arrow represents the 3d moment. For the more distant outer (e.g. 4s) electrons, contraction of the lower-energy (parallel-spin) orbit and dilation of the higher-energy (antiparallel-spin) can lead to negative spin density at interstitial sites (*a*). (This is the intrinsic spin density, but a similar mechanism is envisaged for spin polarisation of the muon screening charge.) For the inner core (e.g. 2s) electrons, compression of the antiparallel-spin orbit leads to negative spin density close to the nucleus (*b*). This latter region may be probed by negative muons. Schematics indicating how the dipolar component of the total field experienced by an interstitial muon can be parallel and antiparallel to the host magnetisation are given in (*c*) and (*d*) respectively.

The zero-field μSR signal can in each case be followed right up to T_N. Here a lattice deformation accompanies and sharpens the magnetic phase transitions, resulting in a discontinuous collapse of the internal field. For MnO, which is insulating in both phases, a one-dimensional expansion of the lattice below T_N economises exchange energy. For V_2O_3, even some hysteresis is apparent (figure 12(*c*)). This material is remarkable in that the volume contraction of the lattice above T_N is sufficient for it to become conducting in the paramagnetic phase: the magnetic and structural phase transition is also a metal–insulator transition.

For both materials, the μSR results corroborate those of earlier neutron scattering and ESR expriments, but in particular give more precise and detailed information on sublattice magnetisation close to T_N. Current μSR measurements on V_2O_3 are concentrating on elucidating the electronic structure in the metallic phase (Chan *et al* 1985). Likewise in ferromagnetic Fe_3O_4, attention is now turning from the magnetic structure and Verweh transition (Boekema *et al* 1985) to a study of the valence fluctuations and the nature of the high-temperature conductivity, namely the polaron behaviour of the 'extra' 3d electrons that populate one sublattice of this material (Boekema *et al* 1986). Here the low-temperature magnetic and electronic structure may be depicted $Fe^{2+}\uparrow \cdot Fe^{3+}\uparrow \cdot Fe^{3+}\downarrow \cdot O_4$ (and so compared with the series of insulating spinel-structure ferrites $M^{2+}\uparrow \cdot [Fe^{3+}\uparrow \cdot Fe^{3+}\downarrow] \cdot O_4$). At high temperatures a hopping transfer of the extra electron leads to narrow-band semiconducting behaviour:

$$\overset{e^-}{\overleftrightarrow{\mathrm{Fe}^{2+}\uparrow\cdot\mathrm{Fe}}}{}^{3+}\uparrow\cdot\mathrm{Fe}^{3+}\downarrow\cdot\mathrm{O}_4.$$

3.1.6. Comments. Some general comments might be made on the above studies of non-conducting magnetic materials. It is important to test any relatively young technique on model materials in this way. The agreement with the results from established techniques in the region of overlap is gratifying; it allows confidence to be placed in those μSR results that are novel, or more precise, or that extend the range of measurements previously accessible. These competent demonstrations are for the most part some years old now, however, and it is curious that μSR is not currently being used more extensively to address topical questions in insulating magnetic systems, e.g. the nature of the phase diagram and transitions in metamagnets, or the effect of random fields introduced through dilution of the pure systems. (μSR should be a useful probe of short-range order here, although the departure from long-range order over length scales of many atomic spacings is more appropriately studied by neutron scattering.) Happily, a more prominent role for μSR in current research can be claimed in metallic magnetic materials, as described below.

3.2. Magnetic metals

3.2.1. Hyperfine fields. In insulating systems, the existence of a hyperfine field (in addition to the distant-dipole field from any localised moments) relies on the degree of covalency in the bonding of the muon, i.e. on the delocalisation of the magnetic electrons. In metallic systems, a hyperfine field representing direct contact with the conduction electrons is always expected. This contribution is a measure of the local spin density. A crucial question is how the intrinsic interstitial spin density is modified by the muon's presence. The formation of polaron states, described in § 5.2, indicates the considerable importance in metals of the effects of electronic screening of the muon charge, and of the local distortion of the lattice. Whereas μSR may report the intrinsic magnetic properties in many non-conducting sytems, there can certainly be no guarantee that this is also the case for metals. The contrary is more usually true.

Are the intrinsic properties necessarily the objective though, if these have been established by conventional methods? Is it not more interesting to ask what new information μSR can give? The history of studies of the ferromagnetic transition metals is instructive here and not untypical of the surprises and puzzles that μSR has revealed in many areas. It happens that measurements of the contact hyperfine field in Ni gave values of the interstitial spin density that were identical with those obtained by neutron scattering (Foy *et al* 1973, Patterson *et al* 1974). As they were also more precise, this was a noteworthy result. On reflection it is somewhat surprising, however. In common with other positively charged impurities in metals, the muon should attract a surplus of electrons to its vicinity, thereby reducing or 'screening' its long-range Coulomb field. The local electron density is expected to be enhanced by a substantial factor, about five for muons in Ni, yet there is apparently no corresponding enhancement of spin density, i.e. of the difference between the densities of spin-up and spin-down electrons, at least in this instance (Patterson and Falicov 1974). Measurements for Fe (Foy *et al* 1973, Gurevich *et al* 1974, Brewer *et al* 1975b) and for Co (Gurevich *et al* 1974, Graf *et al* 1976, Denison *et al* 1979) revealed enhancements of the intrinsic spin density approaching an order of magnitude, however. Considerable progress was required before these factors could be reproduced or modelled theoretically (Jena and Singwi 1978, Kanamori *et al* 1981, Meier 1981, 1984, Lindgren and Ellis 1982, 1984). This stimulus to screening theory has been a particularly valuable outcome of μSR studies in metallic systems.

Perhaps one should take the broader view here that the fundamental interest in magnetic phenomena lies in what can be learnt about the subtleties of electronic behaviour. No metal, magnetic or otherwise, can be said to be understood if its electronic response to this particularly elementary defect—the introduction of a test charge—cannot be modelled.

Interstitial spin density represents the exchange polarisation of the conduction electrons, by the mechanism illustrated in figure 13(*a*). For the transition metals Fe, Co and Ni it is admissible for these purposes to assume a polarisation of the 3d electrons and to consider the exchange interaction with s–p electrons as effectively attracting like spins, and repelling opposed spins. The outer valence electrons (those that are on average more distant from the nucleus than the 3d electrons), then have their orbits somewhat inflated if they have spin antiparallel to the 3d moment, and contracted for spin parallel. In consequence the spin density can change sign across the interstitial space, being positive closer to the atom cores, negative further away. (It is this intrinsic variation that is mapped, for instance, by neutron scattering experiments.)

A similar mechanism can be envisaged for spin polarisation of the muon screening charge. Substantial enhancements of the intrinsic spin density at the muon site result if the screening radius is short compared with the scale of variation of the instrinsic value. This is the case in Fe, where the enhancement factor is about 10, giving a hyperfine field sensed by the muon of -1.1 T; the screening charge can be thought of as mostly 'spin-down' electrons. The assumption here is that there is no on-site moment developed for muons in normal metals, but that the spatial variation of the conduction electron wavefunctions is different for spin parallel and antiparallel to the 3d moments. In certain circumstances the tails of the 3d wavefunctions may themselves overlap onto the muon site and make a direct contribution to the contact interaction. The situation in the absence of spontaneous ordering, but in the presence of an externally applied field, is considered in § 3.3.

3.2.2. Core polarisation. In parenthesis, just the opposite effect occurs in the polarisation of inner or core electrons. Here the orbit of like spins is dilated and that of unlike spins compressed, leading to negative spin density at the centre of the atom (figure 13(*b*)). This effect may be probed using *negative* muons since these, in their role as heavy electrons, occupy scaled-down electronic orbits very close to the atomic nucleus. Their μSR frequency is therefore a measure of the hyperfine field in this region. For an element of nuclear charge Z, the outer electrons see the $(\mu^- Z)$ nucleus as equivalent to $(Z - 1)$, so a comparison with NMR or Mössbauer measurements of the nuclear hyperfine interaction in the $(Z - 1)$ element is relevant. As a result of the core polarisation, the so-called hyperfine anomaly is much greater between Z and the muonic species $(\mu^- Z)$ than between Z and $(Z - 1)$. Results given by Baumeler *et al* (1984) and Imazato *et al* (1984) make this comparison between μ^-Ni (i.e. negative muons implanted in Ni) and **Ni**Co (i.e. Co as a dilute substituent in Ni). A similar 'giant' hyperfine anomaly can be expected between μ^-Fe and **Fe**Mn.

μSR studies using negative muons, and the related studies of the so-called exotic atoms are not otherwise mentioned in the present review. The interested reader is referred to Yamazaki (1984a), Yamazaki and Nagamine (1984b) and Horvàth and Lambrecht (1984).

3.2.3. Elemental ferromagnets: structural studies. Returning to the μ^+SR studies of the spontaneous internal fields, data for the transition metals Fe, Co and Ni and for the rare earths Gd and Dy demonstrate those aspects that are understood as well as details that are not. These are the familiar elemental ferromagnets (although Dy also has an antiferromagnetic phase). The emphasis of the studies varies according to the relative values of the dipolar and hyperfine components of the measured fields. A complication here is that the dipolar sums are not as 'well behaved' for ferromagnetic as for antiferromagnetic spin alignments. There are typically large corrections from surface integral terms, namely the Lorentz field (relating to the local or single-domain magnetisation and the demagnetising field (relating to the overall magnetisation, via a shape-dependent factor).

In Co, which exhibits a variety of magnetic and crysetallographic phases, it is the dipolar component that is responsible for the remarkable temperature dependence of the field experienced by implanted muons (Gurevich *et al* 1974, Denison *et al* 1979). The structure-dependent part actually changes sign in the narrow temperature range where the Co moments tilt at 90° from the *c* axis: a simplified schematic illustrating how this can occur is given in figure 13(*c*),(*d*). (This is the so-called spin-rotation—not to be confused with the precession of the muons! It is by no means as abrupt as the Morin transition in Fe_2O_3 (figure 12(*a*)) but the magnetisation, i.e. the magnitude of the Co moments, varies only slightly over this range.) Then at the temperature of the structural phase transition of the Co lattice from HCP to FCC, the dipolar sum vanishes at the muon site and the μSR frequency changes discontinuously by a factor of two. (By symmetry, the ferromagnetic dipolar sum is identically zero at all cubic sites in an FCC lattice.) The magnetisation, by comparison, jumps only 2% at this transition.

A similar strong temperature dependence of the magnetic anisotropy is found in Gd, and is reflected in the μSR data (Gurevich *et al* 1975, Graf *et al* 1977). Here it was possible to determine precisely the direction of easy magnetisation, corroborating evidence from other techniques on how this cants with respect to the crystallographic axes as a function of temperature.

The way in which different terms in the field experienced by the muon can be disentangled is explained by Denison *et al* (1979) and by Meier (1984). The extracted dipolar term may be used to determine the muon site (as in Co) or to check the spin structure (as in Gd). The extracted hyperfine field may then be compared with the magnetisation curve. The theoretical expectations for all the elemental ferromagnets are considered by Estreicher and Meier (1982). In Ni and in α-Fe, the hyperfine field is measured rather more directly since the structure-dependent dipolar field is in each case zero, though for different reasons (Gurevich *et al* 1974, Patterson *et al* 1974, Graf *et al* 1979). In Ni the lattice is FCC at all temperatures and the dipolar sum is therefore zero. In Fe the lattice is BCC, and the dipolar sums are not individually zero at the possible muon sites. Their mean value, weighted by equal occupation, is zero, however. They are therefore believed to be effectively averaged to zero by rapid movement of the muon, which is hopping from site to site. (Diffusion of this sort is facilitated in a BCC lattice—see § 5.) In both Ni and Fe, the hyperfine fields scale reasonably well with the magnetisation curve, but the correspondence is not one-to-one, as would be expected of a purely contact interaction. The proportional differences are in fact of opposite sign in Ni and in Fe, and rather greater in Ni, as is sketched in figure 14(*a*) (from Butz *et al* 1980). The temperature-dependent discrepancy relates partly to the imbalance of spin-up and spin-down populations, but is complicated by the effects of thermal expansion on the primary process of exchange polarisation. A separate study of the effects of hydrostatic pressure in principle allows the contribution from lattice dilation to be subtracted; again, qualitatively different behaviour is found in the two metals, as is sketched in figure 14(*b*). These are the raw data for the field experienced by the muon, however. The corrections to be applied for the Lorentz field are severe, with the results that the hyperfine field is found to decrease with increasing pressure in both metals (Butz

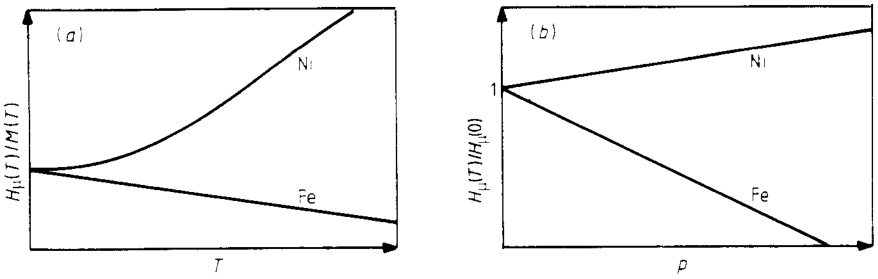

Figure 14. The dependence of the local field on (*a*) temperature (relative to the bulk magnetisation) and (*b*) pressure.

et al 1980). This must be due primarily to a decrease of the atomic moments: squeezing the lattice broadens the bands through increased overlap of the atomic orbitals; the 3d polarisation is therefore decreased by this reduction of the density of states. Exchange polarisation of the outer valence electrons and screening charge should be reduced in consequence. Quantitative understanding is claimed in the case of Ni (Katayama *et al* 1979). Calculations of hyperfine field revealing a delicate balance of opposing contributions from band-like states near the Fermi surface and bound states well below it have been performed for Fe, Ni and Co by Lindgren and Ellis (1984).

Such a discrepancy between hyperfine field and bulk magnetisation is not unique to μSR, but is a topical problem in the measurement of hyperfine fields by local probes, NMR and Mössbauer spectroscopy included. The effect seems to be particularly pronounced for μSR, however, and may relate to the large zero-point motion of the muon, which is 10–20% of a lattice spacing. Unlike the dipolar field, the hyperfine field depends crucially on the amplitude of the harmonic motion, especially for exchange interaction terms with an oscillatory range dependence (Estreicher and Meier 1982, 1984).

Further information is provided by the dependence of the internal fields on strain (Namkung *et al* 1984), by the alloying of Fe and Ni with other elements and by the observations of Mu^+ trapped at vacancies in electron-irradiated Fe (Weidinger 1984a).

3.2.4. Spin dynamics in metals. In the paramagnetic phase, can μSR probe the spin dynamics and critical behaviour as successfully in metallic as in insulating systems? Certainly it can, but a word of justification is in order here as it is generally taken for granted that there is no conduction electron contribution to the μSR linewidth.

This may be demonstrated using the elementary calculation of nuclear relaxation times in metals represented by equation (3.5) (Abragam 1961).

$$\frac{1}{T_1} \sim |\mathcal{H}_1|^2 \frac{\hbar}{E_\mathrm{F}} \frac{kT}{E_\mathrm{F}}. \tag{3.5}$$

For the purposes of the estimate, an upper limit to the strength of the muon–electron interaction may be taken as $|\mathcal{H}_1|^2 < \hbar^2 A_0^2$ with A_0 the muonium hyperfine constant. The factor $\hbar/E_\mathrm{F}$ represents the time for which a conduction electron may be localised in the vicinity of the muon. The perturbation is random and the correlation time short ($A_0\hbar/E_\mathrm{F} \ll 1$) so equation (3.5) applies equally to transverse and longitudinal relaxation; $1/T_2 = 1/T_1$. The factor kT/E_F represents the proportion of conduction electrons within the thermal shell around the Fermi energy E_F that are able to participate in the relaxation. For normal metals below liquid nitrogen temperatures the estimate gives a depolarisation rate not exceeding 10^3 Hz, which is typical of Korringa relaxation and negligible on the μSR timescale. (The case of semimetals, and the connection with the muonic Knight shift, are touched on in § 3.3.)

This absence of muon depolarisation by the conduction electrons is implicit throughout the discussion of muon localisation and diffusion in § 5, where the muon depolarisation rate is largely determined by the dipolar fields from the metallic nuclei (or interstitial protons). When localised atomic moments are present, these will dominate the μSR depolarisation rate or linewidth. As for the magnetic insulators, the correlation time τ_c that characterises the fluctuation of these moments may be readily extracted when (3.1) and (3.2) are satisfied. Measurements of the transverse relaxation rates in Ni, for example, for both the paramagnetic and ferromagnetic regions close to T_c, are given by Patterson *et al* (1974), and Nishiyama *et al* (1983).

In the hard magnets, the rare earths and their alloys, the quantity $\langle \delta H^2 \rangle$ in (3.1) is huge, so very short values of τ_c may be measured. With local dipolar fields in the range 0.1–1 T (resulting from the dominant orbital contribution to the magnetisation and generally much larger in these materials than the contact term), direct linewidth measurements (in the inverse microsecond range) allow determination of τ_c values in the range 10^{-12}–10^{-14} s. This is exactly the range expected for non-S-state rare-earth ions and it is not readily accessible by other techniques. μSR appears to be unique in opening up this particular time window. It bridges the gap between NMR on the one hand and perturbed angular correlation or neutron spin-echo techniques on the other (Kalvius *et al* 1985, Asch *et al* 1985). For the hard magnets, NMR is virtually useless for dynamical and critical studies. More generally, it will surely become commonplace for NMR and μSR to complement each other, μSR taking over the measurements when NMR lines broaden beyond detection. μSR will be especially valuable in this situation at high temperatures, where NMR is insensitive, being greatly disadvantaged by the Boltzmann factor (Curie's Law).

An interesting difference with the softer magnets and non-metals may be noted here: it is no longer a prerequisite for studies of the spin dynamics that the muon probe be stationary in the lattice. The μSR measurements in hard magnets are insensitive to muon mobility because the spin fluctuations are so much faster than any likely hopping rate. In fact the following inequality probably holds for the temperature range of interest (Kalvius 1985):

$$\tau_c \text{ (atomic moments)} < 10^{-12}\text{ s} < \text{muon jump time} < 10^{-6}\text{ s} < \tau_c \text{ (nuclear moments)}.$$

In this case any nuclear contribution to the depolarisation rate, already negligible compared with that of the atomic moments, is in fact averaged to zero.

The origin of the fluctuation of the atomic moments is different in different temperature regimes. At high temperatures it is the spin–phonon interaction, i.e. spin–lattice relaxation by Orbach or Raman processes. At intermediate temperatures it is spin exchange with the conduction electrons; this is Korringa relaxation (demonstrated above to be unimportant for the smaller moment of the muon probe). A comparatively weak temperature dependence of the μSR linewidth is expected to result from these mechanisms. In the critical region however, close to the transition temperature T_c, the origin of the fluctuation is the same spin–spin interaction between the rare-earth moments themselves that is responsible for the long-range order below T_c. A divergence of the μSR linewidth is then expected (as for the magnetic insulators, § 3.1) corresponding to the critical slowing down of these fluctuations, i.e. the onset of long-lived correlations (here ferromagnetic) between neighbouring spins.

A careful study of the whole series of rare-earth aluminides (REAl$_2$ with RE = Ce, Pr, Nd, Gd, Dy, Ho, Er and Tm) has revealed some surprising results, which are sketched in figure 15(*a*) (Asch *et al* 1983, 1985). These materials order ferromagnetically with values of T_c between 10 K (ErAl$_2$) and 160 K (GdAl$_2$). At high temperatures well above T_c (i.e. at room temperature, with the possible exception of GdAl$_2$) the μSR linewidths are consistent with the various expected contributions to the spin–lattice relaxations, notably the Korringa mechanism. A much stronger temperature dependence is found at lower temperatures, towards T_c, than can be attributed to any mechanism of spin–lattice relaxation, however. This must be associated with the magnetic transition: the extra depolarisation rate may be fitted to a power-law variation of the form $(T - T_c)^{-x}$ with exponents x of typically 0.6. The astonishing feature is that this apparently critical divergence sets in, for most members of the series, far above the respective Curie points. Thus in DyAl$_2$ the divergence begins as high as $5T_c$, in PrAl$_2$ and GdAl$_2$ at $3T_c$. This is to be compared with the 'critical region' which, conventionally at least, is confined to the range $(T - T_c)/T_c < 0.01$, i.e. to within a few degrees of T_c in these materials. The effect is not so pronounced for some other members, e.g. HoAl$_2$, so it is difficult to tell just how general the phenomenon is. It may be simply masked by Korringa relaxation in the members with weaker exchange. These provocative results are interpreted by Asch *et al* (1985) in terms of pairwise correlations between neighbouring rare-earth moments, the muon being suitably located in the lattice to be sensitive to these. Pair correlations are considered to set in at a higher temperature, and to show a less pronounced temperature dependence (i.e. a smaller exponent) than the many-body correlations whose critical slowing down is confined to the much narrower range.

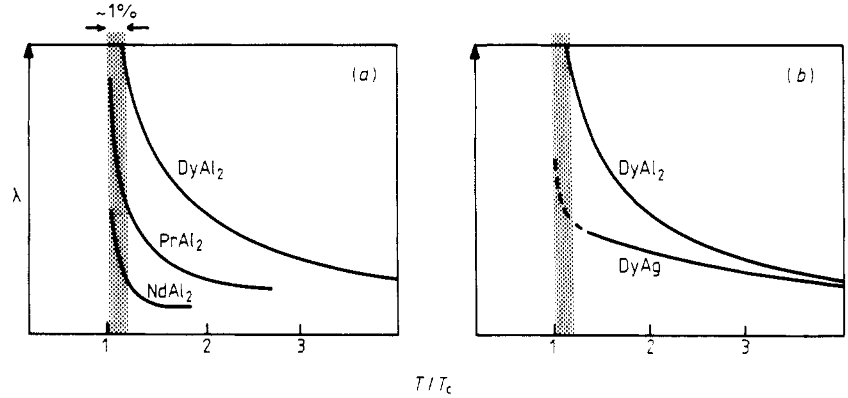

Figure 15. μSR linewidth measurements (absolute scale) in the paramagnetic phase (reduced temperature scale) for some rare-earth alloys. A divergence beginning well outside the conventional (shaded) critical region is shown for several members of the series REAl$_2$ in (*a*). In (*b*), the measurements are contrasted for DyAl$_2$ (which orders ferromagnetically at 64 K) and for crystalline DyAg (which orders antiferomagnetically at 60 K); similar values are found at room temperature, but DyAg shows only the weaker temperature dependence characteristic of spin–lattice relaxation (adapted from Asch *et al* 1984, 1985).

No such early onset of apparently critical behaviour is observed in the rare-earth material DyAg, which in its crystalline form orders antiferromagnetically (Asch *et al* 1984). These results are sketched for comparison in figure 15(*b*). The authors suggest that the sign of the exchange could therefore be important to the formation of spin correlations or that anisotropy or crystal-field effects play a major role. (It could perhaps be, however, that the muon site in this material is symmetrical, or nearly so, with respect to the antiferromagnetic sublattices, and therefore insensitive to antiferromagnetic fluctuations.) It is noteworthy that *amorphous* DyAg has also been studied by μSR in the paramagnetic phase, and the results compared with those from the crystalline version (Asch *et al* 1984). At room temperature the relaxation functions recorded in the amorphous and crystalline samples are not significantly different, implying that the mean square field distributions (and therefore also the nearest-neighbour distances, which dominate these) are largely similar. This is the first reported application of μSR to the study of an amorphous magnetic system. Preliminary results have also been obtained on amorphous DySi (Kalvius 1985). Here the relaxation function studied was actually that for longitudinal relaxation, recorded in zero field; this technique has been extensively employed in the study of dilute (but crystalline) magnetic alloys, notably the spin glasses. This is the subject of § 7, where these topics are presented as illustrations.

3.3. *Local electronic structure and screening*

The contact hyperfine field experienced by interstitial muons in the elemental ferromagnets generates characteristically high frequencies in their μSR spectra. It can be comparable in magnitude (although opposed in sign) to the molecular or Weiss field at the regular lattice sites, reflecting the extent of the exchange polarisation of the conduction electrons and screening charge. In the absence of magnetic ordering, however, i.e. in transition metals in the paramagnetic phase or in simple metals, electron spin density at the muon is induced only in the presence of an externally applied magnetic field. It then results in just a small proportional shift K_μ of the Larmor frequency from the value appropriate to a free muon. (Such shifts are well known in NMR for the host and impurity nuclei in metallic systems, and are known as Knight shifts: see for instance Abragam 1961.) Equivalently, the Zeeman energy $\gamma_\mu H I_z$ for a free muon becomes $(1 + K_\mu)\gamma_\mu H I_z$ in a metal, with the additional energy given by

$$K_\mu \gamma_\mu H I_z = (8\pi/3)\beta\gamma_\mu I_z(\rho_\uparrow - \rho_\downarrow). \tag{3.6}$$

The spin density at the muon is expressed in an obvious notation in (3.7) and, following Hintermann *et al* (1981), some insight into the contributing factors may be gained from a suitable rearrangement of terms, as in (3.8):

$$\rho_\uparrow - \rho_\downarrow = n_\uparrow |\psi_\uparrow|^2 - n_\downarrow |\psi_\downarrow|^2 \tag{3.7}$$

that is

$$\rho_\uparrow - \rho_\downarrow = \tfrac{1}{2}(n_\uparrow - n_\downarrow)(|\psi_\uparrow|^2 + |\psi_\downarrow|^2) + \tfrac{1}{2}(n_\uparrow + n_\downarrow(|\psi_\uparrow|^2 - |\psi_\downarrow|^2). \tag{3.8}$$

The first term in (3.8) need be evaluated only at the Fermi surface. In simple treatments only this term is retained, the possible difference between spin-up and spin-down wavefunctions being ignored. Knight shifts of the host-metal nuclei themselves represent predominantly 'direct' contact interactions of this sort: the difference in *occupation* of the spin-up and spin-down states, $n_\uparrow - n_\downarrow$, is directly proportional to H (via the spin susceptibility) so Knight shifts may be defined as in (3.6). With few exceptions, those for simple metals are (i) positive, (ii) isotropic and (iii) independent of field and temperature, reflecting as expected the Pauli spin susceptibility. Metal Knight shifts, and those of *substitutional* impurities, are typically of order 1%. Values for *interstitial* muons (or protons) in different metallic hosts are mostly two orders of magnitude smaller (only in a few instances exceeding 100 ppm). This factor may be thought of as representing the much smaller amplitude of the Bloch waves at interstitial sites relative to substitutional sites, and also the low atomic number, $Z = 1$, for the hydrogen isotopes, albeit partially compensated by the accumulation of conduction electron density at the muon or proton site and a corresponding local enhancement of the spin susceptibility.

The fundamental interest here lies in how electron charge density and spin density respond to the introduction of a unit test charge. The local accumulation of electron density about a charged impurity is readily calculated within the so-called 'jellium' model, namely for a free-electron gas moving in a uniform background potential. In the simplest semi-classical treatment it results in an exponential damping of the Coulomb potential, with excess charge effectively screened in a distance comparable with interatomic spacing. The absence of electronic wavefunctions with sufficiently small wavelengths to accomplish this actually results in oscillations in the electron density at large distances. (These are variously known as Friedel or Rudermann–Kittel oscillations. Ziman (1964) describes them as diffraction haloes from the scattered electron waves.) Unlike certain heavier ions, where the presence of core electrons can attenuate the effect, muons or protons create too great a disturbance to be represented by a simple adjustment in the population of conduction electron states (i.e. linearised screening). Self-consistent treatments are necessary, revealing changes in the electron wavefunctions themselves (i.e. non-linear screening; see Jena *et al* (1978), Estreicher and Meier (1983), Ellis and Lindgren (1984)). Except in metals with the highest electron densities, the local enhancement of spin density over the average polarisation does not scale with the enhancement of charge density. Figure 16 shows profiles of the enhancement of electron charge density and spin density (for an average electron density where differences are just beginning to show) adapted from a figure due to Jena (1979). Calculations that include a realistic lattice potential are more difficult again; these can

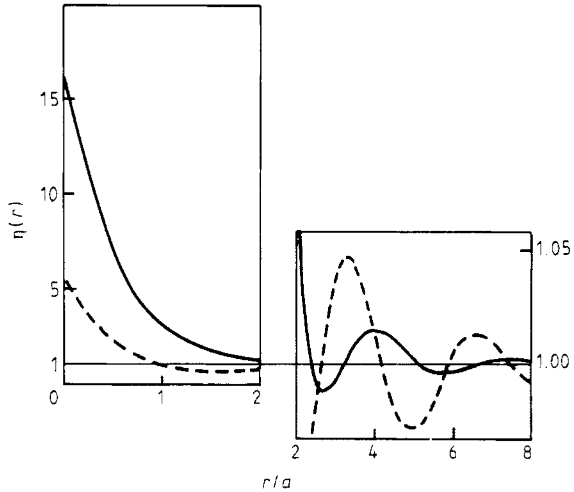

Figure 16. Profiles for the enhancement $\eta(r)$ of the electron charge density (full curve) and spin density (broken curve) in the vicinity of a positive muon (after Jena 1979). The vertical scale is expanded by a factor 100 to show the oscillatory behaviour at large distance. The spin density at the origin is enhanced to a lesser degree than the charge density, and the Friedel oscillations lag in phase by about $\pi/2$.

simulate the formation of muon–host bonding states, which may be regarded as an extreme example of non-linear screening.

Thus the second or 'indirect' term in equation (3.8) becomes important when polarisation of the host atoms leads to a field-dependent modification of the conduction electron wavefunctions (cf. figure 13) so spin-up and spin-down wavefunctions do not have the same spatial distribution. This second term must be averaged over states of all energies and therefore subsumes the effect of electrons well below the Fermi surface.

To these terms must be added contributions from diamagnetic screening, representing circulating loops of charge with no density at the muon. These are negative and in the simplest treatments merely reduce the effective spin susceptibility by about 30% (corresponding to the opposition of Pauli paramagnetism and Landau diamagnetism). Diamagnetic screening can be highly anisotropic if the participating electrons are constrained to move in particular orbitals, e.g. if they participate in chemical bonds. For diamagnetic muon states in insulators it will be the dominant term, of course, constituting a 'chemical shift' of the Larmor frequency. (Although potentially informative as to how muonium is covalently bound in the host mulecules, chemical shifts are not expected to exceed 10 ppm and have received no attention to date; see § 4.1.1.)

3.3.1. Muon Knight shifts. Systematic measurements of K_μ have been made for many metals across the Periodic Table, including virtually all non-transition metals, as well as for a variety of alloys and alloy hydrides. Except when the shifts K_μ are exceptionally large (see, e.g. Hartmann *et al* 1979) they are difficult to determine from the μSR precession signals as usually displayed. As is generally true for precision determinations of frequency and shifts of frequency, measurements obtained via the phase of the precession against a reference signal are preferable. Here it is the development of *stroboscopic* μSR that has permitted such an extensive and accurate survey (The technique exploits a favourable periodicity of the SIN† muon source; see Schenck (1976), Camani *et al* (1978), Klempt *et al* (1982).)

Compilations of the available values, and discussions in relation to the various theories of screening are given by Schenck (1982, 1985a). For an illustration of the systematics—and the apparent exceptions—some of the data for simple metals are reported in figure 17. Absolute values have proved difficult to ascribe, indicating the importance of comparable and competing contributions to K_μ. By the same token, however, these values should ultimately provide decisive tests of the detailed theories. It was apparent from the outset that calculations based on the simple jellium model were inadequate. These consistently overestimate K_μ and fail totally to reproduce the detailed systematics from metal to metal (the measurements showing no simple monotonic dependence on average electron density).

Simple jellium predictions are generally held to give an adequate description of purely electrostatic properties, e.g. the profile of the *charge* density cloud and its role in determining the muon site and motional behaviour (§ 5). Enhancement of the *spin* density, however, is evidently much more sensitive to details of the lattice potential.

Significant progress has been made in the 'spherical solid model', i.e. using an effective lattice potential that is spherically symmetric about the muon site (Manninen 1983). The direct conduction electron contribution to K_μ (the first term in (3.8)) is then smaller than in the simple jellium model and the indirect or core contribution (the second term, and negative) is larger, giving better estimates of absolute values. The distinctive

---

† Swiss Institute of Nuclear Research (Villigen, near Zürich).

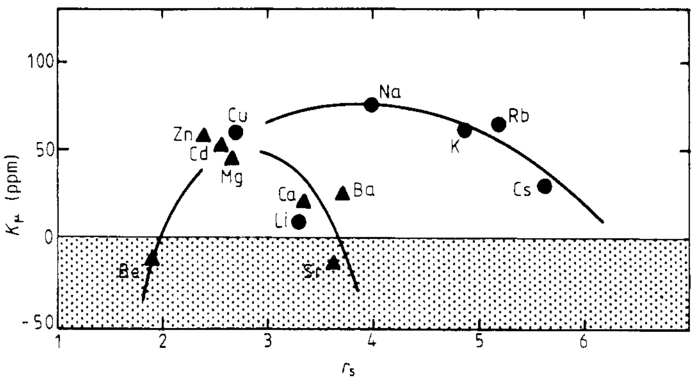

Figure 17. Muon Knight shifts for the monovalent (●) and divalent (▲) simple metals. The radius r_s of the free-electron sphere is used as a parameter of the conduction electron density and the curves are drawn to guide the eye (see, however, Manninen 1983).

dependence of K_μ on valence is also reproduced as is, to a certain extent the qualitative variation between metals of given valence. A feature that emerges from these calculations is that in divalent metals, where the lattice potential is stronger than in monovalent, K_μ is sensitive to the type of interstitial site that the muon occupies. This may provide a means of site identification in non-magnetic metals (compare § 5.1). A suitable normalisation of the data, yielding the induced hyperfine field *per atom*, removes the dependence on lattice structure and muon site. The logarithmic correlation of this quantity with the density of states at the Fermi level, established empirically (Schenck 1981, Gygax *et al* 1984b), is also reproduced by these calculations (Manninen 1983).

Certain data cannot be accommodated within this framework, however, even amongst the simple metals. Thus the particularly low value of K_μ for Li and the *negative* value for Be (see figure 17) imply that the nature and density of states at the Fermi level is not monitored in these measurements, but that core polarisation is dominant. (In this context, the term 'core polarisation' refers to the *host* atoms.) Here cluster calculations appear to be notably successful, although (for the purposes of calculating K_μ, at least) these have been performed only in relatively few instances (Keller and Schenck 1979, Castro *et al* 1979, Shillady and Jena 1984, Martin 1984). In a microscopic cluster the potential is determined by short-range interactions; the formation of muon–host bonding states (the extreme example of non-linear screening) and diamagnetic shielding are well modelled. The success of these calculations would seem to indicate that long-range disturbances (e.g. the Friedel oscillations, which can be accommodated in jellium-based models) are not relevant here. It is surprising that these microscopic first-principles models of the muon impurity have not been pursued for other hosts.

Another notable exception is Cd, where K_μ is anisotropic and highly dependent on the temperature. A consequence of the nearly full band is that K_μ is sensitive to the particular topography of the Fermi surface (which is dependent on temperature, via a lattice distortion) and actually reflects Van Hove singularities in the density of states. Here, and in various alloys of Cd, it is apparent that the interstitial muon monitors electronic properties that are inaccessible to substitutional probes (Studer *et al* 1984).

Although this latter example is exceptionally rich, there is a general possibility for the transition metals that electrons that have no contact interaction with the *host* nuclei may contribute directly to the *interstitial* hyperfine field. Thus d states at the Fermi level may contribute directly to the muon or proton Knight shifts (i.e. to the *local spin* susceptibility) via the extension of their wavefunction tails into the interstitial region or via their hybridisation in bonding states. For the transition metals especially, values of K_μ in principle offer tests of band-structure theory, although calculations have been performed in only a few instances (e.g. in ferromagnetic Ni; Katayama *et al* (1979)). The question may be raised here, however, of whether band-structure calculations are appropriate to a probe that destroys the periodicity of the lattice on which they are based. That is, whether the interstitial positive charge is too strong a scattering centre for Bloch waves to remain a useful basis (Schenck 1985b).

The use of K_μ simply to monitor electron susceptibility, especially as it varies with temperature in the neighbourhood of a phase transition, is noteworthy here. Thus its variation in paramagnetic Ni has been studied as the Curie point is approached from above (Schenck 1982, Nishiyama *et al* 1983). Likewise its variation across valence transitions has been studied in appropriate rare-earth alloys and intermetallic compounds (Wehr *et al* 1984). More recently, attention has turned to heavy-fermion systems, with the whole range of μSR techniques now being brought to bear in the hope of elucidating their extraordinary magnetic and electrical properties (Stewart 1984, Cooke *et al* 1985, Barth *et al* 1985). Here, for instance, a deviation has been found for certain alloys from the usual linear relationship between muon Knight shift and magnetic susceptibility; correlation with specific heat data proves informative about the heavy-electron band width (Heffner *et al* 1985).

3.3.2. Comparison with proton Knight shifts. Of course, muon and proton Knight shifts would be identical for the stationary particles located at identical interstitial sites. In fact the low solubility of hydrogen in many metals precludes such a systematic survey by proton magnetic resonance as has been achieved by μSR. An explicit comparison has been made for Va, Nb and Ta (Schenck 1982, 1985a). (Hydrogen is readily soluble in these metals; as a result they have attracted considerable attention in comparative studies of muon and proton behaviour, see also § 5.) A small isotope effect indicates that muons and protons scan their local environment somewhat differently, by virtue of their different zero-point energies.

Given that the effect is relatively small, muonium is an invaluable substitute for hydrogen for Knight shift measurements, greatly extending the range of metals that can be studied. The fundamental question of how the electron gas responds to a unit test charge then takes on a more practical bias: what becomes of a genuinely isolated hydrogen atom implanted in a metal? This is the starting point for the discussion of all problems relating to hydrogen in metals.

3.3.3. Antimony and the metals paradox. In an early measurement on the semimetal Sb (Hartmann *et al* 1979), a particularly large muon Knight shift—about 1%—was found. This value could be interpreted in terms of incipient muonium formation. It is instructive to pursue the description of a hydrogen-like centre literally. In the semimetals the electron density is low and the screening of the muon charge imperfect. When an electron encounters the impurity it can therefore be envisaged as caught in a hydrogen-like s state. Instead of the ensemble average (3.6), the hyperfine interaction with this single electron takes the form $hA\boldsymbol{I}\cdot\boldsymbol{S}$; that is, the muon sees a hyperfine field $\pm\pi A/\gamma_\mu$ according to whether the muon and electron spins are parallel or antiparallel. Suppose that this state has a characteristic duration τ_e, after which the electron flips, or is replaced by another of opposite spin orientation. Here an upper limit on A is $A_0 = 4.5$ GHz, the value for vacuum-state muonium. If the criterion $A\tau_e \ll 1$ is satisfied, the time average of this field results in a paramagnetic shift $A\langle S_z \rangle$ of the muon Larmor frequency, where the electron spin polarisation takes the value given by the appropriate Brillouin function. A temperature dependence suggestive of this behaviour (i.e. that of a localised paramagnetic centre) is found in Sb. The shift should diminish as the metallic character increases: the contact interaction A decreases as the atom dilates (due to improved screening of the muon's Coulomb potential); also the electronic polarisation tends to a smaller value for any given field and temperature (and in the limit of rapid exchange with the conduction electrons would take the temperature-independent value appropriate to Pauli paramagnetism as above). This is consistent with measurements in Sb as a function of hydrostatic pressure: the muonic 'Knight shift' decreases as the lattice is squeezed[†].

So huge a paramagnetic shift is unique to Sb, however. (No such value is observed even amongst the other semimetals: K_μ is fairly large but negative in Bi, for instance.) It is a nice paradox that the only materials in which muonium is *not* formed, in general, are metals. One could be forgiven for thinking that these were the very materials where electrons are most 'available', so the muon could most easily acquire one to form Mu $= \mu^+e^-$ (or two, to form the muonic hydride ion $\mathrm{Mu}^- = \mu^+e^-e^-$, although this latter would be again diamagnetic). Of course the above description of electrons hopping on and off a hydrogenic state in Sb disguises a conceptual difficulty here, namely that any such state (singly or doubly occupied) will always be degenerate, or 'resonant' with conduction band states in materials with zero band gap.

The facile solution to the paradox is that, for electron densities found in metals, the muon's Coulomb potential is reduced by screening to the extent that a bound state with any individual electrons is impossible. (The criterion for the existence of bound states within a Yukawa potential is given, for instance, by Stoneham 1985b.) Equivalently, the hydrogenic Bohr radius is not short compared with the screening length. Thus, within the jellium model, Estreicher and Meier (1983) find bound states to be excluded above a certain electron density (corresponding to a radius for the free-electron sphere of $r_s = 1.9$, approximately equivalent to Ba or Sr). The screening charge is then entirely due to scattered conduction electrons. At lower densities, states with 1s character condensed out of the conduction band in principle contribute a proportion of the screening charge (25% at $r_s = 2.07$ (e.g. Al), 80% at $r_s = 5$). These are so shallow, however (less than 1% of the free-hydrogen ionisation potential, for $1.9 < r_s < 6$) that lifetime broadening is likely to exceed their binding energy, so they are more properly regarded as resonant states (Jena and Singwi 1978). As Chappert and Karlsson (1983) put it, the muon 'flirts' with many electrons, but does not commit itself to a particular partner! The situation is different in semiconductors and insulators, where the muon potential cannot be screened by mobile charges, so localised or bound electron states may be anticipated. These evidently lie below the lowest 'free-electron' state; it is also likely that an extra electron will be accommodated in a higher energy level than the

---

[†] In parenthesis, the correlation time τ_e determines the *width* of the shifted μSR line; the fluctuating component $A(S_z(t) - \langle S_z \rangle) \simeq AS_z(t)$ causes a line broadening or depolarisation rate given by $\lambda = A^2\tau_e$. (Since $A\tau_e \ll 1$, this is the limit of rapid 'switching' between two frequencies: Abragam 1961.) This result, for a rapidly relaxing paramagnetic centre, may be compared with (3.5); it is significant that the extreme narrowing limit obtains, i.e. no conduction electron depolarisation is observed even in a material that exhibits such a large muon Knight shift. It has yet to be demonstrated whether materials can be found with a low enough carrier density for spin-flip scattering with the carriers to be detectable from a broadening of this 'diamagnetic' signal. In such a case μSR might be able to probe the metal–insulator transition (Catterall 1984). Spin-flip scattering has been invoked in doped semiconductors, to explain the broadening and loss of muonium precession signals as the concentration of electrically active impurities is increased (Albert *et al* 1984).

normal valence electrons, i.e. that localised states (or at least their singly occupied levels) lie in the energy gap between valence and conduction bands. The nature of the paramagnetic muonium centres in these materials, and the extent to which these have hydrogenic or molecular character, is the subject of the following section.

4. Muonium studies

As a unique analogue of hydrogen, muonium has a special place in atomic physics, in chemistry and in chemical physics. The principal concern of this section is with muonium in solids, but a brief mention of the other subjects is in order here.

Of importance in atomic physics are the precise values of the vacuum-state spectroscopic parameters such as hyperfine constant and Lamb shift. Since the muon is believed to be point-like, i.e. to have no spatial extent, the theoretical values of these parameters may be calculated without the corrections from nuclear size effects that complicate the same calculations in hydrogen (i.e. protium). The experimentally measured value of the ground-state hyperfine constant due to Casperson *et al* (1977) (see also figure 25 below) is

$$A_{\mathrm{Mu}} = 4.463\,302\,88(16)\ \mathrm{GHz}\ (0.04\ \mathrm{ppm}). \tag{4.1}$$

This extraordinary precision almost matches that of the theoretical calculations and therefore comes close to providing a significant test of conventional theory, or to identifying unconventional corrections (Hughes and Kinoshita 1977)†.

For this purpose, determination of the muonium Lamb shift is not yet sufficiently precise; probably the muonium $2P_{1/2}$ lifetime will always impose an unfavourable limit here. Measurements by Oram *et al* (1984) yield a result with an uncertainty of 1% and differing by two standard deviations from the theoretical value (see also Badertscher *et al* 1984). The Lamb-shift experiments are noteworthy, however, as a demonstration of muonium formation in the 2S state. This is achieved by a beam foil technique illustrated in figure 18: energetic muons strip and capture electrons in traversing a thin diaphragm, emerging as neutral muonium in the vacuum space beyond (see also Bolton *et al* 1981, Oram *et al* 1981, Fry *et al* 1984). Otherwise, e.g. for the ground-state measurements, there are other means of optimising the muonium yield (per incident muon) whilst still approximating the vacuum state. Thus muonium may be formed when muons are stopped in a gas; the free-atom state is then approximated at sufficiently low pressure. Likewise when muons are stopped in very finely divided quartz (and certain other oxide powders), a good yield of muonium is found in the space between the particles where again, subject to some interaction with the surface, the free state is approximated (Marshall *et al* 1978 Kiefl *et al* 1979, 1982). The key feature here is that the muon acquires its electron to form muonium via its interaction with matter, at some stage during the normal process by which it slows down and loses its initial kinetic energy.

Muonium formation was first observed in argon gas (Hughes *et al* 1960), and subsequently in a great variety of substances—gaseous, liquid and solid. Muonium is by no means formed in every material, however (or if formed, does not necessarily

---

† Neither these bound-state muonium measurements, nor the earlier high-precision measurements of the muon's static properties such as magnetic moment or gyromagnetic ratio, give any indication that there is any fundamental difference other than mass between the muon and the electron (Wu and Hughes 1977).

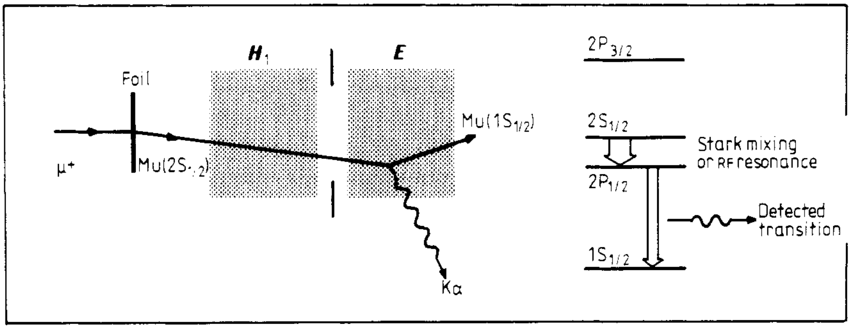

Figure 18. Observation of excited states of muonium, and measurement of the Lamb shift. A small proportion of the muonium atoms formed in the foil emerge from it in the excited state $2S_{1/2}$. This is metastable, the direct transition $2S_{1/2} \rightarrow 1S_{1/2}$ being forbidden. Partial conversion $2S_{1/2} \rightarrow 2P_{1/2}$ by a strong electric field $\boldsymbol{E}$ in the flight zone allows observation of the Lyman-α optical transition $2P_{1/2} \rightarrow 1S_{1/2}$ (Oram *et al* 1981, Fry *et al* 1984). A resonant decrease of the photon count rate is observed when the Lamb shift transition is driven by an RF field $\boldsymbol{H}_1$ (Oram *et al* 1984, Badertscher *et al* 1984).

remain stable on the μSR timescale). This is already apparent from § 3: the metals paradox has been noted above (§ 3.3), and also the absence of clear evidence to date for muonium in magnetic insulators, where the cations have partially filled 3d or 4f shells (§§ 3.1 and 3.2). The questions currently being addressed are therefore as follows:

(i) In what materials is muonium formed? What are the criteria for its formation or otherwise?

(ii) What is the subsequent chemical behaviour, i.e. the reactivity of muonium towards particular molecules?

(iii) What is the influence of the host medium on the muon–electron hyperfine coupling, i.e. on the spin density at the muon?

If a chemical reaction is rapid, and the reaction product is itself paramagnetic, these last two questions are clearly inseparable. This is commonly the case in solids. The word 'prompt' is used here to describe processes that ocur within the timescale for thermalisation of the incoming muons.

Much of the early literature is in fact preoccupied with the precise mechanism of formation of muonium and other muonic species—in particular whether this occurs promptly at epithermal energies or as a result of thermal or near-thermal reactions of the radiolysis products (see, e.g., Percival *et al* 1978, Fleming *et al* 1979, Percival 1979, Walker 1983). In liquids, the bulk of the evidence tends to favour this latter view though there are still a number of open questions (Roduner 1986a, Cox and Symons 1986a, Percival and Mogensen 1986). A remarkable feature of μSR spectroscopy, of especial interest in radiation physics and chemistry, is its ability to single out the ionising particle for observation, and to determine its final chemical state. It shares this distinction with positronium chemistry, which is also able to study radiolytic end-of-track processes. The muon creates a concentration of charged and paramagnetic species around its terminal track, principally by electron ejection, and neither the muon itself nor muonium (if formed) necessarily escape this region without chemical or magnetic interaction with these species. In non-metallic solids there is also the question of whether radiation damage to the lattice, namely point defects, plays any role in the trapping of muonium (see §§ 4.3, 4.7).

The major importance of muoniumin chemistry is that it may be considered a genuine light isotope of hydrogen. Here it may be contrasted with positronium, which has no central nucleus and only half the binding energy of hydrogen. Muonium has essentially the same Bohr radius and ionisation potential as the familiar hydrogen isotopes (the reduced mass differing from that of protium by about 2% only). Together with deuterium and tritium, therefore, muonium extends the available isotopic mass ratio from 3 to about 27, a range that is unique in chemistry and chemical physics. The interpretation of isotope effects is therefore of especial interest. Section 6 describes such effects in the studies of molecular dynamics, in molecules where a hydrogen atom is replaced by muonium. The effects are appreciably greater than those obtained by deuteration or tritiation of the molecules, which is the more familiar isotopic substitution; their interpretation is correspondingly more certain.

Huge 'normal' and 'inverse' isotope effects are found in comparisons of the reactivities of muonium and atomic hydrogen. (Here 'normal' means an *increase* in rate constant, although the purely kinetic factor expected is only $(m_H/m_{Mu})^{1/2} \sim 3$, the mean thermal velocity and collision frequency of muonium being greater by this factor.) In the liquid (or gaseous) phase there is often the possibility of adjusting the muonium reaction rate by the addition of inert diluent (and also by varying the temperature) so that it falls into the inverse microsecond range where it may be measured directly. Thus muonium is formed, and remains stable on the μSR timescale, in pure water and in a variety of saturated hydrocarbon solvents. From the reduction of its lifetime with suitable concentrations of reactive solute, as in figure 5, rate constants for muonium reactions are readily determined. Certain reactions are greatly enhanced, others virtually suppressed, as summarised in figure 19 (Garner *et al* 1978, Roduner and Fischer 1979, Ng *et al* 1981). A record enhancement factor approaching 10^5 is reported in one instance (Roduner and Munger 1984). (The equally surprising absence of an isotope effect has been noted for some reactions that are diffusion-controlled, i.e. that proceed at every collision (Ng *et al* 1981). This is noteworthy in that it suggests that a large cluster of solvent molecules, or a void, accompanies the reactive atom in its diffusion.)

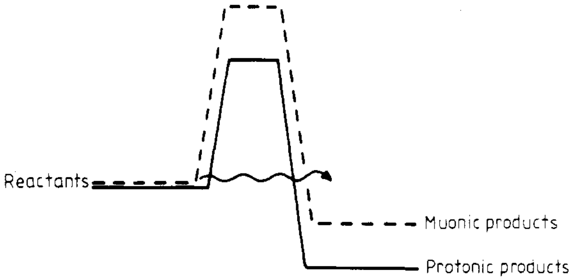

Figure 19. A schematic energy level diagram for the reactants and products in a chemical reaction together with the intervening barrier (or transition state). Muonium is better able to tunnel through the barrier than heavier hydrogen, and certain reaction rates are much enhanced at low temperature for this reason. On the other hand the zero-point energy for muonium bound in the product molecule is greater than for hydrogen in the same position. Muonium reactions can be correspondingly less exothermic, or even endothermic; these latter are virtually suppressed.

Muonium chemistry is reviewed, for instance, by Fleming *et al* (1979), Percival (1979) and Webster (1984), and in a monograph on this subject by Walker (1983). Chemical physics aspects, and the use of 'muonium labelling' of larger molecules (notably organic radicals), are touched on in § 6.

4.1. *Muonium spectroscopy*

In materials where muonium *is* formed, then, how can its formation and existence be recognised? And what can be told of its physical and chemical properties in different materials? In condensed phases one is concerned with muonium in its electronic ground state, and it is by its magnetic properties—by the Zeeman effect—that it is recognised.

The Breit–Rabi diagram, figure 20, is invaluable in the interpretation of all μSR studies of muonium, and of its related paramagnetic centres. Conceived for atomic hydrogen, it shows the energy levels for a system of two spin-$\frac{1}{2}$ particles (electron spin $S = \frac{1}{2}$, muon spin $I = \frac{1}{2}$) as a function of magnetic field, and in this version allows for an isotropic hyperfine interaction $A\boldsymbol{I} \cdot \boldsymbol{S}$ between the two (compare figures 24 and 45, below). At sufficiently low fields, the muon–electron hyperfine interaction is dominant. It is symmetric in the electron and muon spins (i.e. the scalar product term is unable to distinguish electron and muon) so the eigen-states must be symmetric and anti-symmetric combinations. They group into a singlet and a triplet, separated in zero field by an energy splitting equal (in frequency units) to the hyperfine constant A itself. Here total spin ($F = 1$) is the good quantum number. The electron Zeeman energy

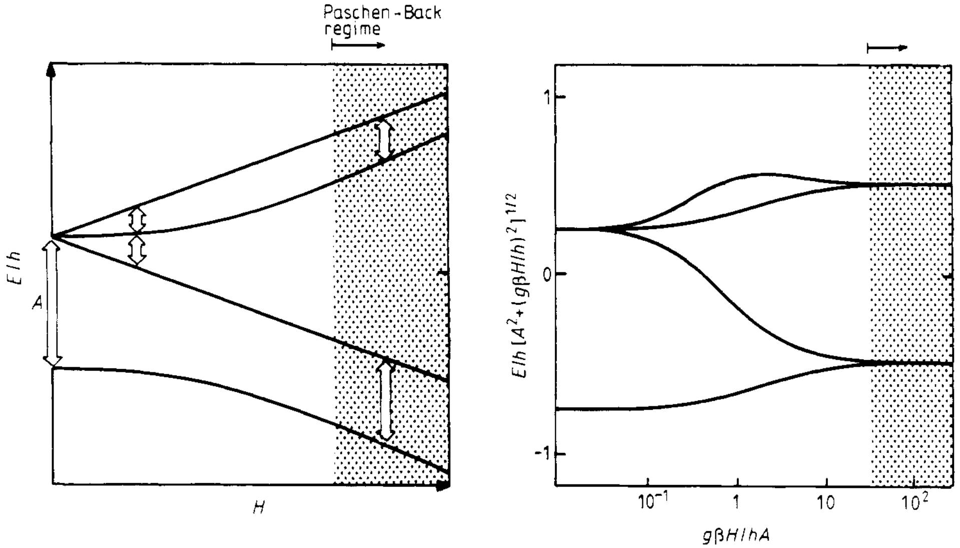

Figure 20. The Breit–Rabi diagram for muonium. In its conventional form (*a*) the μSR transitions discussed in this section, namely in the zero-, 'low'- and 'high'-field regimes, are indicated. The diagram also applies to muonated radicals in the liquid phase and to muonium centres in solids where the muon–electron hyperfine constant A is isotropic and no other dipolar nuclei are involved. In the version drawn in (*b*), the normalised scales emphasise the decoupling of electron and muon spins in the high-field (Paschen–Back) regime (see, e.g., Poole and Farach 1985); this is reached for muonium above ~2 T, and for organic radicals typically above 0.3 T.

dominates the muon Zeeman energy by a factor of about 200 (the ratio of their magnetic moments) at all fields. When it also dominates the hyperfine interaction, i.e. at sufficiently high fields, $g\beta H/h \gg A$, the muon and electron spins are decoupled and the quantum numbers m_S, m_I are appropriate. Figure 20(*b*) emphasises how this 'high field' or Paschen–Back regime is reached at lower fields for the muonic radicals and other centres than for muonium itself.

Between these four levels, all transitions that would be observable in a conventional magnetic resonance experiment (all transitions that constitute a 'flip' of the muon spin) are also permitted in μSR. This is evident for the genuine *resonance* experiments (some examples of which figure in § 8). It is equally true for the more usual *rotation* experiments in which the μSR signal appears spontaneously without being induced by an RF field. This is because the muons are implanted in a non-stationary state, which is a coherent superposition of spin-up and spin-down components. Each and every state that contains one of these components is subsequently occupied, therefore, with a probability that oscillates sinusoidally in the usual fashion. As for the polarisation of the ensemble (whether it be a simple spatial average, as would be the case for a burst of muons implanted all together, or an ensemble average taken with regard to the separate arrival times of muons implanted one-by-one, as is the case for a continuous beam), its behaviour is equivalent to precession or oscillation at the corresponding frequencies.

4.1.1. Low magnetic fields: muonium fraction, diamagnetic and missing fractions. The μSR precession signals most readily observed correspond to transitions within the triplet. At very low fields, typically ~1 mT, the two possible transitions have identical frequencies and a single-component precession signal is observed. It is by means of this signal (called in the literature the 'triplet precession'), that muonium was first directly identified (Hughes *et al* 1960), and the bulk of subsequent muonium searches performed. (In fact its existence had previously been inferred from other measurements: see § 7.2.) Figure 21 illustrates the features to be expected. Note that only half the initial muon polarisation is visible—there is a 50% chance that the muonium atom will be formed in eigen-states that do not participate in these transitions (referred to

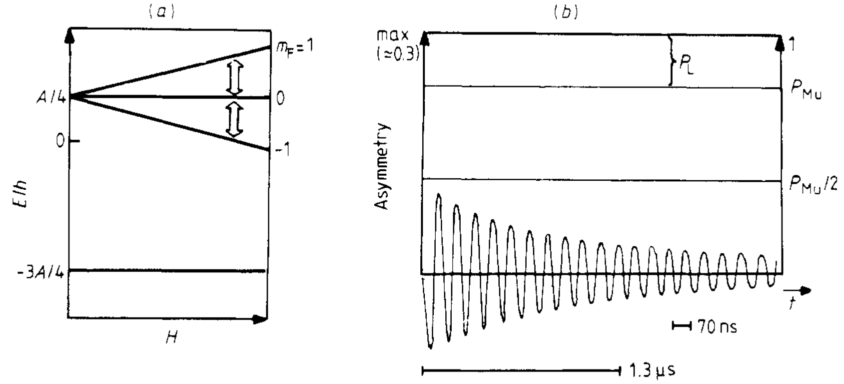

Figure 21. Low-field triplet transitions (*a*) and parameters of the precession signal (*b*). Values are typical of muonium in crystalline and amorphous silica at 1 mT and room temperature. Transitions between the singlet state and the triplet ($m_F = \pm 1$) states in principle contribute components of much higher frequency, which are not normally visible.

in the literature rather improperly as 'singlet muonium'). The vector addition of the muon and electron spins, and the consequent evolution of polarisation, has been treated rigorously by Brewer *et al* (1975a).

These features may be illustrated in gases, solids and liquids with the following few examples. Gaseous Kr and Xe, for instance, show the maximum possible asymmetry, i.e. all the incident muons form atoms of muonium (above about 2 atm pressure). This is exceptional and relates to the mechanism of muonium formation that is effective here, namely charge exchange: the ionisation potential of these gases is less than that of hydrogen so the incident muons readily strip electrons from the host. (It is equally noteworthy that *no* muonium is formed in He, which has a considerably greater ionisation potential.) Muonium yields in the other rare gases (and various molecular vapours) are reported and interpreted by Fleming *et al* (1982, 1984). In silica, the triplet precession signal is also easily visible. For a solid, this material shows a particularly high proportion of the maximum possible asymmetry in both its crystalline and amorphous forms, as though about 65% of the incident muons formed atoms of muonium. (Quartz was in fact the first solid in which long-lived muonium was detected (Myasischeva *et al* 1967).) This 'muonium fraction' is denoted P_{Mu}. In water, the corresponding fraction is $P_{\mathrm{Mu}} = 20\%$ only. (Water was the first liquid in which long-lived muonium was detected (Percival *et al* 1976).) Here a much larger proportion, about 60%, of the incoming muons are observed to process at a frequency that is indistinguishable from the muon Larmor frequency appropriate to the applied field. These muons must be in a state or environment that is locally diamagnetic, and this proportion is called the diamagnetic fraction, denoted P_{D}. A diamagnetic signal is observed in most materials. In water, for instance, a probable sequence of events is the following (Percival 1979, Percival *et al* 1978):

$$\mu^+ + \mathrm{H_2O} \rightarrow \mathrm{MuOH_2^+} \tag{4.2}$$

$$\mathrm{MuOH_2^+} + \mathrm{H_2O} \rightleftharpoons \mathrm{MuOH} + \mathrm{H_3O^+}. \tag{4.3}$$

The muon–proton exchange (4.3) is reversible (and extremely rapid) but the statistically overwhelming probability is that the muon remains in the stable, neutral species MuOH, a species that might be called 'light water'. Muons that are stabilised as in (4.2) may still form muonium by accepting *excess* electrons (e.g. those generated radiolytically, and which themselves may be wholly or partially solvated). They are unable to *extract* electrons from the host molecules, however, i.e. to form muonium via cold charge exchange, since the difference in ionisation potentials between muonium and most solvents does not exceed the muon solvation energy.

Unfortunately the diamagnetic fraction cannot be directly identified. A contrast may be made here with high-resolution proton NMR where the chemical shift is usually an unambiguous signature of the position of hydrogen within a molecule, i.e. of its immediate chemical environment. No such shifts have yet been measured for diamagnetic muons in non-metals, although this may prove possible using resonance techniques in a suitably high field (see § 8.3). In the case where more than one diamagnetic species is present, however, the muon radioactive lifetime will undoubtedly preclude the resolution of their separate chemical shifts. 'High-resolution μSR' cannot be envisaged. Here recourse to the different relaxation rates of the various species has been shown to be of some use (Newman *et al* 1985).

An interesting possibility, in situations where quadrupolar nuclei are adjacent to the muon, is that the diamagnetic species may be identified from characteristic quadrupolar splittings, measured via level crossing resonance (see § 7).

The muonium signal and the diamagnetic signal have quite different characteristic frequencies: there are just two orders of magnitude between them. The triplet precession corresponds to transitions of the total spin with a frequency characteristic of ESR (14 MHz mT^{-1}, which is just half the value for transitions of free-electron spins alone); the diamagnetic signal corresponds to transitions of the muon spins alone, with a frequency characteristic of NMR (140 kHz mT^{-1}, which is about three times that for protons). When both fractions are present, the two signals appear superimposed, with the somewhat curious result illustrated in figure 22. Very often a fraction of the incoming muons—or rather of their initial polarisation—is lost. That is, the sum of the intensities of the muonium triplet signal and the diamagnetic signal is less than is expected, knowing the initial beam polarisation. In water, for instance, some 20% of the initial polarisation is unaccounted for. Known in the literature as the 'missing' or 'lost' fraction, $P_L = 1 - (P_{Mu} + P_D)$, this has been a long-standing puzzle and the source of considerable conjecture.

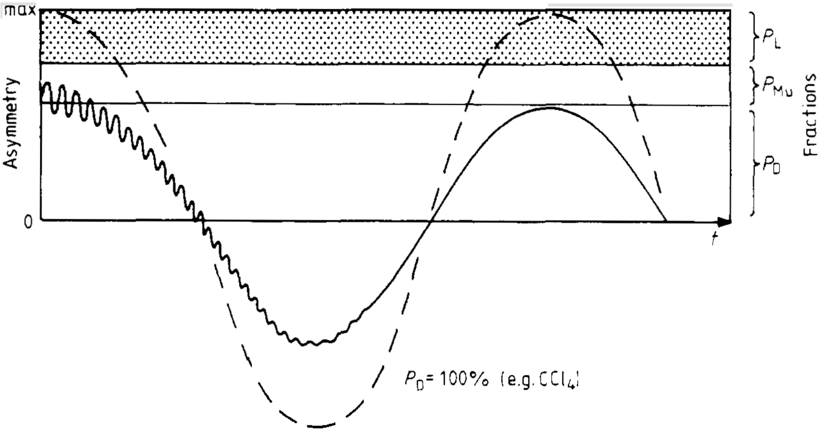

Figure 22. A sketch of the appearance of muonium and diamagnetic precession signals superimposed (cf figure 5) and the measurement of the corresponding fractions. Materials such as graphite, carbon tetrachloride and most simple metals show maximum asymmetry of the diamagnetic signal and are commonly used for calibration.

The missing fraction is now generally thought to correspond to muonium which is depolarised by spin-flip encounters with other paramagnetic species generated radiolytically. The real muonium yield is in this hypothesis $P_{Mu} + P_L$, with P_{Mu} the proportion that escapes encounter. This has been demonstrated for water (Percival *et al* 1982, Miyake *et al* 1984) and is probably usually so. In the materials mentioned so far, thermal muonium is stable on the μSR timescale. Otherwise, in substances or solutions where it reacts chemically, polarisation is also lost when the reactions are not sufficiently fast to ensure its coherent transfer from precursor to product (Percival and Fischer 1976). Precession signals from precursor and product are rarely simultaneously visible in μSR spectra for this reason, though the time evolution of the muon state may in principle be analysed via resonance techniques (§ 8).

4.1.2. Intermediate fields: measurement of the hyperfine constant. As the applied field is increased, the curvature of the central level of the triplet takes its effect and the

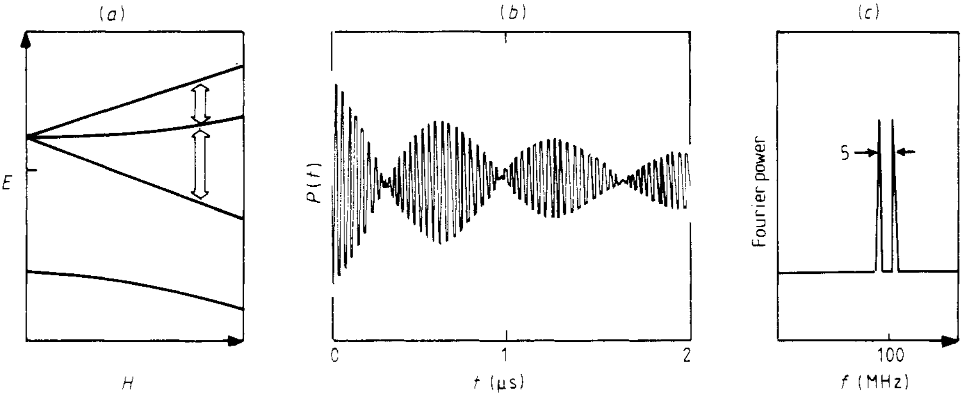

Figure 23. Intermediate-field triplet transitions, differing slightly in frequency (*a*), together with the corresponding (simulated) precession signal (*b*) and frequency spectrum (*c*). Values are typical for muonium in quartz at 7 mT. More generally, the separation of the two frequencies is equal to $(g\beta H + \gamma_\mu H)^2/2A$ (i.e. is quadratic in the applied field and increases for muon–electron couplings that are smaller than the free muonium value). (See for instance Gurevich *et al* 1971.)

two transitions within the triplet begin to differ in frequency (figure 23(*a*), (*c*)). As long as the difference is less than the linewidth it is not resolved, but can have misleading consequences for the measurement of the intrinsic or underlying linewidth if it is not allowed for. It has been suggested that the dephasing between the two components of the signal was actually mistaken for a genuine relaxation or depolarisation of muonium in some early experiments. Certainly recent measurements by a pulsed μSR technique, which permits the use of very low applied fields, give a lifetime of muonium in water in excess of 20 μs, which is much larger than was indicated by measurements using continuous beams (Magamine *et al* 1982).

In intermediate fields, this dephasing becomes a recognisable beating in the precession signal, simulated in figure 23(*b*). A corresponding splitting of the μSR line is resolvable in the Fourier transform spectrum, as in figure 23(*c*).

This splitting is quadratic in the applied field, and depends on the hyperfine constant, which can therefore be determined. In quartz, which is a particularly inert medium with large interstititional cavities, the hyperfine constant is close to its vacuum-state value (4.1): $A \simeq 4.5$ GHz (Gurevich *et al* 1971). Detailed studies in fact reveal a discrepancy of a few ppm, as well as a similar degree of anisotropy, so the interaction with the lattice is not entirely negligible (Brewer *et al* 1979, 1981a, c, Holzschuh *et al* 1982). It is also apparent that muonium is mobile in the lattice above about 75 K (Brewer 1981) and it is fascinating that muonium is evidently ejected from the lattice when it reaches the surface of sufficiently fine grains of SiO_2. Similar behaviour is found in Al_2O_3 and MgO (Kiefl *et al* 1979). (The resultant high yield of nearly vacuum-state muonium has been exploited here in an experiment to set an upper limit on the muonium–anti-muonium conversion rate (Marshall *et al* 1982).) Studies of muonium on the *surface* of SiO_2 powder are likewise noteworthy and yield information on diffusion rates and surface trapping (Kiefl *et al* 1982, 1984, Harshman et al 1984).

In other bulk materials, substantial deviations from the free-atom hyperfine constant are found. There was already an indication from longitudinal-field measurements (see § 7) of some form of muonium with a low hyperfine coupling in Ge and Si, for example (Feher *et al* 1960), and this was confirmed by observation of the triplet precession signal. Isotropic coupling constants of about 50% of the free-muonium value were measured in Ge (Gurevich *et al* 1971), the precise value being revised somewhat by Holzschuh *et al* (1979), and in Si (Brewer *et al* 1973). Completing the series of group IV elements with the diamond-type lattice, a value of 83%was found for diamond itself (Holzschuh *et al* 1982). (No muonium is seen in α-Sn, which is presumably too conductive.) These low values indicate a considerable interaction with the host lattice, yet the muonium is still mobile (Holzschuh 1983, Barsov *et al* 1984). For Si, these studies have been pursued down to dilution-refrigerator temperature (Bucci *et al* 1981).

Other surprises were in store. The direct spectroscopic studies revealed the presence of additional frequencies in the μSR spectrum of Si (Brewer *et al* 1973). These represent the coexistence of a muonium centre with surprisingly weak anisotropic muon–electron coupling. Subsequently identified in Ge (Holzschuh *et al* 1979) and in diamond (Holzschuh *et al* 1982), this state has no known hydrogen analogue and has become known in the literature as 'anomalous muonium' or Mu* (pronounced mu-star). By default, the isotropic centre has become known as 'normal muonium', although a different nomenclature is introduced in § 4.3 below to distinguish these defect centres from the free atom. The nature of the various centres, isotropic and anisotropic, and the factors that determine the spin density at the muon, are the subject of §§ 4.4–4.6 below.

4.1.3. Zero field: direct measurement of the hyperfine constant. The study of the influence of the host medium prompted the need for a more precise measurement of hyperfine constant than is possible by this 'two-frequencies' method. A direct measurement is in principle provided by the zero-field transition between singlet and triplet states (figure 20). Called by Patterson (1984a) the 'heart-beat' signal, this has a frequency in the GHz range, which is technically much harder to detect than the triplet precession. Most 'conventional' μSR spectrometers have a pass-band of about 500 MHz, limited about equally by alternative light paths inside the scintillators and lightguides, by the photomultiplier response, and by jitter in the subsequent electronics. A much improved timing resolution is therefore required both of the particle detectors themselves, and of the data-acquisition electronics. Such a spectrometer has been developed for this purpose (Holzschuh *et al* 1982, Holzschuh 1983), and used to detect the heart-beat signal firstly in germanium and subsequently in a variety of other materials. In quartz itself, the hyperfine constant has been determined directly in this manner to a precision of 10 ppm, which is a remarkable achievement, and in germanium, sufficiently precise measurements can be made to follow the small proportional variation with pressure or temperature. This variation may then be confronted with, for instance, the prediction of a Debye model (Holzschuh 1983).

4.1.4. High field: decoupling of electron and muon (and other nuclear) spins. The absence of a triplet muonium signal in low or intermediate fields is not an unambiguous result; it does not necessarily imply that muonium is not present. Of course if the diamagnetic fraction is 100%, as is the case in liquid CCl_4 or graphite, for example (both commonly used as standards of asymmetry for calibration purposes as illustrated in figure 22), and in most metals, the diagnosis is clear: either muonium is not formed, or it reacts promptly to give diamagnetic products. The question is whether any missing fraction can be attributed to muonium. Depolarisation by radiolysis products is mentioned above (paramagnetic impurities are likewise effective); in the following the intrinsic interaction with the host medium is considered.

The triplet muonium frequency is 1.4 MHz^{-1} G, so field inhomogeneities of a few gauss or more are sufficient to broaden the triplet precession signal beyond detection. In the presence of dipolar nuclei, therefore, with local fields of this order, muonium is only seen if the field distribution is motionally narrowed, e.g. by rapid tumbling of the host molecules (as in water and hydrocarbon solvents) or by rapid diffusion of the muonium (as in ice). It is no coincidence that silicon, germanium and diamond have received so much attention; the abundant isotopes of these elements have no nuclear spin. The various metal oxides and other materials in which the triplet muonium signal has been sought have likewise been carefully chosen (Spencer *et al* 1984).

In a molecular radical, hyperfine coupling of the unpaired electron to dipolar nuclei other than the muon itself broadens the μSR lines or splits them into many components, rendering them invisible in the regimes of low and intermediate field. Thus in the organic radicals described in § 6 the μSR lines cannot usually be detected below about 0.1 T due to proton multiplicity. This is a problem of resolution and statistics (i.e. signal-to-noise ratio) and is not avoided in liquid samples. The situation is illustrated later, in figure 45, for a radical (or muonium centre) with hyperfine coupling to one other spin-$\frac{1}{2}$ nucleus (i.e. total spin $F = \frac{3}{2}$; Roduner 1979); the increasing complexity of the Breit–Rabi diagram as more nuclei are added can readily be imagined (see e.g. Poole and Farach 1985). For muonium centres in crystalline solids, delocalisation of spin density onto the surrounding atoms (possibly over successive shells: nearest neighbours, next-nearest neighbours etc) has the corresponding effect. This is variously known as the superhyperfine interaction, covalent super-transfer etc.

In sufficiently high fields, i.e. in the Paschen–Back regime, the muon and other nuclear spins are effectively decoupled from the electron spin. In the simple Breit–

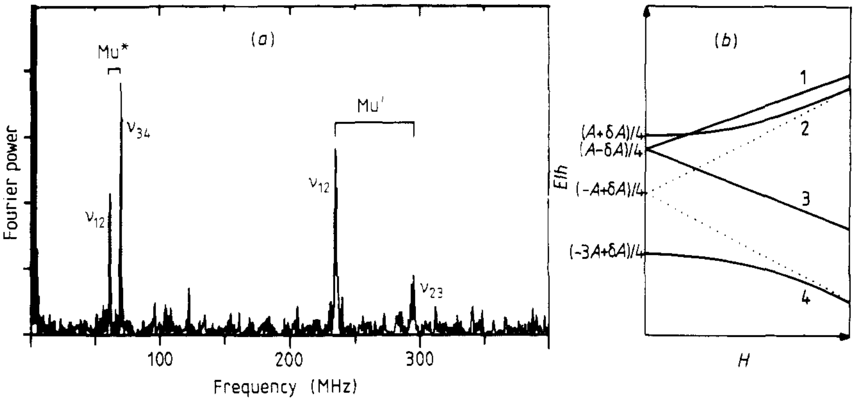

Figure 24. The μSR spectrum of Si recorded at 7 mT (courtesy of the Konstanz group). The two upper lines are asigned to 'muonium' (compare figure 23) with an isotropic hyperfine constant of about 50% of the free-atom value. The species is designated Mu' to distinguish if from the free atom. The complex group of lines at lower frequency is assigned to Mu* or 'anomalous muonium'. (The contrasting spectra of Si and SiO_2 published by Brewer *et al* (1973) illustrate the reduced hyperfine coupling for Mu, and the discovery of Mu*, particularly beautifully.) For Mu* the hyperfine interaction has axial symmetry and may be written $AI \cdot S + \delta A I_z S_z$ (with z along the $\langle 111 \rangle$ directions). The modified Breit–Rabi diagram appropriate to Mu* is constructed in (*b*) (this is for a particular orientation; the dotted lines are high-field asymptotes).

Rabi diagram two transitions are then allowed, indicated in figure 25. The sum of their frequencies in this regime is exactly equal to the hyperfine constant and so provides a particularly direct and precise measurement. It is the detection of these transitions by microwave *resonance* techniques in gas-phase muonium studies that has yielded a value (4.1) precise to eight significant figures used to confront the theoretical predictions (Casperson *et al* 1977). Ignoring the small differences, which are of importance in atomic physics, this value (in frequency units) is simply the hydrogen value increased by the ratio of magnetic moments of the muon and proton. In units of field (or spin density of the nucleus) and as a starting point for discussing hyperfine fields and spin density at the muon in condensed phases, the values for free muonium and free atomic hydrogen may be considered identical.

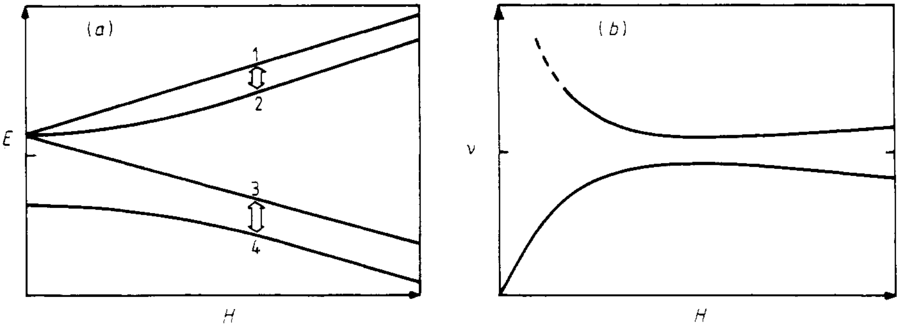

Figure 25. The simplified Breit–Rabi diagram (*a*) and the evolution of the frequencies of the transitions allowed in high field (*b*). For vacuum-state Mu, $A_{\mathrm{Mu}} = 4.5$ GHz and the frequencies are stationary near 1.2 T. (The crossover of levels 1 and 2 ($\nu_{12} \rightarrow 0$) is only reached at $B = 3.7 A_{\mathrm{Mu}}(\mathrm{GHz}^{-1})T$; this is 16T for vacuum state Mu, but can be at much more accessible fields for the muonium-substituted organic radicals.)

These high-field transitions are essentially flips of the muon spin alone, decoupled from the electron spin. The μSR spectrum characteristic of muonium radicals or defect centres is therefore also a simple pair of lines, giving the muon–electron hyperfine coupling in the same manner, $A = \nu_{12} + \nu_{34}$, irrespective of the presence of other nuclei. Referring to figure 25(*b*), these evolve with the field as the muon gyromagnetic ratio and are correspondingly less sensitive to dipolar-field inhomogeneities than the triplet muonium frequencies. There is even a particular intermediate field at which the frequencies are stationary, chosen by Kiefl *et al* (1985b) for the observation of muonium in compound semiconductors (GaAs and GaP) and other materials where nuclear magnetism is not absent. The technical achievement is also noteworthy here, namely the development of a μSR spectrometer with a timing resolution comparable with that of the zero-field instrument, but with the added complication that the photomultiplier tubes (of necessity very close to their respective scintillators) must be adequately screened from the high applied field. The technique will undoubtedly supersede the triplet precession method in the search for muonium in different materials, and the measurement of the hyperfine constant.

In parentheses, no such sophistication is necessary for observation of the 'high-field' spectrum of the organic radicals described in § 6. Here the characteristic frequencies are lower (typically less than 500 MHz) corresponding to the lower hyperfine constants.

Referring to figures 20, 25 and 45 (below), the Paschen–Back regime is achieved in a correspondingly lower field (Roduner 1969).

4.2. *Muonium centres in semiconductors*

The discovery of muonium centres in silicon and germanium was a particularly significant achievement for μSR spectroscopy, since no analogous paramagnetic centres incorporating normal hydrogen (i.e. protium) are known from ESR studies of these materials. Likewise no hydrogen centres are known in diamond, which for this purpose is classed with the group IV elemental semiconductors (the relevant common features being the identical lattice structures and the totally covalent bonding). Hydrogen is only weakly soluble in these materials and in any case dissolved hydrogen remains strongly bound as H_2. Using proton bombardment, the hydrogen centres (if formed) cannot be singled out from the other paramagnetic radiolysis products by conventional magnetic resonance (Estle and Brower 1985). No characteristic proton splittings are visible in the ESR spectra (Symons 1985). There may be a question of timescale here. Thus hydrogen, on the timescale appropriate to equilibrium ESR, can seek out impurities or defects (de-activating acceptors, saturating dangling bonds etc), or encounter other hydrogen atoms, in each case forming a diamagnetic centre. The greater selectivity and shorter timescale of μSR spectroscopy is therefore of importance here, and muonium a unique substitute for hydrogen. Yet these centres have also provided the subject with its most long-standing puzzle. Despite intensive investigation, both theoretical and experimental, neither the muon sites within the diamond-type lattice, nor the local electronic structure, nor the energy of these states, have been established with any certainty or with any consensus.

The two distinct types of paramagnetic centre observed in the elemental semiconductors are usually designated Mu and Mu*. Their characteristics are reviewed, for instance, by Patterson (1984a) and Estle (1985a,b), and may be summarised as follows. The muon–electron hyperfine coupling is isotropic for Mu, which appears to be mobile down to very low temperatures. This coupling is only about 50% of the free-muonium or vacuum-state value in Si and Ge, however, and only 83% in diamond. For Mu*, the coupling is far smaller again and highly anisotropic, with axial symmetry along the $\langle 111\rangle$ directions (Patterson *et al* 1978). These are the bond directions in the diamond-type lattice. Spectra for Mu* are observed from the inequivalent $\langle 111\rangle$ directions, so Mu* is localised and immobile in the lattice. Mu and Mu* are observed simultaneously in μSR spectra, so both are formed promptly on implantation of muons, but some thermally activated conversion of Mu to Mu* can also be demonstrated. Mu* is therefore the more stable state, at least in diamond (Holzschuh *et al* 1982). Diamond is remarkable in that the Mu* signal increases dramatically in intensity between 600 and 800 K and remains visible up to 1100 K, the highest temperature investigated (Patterson *et al* 1984). Presumably Mu* is also the more stable state in Si and Ge; its disappearance at more modest temperatures in these materials may be attributed to depolarisation by conduction electrons (Albert *et al* 1984).

The parameters of the Mu* spin Hamiltonian—the principal values of its hyperfine tensor—have been established in careful single-crystal studies for the three materials, Si, Ge and diamond (Patterson *et al* 1978, Holzschuh *et al* 1979, 1982, Hintermann *et al* 1980). (As a result of the anisotropy, precession signals are only visible in polycrystalline samples at a 'magic' value of the applied field, for which the various transition frequencies happen to coincide (Boekema *et al* 1981a). The appropriate form of the Breit–Rabi diagram (Patterson 1984) is sketched in figure 24(*b*). As a result of the splitting of the triplet, the zero-field spectrum for Mu* comprises three lines (Holzschuh *et al* 1982).

Studies of these centres were until recently confined to materials in which nuclear magnetism is weak or absent (superhyperfine splittings broadening the low-field μSR spectra beyond detection, as mentioned above)—hence the focus of attention on the elemental semiconductors. Since the removal of this constraint by the development of high-field spectrometry, these studies are rapidly being extended to other materials. A particularly beautiful high-field spectrum of Mu and Mu* centres in GaAs is to be found in the publication by Kiefl *et al* (1985b). Although isotropic Mu centres are currently being reported in a variety of other compounds, including the more ionic insulators, the III–V compound semiconductors are the only other class of materials in which Mu* centres have been detected. (The models described in § 4.4 below imply that Mu* centres are not expected in materials of much greater ionicity.)

4.3. *The nature of the centres and nomenclature*

Implicit in virtually all the literature to date is the assumption that muonium essentially retains its hydrogenic character in the isotropic centres, i.e. that these represent muonium atoms contained within an interstitial cavity of the lattice (figure 26(*a*)). (Hydrogen, although it cannot be directly observed via ESR or ENDOR experiments, is likewise presumed to exist as a non-ionised interstitial atom (Reiss 1956).) The 'tetragonal' site is the only intrinsic interstitial site with cubic symmetry and so is the only site compatible with an isotropic hyperfine coupling, unless tunnelling states are involved. The mobility of Mu is explained as a hopping motion between equivalent tetragonal sites. This site is still favoured for Mu although it is challenged below. Early ideas likewise put Mu* at the hexagonal interstitial site (figure 26(*b*)), this having the required axial symmetry. It is difficult to see how bonding at the hexagonal site could be so much stronger that it immobilises this centre, and reduces the spin density so substantially, although the implied combination of atomic orbitals is given by Estle (1981). Alternative sites for Mu* are considered below.

As to the reduction of the hyperfine constants from the free-atom value, it was quickly apparent that shallow-donor models (see e.g., Feher *et al* 1960) were not appropriate. For Mu, the assumption of a uniform dielectric constant and low effective mass would lead to very much smaller electronic density at the muon than is observed. Extensive delocalisation of the electron would also essentially leave the muon unbound

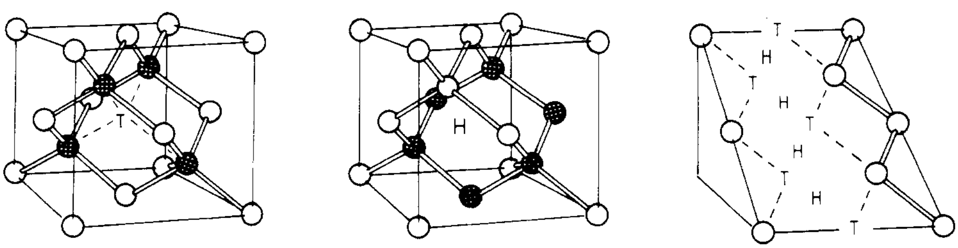

Figure 26. The diamond-type lattice showing (*a*) a tetrahedral (body-centred) and (*b*) a hexagonal interstitial site (nearest neighbours shaded). The various tetragonal and hexagonal sites in a ⟨110⟩ plane are shown in (*c*) (adapted from Mainwood and Stoneham 1984).

in the lattice (quite unlike the situation for the familiar substitutional donors, e.g. P in Si, which remain tetrahedrally bonded even when ionised); this is inconceivable for so reactive a particle. In the deep-donor model of Wang and Kittel (1973) this 'dielectric swelling' of the muonium atom is limited by representing the immediate environment as a spherical cavity within a dielectric medium. The cavity simulates the interstitial volume which is available and is 'rounded off' with a suitable radial dependence of the dielectric constant. A critique of the model, and an alternative treatment that includes a lattice potential (in the spherical solid model), as well as the effects of the muon zero-point motion, are given by Manninen and Meier (1982). An essentially equivalent description (to any treatment that invokes the dielectric constant) is that the relatively small band gap in Si and Ge encourages a degree of delocalisation. The overall correlation between hyperfine constant and band gap in figure 28 below indicates that this is in a certain sense true, since the dielectric constant may be related to the band gap. However, a rather different *microscopic* interpretation of this correlation is given in § 4.5, with due regard for details of lattice structure and bonding. Although the electronic wavefunction for the isotropic centres retains largely s character at the muon, delocalisation of spin density as high as 50% onto the surrounding atoms cannot be described in terms of purely hydrogenic wavefunctions centred on the muon alone; a molecular orbital treatment is more appropriate. The nomenclature 'normal muonium' is therefore dropped in the following in favour of muonium defect centres, designated Mu′. This reserves the symbol Mu for the free atom and the chemical element.

For Mu* the electronic density at the muon is surprisingly low, so there is a certain superficial resemblance to shallow states (especially with those where the wavefunction is p-type at the impurity centre). However, the thermal stability of the Mu* centres is not consistent with a low ionisation potential (Estle 1984). (Since these turn out to be *more* stable than the Mu′ centres, the nomenclature 'anomalous muonium' is likewise dropped in the following.) Also although the electronic wavefunction has virtually no s character at the muon itself, the electron is nonethelesss located very close by: the large value of the anisotropic or pseudo-dipolar coupling is not consistent with an extended wavefunction. Of the various 'microscopic' models devised for these various centres (i.e. models taking proper account of the local atomic structure) the cluster calculations are noteworthy. For Mu′, those of Sahoo *et al* (1983) and Estreicher *et al* (1985) predict that the tetrahedral site is stable, though there remain questions as to how big a cluster is required, and how its surface bonds should be terminated, in order to represent the muon's crystalline environment adequately. Using larger clusters, Mainwood and Stoneham (1983) have calculated the total-energy surfaces for muonium in various charge states, in Si and C. They conclude that all minima are shallow (finding, in fact, an energy maximum at the tetrahedral site!) and raise the question of whether defect- or impurity-related states, or even bound-exciton complexes ($\mu^+e^-e^-h^+$), might be involved. For Mu*, the various defect-related states that need to be considered on symmetry grounds are examined by Estle (1984). Substitutional models, in which muonium is trapped at a vacancy, have received particular attention, for instance in the calculation of Sahoo *et al* (1985), which successfully reproduces all the known features of the Mu* hyperfine tensors.

It is likely, however, that cluster calculations in which atomic coordinates are held fixed will overlook or artificially exclude intrinsic trapping sites, since these entail a local relaxation of the lattice. Intrinsic sites that may be stabilised by a suitable local distortion are therefore reconsidered in §§ 4.4 and 4.5.

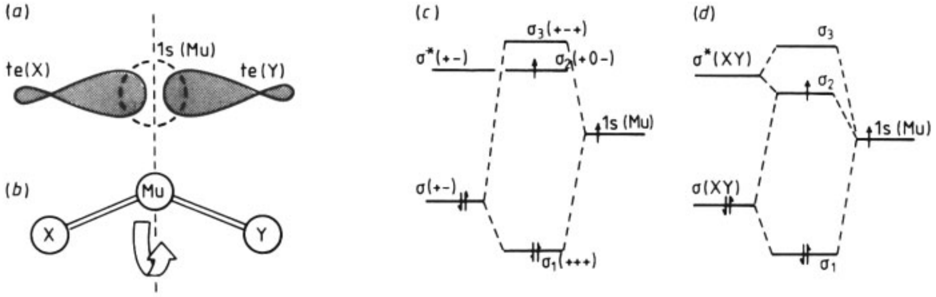

Figure 27. Structure for Mu*, corresponding to insertion of the muon into an elongated X–Y bond at its centre (*a*) or off-axis (*b*) (rotation or tunnelling as depicted in (*b*) would secure effective axial symmetry). The symmetric situation appropriate to the diamond-type lattice (X = Y) is shown, with the muon located at the nodal plane of the σ^* orbital, i.e. in a region of high charge density, but zero spin-density. The singly occupied molecular orbital is then non-bonding, $\sigma_2 = \sigma^*$, as in (*c*). In the zincblende lattice (X $\neq$ Y), positive spin density on the muon results from the admixture with 1s (Mu), as in (*d*). (te = tetrahedral hybrid.)

4.4. The Mu centres*

4.4.1. The elemental semiconductors. A legitimate starting point for predicting the solid state chemistry of muonium (or of atomic hydrogen) is to consider the expectations for its interaction with a particular pair of atoms X–Y. In figure 27(*a*), (*b*) the muon is shown accommodated symmetrically with respect to the two atoms, close to the bond centre. This is the model proposed by Symons (1984a,b) for the Mu* centres in the elemental semiconductors (X = Y = Si, Ge or C). In the corresponding molecular orbital diagram (figure 27(*c*)) the interaction is treated as a three-centre, three-electron problem. The initial levels for the *X–Y* bond are the doubly occupied or bonding orbital, denoted σ, and the vacant anti-bonding orbital, denoted σ^*. Interaction with the muonium 1s orbital creates three new molecular orbitals, denoted σ_1, σ_2 and σ_3. The essential feature of the model is that the unpaired electron occupies the anti-bonding orbital, which has a node at the bond centre, i.e. $\sigma_2 = \sigma^*$, so that first-order spin density on the muon via the direct or contact interaction is very low. This orbital is therefore non-bonding on the muon, but the structure is stabilised by the depression of σ_1 relative to σ (representing the symmetric overlap of 1s(Mu) and σ(XY)). Some stretching of the original X–Y bond is certainly required to accommodate the muon, which may also be displaced laterally from the bond centre, but still lying in the nodal plane of the σ^* orbital. There is then no first-order spin density on the muon. It is instructive to decompose the principle values of the hyperfine tensor into an isotropic term plus an anisotropic term that has dipolar character, as in table 1. (The signs of $A_{\parallel}^*$ and $A_{\perp}^*$ have been chosen so as to give a positive dipolar constant, the raw spectroscopic data providing only relative signs; this contradicts the arbitrary assignment of Kiefl *et al* (1985b) but is consistent with that from an analysis of the polarisation transfer from Mu to Mu* (Patterson *et al* 1984).) It then appears that the isotropic term is negative for Si, Ge and diamond. This *requires* the singly occupied molecular orbital to have zero amplitude at the muon and is readily understood in terms of spin polarisation of the bonding electrons (i.e. the σ orbital).

Likewise the close proximity of the unpaired spin (50% on each adjacent atom in the three-centre model, but with some further delocalisation onto next-nearest neighbours in practice) accounts for the surprisingly large anisotropic component, as

Table 1. Hyperfine coupling constants for Mu* in MHz. The measured values $|A_\parallel^*|$ (Mu*) and $|A_\perp^*|$ (Mu*) are taken from Patterson (1984a) and from Kiefl *et al* (1985b). The derived isotropic and anisotropic components are appropriate to a Hamiltonian of the form $\mathcal{H} = A_{\rm iso}\boldsymbol{I}\cdot\boldsymbol{S} + B(3I_zS_z - \boldsymbol{I}\cdot\boldsymbol{S})$, i.e. $A_\parallel^* = (A_{\rm iso} + 2B)$ and $A_\perp^* = (A_{\rm iso} - {\rm B})$. Signs are chosen to give a positive dipolar parameter $2B$ and to accord with the requirement that $A_\parallel^*$ and $A_\perp^*$ have opposite signs for C, but like signs for Si and Ge.

Mu* host	$A_\parallel^*$	$A_\perp^*$	$A_{\rm iso}$	$2B$
C (diamond)	+168	−392.5	−206	+374
Si	−16	−92.6	−67	+51
Ge	−26.8	−130.7	−96	+69
GaP	219	79	126	94
GaAs	218	89	132	86

well as its axial symmetry. Indeed, the requirements of these parameters are so stringent that this is possibly the only *intrinsic* site that is able to satisfy them.

4.4.2. The III–V semiconductors. Essentially similar models may be envisaged for binary compounds that have tetrahedral coordination (Cox and Symons 1986b), i.e. for structures of the zinc sulphide type. Here the lattice resembles that of diamond, but has alternate atoms of different species. The geometrical symmetry of the Mu* structure is lost in these materials, however. The muon can no longer sit precisely at a node of the singly occupied orbital (i.e. this loses its purely non-bonding character) and accordingly the contact term is positive, representing first-order spin density at the muon. This explains the qualitative difference between the elemental and compound semiconductors noted by Kiefl *et al* (1985b), namely that $|A_\parallel|$ is greater than $|A_\perp|$ in the former case, less in the latter (table 1). This model for Mu* relies heavily on the assumption that tetrahedral hybrid atomic orbitals remain a good basis for the description of the σ (bonding) and σ^* (anti bonding) molecular orbitals. Mu* centres are not therefore expected in more ionic materials, i.e. when the anion p orbitals are not involved in bonding to the cation and the electronic density falls to zero between the ions.

4.5. The Mu′ centres

4.5.1. Other crystalline solids. Although Mu* centres have not been detected other than in the group-IV and compound III–V semiconductors, *isotropic* centres are currently being reported in a variety of binary systems, notably in SiC, in certain II–VI compounds (ZnSe, ZnS, MgO) and in the alkali and cuprous halides (Baumeler *et al* 1985, Kiefl *et al* 1985a, Estle 1985, Kiefl 1986). The existence of muonium in certain of these was known previously (e.g. KCl (Ivanter *et al* 1972) and MgO (Spencer *et al* 1984)) but these observations represent the first systematic measurements of hyperfine coupling by the high-field technique and are undoubtedly the prelude to a survey of a great variety of non-metallic solids. The overall picture is presented in figure 28, where reported values of hyperfine coupling A for the isotropic centres are expressed as a proportion of the free-muonium value $A_{\rm Mu}$.

It is natural to examine the systematics of these values and to look for correlations with essential parameters; here they are plotted against the band gap for each host

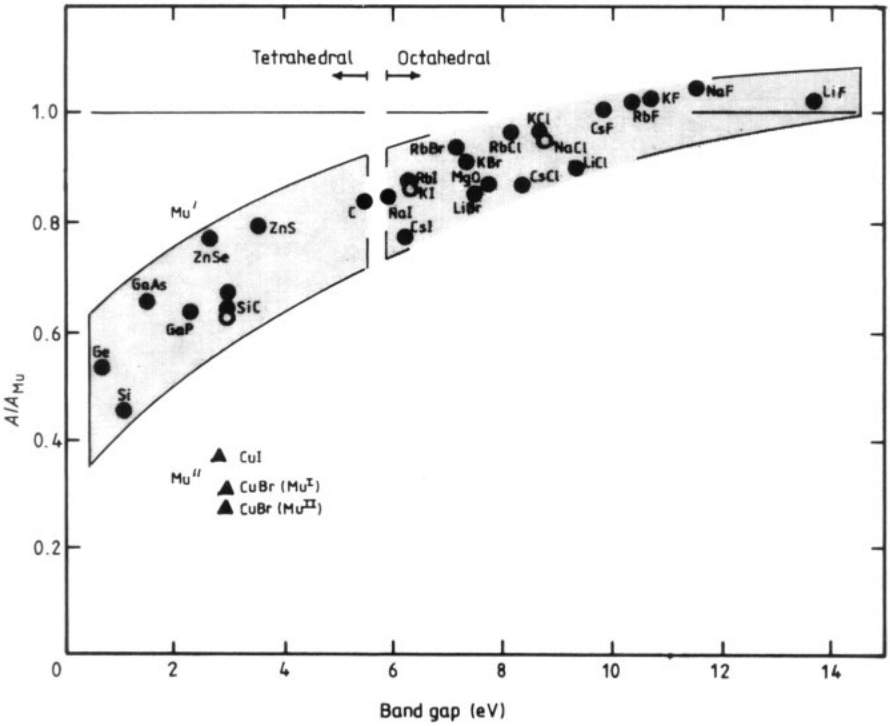

Figure 28. Correlation of spin density at the muon with the band gap of the host material, for isotropic centres. Hyperfine constants A are taken from Patterson (1984a), Baumeler *et al* (1985), Kiefl *et al* (1985a), Estle (1985a) and Kiefl (1986). Values for the band gap are taken from standard texts.

material. It would be unreasonable to expect a monotonic dependence on a single parameter, and the detailed variations within particular categories of material are considered below. However, a broadly successful correlation is apparent which includes the elemental semiconductors together with the majority of (more or less ionic) binary compounds investigated to date. These centres are all labelled Mu′ rather than Mu, to distinguish them from the free atom, although clearly the distinction is lessening towards the right of the plot, and virtually vanishes for the alkali halides. It is noteworthy that hydrogen defect centres are well known in the oxides and halides (unlike in the semiconductors), and the proton hyperfine couplings are known from ESR studies, so in these materials an isotopic comparison is possible. In the alkali fluorides , values of spin density are found that actually exceed the free-atom values, both for muonium and hydrogen. In this limit, therefore, a trapped-atom model is legitimate, with the hydrogenic wavefunction slightly compressed in the interstitial cavities. Any lower value of spin density represents admixture with the surrounding atomic wavefunctions. In fact the small isotope effect that is noted by Baumeler *et al* (1985), namely that reduced values of hyperfine coupling are somewhat less for the muonium than for the analogous hydrogen defect centres can be understood in these terms. Delocalisation is enhanced by the greater amplitude of zero-point motion for a muon, as compared with a proton in the same potential well, the muon spending relatively more time close to the surrounding atoms. A simplified approach to the molecular orbital problem is presented in § 4.5.2. The correlation of hyperfine coupling with band gap, and the structures appropriate to the wide range of materials depicted in figure 28, may also be understood in these terms. Notable exceptions to this correlation are the centres labelled Mu″, which to date are unique to the cuprous halides. These are examined separately in § 4.6.

4.5.2. The three-electron model. Considering again the interaction of muonium with an atom pair X–Y, reaction (4.4) describes a process in which the muonium atom is envisaged as approaching the atom X along the line of the X–Y bond, i.e. from a tetragonal site towards one of the four nearest neighbours. For the elemental semiconductors (X = Y), as well as for compounds with predominantly covalent character (except the cuprous halides), this implies a partial breaking of the intrinsic bond.

$$\mathrm{Mu}^{\bullet} + \mathrm{X{-}Y} \rightarrow \mathrm{Mu{-}{-}{-}X{-}{-}{-}Y} \tag{4.4}$$

$$\mathrm{Mu}^{\bullet} + \mathrm{X{-}Y} \rightarrow \mathrm{Mu{-}X} + \dot{\mathrm{Y}}. \tag{4.5}$$

If the reaction could be carried to completion, breaking the bond as in (4.5), this would transfer the unpaired spin to Y. Such displacement reactions are well known in gaseous and liquid-phase chemistry†. In a crystalline solid, the progress of reaction (4.4) is obviously limited by the lattice forces that hold atoms X and Y in position. Thus for the particularly hard lattice of diamond, the transfer of spin density away from the muon is limited to about 17%. For the softer lattices of Si and Ge, further progress along the reaction coordinate is permitted, and about 50% transfer achieved. Contrary to the formation of the more stable Mu* centre, which must require an activation energy, no significant barrier is expected for the formation of Mu′ centres via reaction (4.4). The corresponding molecular orbital diagram, again treated as a three-centre, three-electron model, is given in figure 29 (Cox 1986). The structure is stabilised by the depression of the doubly occupied level σ_1 relative to σ since this more than offsets the change in energy from 1s (Mu) to σ_2, which is singly occupied.

For the elemental semiconductors, the σ and σ^* levels correspond to symmetric and anti-symmetric combination of sp^3 atomic hybrid orbitals. The model is readily extended to the binary compounds if, for the Mu′ centres, muonium is associated with the more anionic species (Cox and Symons 1986b). As the degree of ionicity increases, the σ level takes increasing atomic *p* character and in the completely ionised limit corresponds to retention of the two bonding electrons by the anion (the σ^* level then corresponding to vacant cation states). The essential feature, however, is that as the σ–σ^* splitting for X–Y increases, as in figure 29(*b*), the degree of admixture diminishes and the 'muonium' retains more and more free-atom character. That is, the hyperfine coupling increases towards the free-atom value. Taking the band gap as a convenient measure of the initial σ–σ^* separation, the general trend apparent in figure 28, with spin density on the muon increasing from about 50% in Si and Ge to about 100% in the alkali halides, is readily understood. The σ–σ^* separation is so great in the ionic insulators that admixture with the cation states is negligible, i.e. the model is reduced

---

† The product of reaction (4.5) might seem at first sight to be a good model for Mu*. However the electron spin is then too remote from the muon to account for the remarkably large anisotropic couplings observed, either via the purely dipolar interaction or (since the intrinsic or direct X–Y bond is broken) via spin polarisation of bonding electrons. The Mu* centre may be thought of instead as the product of a solid state reaction in which muonium approaches the X–Y pair along the median plane between the two atoms, i.e. perpendicular to an intrinsic X–Y bond, as explained in § 4.4 above.

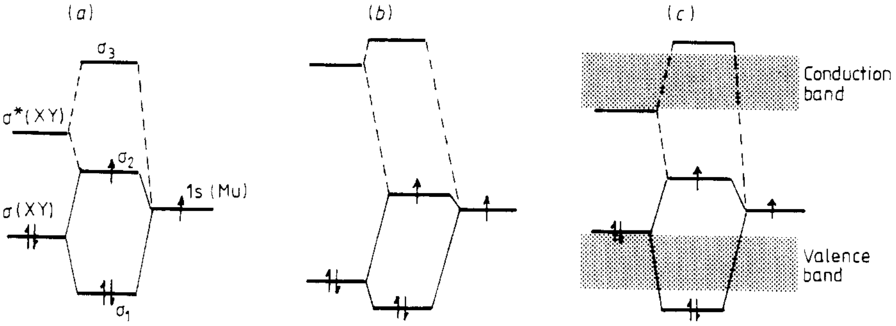

Figure 29. The three-electron model for the Mu′ centres, illustrating the partial anti-bonding character of the singly occupied molecular orbital σ_2 for the case of large admixture (*a*), and increasing atomic hydrogen character as the degree of admixture diminishes (*b*) (Cox and Symons 1986b). The bonding state σ for an X–Y pair characterises states in the valence band for the solid. The paired and unpaired electrons remain closely localised if the molecular orbital states are detached from the bands (*c*).

to a two-centre, three-electron problem. How the energy levels σ_1, σ_2 and σ_3 in this admittedly simplified description relate to the band structure (figure 29(*c*)) must await detailed calculations. However, it is noteworthy that the paired and unpaired electrons will remain closely localised if these levels are detached from the bands and the correspondence can be made here with calculations performed for the semiconductors (Katayama-Yoshida and Shindo 1984).

Evidently the σ–σ^* separation is a more important parameter in determining this progression than, for instance, ionicity, since virtually identical spin density is found on the muon in diamond and in MgO. Diamond is totally covalent with tetrahedral coordination, whereas MgO has a high ionicity parameter and octahedral coordination. Points to the left of (and including) C in figure 28 represent materials that all have tetrahedral coordination. To the right of C in figure 28, the materials have octahedral coordination. Nonetheless no discontinuity or change of slope in the curve is apparent at this point. A correlation with ionicity can certainly be found within each category of material, however, as noted by Kiefl *et al* (1985a). Ionicity is also important with regard to the siting of the muon, as discussed below.

4.5.3. Mu′ sites in covalent and partially covalent hosts. For compounds in which tetrahedral atomic hybrid orbitals remain a good basis for the description of bonding, the solid state reaction (4.4) determines the muon site. Muonium is, in effect, attached to the back-lobe of an sp^3 orbital centred on XZ, as in figure 30(*a*). Here X is the more anionic species.

It is noteworthy that these anti-bonding sites have not to date been identified as stable in any *ab initio* calculations of energy surfaces. However, the weakening and consequent stretching of the X–Y bond, which is a requirement of this simple model, implies that they will be artificially excluded by any cluster calculations that hold the host atoms at fixed coordinates and that do not include the possibility of local bond stretching. Using the adamantane molecule $C_{10}H_{16}$ to simulate the carbon-atom cage surrounding muonium in diamond, Estreicher *et al* (1985) note that the anti-bonding sites are partially stabilised when the outward-pointing C–H bonds are stretched beyond the normal C–H bond length. These authors dismiss the importance of these

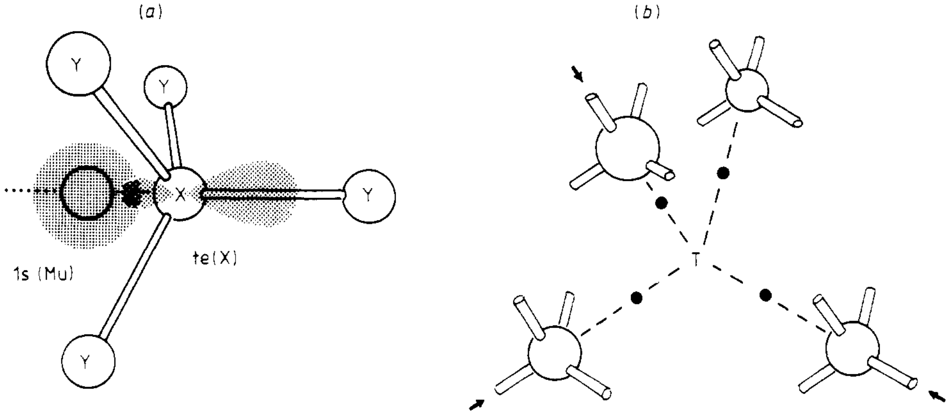

Figure 30. The postulated structure of the 'anti-bonding' site for Mu′ in materials with tetrahedral coordination (*a*) and four equivalent anti-bonding sites surrounding a 'tetragonal site' T (*b*). In the binary compounds (except the cuprous halides) the sites involved are associated with the more anionic species. A possible *contradiction* of the tetrahedral cage is indicated in (*b*). (te = tetrahedral hybrid.)

sites, regarding them as an artefact of the 'partial saturation' of these bonds. In terms of the present model, however, a weakening of one or more of the outward-pointing bonds is exactly the chemical expectation, as expressed by reaction (4.4) and figures 29 and 30; such a distortion may therefore be expected to *stabilise* the structure of the Mu′ centres.

These same anti-bonding sites are also invoked in various models for hydrogen defect centres in Si and Ge (Falicov *et al* 1985, Johnson *et al* 1986); these authors consider hydrogen only adjacent to, or in the vicinity of, other substitutional impurities, however, and the states in question appear to be too shallow to account for the stability and other properties of the Mu′ centres. The possible role of defects and impurities has been discussed elsewhere (Mainwood and Stoneham 1984, Cox and Symons 1986b) but there is no compelling evidence for Mu′ centres being at other than intrinsic sites.

4.5.4. Dynamical models. Since the hyperfine coupling for Mu′ centres is isotropic, some form of dynamic averaging must be introduced into the model. Sufficiently rapid motion between equivalent anti-bonding sites would secure the effective isotropy, since such sites are symmetrically disposed about the 'tetragonal site', labelled *T* in figure 30.

A potential well with four local minima can be envisaged within the interstitial cavity centred on *T*. Pending detailed calculations of this energy surface for the relaxed lattice there are various possibilities. If the energy barriers between adjacent minima are small, and exceeded by the muon zero-point energy, the muon explores the whole cavity and is effectively centred at *T*. For intermediate barrier heights, tunnelling states between the four sites may be possible (see also § 4.6.2). In either case the bond-weakening is distributed over all four outward-pointing X–Y bonds, and readily accommodated by the lattice. For larger barrier heights the muon may be 'self-trapped' at a particular anti-bonding site, in which case an activation energy is implied for hopping to neighbouring sites. Whether the motion is of long range, or restricted to a particular 'cage', will depend on the properties (e.g. the hardness) of individual materials. In either case the centre is *magnetically* indistinguishable from a spherically symmetric entity centred at a tetragonal site. If the model is correct, however, an instantaneous muon position displaced off-centre from the tetragonal site is always favoured, and this prediction may be compared with the interpretation of various channelling experiments (Picraux and Vook 1978, Patterson 1984b, Flik *et al* 1986). That the same sites are occupied by pions in the supposedly analogous 'pionium' centres (Flik *et al* 1986) is particularly noteworthy.

In the elemental semiconductors it seems likely that the mobility of the Mu′ centres is of long range. In the compound materials the inequivalence of adjacent tetragonal sites along connecting paths through the lattice must imply a barrier to long-range motion. This is borne out by the variation with temperature of the μSR linewidths. Superhyperfine coupling is not completely averaged in binary compounds, and the Mu′ centres appear to become localised at lower temperatures (Kiefl *et al* 1985b).

4.5.5. Highly ionic compounds. To the right-hand side of figure 28, the bonding in the host materials is primarily ionic, i.e. there is negligible electron density between anion X^- and cation Y^+. The muon site is not in this case determined by directional orbitals. For the alkali halides, Baumeler *et al* (1984) note the correlation between muon–electron hyperfine coupling in the Mu′ centres and proton–electron coupling in the corresponding hydrogen U_2 centres. Accordingly they assign the muon to the interstitial U_2 sites. They also note that the halogen species (rather than the alkali metal) has the dominant influence on hyperfine coupling. This is expected in terms of the three-electron model (the initial σ level of figure 29(*b*) deepening substantially in the order XBr, XI, XCl, XF), and is also evident in figure 28. The implication of this model is that spin density is partially delocalised from the muon onto the anions only. It may prove possible to detect this and measure the halogen–nucleus couplings in a 'level crossing resonance' experiment (see § 7).

For a given halogen, a slight variation of muon–electron coupling is found for different alkali cations, the trend running contrary to the general increase of coupling with band gap (figure 28). This subsidiary dependence on another parameter may be explained in terms of competition between muonium and the alkali metal ions for bonding to the halogen. Thus the Mu′ centre retains greater atomic character as the electronegativity of the cation increases. Similar trends are seen here for the II–VI and III–V categories of compound.

4.6. The Mu″ centres

4.6.1. The one-electron model. In the completely ionised limit, both anion and cation normally have filled p shells outermost. Filled anion p states lie at the top of the valence band and vacant cation s states at the bottom of the conduction band. Wide-band-gap materials of this sort exhibit nearly atomic-like Mu′ centres. The situation differs for the cuprous halides in two respects. Firstly the Cu^+ cation has a filled d shell outermost. These cation d states are positioned energetically close to the anion p states, the near degeneracy resulting in considerable p–d mixing (e.g. Goldmann and Westphal 1983, Smolander 1983). This is the origin of the partially covalent character in these compounds. The presence of cation states in the valence region is unique, amongst the materials portrayed in figure 28, to the cuprous halides. Secondly, the Cu^+ cation has vacant s states lying very much closer to the top of the valence band than, for instance, the alkali cations. These key differences are strongly supportive of the proposal, due to

Symons, that muonium is associated with the Cu^+ cation. (These characteristics are shared with the noble-metal cations, notably Ag^+ (Kunz 1982), although to date no Mu″ centres have been detected in the silver halides.) The interaction is expressed in reaction (4.6), and in the qualitative molecular orbital diagram of figure 31, where it is represented as a one-electron bond:

$$Cu^+ + Mu^{\bullet} \rightarrow (Cu^{\bullet}Mu)^+. \tag{4.6}$$

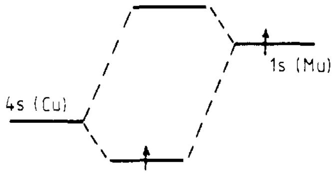

Figure 31. The one-electron model for the $(Cu^{\bullet}Mu)^+$ radical cation, due to Symons, placing major spin density on copper. (There must in fact be a degree of admixture with other vacant Cu^+ orbitals, limiting the magnitude of the copper nuclear hyperfine coupling to less than its purely s state value.)

Here the Cu^+ electronic configuration is taken to be $3d^{10}4s^0$. Relatively little energy is required† to promote this to $3d^94s^1$. ESR results for the $(Ag^{\bullet}H)^+$ radical cation, however, suggest that no such excitation need be invoked here; these are entirely explicable in terms of a singly occupied molecular orbital involving the atomic s orbitals only (Eauchus and Symons 1970). It seems reasonable to extrapolate to copper, although the $(Cu^{\bullet}H)^+$ species has not yet been studied by ESR spectroscopy. Upper limits on the nearest neighbour hyperfine coupling constants estimated from linewidth data by Kiefl *et al* (1985b) suggest that the metal cation orbital cannot be purely s state in $(Cu^{\bullet}Mu)^+$, if this is indeed the species observed, but that hybridisation with other vacant orbitals must be involved.

In fact, two Mu″ centres, designated Mu^I and Mu^{II} by Kiefl *et al* (1985b) and having coupling constants differing by only about 10%, are observed in CuCl, and likewise in CuBr. These authors suggest that the two centres arise because there are two inequivalent tetrahedral sites in the crystal. It could well be that bonding to Cu^I is more sterically resisted for one site than the other, weaker bonding giving a lower coupling constant. It would be of great interest to determine the hyperfine coupling to ^{63}Cu in these centres both measure the 4s component and to see how many equivalent copper nuclei are involved.

4.6.2. Tunnelling states. The one-electron bond between Cu^+ and Mu is not directional, and so does not determine the muon site (as does the three-electron bond for Mu′ centres in the other tetrahedrally coordinated materials). However, it is legitimate to assume that the Mu″ centres are instantaneously displaced towards a particular Cu^+ cation. Figure 32(*a*) depicts the possible sites within the tetragonal cage defined by four cations. An interesting possibility is that Mu^I and Mu^{II} represent the singlet and triplet states (figure 32(*b*)) associated with local tunnelling between four such sites. This would account for the small difference in coupling constants. The singlet and triplet states have

---

† For the Ag^+ cation, the promotion $4d^{10}5s^0 \rightarrow 4d^95s^1$ is responsible for the abnormally high concentration, polarisability and mobility of interstitial Ag^+ (all crucial to the photographic process (Slifkin 1986)).

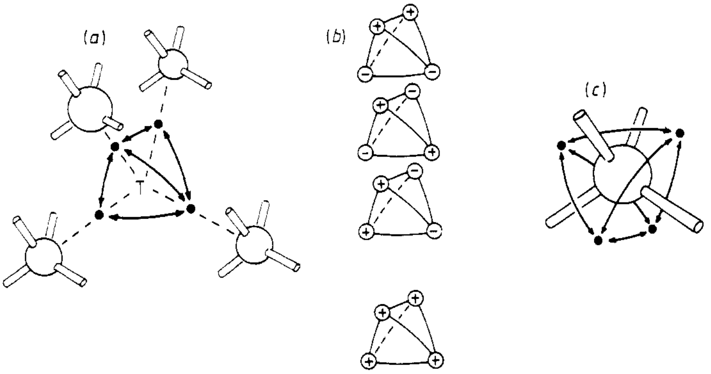

Figure 32. Tunnelling models for the Mu″ centres in which the muon is delocalised over four cation-related sites. Four sites within an interstitial cage are shown in (*a*), for which two tunnelling states (a singlet and degenerate triplet) are expected (*b*), which could correspond to $\mathrm{Mu^I}$ and $\mathrm{Mu^{II}}$. An alternative choice of four sites with the required symmetry is shown in (*c*).

slightly different spatial distributions of probability density for the instantaneous muon position; as spin density at the muon is a sensitive function of its position, this results in different averages for the hyperfine coupling. Nevertheless only cation-related sites are involved.

The tunnelling model proposed here is conjectual, but is consistent with the temperature variation of μSR amplitudes, linewidths and frequencies (Kiefl *et al* (1985c); in particular, that the depolarisation rate for the $\mathrm{Mu^{II}}$ varies only slightly in the region where that for $\mathrm{Mu^I}$ diverges and its signal is lost, if the following interpretations are made. The separation of singlet and triplet is greater than kT (for all temperatures investigated to date) so, in thermal equilibrium, the population of the upper state is negligible. Nonetheless both states are populated on implantation of the muon. The upper state, corresponding to $\mathrm{Mu^I}$, is even populated preferentially by 'capture' of the still slightly energetic muon, i.e. before complete thermalisation. (Also a triplet upper state would have greater statistical weight.) At low temperatures, the two states can coexist by virtue of a slow interconversion rate. The conversion rate increases with temperature, and above e.g. 150 K becomes so rapid that only the more stable state ($\mathrm{Mu^{II}}$) is observed. An alternative choice of four sites with the required symmetry is depicted in figure 33(*c*). These surround a single $\mathrm{Cu^+}$ cation.

4.7. *Trapping mechanisms and the diamagnetic fraction*

The mechanisms by which muonium is formed and trapped in these centres is not clear. In the above (bond-centre) model for Mu*, conversion from Mu′ requires a minor migration of the muon together with a local rearrangement of the lattice, and this may be thermally activated—yet both Mu′ and Mu* are formed promptly on implantation. For the prompt Mu* fraction, therefore, the activation energy must be provided by the residual kinetic energy of the muon: by implication the distribution of polarisation between Mu′ and Mu* states is determined at epithermal energies. If instead muonium is thermalised before trapping, it is necessary to consider the possible roles of defects of impurities, since bonds that are *already* elongated should preferentially trap muonium. Substitutional C in Si, for instance, provides such sites and is available in significant concentration even in the purest silicon samples. In view of its stability, it is possible that Mu* could be associated with such defects.

Defect-related models readily account for the conversion of Mu to Mu* in terms of encounter and trapping, and likewise for the stability of Mu*. Studies of samples in which the vacancy concentration has been increased by electron irradiation reveal an increased Mu* fraction (Albert *et al* 1983). This seems at first sight to be supportive of the substitutional model (Sahoo *et al* 1985). The result should properly be interpreted in terms of trapping of charge carriers at the vacancies however, rather than muonium trapping, thereby suppressing a depolarisation mechanism (Weidinger 1985). The *intrinsic* vacancy concentration, e.g. in diamond, is known to be too low to explain the Mu* fraction that is formed promptly, if muons thermalise at random in the lattice. Substitutional models therefore require the energetic incoming muons to thermalise preferentially near vacancies (which is not inconceivable—see § 5) or else *to create their own*. In this latter hypothesis the Mu* fraction would then represent the probabiity that a muon is trapped promptly, and the Mu′ fraction the probability that it escapes the region of radiation damage without capture. It is then difficult to understand, however, why the Mu* fractions are so similar in materials of such different hardness (bond strength).

On these grounds the intrinsic models of §§ 4.4 and 4.5 are to be favoured but verification must await experimental tests such as channelling site determinations for the mobile centres, or measurements of the spin density on neighbouring nuclei for the immobile centres. Level crossing resonance (§ 7) is in principle able to provide a detailed map of spin density in the vicinity of the muon and should prove decisive for identification of the Mu* centres. Preliminary results (Kiefl 1986) are supportive of the bond-centre model.

Each of these models is susceptible to electron capture or electron loss. Thus $(\mathrm{Mu}')^- = \sigma_1^2\sigma_2^2$ or $(\mathrm{Mu}')^+ = \sigma_1^2\sigma_2^0$ (cf. figure 29), and likewise $(\mathrm{Mu}^*)^\pm$ (cf. figure 27) would represent diamagnetic states. The diamagnetic fractions in the various materials, and their variations with temperature, do not correspond to thermal ionisation of the paramagnetic centres, however (by the same token the energies of the paramagnetic states, relative to the conduction and valence bonds, have not been determined). Diamagnetic states may be formed promptly, but it must also be borne in mind that Mu′ is sufficiently mobile to seek out and saturate dangling bonds, deactivate acceptors etc. μSR studies of *amorphous* Si (with and without hydrogen loading) might be valuable here.

Whereas in the elemental semiconductors there are no lone electron pairs that could trap muons (or protons), and no low-lying unoccupied orbitals that could capture excess electrons, these possibilities do exist in the ionic materials. Such processes can provide routes to the formation of the radical centres, as is the case in certain organic materials (Cox *et al* 1982, Hill *et al* 1985, Cox and Symons 1986a; see also § 6), but equally can stabilise the diamagnetic states and thereby inhibit or delay muonium formation. There may be a clue here to why muonium centres are not found in every non-metallic and non-magnetic compound. Assuming the experimental results to be unambiguous, Stoneham (1984a) envisages the following situations in which the formation of stable muonium could be inhibited:

(i) in ionic crystals that show cation Frenkel disorder (M^+ interstitials or vacancies)—here Mu^+ could be localised at sites where the Madelung potential favours a positive charge;

(ii) in ionic crystals that show anion Frenkel disorder—here the muonic hydride ion ($Mu^- = \mu^+e^-e^-$) could be stabilised;

(iii) in materials where formation of molecular ions is favoured, e.g. $(OMu)^-$ ion oxides or $(FMuF)^-$ in fluorides (see § 3), $(HMu)^-$ in hydrides, metal ligands etc. In this latter case, the interaction (4.7) or (4.8) may be favoured, depending on the Madelung potential and the valence state of the transition-metal ion:

$$M^{n+} \ldots Mu^+ \rightarrow M^{(n+1)+}Mu \tag{4.7}$$

$$M^{n+} + Mu^{\bullet} \rightarrow M^{(n-1)+} \ldots Mu^+. \tag{4.8}$$

No detailed predictions are available, but presumably the great disparity of muonium yields in the metal oxides, for instance (Spencer *et al* 1984), represents the result of competition between these various possibilities for bonding and the degree to which the intrinsic metal–oxygen bond is broken.

5. Dynamical studies in metals

The nature of the muon state in *metallic* systems, and its evident mobility in many pure metals, are the subjects of this section. Here it is the comparison with the behaviour of other light interstitial particles—notably protons—that is of interest. Indeed, for this reason, experimentalists working on hydrogen in metals were amongst the first to exploit the μSR technique (see, for instance reviews by Kehr (1978), Seeger (1978) and Karlsson (1982)). The substantial isotopic mass ratio provides a more severe test of models for hydrogen behaviour than does comparison with deuterium or tritium, and the use of a *lighter* isotope favours observation of specifically quantum effects.

Another particular interest in implanted muon studies stems from their ability to monitor the genuinely isolated interstitial particle. This is a consequence of the remarkable sensitivity of μSR and contrasts with proton studies via NMR (see, for instance, Cotts 1978) or neutron scattering (Richter 1983, Hempelmann 1984), which are only possible in metals in which hydrogen is sufficiently soluble to be detected. At the hydrogen concentrations required, the correlation between neighbouring protons (or even cooperative phenomena) then often dominates the behaviour. Proton studies below liquid nitrogen temperature are precluded in many instances by the miscibility gap, that is the tendency for the hydrogen to precipitate out, leaving domains of hydride and virtually pure metal. In most μSR experiments, on the other hand, there is literally only one muon in the entire sample at a time; even using pulsed implantation the probability of pairwise interactions is negligible at the intensities available for the foreseeable future. By the same token, μSR allows the behaviour of the isolated interstitial to be followed down to the lowest temperatures available—liquid helium and below†.

The combination of studies of isotope effects and temperature dependences over an extended range has proved extremely valuable. The principal problems addressed are:

(i) the mechanism of localisation of the proton or muon at sites of specific crystallographic symmetry (§§ 5.1 and 5.5);

---

† It is also noteworthy that NMR signals may be obtained only from the surface layer of bulk metallic sample, so foils or powders are commonly (though not exclusively) used. The RF penetration or 'skin' depth is typically 10–100 μm at 50 MHz, for example. Low-momentum muon beams (i.e. 'surface muons', see § 2) penetrate to a depth of typically 0.1 mm; the higher-momentum ('decay channel') beams may be used to implant muons approximately uniformly in bulk samples, facilitating single-crystal studies.

(ii) the mechanism of the elementary diffusive step, which allows the particle to migrate between equivalent sites, and the variation of this mobility with temperature (§§ 5.2—5.6);

(iii) the nature of the trapping of the muon or proton at imperfections (§ 5.5); and

(iv) the additional information that may be obtained from μSR studies of the concentrated metallic hydrides themselves (§ 5.7).

These are fundamental questions which are each the subject of some topical controversy. They also relate to a number of problems in practical metallurgy. Their understanding is a necessary prerequisite to an understanding of the surprising rapidity of hydrogen diffusion in metals—for instance, to the choice of hydrides for energy storage media or to the choice of constructional materials (e.g. for containment vessels), which are exposed to hydrogen.

5.1. *μSR linewidth and muon site determination*

In these studies, the *μSR linewidth* is the primary source of information. This characterises the effective distribution of local fields from surrounding nuclei (most commonly from the metallic nuclei themselves but also, in the case of the metal hydrides, from the nearby protons too)†.

For a muon at rest, embedded in a regular array of dipolar nuclei, the depolarisation is approximately gaussian, as in (5.1) (see, for instance, Hartmann 1977a). So also, therefore, is the μSR lineshape, with a mean square width given by a static dipolar sum, as in (5.2). This is the classic calculation of the second moment of an NMR line due to Van Vleck (1948), with the proviso that the probe spin is distinct from the host spin species, as for a rare or dilute nuclear species (see, for instance, Abragam 1961), and also that it is usually positioned at an interstitial, rather than a substitutional, site‡. By 'at rest' is meant here localisation at a particular site for times greater than this calculated inverse width. Motion from one site to another faster than this effectively averages the distribution; the resultant narrowing of the observed μSR line is the source of information, albeit somewhat indirect, on the muon mobility in pure metals (§§ 5.2–5.6) or on the proton mobility in the concentrated metal hydrides (§ 5.7). The μSR linewidth is not altered, however, by the vibratory motion of the muon at a particular site, as long as this is isotropic: harmonic zero-point motion is sufficiently rapid and of sufficiently small amplitude (typically about 10% of the atomic spacing) for the second-moment calculation to be unaffected:

$$P_x(t) = P_x(0)\exp(-\sigma^2 t^2) \qquad \text{with } \sigma^2 = \tfrac{1}{2}\gamma_\mu^2\langle\delta H^2\rangle \tag{5.1}$$

$$\langle\delta H^2\rangle = \tfrac{1}{3}\gamma_I^2\hbar^2 I(I+1)\Sigma(1-3\cos^2\theta)^2/r^6. \tag{5.2}$$

In the sense that only secular terms are included in the dipolar sum, this is inhomogenous broadening: there is no significant lifetime broadening of the muon spin states. The

---

† These studies therefore rely on the linewidth or depolarisation rate being measurable; other methods must be contrived when nuclear magnetism is weak or absent or when the muon in highly mobile at all temperatures (Seeger 1984a, b, Kehr 1984). It is noteworthy here that the related studies of muon or positron 'channelling' do not rely on any magnetic properties of the host (Maier and Seeger 1983, Maier 1984, Carstanjen and Seeger 1984, Patterson 1984b) but require instead near-perfect crystals.

‡ That is, the muon is interstitial with respect to the metal lattice. The case of muons that are substitutional in the sense of being trapped at a vacancy is touched on briefly below. In the metal hydrides, if the important spins are those of the protons, the muon may be regarded as substitutional in the proton lattice.

decay of transverse polarisation can be thought of simply as a dephasing of the ensemble, as different muons precess in slightly different local fields. The μSR line is also inhomogenous in the sense that single or isolated muons have no muon–muon dipolar interaction to constitute a thermodynamic system, and therefore cannot come to *dipolar* equilibrium with the host spins. *Zeeman* equilibrium is in principle possible, but spin–lattice relaxation is invariably too slow on the μSR timescale for this to be achieved. In particular, depolarisation of the muons via their interaction with the conduction electrons (i.e. Korringa relaxation) is negligible in normal metals, as demonstrated in § 3.2.4; there is no conduction electron contribution to the μSR linewidths. The dipolar sum depends on the direction of the host spin quantisation, relative to the crystalline axes, so the orientation dependence of the static μSR linewidth defines the symmetry of the site adopted by the muon within the lattice.

Another method of site determination, which is experimentally more convenient, is available for most metals, namely those with quadrupolar nuclei. The Van Vleck expression (5.2) is valid only in an applied field that is sufficiently high to determine the quantisation axis of each spin. In low fields, quadrupolar nuclei neighbouring the muon do not line up with the applied field but with the electric field gradient from the muon charge itself. The field dependence of the μSR linewidth consequently exhibits a step change to the Van Vleck value at the field sufficient to break this orientation (Hartmann 1977b, Camani *et al* 1977). The direction and magnitude of the step often uniquely characterises the occupied site; its position also characterises the strength of the nearest-neighbour quadrupolar interaction although this may now be determined more precisely by other means (§ 7.3). Several steps in the field dependence would correspond to the quenching of the interaction on successive shells (e.g. next-nearest neighbours, nearest neighbours).

These methods, illustrated in figure 33, were the starting point for systematic μSR studies of many metals. In all cases established to date, these are the same interstitial sites as are adopted by protons at low hydrogen loadings (i.e. in the solid solution or α phases)—hence the interest in comparative studies. In the following, the information available on the localisation and diffusion of muons is illustrated principally with results obtained for Cu, Al and Nb. In fact hydrogen is not sufficiently soluble to be detected easily in Cu or Al, so in these cases muons are a unique substitute; Nb has a considerable capacity for dissolved hydrogen. References to work on other metals are listed by Schenck (1985a).

In fact the site determination may not always be clear-cut. This is the case in niobium, for instance. Nb has been much studied because of its relatively large nuclear moment, resulting in a readily measured static depolarisation rate. Nb has a BCC lattice, in which the most likely interstitial sites for a positively charged impurity are (i) the face centres, which are the centres of *octahedra* of Nb atoms, and (ii) the corners of the Wigner–Seitz unit cell, which are the centres of *tetrahedra* of Nb atoms (figure 33(*a*)). The second-moment measurements for Nb indicate that the muon site has dominant, but not perfect, tetrahedral character. Also the small departure from cubic symmetry appears to increase as the temperature is lowered. Gygax *et al* (1984a), whose results are sketched in figure 33(*c*), argue that an unreasonably large distortion of the tetrahedral site, or conversion of the entire Nb lattice to lower symmetry at low temperature, would be required to explain the discrepancy. The possibility of two inequivalent muon sites, weighted with an occupation probability, is therefore not excluded. The octahedral and tetrahedral sites within an FCC lattice are shown in figure 33(*b*). In Al, which is FCC, a change in the preferred site with temperature is apparent, from octahedral below 5 K to tetrahedral

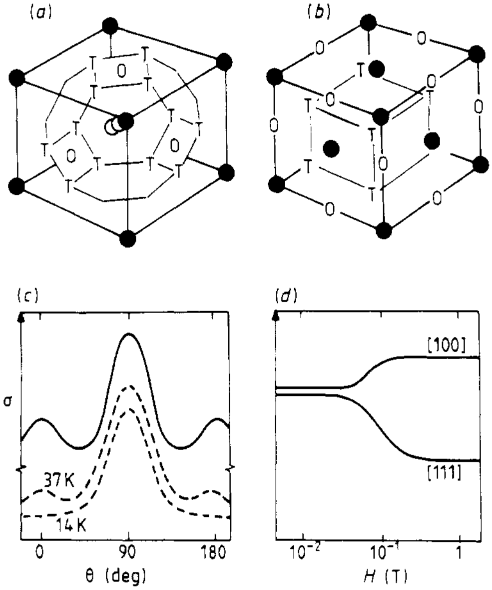

Figure 33. Site determination. The interstitial tetrahedral (T) and octahedral (O) sites are shown for the BCC lattice in (*a*) and for the FCC lattice in (*b*). These may be distinguished by the orientation (*c*) or field (*d*) dependence of the μSR linewidth. The full curve in (*c*) sketches the prediction for BCC tetrahedral sites in Nb; the dotted curves represent the experimental results of Gygax *et al* (1984c) at two different temperatures. The curves in (*d*) sketch the predictions for the octahedral sites in Cu and are confirmed by the results of Hartmann *et al* (1980) at 2 K and at 100 mK.

around 15 K (Hartmann *et al* 1980). In Cu, also FCC, the octahedral site is favoured at all temperatures (figure 33(*d*))—see § 7.3.1. The occupation of metastable sites has also been invoked in certain instances (see, e.g. Teichler and Seeger 1981, Browne and Stoneham 1982).

5.2. *The small-polaron model*

The microscopic disturbance caused by the introduction of an interstitial muon in an otherwise perfect metal lattice is depicted in figure 34. Since the muon (or proton) is positively charged, its introduction will

(i) attract conduction electrons, increasing their charge density in its immediate vicinity (this is the screening charge, touched on in § 3); and

(ii) distort the lattice locally, by repelling the neighbouring nuclei (since the screening cannot be totally effective at short range).

The whole entity is called a small polaron. This concept, which is borrowed from transport theory (specifically the description of localised electron and hole states; see, e.g. Holstein 1959), is now generally considered appropriate to the description of hydrogen in metals as well (see, e.g. Kehr 1978, Hempelmann 1984). The interstitial potential is altered at the site occupied by the impurity: the particular well is deepened by its presence. If this deepening is sufficient to localise the particle wavefunction, as is invariably the case for muons and protons, the particle is said to be self-trapped.

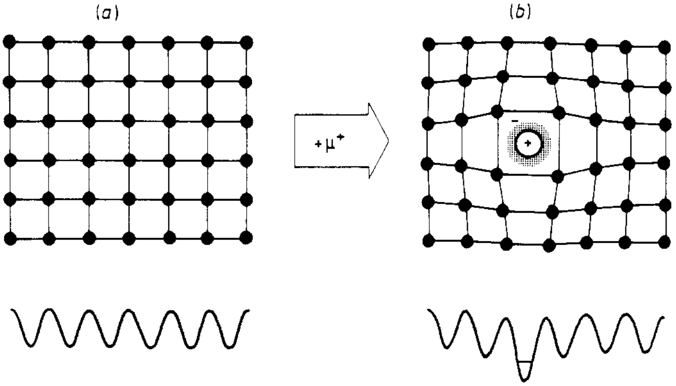

Figure 34. Self-trapping or localisation of muons or protons in metals. In the perfect lattice, the interstitial potential (as measured by a probe that does not perturb its surroundings) is periodic (*a*). The distortion of the lattice on introduction of a charged interstitial impurity, and the consequent lowering of the potential of the occupied site are illustrated in (*b*).

Displacements of the nearest neighbours are estimated to be typically a few per cent of the inter-atomic spacing (see, e.g. Camani *et al* 1977, Perrot and Rasolt 1981)†.

For more distant neighbours, this lattice strain should fall off fairly gradually, as a power law in distance (see e.g. Stoneham 1969, 1984a) although the total disturbance is usually treated as confined to a single unit cell. Screening is discussed in relation to the preferred muon sites and the likely diffusion paths through the lattice by Estreicher and Meier (1983). The gross features of the screening charge fall off exponentially with distance (i.e. much more rapidly than the strain field, the muon potential often being screened within less than a lattice spacing; see § 3). The longer-range Friedel oscillations (cf. figure 16) can also be significant, however, via their interaction with the lattice potential. In an elementary harmonic oscillator model, the zero-point energy of a muon will be greater than that of a proton in the same well by a factor $(m_p/m_\mu)^{1/2} \simeq 3$. The wavefunction is correspondingly more extensive and tunnelling probabilities greater. (The lowest level for muon corresponds approximately to the first excited level for a proton. Excited vibrational states for the muon are likewise more widely spaced so fewer, if any, are bound than for the proton; they play no significant role in the muon mobility at temperatures investigated to date.)

The question arises of how the self-trapped polaron—the interstitial muon or proton—can move fron one site to the next, given that the screening charge must also be transferred, and the metallic ions relaxed about the new position. The problem may often be formulated as follows. Supose that the lattice is rigid and insulating and that the particle is initially located at a particular interstitial site. The subsequent leakage of its wavefunction onto a neighbouring site is determined by a tunnelling matrix element J_0. Variously known as the 'transfer' or 'hopping' integral, this is the overlap of the muon wavefunctions describing localisation at adjacent sites, $J_0 = \langle \psi^{\mathrm{i}}_\mu | \psi^{\mathrm{f}}_\mu \rangle$. In real metals the tunnelling matrix element is reduced from this value, both by the elasticity of the lattice and by the presence of the conduction electron gas. The mobility is reduced when the particle has to drag with it a distortion field and a screening charge, i.e. when the muon

---

† The experimental estimate of the distortion in Cu (Camani *et al* 1977) was deduced via expression (5.2) assuming the muon to be static in the lattice; allowance for the degree of mobility which is now known to exist (see § 5.4) suggests that the distortion may in fact be much less than was first thought (Brewer 1986).

is 'dressed' with clouds of phonons and electrons. Equation (5.3) assumes that these two effects can be represented by separate factors (both less than unity):

$$J_{\text{eff}} = J_0 \langle \psi_L^i | \psi_L^f \rangle \langle \psi_E^i | \psi_E^f \rangle . \tag{5.3}$$

The elastic reduction factor represents the overlap of the wavefunctions ψ_L which describe the lattice, relaxed about adjacent sites. This may be written in the form $\langle \psi_L^i | \psi_L^f \rangle = \exp(-S)$ where the parameter S, in the zero-temperature limit, characterises the ratio of the relaxation energy (the elastic energy of distortion) to the Debye energy (Stoneham 1972, Kehr 1978). The softer the lattice, the smaller the factor, i.e., tunnelling is suppressed for a muon carrying a long-range distortion field. For illustration, $\langle \psi_L^i | \psi_L^f \rangle (T = 0) \simeq 0.01$ (i.e. $S \simeq 4.5$) is estimated for muons tunnelling between octahedral sites in copper. How this is modified at finite temperatures, when thermal fluctuations may create configurations that enhance or induce tunnelling, is the subject of § 5.3.

The electronic reduction factor is likewise the overlap of the electronic wavefunctions ψ_E when the screening charge is centred at adjacent sites. The problem of the ability of the screening charge to follow the muon motion has only recently been addressed (Kondo 1984, Yamada 1984). Substantial further reductions are calculated at low temperatures, e.g. $\langle \psi_E^i | \psi_E^f \rangle \simeq 0.01$ for Cu at 1 K. This is the subject of §§ 5.4 and 5.6.

The mechanism by which the polaron state is formed following implantation of the muon is considered in § 5.5. Its subsequent motion may be described from two different standpoints. One is the assumption of an *incoherent* or 'hopping' motion from site to site, step by step in a random walk. In the detailed theories, the probability of such a step is then calculated from the effective tunnelling matrix element J_{eff} via various formulations of Fermi's Golden Rule (5.4):

$$W \simeq J_{\text{eff}}^2 \rho_{\text{eff}} . \tag{5.4}$$

Here ρ_{eff} is an appropriate density of final states and the transition probability W is often referred to as the 'hopping rate' or inverse 'jump time'. (This latter term is inappropriate since the muon spends a far greater proportion of its time localised at particular sites than is involved in the jumps themselves, i.e. the overlap J_0 is small—the muon wavefunction ψ_μ has no significant amplitude *between* its preferred sites.) Inverse 'residence time' is a better choice of words, and is adopted in the following. It is common to relate this to a diffusion coefficient D, as in (5.5), where d is the step length and z is a coordination number representing the choice of neighbouring interstitial sites. For isolated muons, D is a notional quantity; of interest is the comparison with diffusion constants deduced for protons by other means:

$$D = (1/z) d^2 W . \tag{5.5}$$

An alternative approach is to attempt the construction of band-like or Bloch states describing the *coherent* propagation of the small polaron through the lattice. Here, to within a numerical factor, J_{eff} describes the band width of such states. (In a tight-binding description, $B = 2zJ_{\text{eff}}$.) In this description, temperature-dependent factors in the muon diffusion are best displayed via the classical expression (5.6), where v is the (group) velocity of the propagating state and Λ its mean free path between scattering collisions (or, equivalently, $\tau_{\text{tr}} = \Lambda / v$ is a transport lifetime):

$$D = v\Lambda = v^2 \tau_{\text{tr}} . \tag{5.6}$$

The RMS velocity v takes its average value $J_{\text{eff}} d$ over the polaron band, or its classical value $3kT/m$, according as the band width is less or greater than the thermal energy kT (Kehr *et al* 1982). Scattering mechanisms are considered in § 5.4. Whether the concept of coherent motion is valid if kT exceeds the band width, whether tunnelling without dissipation is ever observed and whether the apparently competitive descriptions of coherent and incoherent motion can be reconciled are considered in § 5.6.

5.3. *High-temperature mobility*

At high temperatures—but not high enough for a classical over-the-barrier motion—there seems little doubt that the motion is by incoherent tunnelling, and that the process is phonon-assisted. An appealing description is that the phonons 'dig a hole' for the muon or proton. The usual picture is that shown in figure 35: the lattice vibrations momentarily equalise the potential wells at adjacent sites, allowing the muon to tunnel through the remaining barrier.

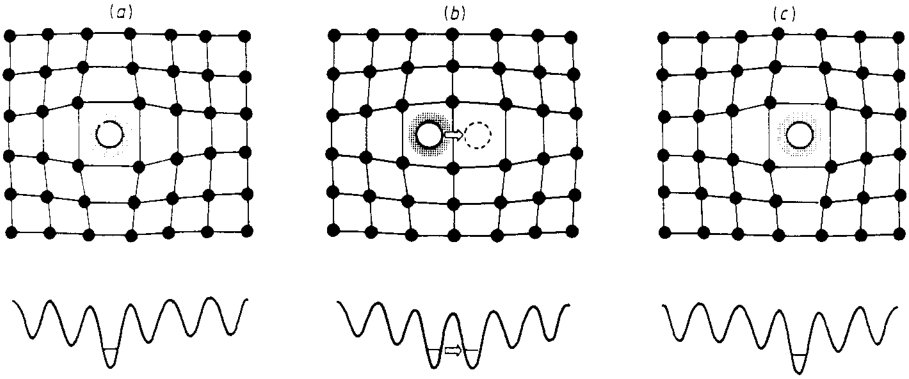

Figure 35. The elemental step in intrinsic diffusion via phonon-assisted tunnelling. Thermal fluctuations provide a favourable intermediate configuration, (*b*), for tunnelling between initial and final states, (*a*), (*c*).

The mobility of the muon increases with temperature in this phonon-assisted process, and this shows up in the temperature dependence of the μSR linewidth. Whilst the muon is immobile, the linewidth shows a plateau whose value characterises the static dipolar sum (5.2). At higher temperatures, where the muon begins to move, it averages over differences of the local field at different sites and a reduction of the μSR linewidth is apparent (Gurevich *et al* 1972). This is motional narrowing, common in NMR. The timescale on which the muon changes its magnetic environment is characterised by the residence time, $1/W$. In the limit of rapid motion, $\gamma_\mu\langle\delta H^2\rangle^{1/2}/W \ll 1$, the profile of the μSR precession signal is not gaussian, as in (5.1), but exponential, as in (5.7), so W may be extracted from the damping rate. Equivalently, the μSR lineshape goes over from gaussian, when the muon is static in the lattice, to lorentzian, when the muon is diffusing rapidly.

$$P_x(t) = P_x(0)\exp(-\lambda t) \qquad \text{with } \lambda = \gamma_\mu^2\langle\delta H^2\rangle/W. \tag{5.7}$$

(Equation (5.2) for $\langle\delta H^2\rangle$, the mean square local field at the muon site due to the nuclear dipoles, remains valid in this expression.) The correspondence can be made here between this narrowing due to spatial motion, and the exchange narrowing of the μSR line in certain magnetic materials, where the magnetic environment of the muon is fluctuating due to rapid flips of the host spins; cf equations (3.1) and (3.2)).

Early results for Cu are a textbook example of this behaviour, and are sketched in figure 36 (Gurevich et al 1972, Grebinnik *et al* 1975). These show a temperature dependence with an Arrhenius form $W = \nu_0 \exp(-E_a/kT)$, but with an activation energy E_a and a pre-exponential factor ν_0 which are both very much lower than would be expected for classical over-the-barrier hopping. This is a clear indication that the motion is via quantum mechanical tunnelling *through* the inter-site barriers and it is generally accepted that the process is adequately described by the mechanism of phonon-assisted tunnelling devised for hydrogen diffusion by Flynn and Stoneham (1970). The model has been adapted for muon diffusion by various authors (e.g. Kagan and Klinger 1974, Teichler 1981, Emin 1981). Referring to figure 35, energy is taken from the phonon bath between frames (*a*) and (*b*). Between (*b*) and (*c*) it is given back, but redistributed amongst the phonon modes. This identity of the initial and final polaron energies causes some mathematical difficulties in the calculation of the transition probability; these are resolved in different ways by the above authors. The essential feature is that E_a represents the energy required to create a configuration in which adjacent levels are momentarily coincident (frame (*b*)), allowing tunnelling to occur, and that this is much less than the static inter-site barrier. Here it is noteworthy that whereas the proton exhibits this sort of tunnelling in BCC lattices, the heavier particle cannot squeeze between the intervening atoms so readily in FCC lattices. In these latter the step length is longer and the overlap integral J_0 is correspondingly smaller; protons are restricted to almost classical behaviour. Over-the-barrier motion has not been reported for muons in any metal. Certainly somewhat different behaviours are found in the BCC and FCC metals, so the tunnelling models have to be extended beyond the Condon approximation (Flynn and Stoneham 1970, Teichler 1981). The Flynn and Stoneham description appears to be satisfactory in the BCC metals; in other lattices complications due to inequivalent sites, excited states, or perhaps local tunnelling, may modify the description (Stoneham 1984a).

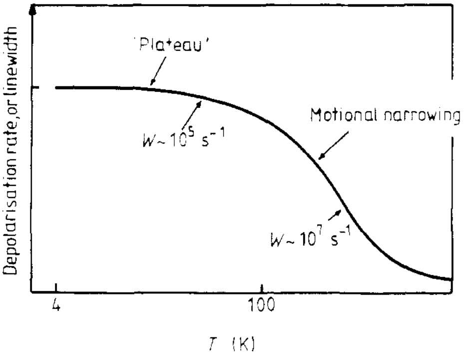

Figure 36. The temperature dependence of the μSR linewidth in copper indicating the onset of muon mobility above liquid He temperatures. (This is the qualitative behaviour: in a precise characterisation of the width of the μSR line one must bear in mind that this changes from gaussian in the 'plateau' to lorentzian in the motionally narrowed regime.)

These processes, characterised by the exponential temperature dependences are 'multi-phonon'. The power-law dependences (T^7 or T^9) predicted for two-phonon processes at somewhat lower temperatures (Flynn and Stoneham 1970, Kagan and Klinger 1974, Fuji 1979) have not been reported and are perhaps only effective over too narrow a range of temperature. Single-phonon or 'direct' processes are forbidden when the initial and final polaron energies are identical. They become allowed, however, when this degeneracy is lifted, e.g. when inequivalent sites are involved, or when the potential wells at adjacent sites are detuned by static strains, e.g. in the neighbourhood of defects or impurities. In this latter case, a characteristic 'downhill' motion is expected towards the deepest trap, as in figure 38(*c*). Single-phonon processes should be characterised by a direct proportionality to temperature (Teichler and Seeger 1981, Yaouanc 1982). Although they have not been identified with certainty, it is noteworthy that lower power laws (T^n with $\frac{1}{2} < n < 2$) are common over restricted temperature ranges. Thus this could involve the changeover from octahedral to tetrahedral sites in Al (Kehr *et al* 1981) or the strain field from Ni impurities in Cu (Chappert *et al* 1982).

5.4. *Low-temperature mobility*

A surprise came at temperatures in the dilution refrigerator range. The *complete* information for pure copper, sketched in figure 37(*a*), indicates an apparent motional narrowing at low temperatures too (Hartmann *et al* 1980, 1981). This is most pronounced *below* 1 K. More recent measurements by zero-field μSR, a technique described in § 7, confirm that this is indeed a motional effect rather than a reduction of static linewidth due to a site change (Clawson 1984). Experimental results for Cu from various sources have been collected together by Kadono *et al* (1984); the overall temperature dependence of the inverse residence time or hopping rate has the form sketched in figure 37(*b*)†.

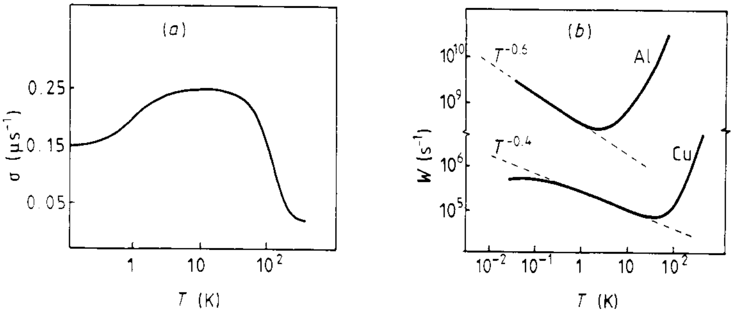

Figure 37. The temperature dependence of the μSR linewidth in copper (*a*), including the low-temperature behaviour (sketched from Hartmann *et al* 1981). A compendium of results for the extracted hopping rate or inverse residence time is sketched in (*b*) from Kadono *et al* 1984). Also included in (*b*) are the corresponding results for Al (from Kehr 1984); note that the behaviour is different in magnitude but similar qualitatively. In the high-temperature domain to the right of the minima, the tunnelling is phonon-assisted (cf figure 35); in the low-temperature domain to the left of the minima the tunnelling is without lattice excitation, but movement of the screening charge requires the excitation of electron–hole pairs (cf figure 41).

---

† The hopping rates in figure 37(*b*), as low as $10^5\ \mathrm{s}^{-1}$, are particularly noteworthy. Thus neutron scattering is sensitive to much faster rates in the range 10^9–$10^{12}\ \mathrm{s}^{-1}$ and for this reason (as well as the hydrogen solubility requirement) is more suited to studies around room temperature. Referring to (5.7), faster hopping rates are accessible to μSR in the presence of atomic, rather than nuclear magnetism, e.g. in α-Fe (Seeger 1984b, c).

An attractive interpretation of the low-temperature results, in which the mobility increases again as the temperature is lowered, is that these represent *coherent* tunnelling. In contrast to stepwise incoherent motion this implies band-like states in which the muon wavefunction is not localised at a particular site, as depicted in figure 34, but instead is extended over many lattice spacings. (The associated lattice distortion is likewise distributed—this is a property that distinguishes this hypothetical propagating state of the small polaron from the 'free' state of the energetic muon on entry into the sample.) The muon is to be envisaged as travelling as a wave packet—a superposition of Bloch-like polaron band states—which is scattered intermittently, with the coherence of its wavefunction destroyed at each scattering collision, as expressed in (5.6). Then it is possible to determine an effective inverse residence time by the somewhat dubious procedure of equating (5.5) and (5.6), giving $W \simeq (v^2/d^2)\tau_{\mathrm{tr}}$. Intuitively at least (although see § 5.6) one would expect the scattering process to increase with temperature so that coherent diffusion decreases, whereas incoherent diffusion requires thermal excitation and increases with temperature, consistent with the turnover in the qualitative behaviour that is apparent in figure 37.

In the purest samples of aluminium, the muon mobility in the dilution refrigerator range has likewise been taken as evidence of coherent tunnelling (Hartmann *et al* 1980). In fact in Al, unlike Cu, the depolarisation rate is low at *all* temperatures, i.e. the intrinsic diffusion is always rapid, so it is necessary to provide traps to immobilise the muon by deliberate doping with impurities, in order to give a measurable linewidth and to enable deductions about the intrinsic mobility to be made. Of the various dopants used, substitutional Mn is particularly suitable for this purpose as it is a gross misfit in the regular lattice and creates a large local strain. Assuming the muon to encounter these traps at a diffusion-limited rate, a diffusion constant varying as $T^{-0.6}$ is found between 35 mK and 1 K (Kehr *et al* 1982). This is not dissimilar to the $T^{-0.4}$ dependence at low temperature in Cu. The overall behaviour for Al is also sketched in figure 37(*b*) (from Kehr 1984).

These temperature dependences have to be compared with the expectations for various different scattering processes. The most obvious would seem to involve lattice imperfections, i.e. vibrations and defects. In fact phonon scattering is readily discounted, as it would be characterised by a very much stronger variation, namely as T^{-7} or T^{-9} (Kagan and Klinger 1974). There is also an enormous discrepancy in the magnitudes of the observed and calculated diffusion constants (Jäckle and Kehr 1983). The general question of the effectiveness of dissipative coupling between tunnelling states and the lattice has been raised by Leggett (1984). He notes that an ω^3 phonon spectrum (or indeed any low-power law that does not have some additional intensity at low frequencies, e.g. local modes) should not in principle result in localisation on a particular site, although the tunnel splitting may be reduced so much that mobility is no longer observable in practice.

Mechanisms involving point defects are discounted by Kehr *et al* (1981), on the grounds that these would give a scattering rate for long-wavelength propagating states that is independent of muon velocity, and therefore independent of temperature. Of course, strain fields may destroy the coherent states not by scattering them between different wave-vectors but by capture. For instance the muon motion may not be uniform, but may proceed by coherent propagation until a deep trap is encountered. The problem of localisation versus coherence is illustrated in figure 38 for the case of a two-well potential. The particle remains located in the lower well if the potential minima are detuned by more than half the tunnel splitting. A similar criterion, relating the

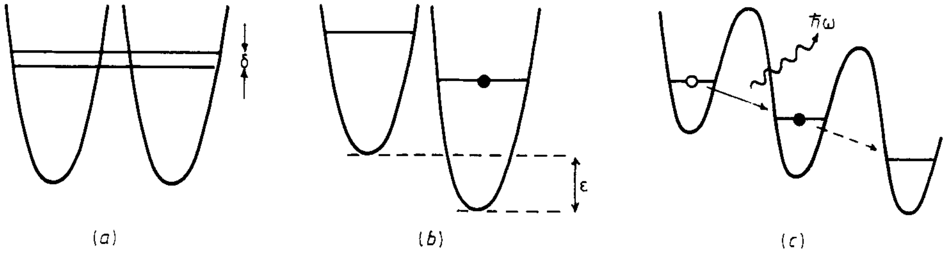

Figure 38. Coherent tunnelling states in a two-well potential (*a*) suppressed by detuning, $\varepsilon > \frac{1}{2}\delta$, which is the criterion for localisation in the lower well (*b*). Incoherent tunnelling between inequivalent wells may be achieved by single-phonon processes, as in (*c*). (When the strains at adjacent sites are correlated, e.g. near an impurity, the muon motion is then characteristically 'downhill' towards the deepest well.)

distribution of potential minima to band width, holds for the extended case. To within a numerical factor, this is $\varepsilon \geqslant B$, where here B is the band width in the absence of strain, and ε is the critical width of the strain distribution (Karlsson 1982), i.e. the minimum strain that is necessary to induce localisation (Browne 1982). Typically the strain due to point defects lies in an appropriate range: $1\ \mathrm{K} < \varepsilon/k_{\mathrm{B}} < 10\ \mathrm{K}$ (Stoneham 1969). This question is reconsidered in § 5.5 below where an alternative interpretation of the experimental results and of the role of impurities is presented.

For uniform motion, the proposition of Jäckle and Kehr (1983) is that collision with conduction electrons is the scattering mechanism that had previously been overlooked. Their model predicts a T^{-1} dependence for the diffusion coefficient, which may be traced from the elementary formula (5.6) as follows. On the assumption that the muon mobility is not limited by the transfer rate (i.e. band width $2zJ_{\mathrm{eff}} \gg kT$) the mean kinetic energy is given its classical value, kT, so v^2 is proportional to T. The scattering rate, τ_{tr}^{-1} is found to be proportional to T^2, with one factor of T representing the fraction of conduction electrons susceptible to scattering to unoccupied states across the Fermi surface, and a further factor of T representing the decrease in scattering angle with decreasing temperature (somewhat reminiscent of the Bloch theory of conductivity). Hence D is proportional to T^{-1}, close to the observed qualitative dependence in Al ($T^{-0.6}$) and Cu ($T^{-0.4}$). The derivation by Jäckle and Kehr (1983) of the *magnitude* of D, by the standard methods of transport theory, nonetheless gives values very much greater than those determined experimentally.

The remaining discrepancy arises from an inadequate treatment of the screening charge cloud which, in the coherent propagation model, turns out to be the dominant source of scattering. Yamada (1984) points out the neglect of the overlap integral between screening clouds at adjacent sites, i.e. the electronic reduction factor in the evaluation of J_{eff} by equation (5.3). This factor was first evaluated by Kondo (1976) as

$$\langle \psi_{\mathrm{E}}^{\mathrm{i}} | \psi_{\mathrm{E}}^{\mathrm{f}} \rangle \sim (T/\Delta)^{K}. \tag{5.8}$$

Here Δ is not precisely defined, but is of the order of the *electronic* band width or Fermi energy (see below) and K is a muon–electron coupling constant characterising the phase shift of the scattered electrons. This factor reduces the band width for coherent muon propagation to the point where it is less than the thermal energy: $B = 2zJ_{\mathrm{eff}} \ll kT$. The quantities in equation (5.6) then require a different interpretation. The mean square velocity takes the non-classical value:

$$\overline{v^2} \sim (J_{\text{eff}})^2 d^2 \propto T^{2K}. \tag{5.9}$$

The suppression of the tunnelling matrix element at low temperatures represents the fact that the screening cloud does not follow the muon adiabatically; electrons screening the muon at one site cannot screen it at another†. This temperature dependence is more than offset by that of the scattering rate, $\tau_{\text{tr}} \propto T^{-1}$, which arises from the width of the thermal energy shell at the Fermi surface. Using (5.6), the overall temperature dependence is

$$D \propto T^{2K-1}. \tag{5.10}$$

The coupling constant K cannot exceed 0.5 (Yamada *et al* 1983) so the exponent is always negative, and values of K may be chosen to fit the low-temperature data exactly (i.e. $K = 0.3$ to give $T^{-0.4}$ for Cu; $K = 0.2$ to give $T^{-0.6}$ for Al).

It is now clear, however, that this qualitative agreement is not necessarily evidence for coherent propagation. These temperature dependences may also be fitted on the basis of incoherent tunnelling, when the factor (5.8) is incorporated in the calculation of inverse residence time. This most recent model, due to Kondo (1984, 1985), is described in § 5.6, following a further account of the historical development of the subject (especially with regard to the understanding of impurity effects) in § 5.5.

5.5. *Polaron formation and the role of impurities*

In the absence of a measurable depolarisation rate, mobile muon states that may have quite different characters cannot be distinguished. The question arises in particular as to whether the undamped precession signal represents an intrinsically mobile polaron, as implied above, or whether the polaron is not formed, i.e. the muon does not reach its ground state within its 2 μs lifetime. Polaron formation cannot be immediate, for while the muon has some residual kinetic energy after implantation it will be moving at a speed that does not allow the lattice to respond to its presence. It is then in a 'free' state. Polaron states are lower in energy, but there may be a barrier to their formation (Emin 1981); or there may be a delay because the free state represents propagation via sites having a different symmetry from that of the thermodynamically stable site, so conversion is forbidden by a selection rule. That is, the free states (even those close to thermal energy) may be metastable (Browne and Stoneham 1982).

At high temperatures, it is generally agreed that thermal fluctuations in the atomic positions will induce the transition to the polaron state, and that this will occur at random in the lattice. At low temperatures the mechanism is less certain, and Browne and Stoneham (1982) go so far as to argue that the incoming muons are able to lose their residual kinetic energy, and finally thermalise with the lattice, only by virtue of their collisions with impurites, forming small polarons preferentially in their vicinity (figure 39). This alternative model avoids an embarrassing feature of the standard picture, which is that the hopping rates extracted from μSR data are often too low to explain how otherwise the muons can find the impurity within their lifetime!

---

† An 'orthogonality catastrophe' at zero temperature, $\langle \psi_{\text{E}}^{\text{i}} | \psi_{\text{E}}^{\text{f}} \rangle \rightarrow 0$ as $T \rightarrow 0$, is in fact avoided in a detailed treatment based on a propagating model. The muon motion is represented in the eigen-states (rather than as a perturbation as for the hopping model, see § 5.6) so inclusion of the muon's recoil energy on collision with electrons excludes the possibility of zero-energy excitations. The comparison with the diffusive behaviour of positrons in metals is instructive here.

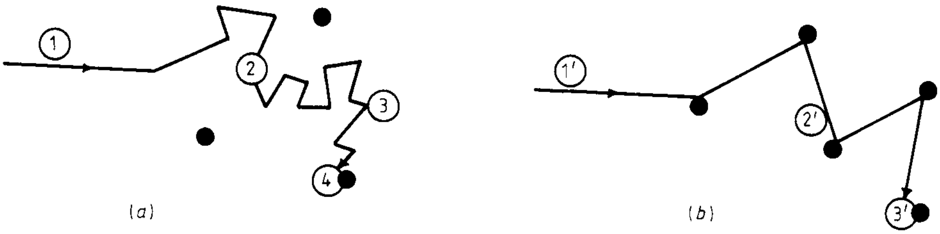

Figure 39. Representations of polaron formation and pinning. (*a*) Standard picture: (1) incoming muon ('free' state); (2) polaron formation at random in lattice; (3) random walk diffusion; (4) chance encounter with an impurity (pinned if the trap is sufficiently deep). (*b*) Alternative picture (Browne and Stoneham 1982, Stoneham 1984a): (1′) incoming muon ('free' state); (2′) thermalisation by collision with impurities or defects only; (3′) preferential polaron formation in close proximity of an impurity (pinned immediately if the trap is deep; subsequent thermal diffusion if the trap is shallow).

Thus the low-temperature results in Al doped with Mn may be understood in terms of capture-limited processes (Browne and Stoneham 1982), as opposed to diffusion-limited processes (Kehr *et al* 1981). Local static strain may be sufficient in itself to localise the muons (cf figure 38), or it may lower the threshold at which thermal strain is effective—in this sense impurities or defects are said to 'catalyse' polaron formation. The different characteristics in this regard of random strain, as in amorphous materials, and of correlated strain, as in the vicinity of impurities in crystals, are emphasised by Stoneham (1984a).

Particularly detailed studies of the effects of impurities have been performed for the case of niobium. Nb typifies metals having a BCC lattice, that is, it has a more open structure in which polaron formation may be more difficult than in the close-packed FCC lattice of Al or Cu. (Tunnelling matrix elements are greater in BCC than in FCC lattices, so the muon may not remain at one site long enough for the lattice to relax about it; Emin (1981) gives as a criterion for immediate polaron formation that the muon residence time should exceed a vibrational period (see also Karlsson 1982).) The results for Nb are sketched in figure 40. Low depolarisation is found at all temperatures in ultra-pure samples. The experimental techniques are noteworthy here since measurements below the superconducting transition, as in Al, must be performed in zero field (see § 7)

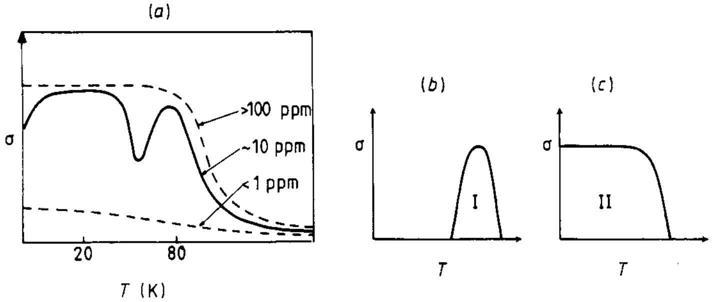

Figure 40. The μSR linewidth in Nb samples of various degrees of purity ('dirty', 'intermediate' and 'ultra-pure'), sketched from Hartmann *et al* (1983), (*a*). This temperature dependence may be simulated by a superposition of features, (*b*), (*c*), associated with different trapping behaviours as described in the text.

and scaled for comparison with the transverse-field measurements made at higher temperatures (Hartmann *et al* 1983). In dirty samples (>100 ppm impurities) a plateau is found in the depolarisation rate below 80 K, but this resolves itself into a more detailed structure for samples of intermediate purity (around 10 ppm). A low-temperature feature is associated with shallow traps in the vicinity of substitutional impurities (typically other metals or carbon). The peak at higher temperatures is associated with deeper traps—deeper because a higher temperature is required to secure the muon's release. These are in the vicinity of interstitial impurities (typically 'gases', e.g. nitrogen or oxygen)†. This assignment is elegantly confirmed by very well characterised samples of niobium doped with substitutional tantalum and interstitital nitrogen (Hartmann *et al* 1983, 1984)‡.

Notice that the structure in the temperature dependence is able to give some indication of whether the muons are immobilised promptly by the impurity or not. Thus for polarons that are formed at random in the lattice, a certain minimum temperature may be required before impurity trapping is effective, i.e. before the intrinsic mobility is sufficient for the muon to explore the lattice and *find* the impurity. Higher temperatures still are required for its subsequent escape. This gives a feature of type I (figure 40(*b*)). Polarons formed preferentially at an impurity, however, may be immobilised immediately. This gives a feature of type II (figure 40(*c*)). Such features are incorporated in the simulation of the μSR data by Hartmann *et al* (1983). It is interesting that even in the dirtiest Nb samples the maximum μSR linewidth falls short of the calculated static or Van Vleck value (5.2); this tends to suggest that there is always a proportion of implanted muons that remain mobile in this material and perhaps never form polarons.

Monovacancies provide especially deep traps for the muon. Thus when these are created in sufficient concentration by electron irradiation in Al, for example, a broad trapping peak appears in the depolarisation rate at correspondingly high temperature (Herlach 1981, Arnold *et al* 1984). The feature disappears on annealing. (Studies of vacancy trapping in magnetic metals are noteworthy here since the substitutional muon, e.g. in Fe, and even the substitutional muon which is pinned at a chemical impurity, e.g. in FeSi, may be distinguished from the interstitial muon by shifts in the μSR frequency (Weidinger 1984a)).

These considerations inevitably case some doubt on the interpretation of the results for Cu. Does the plateau in figures 36 and 37 really represent the intrinsic behaviour? Well there is no clear evidence for any impurity effects in Cu—the plateau is not lowered in ultra-pure samples; nor can one blame natural randomness of the Cu lattice due to the normal mixture of isotopes—the behaviour is not changed in isotopically enriched samples (Walter *et al* 1984)—so for the moment the interpretation of entirely intrinsic behaviour in Cu must be given the benefit of the doubt, and the difference from that of Al remains something of a mystery.

Suffice it to say that there is at present no general consensus on the precise mechanisms of the final stages of equilibration with the lattice, whether this is necessarily always achieved within the muon lifetime and, if so, whether polaron formation is induced by static or by thermal strains, or by a combination of the two.

---

† Neutron scattering results for protons trapped near oxygen impurities in niobium are particularly interesting and show peaks characteristic of tunnelling states, i.e. of coherent local tunnelling between a small number of adjacent sites (Wipf *et al* 1984). This is to date the only clear example of such behaviour.

‡ So sensitive is the depolarisation rate to impurity levels, and so specific is the role of each impurity, that μSR has even been proposed as a means of checking metallic purity and performing a trace analysis (Seeger 1979).

5.6. Kondo theory

A general treatment of the elemental diffusive step in terms of dissipative tunnelling of the localised small polaron has recently been devised by Kondo (1984, 1985). The theory can accommodate diffusion in both metallic and non-metallic lattices, covering the whole of the temperature range that has been investigated experimentally. To date it has been compared explicitly only with the data for Cu, which it explains very satisfactorily, modelling in particular the low-temperature mobility and the transition to thermally activated tunnelling at higher temperatures. Comparison with the data for Al also looks extremely promising.

Two principal features may be noted in Kondo's treatment of the screening charge cloud. Firstly, his expression (5.8) for its overlap at adjacent sites is incorporated. Its movement from one site to the next is described in terms of the excitation of electron–hole pairs, which is seen as becoming too slow at low temperatures for the cloud to follow the muon adiabatically. Secondly, the inclusion of electron–hole excitation gives a spread in energy δE to the final state of the dressed polaron, depicted in figure 41. This allows a straightforward calculation of the transition probability or hopping rate W from one site to another in terms of Fermi's Golden Rule (5.4), where the density of states $\rho_{\rm eff}$ is the inverse of the level broadening δE. It expresses the sharpness of the Fermi surface (i.e. δE is the width of the thermal energy shell), so at low temperatures $\rho_{\rm eff} \propto (kT)^{-1}$. This term dominates the temperature dependence and avoids the 'orthogonality catastrophe' which is suggested by (5.8). The overall dependence is

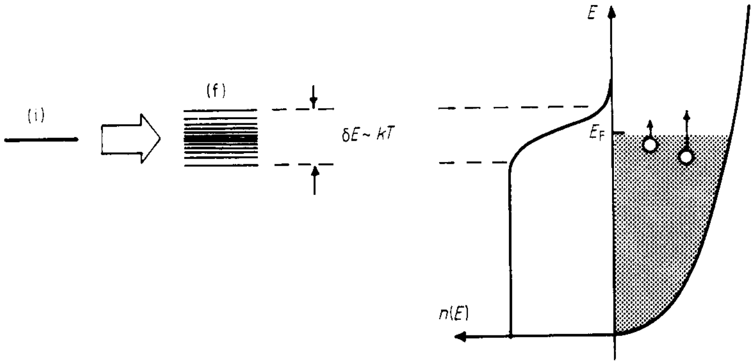

Figure 41. The polaron transition from an initial state (i) to a final state (f) whose energy level is broadened by excitation of electron–hole pairs across the Fermi surface. The tunnelling transition can occur only if energy is conserved, and is therefore facilitated by a high density of final states, i.e. a small energy spread $\delta E \sim kT$ (Kondo 1985).

$$W \propto T^{2K-1} \tag{5.11}$$

which is identical with the dependence (5.10) deduced for the diffusion constant in the propagating model and may likewise be fitted to the low-temperature data for Cu with $K = 0.3$, and for Al with $K = 0.2$. The correspondence between the two models is further underlined by the relation (5.5), and by noting the connection between Kondo's excitation of electron–hole pairs and Yamada's scattering of electrons from initial (occupied) to final (unoccupied) states. For Cu, the absolute *magnitude* of W may also be fitted, assuming $\Delta/k\theta_D = 100$, with the parameters $J_0 = 3.5$ K, and $J_0 e^{-S} = 0.064$ K, i.e. $S = 4$. The inequality (5.12) then holds throughout the temperature range investigated:

$$W/J_{\text{eff}} \ll 1. \tag{5.12}$$

This justifies the hopping model as the more appropriate physical picture for Cu; it indicates that coherence of the muon wavefunction is *not* preserved in the elemental step, even in the lower-temperature regime. The parameters for Cu indicate that coherently tunnelling states would only be a useful concept at unattainably low temperatures, i.e. $W/J \sim 1$ at $T \sim 10^{-4}$ K! For Al, matrix elements an order of magnitude greater are estimated so the validity of the coherent tunnelling concept in this or other materials is certainly not excluded.

The manner in which the Kondo theory accommodates the transition between the 'low'- and 'high'-temperature domains is sketched in figure 42(*a*). There are two key points here. Firstly the turnover in the temperature dependence does not indicate the changeover from incoherent to coherent tunnelling, but is accommodated within the incoherent model. Instead it represents the temperature at which the screening charge begins to become a drag on the muon motion. The very different temperature dependences in the two domains originate in the density-of-state functions $Q(\omega)$ for the relevant excitations. At low temperatures this is electron–hole excitation, with $Q(\omega) = 2K/\omega$, i.e. a high density of states at zero excitation energy, $\omega = 0$. At high temperatures this is phonon excitation with $Q(\omega) \propto \omega^3$, resulting in the Arrhenius-type temperature dependence above about $0.1\theta_D$†. Secondly, the low-temperature dependence is indistinguishable from that calculated by Yamada (1984). Contrary perhaps to intuition, any

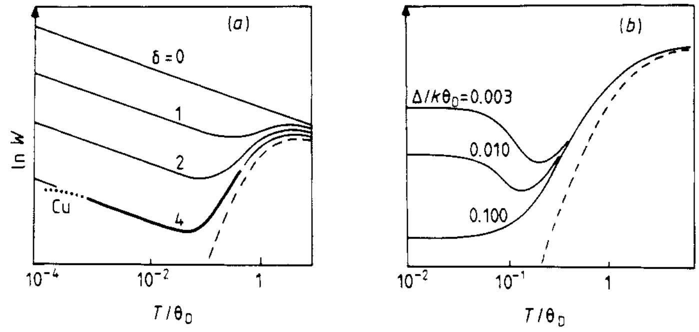

Figure 42. The predictions of Kondo (1984) for the hopping probability of a small polaron in (*a*) a metallic lattice and (*b*) an insulating lattice, but with random strains. The Arrhenius-type temperature dependence of phonon-assisted tunnelling (i.e. the prediction of the Flynn and Stoneham (1970) model) is shown as a broken curve. The region in which the data for Cu may be fitted is indicated in (*a*) (compare figure 37(*b*)). Good fitting is extended to low temperature by inclusion of static strain in the metallic case (dotted curve).

---

† The Huang–Rhys factor $Q(\omega)$ is dependent on the structure; $Q(\omega) \propto \omega^3$ corresponds to the octahedral site in an FCC lattice, as appropriate here for Cu. For BCC lattice $Q(\omega) \propto \omega$. The curves of figure 42 are not greatly sensitive to this difference however.

eventual transition from incoherent to coherent tunnelling will not therefore be signalled by any break in the qualitative behaviour.

In non-metallic lattices, Kondo invokes static strains to provide the spread in final polaron energy that is necessary to his formulation of the Golden Rule. The predictions are sketched in figure 42(*b*). The mobility becomes independent of temperature when phonon-assisted tunnelling is no longer effective, with a large limiting value when the spread in energy is small. It is noteworthy that the inclusion of static strains in the metallic case will limit the indefinite increase in mobility predicted for very low T in figure 42(*a*). This satisfactorily explains the levelling-off of the hopping rate observed in Cu below 100 mK (figures 37(*b*) and 42(*a*)).

The Kondo theory appears to explain the μSR results for Cu very adequately and is attracting current attention accordingly. A close fit to the data is achieved with a small set of parameters. These are tightly constrained and all take apparently sensible values. Theorists should now address the proper calculation of these parameters. Thus the coupling constant K involves the muon–electron interaction potential and will subsume details of the charge-screening mechanisms. The parameter Δ must be related to details of the band structure of a particular metal. Experimentalists should likewise investigate the extent of its application to other systems, including non-metals. Stoneham (1985a) has suggested that the theory could be explicitly tested by investigating the change in behaviour at a superconducting transition. The zero-energy excitation of electron–hole pairs is then suppressed, and the term $(k_BT/\Delta)^K$ in the transfer integral replaced by a temperature-independent term $(\xi/\Delta)^K$, where ξ is the width of the superconducting energy gap.

5.7. *Metal hydrides*

These studies of localisation and diffusion are readily extended to the metal hydrides, and are of especial interest if the preferred sites for muons and protons are again identical in these systems. Figure 43(*a*) illustrates how the onset of motional narrowing is shifted

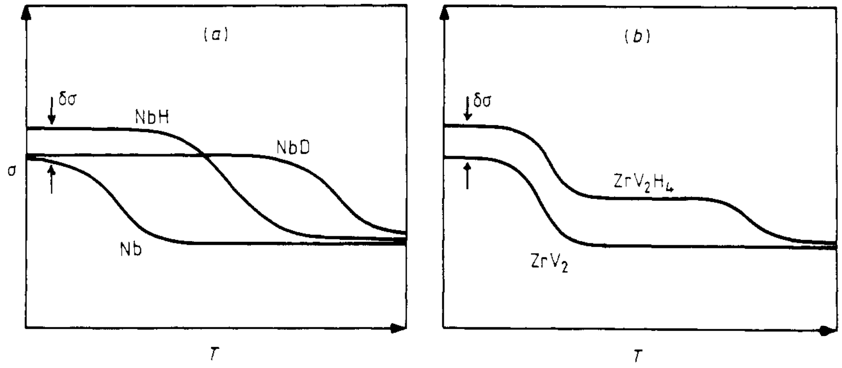

Figure 43. Muon mobility and muon–proton correlation in hydrides. The use of the muon as a tracer for hydrogen (or deuterium) diffusion is illustrated in (*a*). Motional narrowing at about 60 K in unloaded (although not too pure) Nb is shifted to about 170 K in the hydride and to about 200 K in the corresponding deuteride, reflecting the onset of mobility of the heavier isotopes. Partial narrowing in (*b*) may be attributed to a spatially limited or 'cage' diffusion in ZrV_2H_4. The extra depolarisation rate represents the wider distribution of local fields due to the protons.

to higher temperatures when the hydrogen concentration is above the percolation limit, i.e. when the muons cannot find connected paths through the structure. The majority of the preferred interstitial sites are then occupied by protons; the muons manage to find the few remaining empty sites on implantation but their subsequent motion is blocked unless the protons themselves are moving. Richter *et al* (1983) demonstrate that muons may be used in this manner as a radioactive 'tracer' for hydrogen diffusion. These authors give a detailed and systematic study of muon–proton correlation in the system NbH_x for a variety of concentrations x. Below the percolation limit ($x < 0.8$), the depolarisation rate depends in a somewhat complicated fashion on concentration and temperature. The irregularities coincide with known phase transitions, however, and so must reflect the different degrees of hindrance of the muon motion in the various sub-hydrides.

A stepwise descent of the depolarisation rate, observed in the intermetallic hydride ZrV_2H_4 by Hempelmann *et al* (1984), is sketched in figure 43(*b*). Not all the tetrahedral sites are occupied by protons in this material (as they would be in ZrV_2H_6). The authors attribute the partial narrowing to muon diffusion that is confined to a limited number of sites, e.g. within clusters of proton vacancies. Similar curves have been found in γ-TiH_x and γ-YH_x ($x \leqslant 2$) by Kossler *et al* (1986) but attributed by these authors to a change in muon site. In these nearly stoichiometric hydrides the implanted muon finds the majority of favoured tetrahedral sites occupied by protons and at low temperature may be constrained to occupy an unfavoured octahedral site. At higher temperatures the muon is better able to explore the lattice and find a vacant tetrahedral site.

In the unsaturated hydrides, i.e. those in which the metal lattice is loaded to less than its full capacity, the protons are not always randomly distributed. They can order on an interstitial 'superlattice', a process suggestive of a repulsive force between protons on adjacent sites. Since the individual charges are well screened, this repulsive force must represent the interaction of the strain fields surrounding individual polarons. It is interesting to conjecture whether the muon is sufficiently similar in its behaviour to participate in such a structure via a muon–proton repulsion. Preliminary results for $PdH_{0.64}$ (Cox *et al* 1984) indicate a dip in the depolarisation rate around 50 K, at which temperature the protons are expected to order. (The ordered structure of the corresponding deuteride is known from neutron diffraction, but a direct determination is precluded for the hydride by the huge spin-dependent or incoherent elastic scattering of neutrons from protons.) Fluctuations in the proton positions are very slow here so, assuming that the muons are also immobile, this is a structural rather than a dynamic study. The Van Vleck μSR linewidth (5.2) is due to the protons themselves in this material (the contribution from the Pd nuclei being small) and so reflects the average number of nearest-neighbour protons at the muon sites. The onset of short-range order amongst the protons as the transition temperature is approached from above, and the participation of the muons in the ordering as long as proton vacancies are available, are all evident from this study.

6. Studies of organic radicals

The behaviour of non-rigid molecules is the principal subject of this section, again illustrated by the effect of substitution for a proton of a muon (or, equivalently, for hydrogen of muonium, here covalently bonded in the molecule). In this area of dynamical studies, molecules exhibiting low-frequency or large-amplitude normal modes are receiving considerable current attention. (This follows earlier studies, by various spectroscopic techniques, of small rigid molecules, e.g. the symmetric rotors X_2, CH_4, NH_2

etc, asymmetric rotors XY etc). The archetypal system is the methyl group, $-CH_3$, which is often more or less free to reorient within a larger molecule. Of especial interest are:

(i) the nature and origin of the rotational potential;
(ii) the mechanism of reorientation or rotation of the group;
(iii) the effect of isotopic substitution of the methyl protons;
(iv) the influence of the electronic configuration of the molecule (be it paramagnetic or diamagnetic, neutral or charged); and
(v) the relationship with chemical studies.

A certain correspondence can be made here with the dynamical studies of protons and muons in metals of the preceding section, where the appropriate 3D potential is (nearly) periodic in distance. Here the 1D potential is periodic in angle, repeating every 120° in many crystalline solids as illustrated in figure 44, or every 60°, depending on the symmetry of the immediate surroundings. Of course, there are now particles in *each* well, so the wells are of equal depth, at least for the unsubstituted $-CH_3$ group. In the sense used above, the methyl protons are *self-trapped*: it is their presence (via their interaction with neighbouring atoms, i.e. their Buckingham potentials) that determines the depths of their potential wells. Also in the sense used above, they may be mobile: they may exchange positions either by tunnelling at low temperatures or by classical over-the-barrier rotation at high temperatures. Coherent tunnelling in this case is well established; it leads to a discrete splitting δ_{EA} of the single-well torsional states, depicted in figure 44, just as it broadens polaron energies into a band. It is likewise suppressed above a certain temperature, giving way to thermally activated reorientation (see, e.g., Clough *et al* 1982, Press 1981).

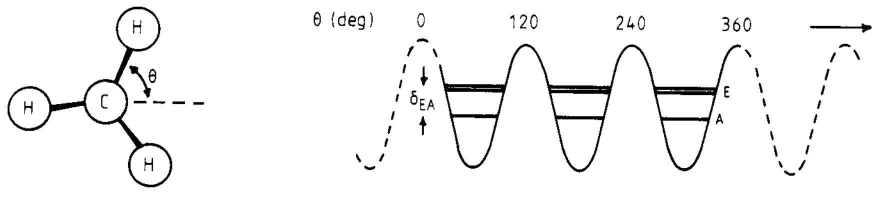

Figure 44. Tunnelling states of a methyl group (viewed end-on) in a V_3 rotational potential.

Isotopic substitution of a methyl proton destroys the inherent symmetry of the rotor by distinguishing one particle. The effect of substitution of a methyl proton by a positive muon is that $-CH_2Mu$ reorients *less* readily than $-CH_3$ (a nice contrast with *isolated* muons and protons in metals!) The key to how this subsitution may be achieved, and its effect studied by μSR methods, lies in reaction (6.1), below. This describes the addition of muonium at a carbon–carbon double bond—for illustration that of ethene (reaction (6.1*a*)). The analogous reaction leading to the ethyl radical $\dot{C}H_2CH_3$ is well known in atomic hydrogen chemistry. The *muonated* ethyl radical $\dot{C}H_2CH_2Mu$ is formed following the implantation of muons in ethene (the exact nature of the primary process, and whether (6.1) necessarily represents the actual route taken, is touched on in § 6.4; of importance here however is that this product is identified in the μSR spectrum). One carbon atom of a host molecule is saturated, thereby creating the labelled methyl group of interest. An unpaired electron is left nominally localised on the other carbon atom;

the product molecule is neutral, with an electronic doublet ground state. It is the hyperfine coupling of the muon with this electron that is the source of information on molecular conformation and dynamics:

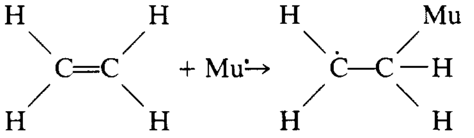

(6.1*a*)

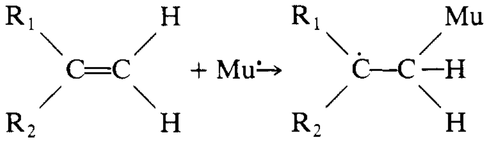

(6.1*b*)

Since the recognition that relatively stable organic radicals could be formed in this way (Roduner *et al* 1978, 1982b, Bucci *et al* 1978, Hill *et al* 1982), numerous species have been prepared and studied (see, for instance, the reviews by Walker (1983) and Webster (1984)). With few exceptions, the corresponding 'normal' radicals are known, having been prepared chemically or by radiolysis or photolysis, and studied by conventional magnetic resonance methods. For aspects of structure and dynamics, interest focuses on the comparison of corresponding proton–electron and muon–electron couplings.

6.1. *The measurement and origin of the hyperfine coupling*

As for the studies of muonium and related inorganic radical centres of § 4, the Breit–Rabi diagram is invaluable for interpreting the measurements. Figure 45 illustrates the

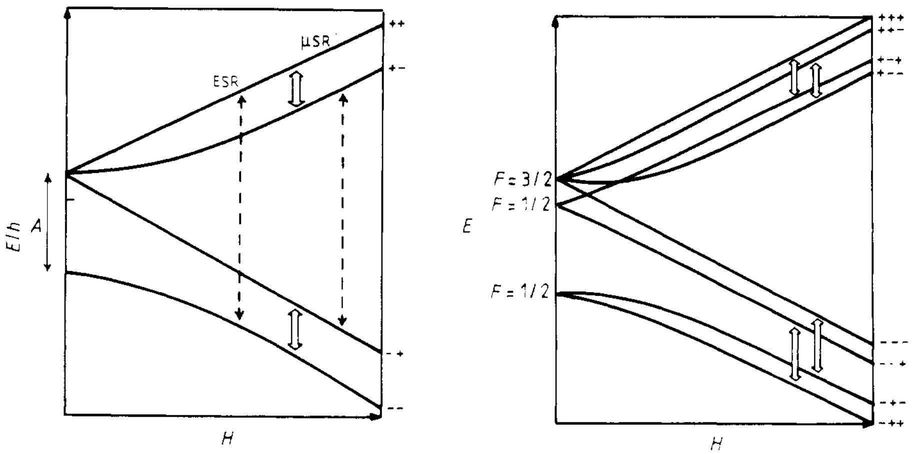

Figure 45. A Breit–Rabi diagram for a radical with hyperfine coupling $\langle A\rangle \mathbf{I}\cdot\mathbf{S}$ to one spin-$\frac{1}{2}$ nucleus (i.e. the muon) (*a*) and to two spin-$\frac{1}{2}$ nuclei (e.g. the muon and a proton) (*b*). The transitions shown as broken lines in (*a*) are those detected by conventional ESR experiments at constant microwave frequency, separated in field by $\langle A\rangle h/g\beta$. The transitions detected in μSR experiments are analogous to ENDOR transitions (full arrows). An example is shown in figure 6. When one other coupling is dominant, as in (*b*), its value may be estimated from the frequency splittings of the μSR transitions in intermediate fields. An example is shown in figure 51. The splittings vanish in sufficiently high fields, when the transitions correspond essentially to flips of the muon spin alone, justifying the use of the simpler diagram (*a*).

high-field transitions usually detected by ESR, by ENDOR and by μSR. There is an evident analogy between μSR and ENDOR spectroscopy (Roduner and Fischer 1981). ESR and ENDOR spectra become more complex when there is hyperfine coupling to more than one nucleus (notably because of proton multiplicity). μSR selects the two lines that, in sufficiently high field, correspond to flips of the muon spin alone (but by the same token, is insensitive to other nuclear couplings). The hyperfine constants in organic radicals are such that fields in excess of a few kG are generally sufficient to secure this decoupling and the precession frequencies obtained lie within the range of most μSR spectrometers. For illustration, figure 6 shows such a characteristic two-line spectrum: that of the *phenyl*ethyl radical, $\mathrm{Ph\dot{C}H{-}CH_2Mu}$, which is formed by reduction of the olefinic bond in styrene, $\mathrm{Ph\dot{C}H{=}CH_2}$ (see equations (6.1*b*) and (6.7*a*)). Other representative spectra are shown in figures 51 and 52 later in this section.

The great majority of such studies have been performed in liquid samples (often at or near room temperature) for which the muon–electron hyperfine interaction is effectively isotropic, of the form $\langle A_{\mathrm{Mu}}\rangle \boldsymbol{I}\cdot\boldsymbol{S}$, any anisotropic component being averaged out by the rapid tumbling of the molecules. The constant $\langle A_{\mathrm{Mu}}\rangle$ is then given exactly by the sum or difference of the two frequencies, according to whether $\frac{1}{2}\langle A_{\mathrm{Mu}}\rangle$ is greater or less than the muon Larmor frequency, so a particularly direct and accurate measurement is possible (Roduner and Fischer 1981, Hill *et al* 1982)†.

The structure of radicals of the general type $\mathrm{R_1R_2\dot{C}{-}CH_2Mu}$, formed as in reaction (6.1*b*), is depicted in figure 46. The unpaired electron occupies an orbital that has essentially non-bonding atomic p_z character, perpendicular to the plane of the portion $\mathrm{R_1R_2\dot{C}{-}}$ of the molecule‡. It is reasonable to suppose that the C–Mu bond to the other carbon atom is essentially similar to a normal C–H σ bond, albeit somewhat longer and weaker by virtue of the greater zero-point motion of the lighter isotope, as emphasised below. In these radicals the main origin of the hyperfine coupling with the methyl muon (or protons) is the overlap or admixture of the doubly occupied σ orbital and the singly occupied p_z orbital. These are nominally orthogonal, and the admixture is known as *σ–π hyper*conjugation. Delocalisation of spin density onto the muon or protons is greatest when this overlap is maximised, i.e. when the p_z orbital (seen from the end-on view of figure 46(*b*) is eclipsed by the C–X bond (X = H or Mu). This is expressed by equation (6.2) for the hyperfine coupling, which has long been established for X = H or D (Symons 1959, Hellar and McConnell 1960, Fessenden 1964, Krusic *et al* 1971):

$$A_{\mathrm{X}}(\theta_{\mathrm{X}}) = A^0_{\mathrm{X}} + B_{\mathrm{X}}\cos^2\theta_{\mathrm{X}} \tag{6.2}$$

$$\langle A_{\mathrm{H}}\rangle = A^0_{\mathrm{H}} + \tfrac{1}{2}B_{\mathrm{H}} \tag{6.2a}$$

$$\langle A_{\mathrm{Mu}}\rangle = A^0_{\mathrm{Mu}} + B_{\mathrm{Mu}}\langle\cos^2\theta_{\mathrm{Mu}}\rangle. \tag{6.2b}$$

---

† For molecular materials that freeze to a glassy solid, anisotropic couplings generally broaden the solid state μSR lines beyond detection, or at best give a featureless spectrum. Determination of the parameters of the spin Hamiltonian requires single-crystal work, as in ESR. Such experiments demand a large allocation of beam-time however. With the exception of elegant studies of the radicals formed in durene (Roduner 1981) and of the muonium (especially Mu*) defect centres in semiconductors (see, e.g., Hintermann *et al* (1981), Patterson (1984); see also § 4) they have received little attention. With the exception of a special case exploited by Boekema *et al* (1981), neither have any studies of powder spectra, comparable with those familiar in ESR, been reported to date.

‡ The carbon atom denoted $\dot{\mathrm{C}}$, which carries the major spin density, is known as the radical centre. Its three bonds are thought to be approximately, if not excatly, planar, although the structure is relatively flexible, with 'pyramidal' deformation possible.

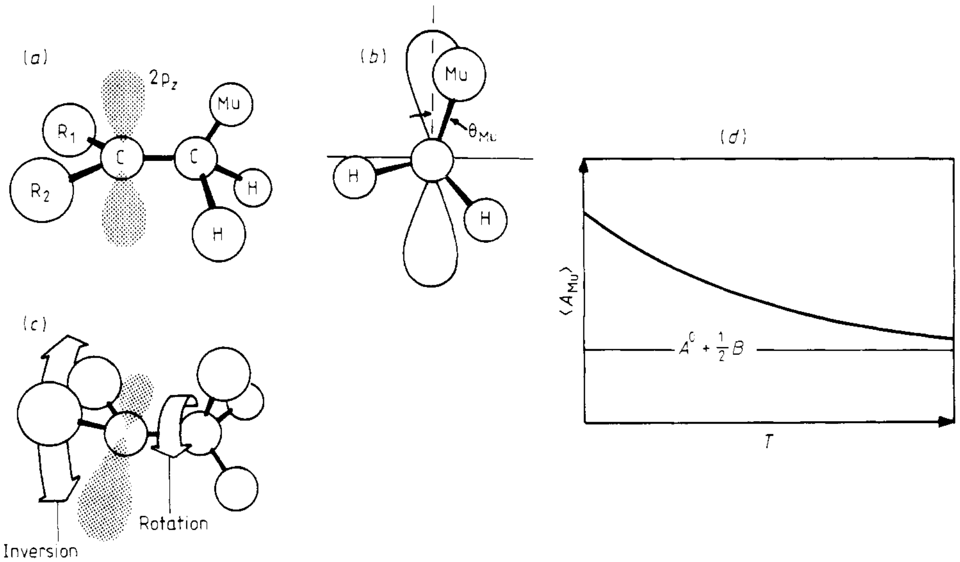

Figure 46. The planar structure of radicals of the ethyl type (*a*) together with an end-on view (*b*). The angle θ defines the orientation of the C–Mu bond (or of a C–H bond) with respect to the carbon-centred p_z orbital. The spin density on the muon (or proton) via hyperconjugation is maximised in the eclipsed position, $\theta = 0$. The probable coupling of intra-molecular rotation to inversion or 'bending' at the radical centre is depicted in (*c*). Variation of the muon–electron hyperfine constant with temperature (sketched from the results of Ramos *et al* 1984a, b) is shown in (*d*). See also figure 55.

Here θ_X is the dihedral angle and A^0_X and B_X are constants; the spin-polarisation contribution, represented by the term A^0_X, is close to zero for the alkyl radicals, so the coupling is small when the proton or muon lies close to the radical plane. The unsubstituted methyl group $-CH_3$ is essentially free to rotate, so an average coupling $\langle A_H \rangle$ given by (6.2*a*) is measured in ESR or ENDOR experiments. For the muonated species, the corresponding couplings $\langle A_{Mu} \rangle$ are generally found to be significantly larger, even allowing for the different magnetic moments of the muon and proton, as in (6.3). This has been noted by various authors (e.g. Roduner *et al* 1982b, Hill *et al* 1982), i.e.

$$(\langle A_{Mu} \rangle / \langle A_H \rangle) \mu_p / \mu_\mu = \eta \qquad \text{with } \eta > 1. \tag{6.3}$$

Temperature-dependent enhancements in the range $1.2 < \eta < 1.4$ are common, but larger factors are also reported in certain instances. These enhancements contrast with the small *reduction* of hyperfine constant for muonium atoms trapped in crystal lattices, relative to the corresponding hydrogen defect centres, that is noted in § 4 (Baumeler *et al* 1985). The key difference here is that major spin density is β to the muon or proton (i.e. located on the next-but-one atom, usually with negligible spin density on the intervening atom) in the organic radicals. Such an isotope effect is not confined to radicals of the alkyl type, but for these at least it may be largely accounted for in terms of different angular averages in (6.2*a*) and (6.2*b*), i.e. $\langle \cos^2 \theta_{Mu} \rangle > \frac{1}{2}$. This suggests that the C–Mu bond adopts a preferred orientation perpendicular to the plane of the molecule: the angular wavefunction weights $\theta = 0$ (or 180°) more heavily than other orientations. The interpretation is confirmed by the variation with temperature: the muon–electron coupling increases as the temperature is lowered. In the approximation where it is assumed that only rotational excitations of the methyl group are populated around room temperature, this represents the reduction in amplitude of thermal libration. Figure 46(*d*) is sketched from the results of Ramos *et al* (1984a, b). (This variation should be roughly balanced by that of the two methyl proton couplings; the effect on the level crossing resonance spectrum, figure 55(*b*) below, is particularly striking.) In an elementary discussion, it is therefore legitimate to look for the dominant contribution to the isotope effect in terms of an effective barrier to rotation.

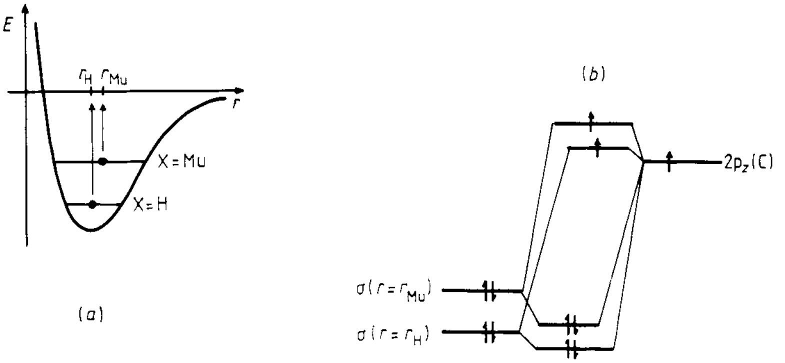

Figure 47. Qualitative energy level diagrams. The curve in (*a*) represents the total energy of the C–X bond as a function of fixed nuclear separation. (The potential energy curve, which represents just one cut through the total-energy surface, is assumed in this description to be the same for X = H and X = Mu. Whether the energy surface is indeed the same for the proton and muon, or whether calculations need to be taken beyond the Born–Oppenheimer approximation, is considered elsewhere (McKenna and Webster 1984, 1985, Fournier and LeRoy 1984, Webster 1985). Non-adiabatic calculations for the simpler muonium-substituted molecules show the corrections to be small.) Zero-point vibrational energies and corresponding average bond lengths are indicated for X = H and X = Mu. In (*b*) orbital levels are depicted for different bond lengths $r = r_H$ and $r = r_{Mu}$ showing the effect of overlap of the σ(C–X) and $2p_z$(C) orbitals for an alkyl radical. The disparity of the initial levels is less for X = Mu than for X = H, favouring delocalisation of the singly occupied orbital (from Cox *et al* 1986).

6.2. The origin of the barrier to rotation

The three methyl proton couplings in a normal ethyl radical (and in radicals of the ethyl type) are all equivalent and independent of temperature over a wide range. The small V_6 barrier (corresponding to different potential energies for the $\theta_x = 0, 60°, 120°$ etc and $\theta_x = 30°, 90°, 150°$ etc configurations) does not significantly hinder the CH_3 reorientation†. The origin of the preferred orientation of CH_2Mu is therefore of especial interest and various possibilities may be envisaged. Their relative importance should be quantified in due course. Firstly, elongation of one of the C–X bonds, which may be used as a model for muonium substitution (see figure 47(*a*)), introduces a V_2 component into the angular potential (corresponding to an enhanced energy difference for the $\theta_X = 0, 180°$ etc and $\theta_X = 90°, 270°$ etc configurations).

† Tunnel splitting measurements in crystalline materials at low temperature in fact indicate that a methyl group is *least* intrinsically hindered when attached via an sp^2 orbital on the neighbouring carbon atom (Clough 1986).

Secondly, the substituted group is no longer a symmetric rotor; its geometrical and inertial axes do not coincide so it 'wobbles' as it rotates, coupling rotation to the other normal modes of the molecule. This is observed by Raman spectroscopy in toluene Ph–CD_2H for instance, where the partially deuterated methyl group –CD_2H also adopts a preferred orientation with the lighter particle perpendicular to the plane of the molecule; in this case and in similar *diamagnetic* molecules, the behaviour may be adequately described in terms of coupling to the stretching mode of the C–H bond (Cavagnat and Lascombe 1982). In the present case, coupling to the inversion mode, i.e. to a bending at the radical centre, may be more important as this has a relatively low characteristic frequency (figure 46(*c*)).

Dynamical couplings of this sort may often be simulated by an *effective static* potential (which in this instance clearly repeats every 180°). Thus Ramos *et al* (1984b), by considering the thermal excitation of torsional states within a V_2 static potential, derive a substantial barrier height hindering the rotation of CH_2Mu in the ethyl radical (this is about 0.03 eV, an order of magnitude greater than that hindering –CD_2H). Such a potential can, equivalently, be parametrised in terms of pairwise interactions between the methyl muons, protons or deuterons and the other atoms or substituent groups of the molecule. In this picture the preferred orientation has often been ascribed to *steric* hindrance, bound muonium being effectively bulkier than bound hydrogen. This is undoubtedly a real effect: the RMS displacement of the muon being greater than that of the proton by virtue of its greater zero-point motion—by a factor of about $(m_H/m_{Mu})^{1/4} \simeq 1.7$, assuming a harmonic oscillator model for H and Mu bound to a much heavier (carbon) atom. This effect will also be present in diamagnetic and paramagnetic molecules alike. Even allowing for such an increased bulk, however, it is difficult to see how rotation could be so drastically hindered in the simple ethyl radical. In other alkyl radicals, steric arguments are certainly by no means always successful in accounting for the stable configurations (Cox *et al* 1986).

Comparison of the barriers to rotation in a variety of species $R_1R_2\dot{C}–CH_2Mu$ should distinguish these two models, since the dynamical coupling of rotation to bending will be weaker, but steric hindrance stronger, for heavier and bulkier groups R_1, R_2.

In paramagnetic species, particular structures may also be stabilised by delocalisation of the singly occupied orbital, i.e. by the same mechanism as is responsible for the hyperfine interaction itself. If steric and conjugative constraints are contradictory, the structure actually adopted is then the result of competition between them. Figure 47 illustrates how conjugative control of the C–X orientation may be effectively stronger for X = Mu than for X = H. The consequences of the greater zero-point energy of bound muonium in this picture are that muonium is bound to carbon somewhat less strongly than hydrogen and that the bond is slightly longer. This facilitates σ–π hyperconjugation. Symons (1984) argues that this should be seen as electron donation from the σ orbital into the half-filled p_z orbital, and that C–Mu σ electrons are more easily released in this manner than C–H σ electrons. This would stabilise the out-of-plane configuration for the muon, in which case the isotope effect follows naturally (Cox *et al* 1986). Whether the implied redistribution of spin density can be detected, e.g. whether there is also any significant difference between the constants used for H and Mu in equation (6.2), remains to be seen. Such a 'residual' isotope effect, over and above the preferred orientation, would be supportive of the model although not a decisive test. A discrepancy of around 20%, i.e. $(B_{Mu}/B_H)\mu_p/\mu_\mu \simeq 1.2$ in (6.2), is in fact suggested by the data of Ramos *et al* (1984b) although this result represents an extensive extrapolation and is open to verification.

In parenthesis, it is by no means standard practice to incorporate zero-point motion explicitly in molecular orbital treatments in the manner suggested in figure 47. Indeed, in the simplest theories, zero-point motion is ignored altogether, being negligible for the heavier atoms. It is therefore a matter of some interest and some debate as to how its effects should best be accommodated. A residual isotope effect may also be understood as follows. Equations (6.2*a*) and (6.2*b*) express explicitly only the rotational averages of the rigid-molecule couplings. Different averages for X=H and X=Mu are to expected over the various other normal modes, notably the stretching modes of the C–X bonds†. Roduner (1984b) points out that increased spin density on X as the C–X bond is stretched may be expected intuitively, since X will take increasing atomic character as it is withdrawn from the molecule. In the most elementary description, the conventional radical structure (i) contains a greater admixture of the other extreme valence bond structure (ii) when X = Mu than when X = H.

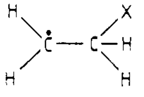

(i)

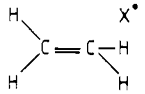

(ii)

(iii)

It is interesting to speculate whether dynamical effects, e.g. coupling of rotation to inversion, or indeed hyperconjugation, are so strong as to result in a distortion of the conventional planar structure depicted in figure 46, i.e. whether the molecule is on average 'bent' at the radical centre‡, and likewise whether there is any as an admixture of a bridged structure (iii).

The situation for radicals formed by addition to a carbonyl oxygen atom is illustrated in figure 48. This depicts the radical formed in acetone, as in (6.4) (Roduner 1980, Hill *et al* 1982, 1985):

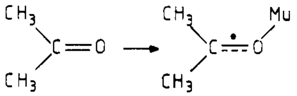

(6.4)

Here it is interesting that it is not strictly necessary to reduce the C=O bond if muonium adds in the plane of the molecule, since in-plane lone electron pairs on oxygen are available for bonding to the muon. (This contrasts with addition to C=C, where the

---

† That is, the greater average bond length and larger amplitude of vibration for C–Mu may result in a greater vibrational average of the coupling. The distinction between this description and that of enhanced hyperconjugation is largely semantic, although the latter term has been criticised as being inappropriate for a comparison between isotopes (Roduner 1985). Certainly for a given fixed geometry the electronic wavefunction is unchanged on isotopic substitution. On inclusion of zero-point and thermal energies, therefore, isotope effects should emerge automatically in *ab initio* calculations. These latter are as yet unable, however, to give reliable values of hyperfine coupling in all but the simplest (diatomic) radicals (Louwrier 1986, Webster 1986). (A similar difficulty in calculating spin density, as opposed to charge density, in metallic systems is noted in § 5.) Model solutions are therefore required, and in this context the concept of isotope-dependent hyperconjugation provides a useful framework for the discussion of structure and coupling (Cox *et al* 1986).

‡ According to Claxton and Graham (1987) the ethyl radical is indeed slightly bent in the 'eclipsed' configuration ($\theta_X = 90°$). Their preliminary calculations yield different force constants for vibration and bending in these two configurations and hence different zero-point vibrational energies which, for X = Mu, they identify as the major contribution to the observed barrier. This simple result would appear to describe an effect of far reaching importance that the μSR studies have highlighted, namely the role of vibrational effects in structural control.

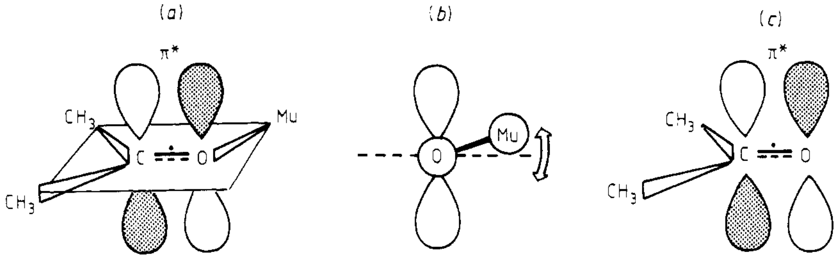

Figure 48. The isopropanol radical formed by addition to carbonyl oxygen in acetone (*a*). The preferred conformation now has the muon in the radical plane, since this maximises conjugation. Out-of-plane excursions (*b*) increase the muon–electron coupling via hyperconjugation. Possible precursors to the formation of this radical following muon implantation in acetone are the radical anion (*c*), in which a radiolytic electron is captured in the π^* orbital, or the diamagnetic cation $(CH_3)_2C{=}O:Mu^+$ (see § 6.4) in which the muon 'sticks' to the lone electron pair on oxygen.

double bond must be opened, the π electrons being the only ones available for bonding.) The planar configuration is preferred in this case, since conjugation between carbon and oxygen is preserved. The carbon–oxygen π bond is greatly weakened by accommodation of the unpaired electron in the anti-bonding σ^* orbital, however, so there is some rotational freedom. The degree of out-of-plane libration (figure 48(*b*)) is expected to be much greater for O–Mu then for O–H, by virtue of the very different moments of inertia of these groups (Roduner 1980). In fact, as the muon is rotated out of the plane, the π bond is indeed opened, localising the unpaired electron on the carbon atom and maximising hyperconjugation in the perpendicular configuration. Applying equation (6.2) to radicals of this sort, the constant A^0_{Mu} is negative and no longer negligible; single occupation of the π^* orbital implies the presence of spin on oxygen (i.e. α to the muon) and confers negative spin density on the muon. The opposition of positive and negative terms results in low values of the average hyperfine coupling and a marked sensitivity to temperature and solvent effects (Hill *et al* 1985).

Although conjugation determines the stable structure in this radical (and similarly in those formed by addition to oxygen in a variety of amides and esters; see Geeson *et al* 1985b), it is again interesting to conjecture whether hyperconjugation is intrinsically stronger in the muonated species. This would destabilise the in-plane site in radicals of the type $R_1R_2\dot{C}.OMu$, just as it would stabilise the out-of-plane site in $R_1R_2\dot{C}.CH_2Mu$.

6.3. *The muon as a passive probe?*

In the above examples, the muonated group is the focus of attention. As in the metals studies, the muon is an 'active' probe—the principal participant in the phenomenon under study. In other circumstances, the muon may also be used as a 'passive' probe to monitor motion of the molecule, which its presence does not significantly perturb. For instance in the case where a radical may be formed in two different isomers, inversion between the two can lead to a lifetime broadening of the spectral lines, so information on the isomerisation rate and its temprature dependence is available from the μSR linewidths (Strub *et al* 1984). In plastic molecular crystals, radical formation has successfully been used to tag the molecular chains (Ricco *et al* 1984) and should provide a convenient label for dynamical studies.

It may also be possible to use the diamagnetic muon signal in a similar manner, so dynamical studies are not limited to radical systems. Thus in a preliminary experiment in calcium hexammine ($Ca(NH_3)_6$, Catterall *et al* 1985) the linewidth of the (diamagnetic) μSR signal follows the same variation with temperature as the proton NMR linewidth. In particular it narrows stepwise at the onset of various types of motion of the surrounding NH_3 groups: tunnelling reorientation, classical rotation (each giving a limited narrowing) and actual translation (i.e. a 'melting' of the NH_3 sublattice, leading to extreme narrowing).

It may even be possible, although this has yet to be demonstrated, to detect a 'resonant' muon depolarisation when the muon Larmor frequency is tuned to the tunnel splitting of neighbouring groups, thereby measuring these splittings directly (Abragam 1984). This would be one valuable application of the cross-relaxation technique described in § 7.

6.4. *Chemical studies*

6.4.1. Reaction kinetics. In the dynamical studies above, the μSR precession frequencies and linewidths are the principal source of information. There are other possible sources of line broadening, namely spin–spin coupling (in liquid samples notably hyperfine coupling to other dipolar nuclei, cf figure 45), spin–lattice coupling and chemical reaction. Fortunately it is often possible to identify the dominant mechanism systematically and unambiguously from the qualitative variation with parameters such as field, temperature and concentration of solution (Cox *et al* 1982). Chemical reaction is a particularly important case since the muon is sufficiently remote from the radical centre not to affect is reactivity. Thus the μSR linewidth gives a direct measurement of the *intrinsic* reaction rate, i.e. of the chemical inverse lifetime; for these purposes also the muon is a passive probe, serving only to label the molecule:

$$R_1^{\bullet} + S \rightarrow R_2^{\bullet} \tag{6.5a}$$

$$R_1^{\bullet} \rightarrow R_2^{\bullet} \tag{6.5b}$$

$$R_1^{\bullet} + R_1^{\bullet} \rightarrow \text{diamagnetic products.} \tag{6.6}$$

Whether the reaction studied is bimolecular as in (6.5*a*), or unimolecular as in (6.5*b*), there is a unique advantage here over conventional chemical studies which require a high radical concentration, namely that termination reactions (6.6) with a second radical are excluded and cannot falsify the measured rate.

As an example of a bimolecular reaction, the linewidths in the spectrum of figure 6 represent the rate of dimerisation of styrene. The monomer is activated as in (6.7*a*) and reacts with another monomer as in (6.7*b*) (Cox *et al* 1982). This is the first stage of polymerisation, *en route* to polystyrene (6.7*c*):

$$\mathrm{PhCh{=}CH_2 + Mu^{\bullet} \rightarrow Ph\dot{C}H{-}CH_2Mu} \tag{6.7a}$$

$$\mathrm{Ph\dot{C}H{-}CH_2Mu + PhCH{=}CH_2 \rightarrow Ph\dot{C}H{-}CH_2{-}CHPh{-}CH_2Mu} \tag{6.7b}$$

$$\rightarrow \mathrm{-(CH_2{-}CHPh)_n-} \tag{6.7c}$$

An example of a unimolecular or rearrangement reaction that has been studied in this manner is reaction (6.8*a*), with the radical prepared as in (6.8*b*). A similar radical, prepared as in (6.8*c*), for which no such rearrangement is possible but that should have the same residual linewidth, serves as a reference in this study (Burkhard *et al* 1984, 1985):

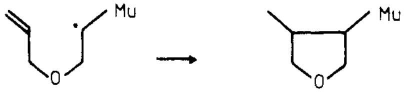

(6.8*a*)

(6.8*b*)

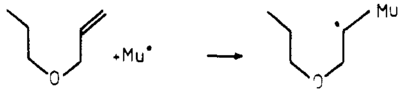

(6.8*c*)

These few examples only touch on the use of the muon as a probe of reaction kinetics, which is by no means confined to radical studies. This large field is reviewed by Roduner (1986b).

6.4.2. Radical formation. In the above studies of reaction kinetics, the product of the reaction is not observed. It would be characterised by different precession frequencies but these do not appear in the μSR spectrum since phase coherence with respect to the incoming muon is lost. This is the result of the (exponential) distribution of chemical lifetimes: signals from individual product molecules are dephased. (More precisely, there is no significant coherent transfer of polarisation from reactant to product when the frequency change exceeds the inverse lifetime: a general treatment is given by Percival and Fisher 1976.) By the same token, the radical *precursor* is too short-lived to be detected directly. Its nature and lifetime (if this is not vanishingly small) may sometimes be deduced from the initial phase of the radical signal, however, as illustrated in figure 49.

The radicals identified to date are all neutral species formed from the host molecules

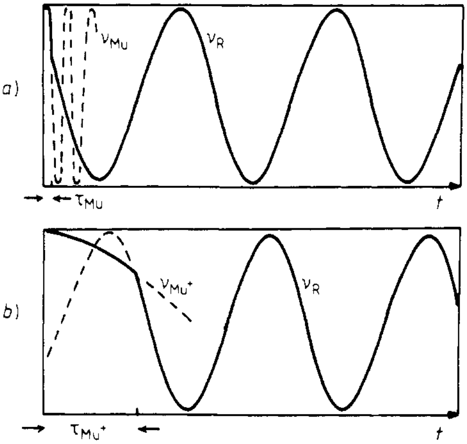

Figure 49. The initial phase of the precession signal. The observed frequency ν_R corresponds to one component of a radical signal (cf figure 6). If the radical is formed promptly, the initial phase of this signal is determined uniquely by the geometrical layout of the spectrometer, i.e. the angle between the positron telescope and the initial beam polarisation. A short-lived chemical precursor shifts the initial phase from this 'geometrical' value. Precursors with higher frequencies (e.g. ν_{Mu} for muonium, as in (*a*)) and lower frequencies (e.g. ν_{Mu^+} for a diamagnetic state, as in (*b*)) give phase shifts of opposite sign and may in principle be distinguished (Cox *et al* 1982).

by the addition of a muon plus one electron. Formally, therefore, their formation may be described as muonium addition (as expressed in reactions (6.1) for the ethyl radicals and (6.7*a*) for the phenylethyl radicals). It was assumed in the early literature that this was the actual route taken, indeed that muonium atoms were the sole and unique precursor to all muonated molecules, paramagnetic and diamagnetic (see, e.g., Myasischeva *et al* 1969). If this is so, questions arise as to the nature of the primary processes by which muonium is first formed following muon implantation, and these are discussed at length elsewhere (see, e.g., Percival *et al* 1978, Percival 1979, Fleming *et al* 1979, Walker 1983). If stable muonium is not formed at epithermal energies, there are other possible routes. In particular the thermalised or nearly thermalised muon will fix itself directly to the host molecule if this has some basic (as opposed to acidic) character. Thus it will 'stick' to a lone pair of electrons, e.g. on the oxygen atom of a carbonyl bond, as in (6.9*a*), or should reduce a carbon–carbon double bond forming a species analogous to the carbocation, as in (6.10*a*). The analogous processes of 'protonation' are well known. The muon, in its role as lightweight proton, will be at least as reactive:

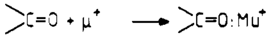
(6.9*a*)

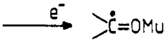
(6.9*b*)


(6.10*a*)

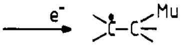
(6.10*b*)

Subsequent encounter with an excess electron, generated radiolytically (or with an anion, if the excess electron is captured by the host molecule in a low-lying unnoccupied orbital) would then give the neutral radical, as in (6.9*a*) and (6.10*b*). These processes are illustrated in figure 50. The muonated cations are diamagnetic, and therefore susceptible to the test of figure 49; the test was shown to be just feasible in experiments on styrene (Cox *et al* 1982) and the results suggest strongly that the phenylethyl radical is formed in this manner. This seems likely to become a standard diagnostic method. In

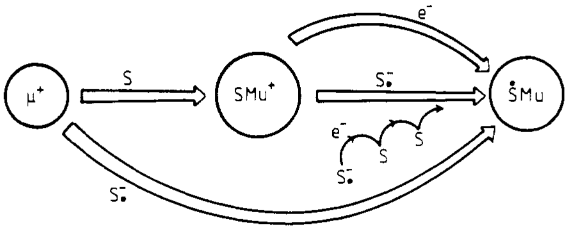

Figure 50. Ionic mechanisms of radical production. S denotes a solvent or reactive solute molecule, and the scheme assumes the radiolytic production of excess electrons by the initially energetic muon (and also by secondary-electron ejection). The majority of these electrons will return to their twin radical cations $S^{+\cdot}$, but some will solvate, or be trapped by individual solvent molecules as radical anions. Both species are denoted $S^{-\cdot}$. Central importance is given to formation of the muonated cation SMu^+. Competitive parallel channels may be favoured depending on the relative affinities of the host S for electrons and protons (muons). A possible hopping transfer of the electron (or even of the muon) may in some circumstances enhance the effective mobilities of the ionic species and so facilitate their encounter. (Adapted from the general scheme of Cox and Symons 1986a.)

subsequent experiments, phase measurements have confirmed that muonium addition is dominant in certain instances (with the muonium formed at thermal energies) and that ionic mechanisms can contribute in others (Roduner 1984a, 1986a). The available results are discussed in relation to chemical expectations by Cox and Symons (1986a).

6.5. *Other radical systems*

Some other archetypal systems formed from double, triple or conjugated homopolar bonds are depicted in (6.11)–(6.14) below. These illustrate different possible sites for muonium addition, and different degrees of localisation of the singly occupied orbital. Thus in (6.11*a*), showing one possible derivative of a diene, terminal addition gives a muonated methyl group. It also allows delocalisation of the unpaired electron over the three remaining carbon atoms; this is characteristic of conjugated systems. Delocalisation of the singly occupied orbital stabilises the radical so that its yield (i.e. its formation probability per implanted muon) is accordingly greater than that of structure (6.11*b*), where the unpaired electron is blocked on the terminal carbon atom by saturation of its neighbour (Roduner and Webster 1983). The interpretation of the *amplitudes* of the μSR precession signals is noteworthy here; these represent the distribution of muon polarisation between the different products and so (to within the uncertainty created by the missing fraction) are a measure of the respective yields, i.e. the formation probability per implanted muon of the different species:

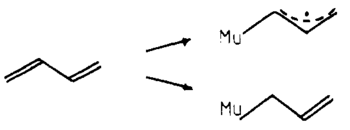

(i.e. $CH_2Mu-\dot{C}H-CH=CH_2$) (6.11*a*)

(i.e. $\dot{C}H_2-CHMu-CH=CH_2$) (6.11*b*)

(i.e. $(\dot{C}_6H_5)HMu$) (6.12)

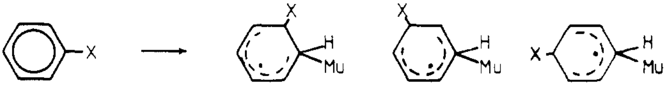

(6.13)

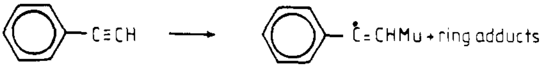

(6.14)

In the cyclohexadienyl radical, derived from benzene as in (6.12), spin density is distributed over the five unsaturated carbon atoms of the ring (Roduner 1979). This is evident from the reduction of the muon–electron coupling by strongly conjugating substituents X at the *ortho* and *para* positions as in (6.13) (Roduner *et al* 1982). No such reduction occurs for substituents at the *meta* position, which is close to a node in the singly occupied molecular orbital. When the benzene substituent X itself contains a multiple bond, this is reduced in preference, thereby preserving the resonance structure of the ring. This is the case in styrene (6.7*a*). It is also the case in phenyl acetylene (6.14) where the major product was the first muonium adduct of a *triple bond* to be identified unambiguously (Geeson *et al* 1985a). The identification is explained in figure 51. Minor products, which may be seen in spectra recorded to very high statistics as in figures 51

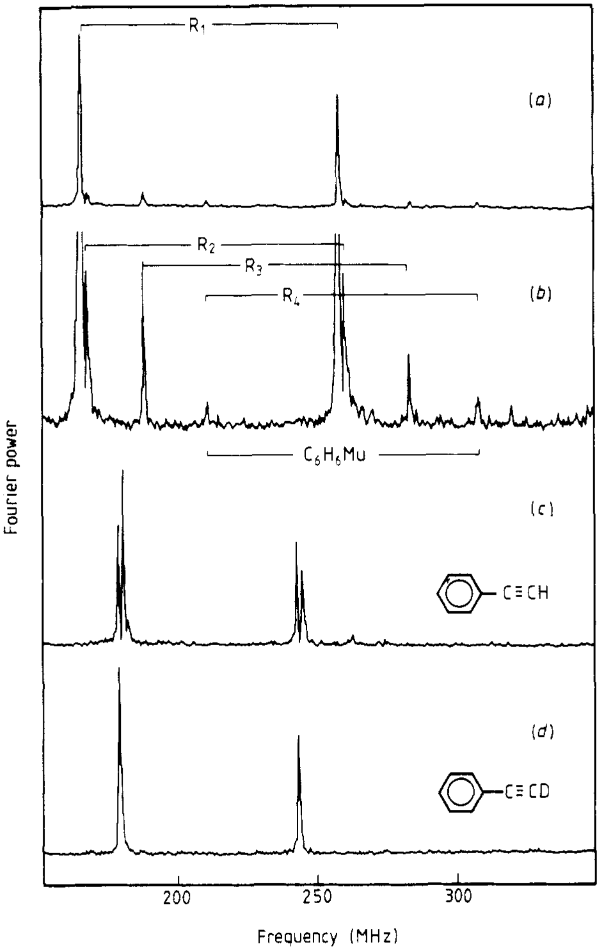

Figure 51. Spectra recorded in phenyl acetylene. The major product R_1 in (*a*) corresponds to the triple-bond adduct. This is identified by the splitting of the lines at lower field (*c*) by the dominant methylene proton coupling, as explained in figure 45; the splitting is absent in the corresponding spectrum of the deuterated material $C_6H_5C{\equiv}CD$ (*d*). With the vertical scale of (*a*) expanded, as in (*b*), minor products corresponding to ring adducts are also visible (Geeson *et al* 1985a).

and 52, show that ring adducts are also formed, both in phenyl acetylene and in styrene (Geeson *et al* 1985a, b). Their detection indicates a site selectivity in the initial addition process, no subsequent internal rearrangement of these radicals occurring on the microsecond timescale†.

As an example of a radical of some topical interest in physics, the reduction of a

---

† The muon has no rotational freedom in the cyclohexadienyl radicals (6.12) or in the vinyl radicals (6.14), so it is somewhat of a coincidence that a very similar isotope effect in the hyperfine coupling is found as for the alkyl radicals (Roduner *et al* 1982b, Geeson *et al* 1985). This may be largely attributed to the greater amplitude of libration of the muon than of a proton in this position (a calculation involving all normal modes has been undertaken for the cyclohexadienyl radical; Munger 1980) but a contribution from enhanced hyperconjugation can also be envisaged for these radicals.

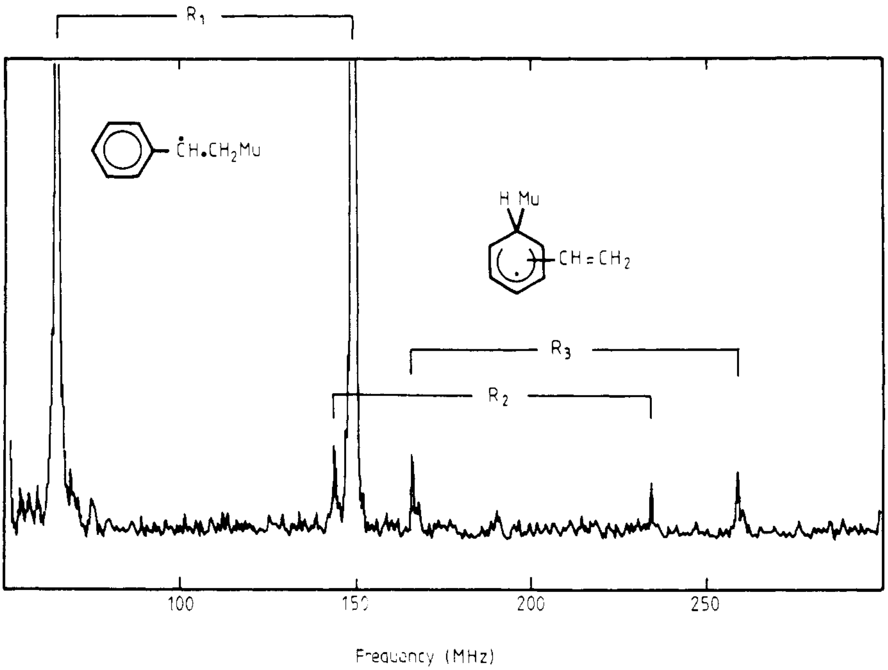

Figure 52. A high-statistics spectrum recorded in styrene (60×10^6 events; Geeson *et al* 1985b). This spectrum is to be compared with the earlier spectrum (corresponding to radical R_1) shown in figure 6, in which the ring adducts (R_2, R_3) are not detectable.

double bond in *trans*-polyacetylene is depicted in (6.15). Here the wavefunction of the unpaired electron does not remain localised adjacent to the saturated carbon atom, as in (6.15*a*), but is extended over many atoms, as in (6.15*b*). It is also mobile: it represents a bond-alternation defect which (in this conformer, though not in *cis*-polyacetylene) is free to migrate along the chain. The μSR data are used here to study the dynamics, not of muons or protons, but of the electronic defect, the so-called soliton (Nagamine *et al* 1984):

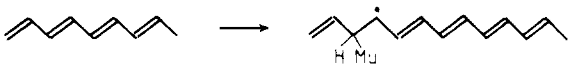

(6.15*a*)

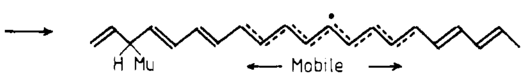

(6.15*b*)

Since the unpaired electron is on average remote from the muon in this radical, the hyperfine coupling is vanishingly small and there is little to be learnt from the transverse-field precession signal. The source of information in this study is muon spin *relaxation*, a technique described in the following section.

Finally it is noteworthy that reduction of a multiple bond always places the major spin density β to the muon (i.e. two atoms removed). In radicals formed by addition to oxygen, conjugation places some spin density α to the muon (i.e. on the adjacent atom, see figure 48(*a*)), but there are no reported examples of organic radicals in which the unpaired electron is predominantly localised on the adjacent atom. It should, however, be possible to form species of the form Mu–ML_n where ML_n is a metal–ligand complex, the additional valence of the transition metal M allowing direct attachment of muonium.

Evidently the constraints of a crystal lattice allow possibilities that are chemically unfavourable in individual molecules; thus the Mu* centres of § 4, observed in the elemental and certain compound semiconductors, have all the characteristics of molecular radicals with spin density α to the muon.

7. Muon spin relaxation

The μSR technique most widely employed to date has undoubtedly been that of muon spin *rotation*, i.e. precession in a transverse field—the principle subject of the preceding sections. Experiments in longitudinal and zero field have also been employed from the outset, however. Their applications span a similarly wide range of topics in solid state and chemical physics and examples are described in this section. The results from zero-field μSR are quite unique, and some particularly exciting new possibilities have very recently been demonstrated using longitudinal fields. In consequence, these techniques are currently accounting for a rapidly increasing proportion of beam-time usage.

7.1. Longitudinal asymmetry and relaxation

Here *longitudinal* means parallel to the initial muon polarisation (usually also parallel to the beam direction). When the applied field is longitudinal therefore, and in the absence of competing local fields within the sample, the muons would be implanted in a stationary spin state and their initial polarisation preserved. The earliest muonium studies, for example, used before the detection of muonium precession signals had been achieved, consisted in a simple time-independent or time-average measurement of longitudinal asymmetry in the positron emission. Indeed, when a precession signal is absent in transverse field, or does not account for the whole initial polarisation, measurement of the longitudinal field required to recover the total asymmetry may still be the only clue to the chemical nature of the missing fraction (§ 7.2). It is now also apparent that particularly precise spectroscopic information on a variety of systems is available in longitudinal fields, via cross relaxation (§ 7.3). With the upgrading of continuous muon sources to higher and higher intensities, there is also a renewed interest in techniques for which a time-average measurement of polarisation is adequate. This obviates the need to correlate individual muons and positrons, so the full available intensity may be used an data rates increased accordingly.

So far, however, the major interest in longitudinal studies has focused on the form of the relaxation function, which is the time evolution of the polarisation measured parallel to its initial direction. In this context the acronym μSR is taken to denote muon spin *relaxation*. A remarkable feature (and one that distinguishes μSR from conventional magnetic resonance techniques) is that the longitudinal relaxation function may be displayed *with or without* an applied holding field in this direction. This is a consequence of the probe spins being implanted in a defined spin state, which obviates the need for a polarising field. In either case the positron asymmetry is measured with counters placed 'forward' and 'backward' as in figure 53. Ideally these would be at 0° and 180° with respect to the initial polarisation, although generally it is necessary to avoid the direct path of the beam by using annular counters or cylindrical arrays, or by rotating the beam polarisation through a small angle. A compromise is made between maximising the event rate (through good coverage of the solid angle) and minimising loss of asymmetry

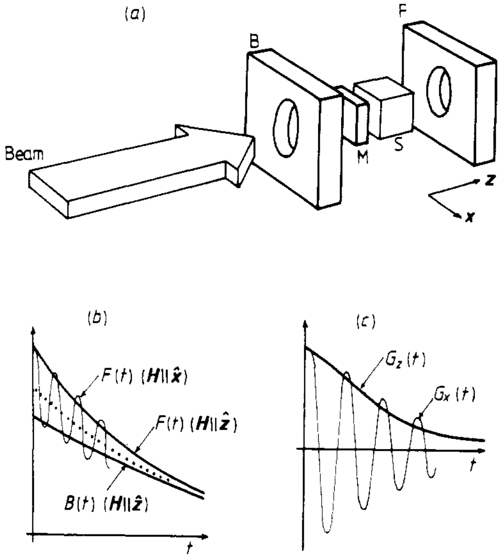

Figure 53. Measurement of the longitudinal asymmetry. In (*a*) F is the forward and B the backward positron telescope (a single scintillation detector for each telescope is often sufficient; otherwise pairs of scintillators may be used in coincidence); M is the muon detector and S represents the sample. The incoming beam is collimated and (if necessary) moderated as usual. In (*b*), the form of histograms recorded in the forward and backward telescopes is sketched. These are given by equations (7.1) and (7.2) and are typical of longitudinal or zero field. The exponential radioactive decay curve for unpolarised muons is shown dotted for comparison, and a transverse-field precession signal (forward telescope) is also shown; such a signal may be used for calibration purposes, and to determine the baseline of asymmetry. The corresponding evolutions of asymmetry are indicated in (*c*) (shown with equal amplitude, as would be the case for diamagnetic muons).

(which vanishes in the perpendicular direction). Other geometrical constraints may be imposed by the apparatus, e.g. the restricted bore of a solenoid magnet.

The positron emission asymmetry does not in this case have the distinctive oscillatory time dependence characteristic of transverse-field measurements, but it may be extracted from deviations from the purely exponential radioactive decay curve in the same fashion. This is explicit in equations (7.1) and (7.2) which describe the histograms recorded in the forward and backward telescopes respectively. $P_z(t)$ is the longitudinal polarisation, and a is the asymmetry parameter defined in § 2 (figure 1). In principle the longitudinal relaxation function $G_z(t)$ may be obtained from either histogram separately; in practice it is obtained most reliably and directly via a sum-and-difference ratio, as in equation (7.3):

$$F(t) \propto \exp(-t/\tau_\mu)(1 + aP_z(t)) \tag{7.1}$$

$$B(t) \propto \exp(-t/\tau_\mu)(1 - aP_z(t)) \tag{7.2}$$

$$G_z(t) = \frac{P_z(t)}{P_z(0)} \propto \frac{F(t) - B(t)}{F(t) + B(t)}. \tag{7.3}$$

Here t is the time elapsed after implantation, and a suitable normalisation of the event rates to account for geometrical factors and counting efficiencies is assumed, as well as the subtraction of any backgrounds from false correlations. The solid angle subtended by the forward and backward arrays at the sample (or rather at the region in which most muons stop, if this is not uniform) should be equalised as accurately as possible so as to avoid large normalisation corrections to the event rates recorded in the individual arrays. The normalisation factors, as well as the precise baseline for the asymmetry, which is crucial to the determination of relaxation functions at long elapsed time, may be determined by the application of a small transverse field in a preliminary calibration experiment, as in figure 53.

In a holding field sufficient to decouple local dipolar or hyperfine fields, $G_z(t)$ describes relaxation of the muon Zeeman energy, analogous to T_1 relaxation familiar in NMR. The muons are implanted with an initial polarisation close to unity but, if they had infinite lifetime, would relax to the polarisation corresponding to thermal equilibrium with the lattice (which is usually negligibly small). For hosts with dipolar *nuclei* only, this spin–lattice relaxation is generally unobservably slow on the μSR timescale, i.e. the initial polarisation is preserved for the lifetime of any individual muon. In the presence of atomic magnetism, however, it can be a sensitive probe of the fluctuation rate of the host moments. Measurements as a function of temperature can test for critical phenomena; measurements as a function of field can map the frequency spectrum of these fluctuations.

In the absence of an applied field, $G_z(t)$ displays the evolution of the muon polarisation in response to totally random local fields, no preferred direction being defined by the sample or its environment. The zero-field relaxation function is readily able to distinguish dynamics and statics, i.e. to differentiate fluctuations of the muon's magnetic enviroment due either to reorientation of the host spins, or to motion of the muon itself, from a change in the basic or 'instantaneous' field distribution. In particular, it is able to detect the onset of very slow fluctuations. It is sensitive to rates that are too slow (by an order of magnitude) to cause any detectable motional narrowing of the transverse-field lineshapes that would be recorded by muon spin *rotation*, or in corresponding NMR (T_2 relaxation) experiments.

7.2. *Repolarisation curves*

The simplest longitudinal measurement is that of the time-averaged or static component of the polarisation. This determines the proportion of implanted muons that adopt a stationary spin state (at least on the μSR timescale, i.e. with the proviso that Zeeman relaxation is not too rapid, as stressed above) in the holding field. Consider the case in which atomic muonium is formed, but where its triplet precession signal is rendered invisible by a distribution of local dipolar fields (the criteria for the formation and observation of muonium in different media are dealt with in § 4). That is, transverse polarisation is lost rapidly. Longitudinal polarisation may be recovered stepwise as in figure 54. The formation of muonium was first deduced from such recoveries (an early experiment by Orear *et al* (1957) is remarkable for its 'integral counting' technique using photographic emulsions!) The detailed field dependence (Ferrell and Chaos 1957) is now variously known as a 'decoupling', 'quenching' or 'repolarisation' curve. The starting polarisation, $P(H = 0)$, is the time average of the zero-field relaxation function, described below (§ 7.4). An initial plateau is reached as soon as the applied field exceeds the local dipolar fields, i.e. when the applied field (rather than the random local fields) determines the quantisation axis. Asymmetry corresponding to just half the muonium fraction is then recovered; here total spin is a good quantum number and half the

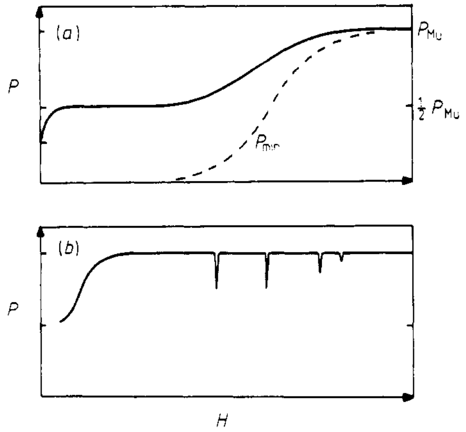

Figure 54. Longitudinal decoupling. An idealised repolarisation or 'quenching' curve is shown in (*a*) for a single paramagnetic species. The full asymmetry is recovered when the applied field 'quenches' the muon–electron hyperfine coupling. More steps in the recovery can indicate the existence of several species, or the successive quenching of superhyperfine interactions (i.e. coupling via the electron to other nuclei). Coupling to other nuclei can also result in the occurrence of sharp dips in the repolarisation curve as in (*b*). These are the result of cross-relaxation to the muon and permit precise relative measurements of the various coupling constants involved.

muonium atoms are formed in eigen-states ($|++\rangle$ or $|--\rangle$) that preserve the initial muon polarisation. (Any promptly formed diamagnetic fraction will also contribute to this plateau, but this can always be checked and measured by application of a small transverse field.) The other half of the ensemble of muonium atoms contributes a longitudinal polarisation that oscillates at high frequency between unity and $P_{\mathrm{min}} = P_{\mathrm{Mu}}x^2/(x^2+1)$ where $x = (\gamma_{\mathrm{e}} + \gamma_{\mu})H/A$, these oscillations being in general undetectable (Brewer *et al* 1975a). The steady component P_{min} becomes appreciable and contributes to the time-averaged longitudinal polarisation only at fields comparable with the hyperfine coupling constant, $H \sim A/\gamma_{\mathrm{e}}$, which is 0.16 T for vacuum state muonium. The full asymmetry is recovered in fields that are sufficiently high for the electronic Zeeman interaction to dominate or 'quench' the hyperfine interaction, $H \gg A/\gamma_{\mathrm{e}}$, i.e. to decouple the electron and muon spins.

An estimate of the hyperfine constant A can be made from the form of the quenching curve (although spectroscopic observations give a far more precise value, and are to be preferred where they are possible). Such an estimate does, for instance, allow atomic muonium to be distinguished from related paramagnetic centres, e.g. molecular radicals. For these latter species the full asymmetry is recovered in lower fields characterising smaller muon–electron couplings. Also the total spin is greater if there are significant super-hyperfine couplings to other nuclei; successive quenching of these couplings can lead to a more complicated stepwise recovery.

It is noteworthy that quenching curves may distinguish between the loss of muonium (or radical) signal due to chemical reaction and that due to physical mechanisms. Thus polarisation is not conserved, by definition, during spin-exchange reactions† or spin-flip encounters with other paramagnetic species. These encounters may occur, for instance,

---

† Calculations of spin-exchange cross sections for muonium, together with a review of early experimental studies, are given by Shizgal (1979).

within the region of radiation damage created by the initially energetic muon itself. This is true of longitudinal as well as transverse polarisation; once lost by such processes it cannot be recovered in a decoupling field.

Transverse polarisation, which determines the amplitude of precession signals, may also be lost in a chemical reaction: it is not coherently transferred between reactant and product when these have different characteristic μSR frequencies. Longitudinal polarisation, on the other hand, is conserved during chemical reactions, even if these are slow. A combination of longitudinal decoupling field and resonance techniques therefore constitutes a powerful method for analysis of the missing fraction. This has been demonstrated using RF resonance by Miyake *et al* (1984) and Ishida *et al* (1984b). Some interesting possible alternatives are described below.

The occurrence of sharp dips in repolarisation curves, as in figure 54(*b*), is exciting considerable current interest. These are one manifestation of a resonant exchange of energy when the muons are 'on speaking terms' with other systems, the subject of the following section.

7.3. *Cross-relaxation*

The determination of energy level splittings by the technique known as level crossing resonance is well known in optical spectroscopy and in conventional magnetic resonance. Its application in μSR studies has recently been proposed by Abragam (1984). A demonstration of the feasibility of the technique was immediately forthcoming, and a large new field of μSR spectroscopy can now be envisaged. The technique consists in tuning a longitudinal field so as to match a μSR frequency to another energy level separation in the system. A much enhanced or 'resonant' muon depolarisation, via cross-relaxation, may then be observed. The precise equality of two energy level separations implies a degeneracy in the energy of the total system (at least to zero or first order, depending on the choice of basis states, see below), whence the name 'level crossing'.

7.3.1. Measurement of quadrupole couplings. In the demonstration due to Kreitzman *et al* (1986), the muon Larmor frequency $\gamma_\mu H/2\pi$ is tuned to match a quadrupole resonance of the muon's nearest-neighbour copper nucleus, allowing a flip-flop transition of the muon and copper spins. Abragam (1984) points out that since the muon has a much larger gyromagnetic ratio than all other nuclei, without exception, such a matching condition can always be met. In the example of a spin-$\frac{3}{2}$ nucleus n, appropriate to Cu, it takes the form

$$|\gamma_\mu H/2\pi| = |Q \pm \gamma_{\rm n} H/2\pi| \qquad (7.4)$$

where Q is the quadrupole coupling constant (also equal to the zero-field splitting, in frequency units, between the $m_z = \pm\frac{1}{2}$ and $\pm\frac{3}{2}$ levels). Here the quadrupole coupling originates in the radial electric field gradient from the muon itself. The level crossing resonance (which occurs in Cu at about 8 mT) constitutes a more precise measurement of this nearest-neighbour interaction than is possible from the field dependence of the transverse depolarisation rate (§ 5 and figure 33). It would be of interest to determine the quadrupole coupling to successive shells of Cu nuclei as (*a*) the direct coupling from the screened muon charge may be oscillatory in distance and (*b*) there may also be an indirect coupling, i.e. a field gradient induced by distortion of the lattice from cubic symmetry, which falls off algebraically with distance. Similar studies may be envisaged in insulators, with the electric field gradients interpreted in terms of lattice polarisation.

Unfortunately the strength of the resonance, i.e. the probability of flip-flop transitions, relies here on dipolar coupling between the muon and nuclear spins and may be too weak for more distant nuclei. Abragam (1984) estimates the strength of the cross-relaxation by relation to the depolarisation rate in zero field.

7.3.2. Measurement of nuclear hyperfine couplings. Cross-relaxation may be effective over a longer range when mediated by an electronic spin. Thus, in a molecular radical, the transition frequencies for the muon may be tuned to match those of the other nuclei n in turn, as in (7.5) (the choice of signs corresponds to the use of the 'upper' or 'lower' transition frequencies (cf figure 45) and again always allows a resonance condition to be found):

$$|\gamma_\mu H \pm \tfrac{1}{2}A_\mu| = |\gamma_\mathrm{n} H \pm \tfrac{1}{2}A_\mathrm{n}| + \text{second-order terms.} \qquad (7.5)$$

Coincidences of this sort result in sharp dips in the repolarisation curve, as in figure 54(*b*). Their position determines the nuclear hyperfine couplings relative to that of the muon very precisely. A complete characterisation of the muonated radicals is therefore possible. Transverse-field μSR gives the muon hyperfine coupling A_μ but (as explained in § 6) is generally insensitive to the other nuclear couplings A_n. Level crossing resonance provides access to these other couplings and also determines their relative sign (this is particularly noteworthy, since relative signs are rarely obtained in conventional ESR or ENDOR studies). The first such results are shown in figure 55(*a*), for the radical $\dot{\mathrm{C}}_6\mathrm{F}_6\mathrm{Mu}$ (Kiefl *et al* 1986). Field modulation was used to avoid systematic errors or drifts in forward–backward asymmetry and to produce this beautiful derivative spectrum. The experiment is noteworthy for the use of integral counting to benefit from a high beam

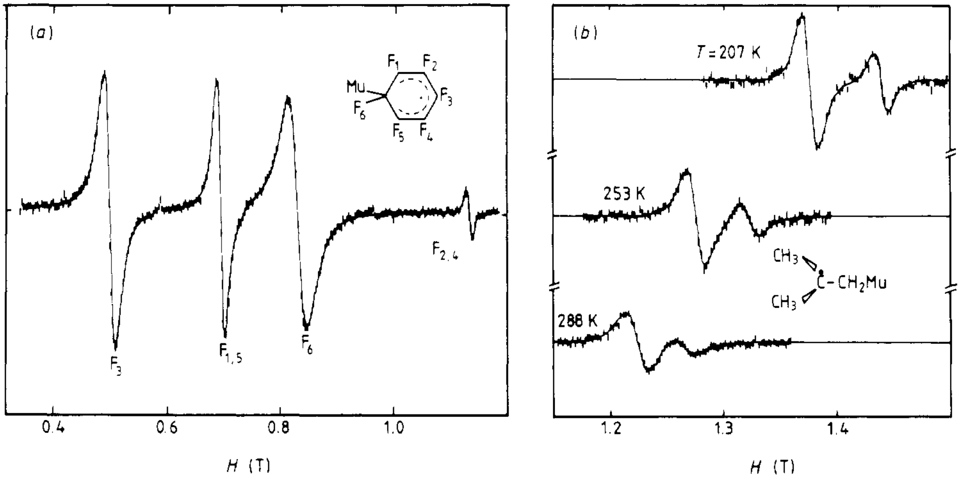

Figure 55. Level crossing resonance for the radicals $\dot{\mathrm{C}}_6\mathrm{F}_6\mathrm{Mu}$ (*a*) (Kiefl *et al* 1986) and $(\mathrm{CH}_3)_2\dot{\mathrm{C}}.\mathrm{CH}_2\mathrm{Mu}$ (*b*) (Percival *et al* 1987). The assignment of the ^{19}F resonances in (*a*) is as shown; even the *meta*-fluorine resonance is detectable (coupling is weak at this position, which is close to a node in the electronic wavefunction). In (*b*) the stronger resonance is with the CH_3 protons, whose hyperfine constant is independent of temperature; the shift with temperature therefore reflects the variation of the muon hyperfine constant (cf figure 46). The weaker resonance is with the $\mathrm{CH}_2\mathrm{Mu}$ protons. The separation of the two decreases with increasing temperature, as free rotation of the $\mathrm{CH}_2\mathrm{Mu}$ group is approached.

intensity; total positron count rates are recorded in the forward and backward telescopes, no correlation with the incoming muons being necessary for this purpose. Couplings to all four inequivalent ^{19}F nuclei are obtained. Even the resonance corresponding to fluorine at the *meta* position is clearly visible; hyperfine coupling is small at this position in the ring, which is very close to a node in the electronic wavefunction.

7.3.3. Future possibilities. This procedure essentially maps the distribution of spin density in the entire molecular radical—a procedure which will now be applied to the various muonium-related paramagnetic centres observed in insulating solids (notably Mu*; see § 4) (Kiefl 1985). This mapping should provide an explicit test for the various electronic structures that have been predicted for these centres (§§ 4.4–4.6). For the muonium-substituted organic radicals, more detailed comparisons with the ESR data on the unsubstituted radicals will now be possible. The ability to determine so precisely the ratio of the hyperfine couplings to nuclei neighbouring the muonium will lead to elucidation of the puzzle of the iostope effect in molecular radicals, for instance; notably it should be possible to establish the importance or otherwise of isotope-dependent hyperconjugation (§ 6.2), via the sensitivity of this mapping to any small redistribution of spin density. Results such as those reported in figure 55(*b*) should prove decisive here.

It is also apparent that a low-order degeneracy between two systems will be lifted in higher order by any non-diagonal element connecting the two. That is, the crossing of the levels is actually avoided, as illustrated in figure 56. Indeed, this is a criterion for detection of the resonance, since no cross-relaxation is possible between isolated systems for which the degeneracy is not lifted. The size of the splitting or energy gap is a measure of the strength of the interaction, and its direct measurement will broaden the scope of this novel spectroscopy considerably. The muonic radicals offer particularly clean

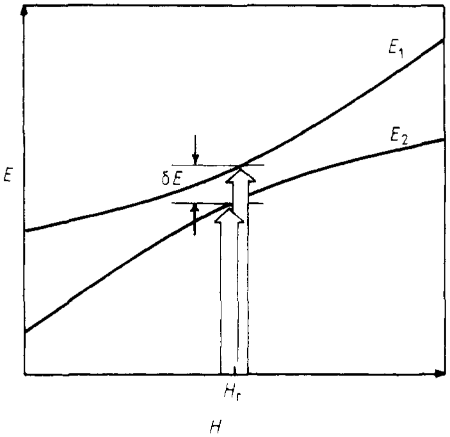

Figure 56. An illustration of the avoidance of level crossing in a two-level system described by the determinant

$$\begin{vmatrix} E_1(H)-\lambda & A \\ A^* & E_2(H)-\lambda \end{vmatrix} = 0.$$

The arrows indicate how a transverse-field μSR line would be split at H_r. ($\delta E = (AA^*)^{1/2}$.)

systems in which an oscillatory evolution of the muon polarisation may be observed at the resonant field, with a frequency equal to the energy gap. An oscillatory exchange of polarisation between the muon and another nucleus is just detectable in the results of Kiefl *et al* (1986). (For this purpose of course, time-differential spectra are required; integral counting gives the Laplace transform of the longitudinal relaxation function, i.e. its average over all muon lifetimes.) For the precession signal observed in transverse field at the resonant value, the energy gap should result in a splitting of the 'conventional' μSR line.

The conditions for cross-relaxation in radical systems are examined theoretically by Heming *et al* (1986), who also give preliminary experimental results for the radical formed in acetone. (These authors prefer to call the technique 'avoided level crossing', for the reasons mentioned above.) Both groups also point out that cross-relaxation within radicals may in principle be observed even when these are formed slowly. Like the RF resonance experiments mentioned above, and the techniques of time-delayed analysis described in § 8, this relies on the conservation of longitudinal polarisation during chemical reaction. Whereas transverse-field signals are lost when the muonium precursor lifetime exceeds about 10^{-10} s, longitudinal-field 'resonances' may still be visible even when the precursor lifetime approaches 1 μs! These four orders of magnitude must permit the observation and study of a vast new class of radicals.

In the demonstration experiments to date, the μSR transitions employed for cross-relaxation represent flips of the muon spin alone (in the case of Cu/Mu^+ as a result of the diamagnetic environment, and in the case of $C_6^{\bullet}F_6Mu$ as a result of the Paschen–Back condition, i.e. decoupling in a sufficiently high field). In principle transitions of the total spin could be employed; those of muonium itself, for instance, could be tuned to very much higher energy level separations (Abragam 1984). A variety of future applications of this spectroscopy may be envisaged. High on the list of priorities, for instance, must be the determination of tunnel splittings, and the chemical identification of the elusive diamagnetic fraction, in suitable materials, via quadrupole resonance.

7.4. *Zero-field relaxation in dense spin systems*

The unique sensitivity of zero-field μSR to motional effects is illustrated in figure 57. This shows the various forms of the relaxation function encountered in the study of dense spin systems, i.e. for an array of magnetic moments arranged on a regular lattice (Hayano *et al* 1980). When these moments are static, the relaxation function $G_z(t)$ exhibits an initial gaussian decay (characterising the gaussian width of the field distribution), but subsequently recovers to a third of its initial value. This distinctive feature represents the proportion of the initial muon polarisation which is held indefinitely by the static, although randomly oriented, local fields.

It is noteworthy that the form of this zero-field relaxation function was calculated in 1967 by Kubo and Toyabe, but found no application to feasible experiments before the advent of zero-field μSR (Yamazaki 1979, Hayano *et al* 1979). Its demonstration is impossible by NMR for instance, without contriving field-switching sequences for polarisation and measurement (Zax *et al* 1985). The one-third recovery is an invaluable signature of a static field distribution (and likewise of a static muon probe), and has been demonstrated in numerous systems, both of atomic moments (e.g. MnSi; Hayano *et al* 1980) and dipolar nuclei (e.g. Cu; Clawson *et al* 1982, Kadono *et al* 1985b). The initial gaussian decay is more rapid than that of high-field transverse relaxation, by a numerical factor that relates the effective widths of the longitudinal- and transverse-field distri-

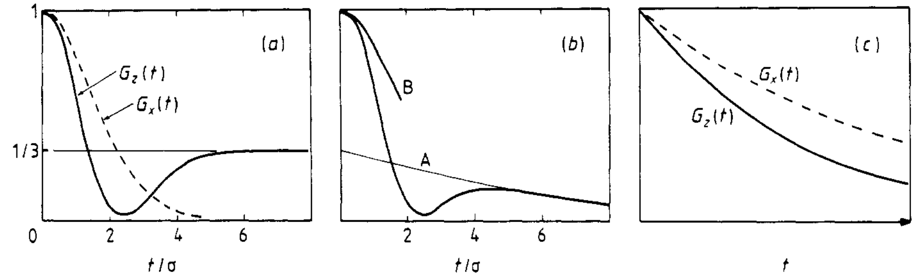

Figure 57. Zero-field relaxation functions $G_z(t)$ for a dense spin system, i.e. with a basic distribution of local fields that is gaussian (of width σ). When this distribution is static, the Kubo–Toyabe relaxation function (*a*) shows a distinctive recovery to a third of the initial polarisation. It is also initially faster than the transverse relaxation $G_x(t)$, shown for comparison as the broken curve. The onset of slow fluctuations, $\nu \ll \sigma$, is first indicated by a decay of the $\frac{1}{3}$-tail (*b*)—see curve A. An increased fluctuation rate, $\nu \sim \sigma$, begins to stretch the initial relaxation (*b*)—see curve B (as well as motionally to narrow the transverse-field linewidth). Note: curves A and B are both for $G_z(t)$. In the limit of fast fluctuation, $\nu \gg \sigma$, the longitudinal and transverse relaxation functions are both exponential (*c*) (the longitudinal rate again being faster by a numerical factor).

butions. The transverse relaxation function $G_x(t)$ is shown for comparison in figure 57 (this is just the envelope of the precession signals, such as in figure 4). These differences are demonstrated, for instance, by data relating to the dense array of proton spins in ZrH_2 (Uemura *et al* 1979).

The origin of the $\frac{1}{3}$-tail to the Kubo–Toyabe function, and the manner in which an applied longitudinal field dominates the random local fields to preserve the whole initial polarisation, are shown in figures 58 (and 60, below). These are adapted from Chappert (1984). This behaviour, including the effect of a small applied field of the same order as

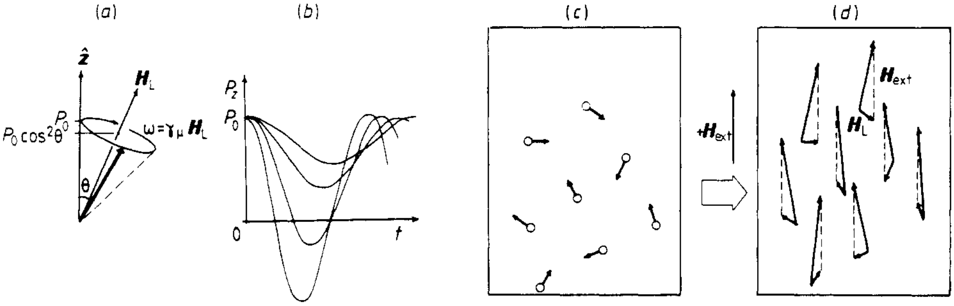

Figure 58. Zero-field relaxation viewed as a precession (*a*) of individual muons about arbitrary local fields H_L. The Kubo–Toyabe relaxation function (Kubo and Toyabe 1967) is a superposition (*b*) of oscillatory terms corresponding to all possible orientations θ of the static local fields, and with a gaussian distribution of H_L. A time-average component $P_0 \cos\theta$ of the initial polarisation P_0 is retained along the initial direction z. Integration over all possible orientations of H_L (i.e. over the ensemble of muon sites, as in (*b*)) gives

$$P/P_0 = \tfrac{1}{2}\int \sin\theta \cos^2\theta \, d\theta = \tfrac{1}{3}.$$

This is the $\frac{1}{3}$-tail of figure 57(*a*). The whole initial polarisation is preserved in a sufficiently large longitudinal field, which adds vectorially to the local fields as in (*c*) and (*d*).

the local fields (Yamazaki 1979) is nicely illustrated by data for MnSi (Hayano *et al* 1980). These data also serve to illustrate the precision with which the ambient magnetic field (i.e. that of the Earth, but often including stray fields from the nearby accelerator) must be compensated if the Kubo–Toyabe tail is to be displayed.

In their formulations developed specifically for the μSR case, Celio and Meier (1983) show that the zero-field relaxation may often show some oscillatory deviation from the Kubo–Toyabe function, associated with the discrete nature of the lattice (figure 59(*a*)) (see also Petzinger and Wei 1984). The additional wiggles have been identified, for example, in copper (Kadono *et al* 1985b). They are accentuated when the muon interacts only with a small number of nearby dipoles. In the alkali and alkaline-earth fluorides a particularly distinctive beat pattern in the relaxation function (figure 59(*b*)) indicates that the diamagnetic muon essentially couples to two ^{19}F nuclei only (Brewer *et al* 1986). Accordingly the muon site is identified as midway between two F$^-$ ions. A good chemical precedent exists for this in the form of the known molecular ion (FHF)$^-$.

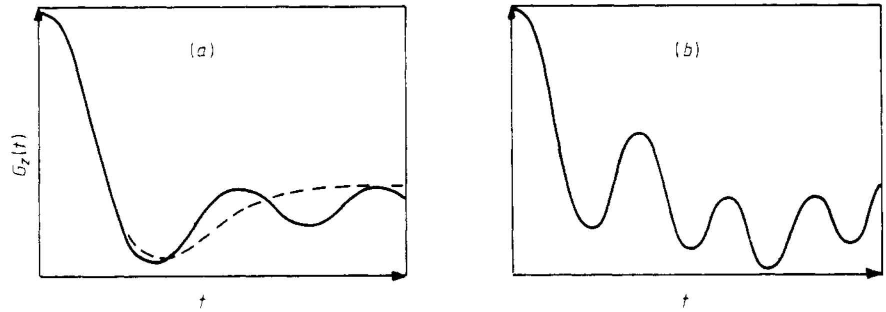

Figure 59. Modification of the Kubo–Toyabe function (broken curve) for a discrete lattice, e.g. Cu (*a*) (sketched from Kadono *et al* 1985b) and an example of extreme behaviour of this sort observed for the (FMuF)$^-$ ion in alkali fluorides (*b*) (sketched from Brewer *et al* 1986).

The onset of slow fluctuations of the host magnetic moments, or slow movement of the muon probe, results in an exponential decay of this $\frac{1}{3}$-tail, as long-term memory of the direction of initial polarisation is lost (Uemura 1981a, Yamazaki 1982). This is already apparent at fluctuation rates that are far too slow to affect the shape of the initial decay, or of the transverse relaxation function (figure 57(*b*), curve A). (Of course, some care is required in distinguishing this second decay from the wiggles of figure 59). Motional narrowing of the field distribution, and the corresponding reduction of the initial decay rate (figure 57(*b*), curve B) is only effective at higher fluctuation rates ν, of the order of the distribution width σ. In the limit of fast fluctuation, both the longitudinal- and transverse-field relaxation functions tend to exponentials (although with the longitudinal rate again faster by a numerical factor—see, for instance, Chappert 1984). The corresponding μSR lineshape functions are then motionally narrowed to lorentzians. In this limit the zero-field and longitudinal-field relaxation functions are identical (Uemura 1981b). Figure 60 emphasises the contrast between the cases of (*a*) static and (*b*) fast dynamic local fields. In this latter case there is no significant change of the relaxation function on application of a longitudinal field.

7.4.1. Diffusion studies using zero-field μSR. Two examples of the power of the zero-field technique in elucidating puzzles in diffusion studies are particularly noteworthy. In

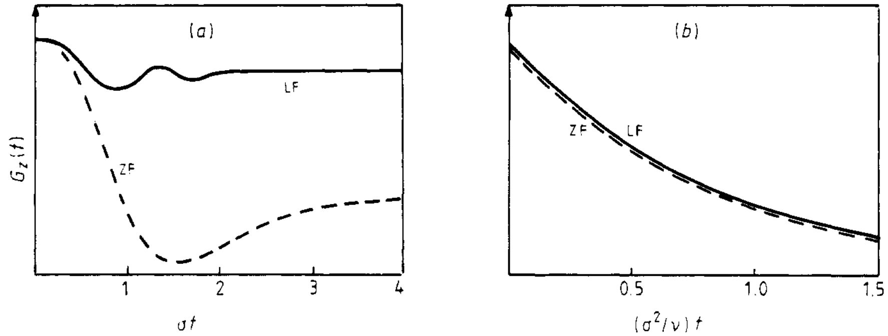

Figure 60. A comparison of the longitudinal relaxation function in zero field and in a longitudinal field. Decoupling of static random fields produces a gross change of relaxation function (*a*), whereas no significant change is detectable in the dynamic case, (*b*), in the limit of fast fluctuation. Note the difference in timescales between (*a*) and (*b*).

copper (referring to figure 37) the plateau exhibited by the μSR linewidth, at liquid helium temperatures, illustrates the loss in sensitivity of the transverse-field method to motional effects when the muon is nearly trapped, i.e. when the characteristic hopping rate ν is small compared with the static dipolar linewidth σ. The question also remains as to whether the apparent narrowing of the line at lower temperatures, in the dilution refrigerator range, is a genuine motional narrowing or a reduction in σ due to a change of the preferred muon site (i.e. to a change in the origin for the dipolar sum). The zero-field relaxation allows independent measurements of σ and ν, the former from the initial gaussian decay of the Kubo–Toyabe function, the latter from the slow decay of its $\frac{1}{3}$-tail. Precise measurements (Clawson 1984, Kadono *et al* 1985a) show the dipolar width to be virtually independent of temperature from below 100 mK to above 100 K (thereby excluding the hypothesis of a site change) and, at the same time yield a temperature-dependent hopping rate consistent with the theory of Kondo (§ 5.6).

In these studies the local fields are taken to be static, and the frequency ν in figure 57 is identified with the muon hopping rate or inverse residence time. Implicit in the formulation is the assumption of a unique value of ν. This assumption fails in the presence of impurity atoms or lattice defects. Lattice conditions are then no longer homogeneous and the muon may be trapped preferentially close to impurities, or at least have a greater residence time in these deeper wells. Increasing temperature increases the muon mobility within the undisturbed lattice but thereby increases the probability of encounter with the preferred traps. Further increase allows escape from these deeper wells. The transverse-field lineshape is narrowed in both cases, and so in itself is not especially sensitive to the different types of motion (although whether it narrows or broadens with increasing temperature is a good clue). Petzinger (1980) demonstrates how the precise form for the zero-field relaxation function is able to distinguish motion *towards* and escape *from* preferred trapping sites. In the former case, if polarisation is preserved until the trapping sites are reached, a $\frac{1}{3}$-tail is then retained indefinitely; in the latter case, no such memory of the initial polarisation is retained.

7.5. Zero-field relaxation in dilute spin systems

The zero-field relaxation functions encountered for sparse or dilute spin systems are illustrated in figure 61. Here μSR has found a major application in the study of spin glass

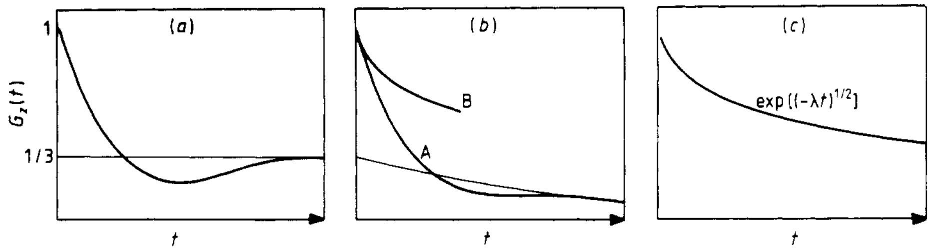

Figure 61. Zero-field relaxation function $G_z(t)$ for a dilute spin system, i.e. with a lorentzian basic distribution of local fields (contrast figure 57). When this distribution is static (*a*) $G_z(t)$ is now lorentzian at short times and recovers to a third at long times. Slow modulation again results in a decay of this ⅓-tail as in (*b*), curve A. No motional narrowing of a lorentzian distribution is expected, yet the spin glass relaxation function is 'stretched' as in (*b*), curve B, as the modulation rate is increased This can be understood as a concomitant narrowing of the effective or underlying distribution of static fields from the 'frozen moments', as the order parameter decreases in magnitude towards T_g. In the limit of fast fluctuation the relaxation function takes a 'root exponential' form (*c*).

systems, where magnetic atoms occupy at random a small proportion of the lattice sites in a non-magnetic host. Attention has focused on the dilute magnetic alloys (consisting of a fraction of an atomic per cent of Mn in a matrix of Cu, for example, denoted **CuMn**; likewise **AuFe**, **AgEr** etc) but some insulating systems have also been studied (Heffner *et al* 1982, Emmerich *et al* 1983, 1985, Yamazaki 1984b, Uemura *et al* 1980, 1985).

In these materials, the phenomenon known as frustration, i.e. the competing tendencies for a particular spin to align ferromagnetically or antiferromagnetically with its immediate neighbours, precludes any long-range magnetic ordering. Each spin receives contradictory messages, via different exchange paths, as to which way it should point. The spins are believed to be frozen in a so-called spin glass order below a certain temperature T_g (known variously as the 'glass' or 'freezing' temperature, at which the AC susceptibility exhibits a characteristic cusp; see, for instance, Mydosh 1978). Individually the moments have a time-average value that is retained in magnitude and orientation, although no long-range correlation of the orientations exists. Well above T_g, these systems are certainly paramagnetic, and the moments free to reorient at random. Yet despite intensive investigation, both experimental and theoretical, the existence or otherwise of a genuine phase transition and associated critical phenomena in the vicinity of T_g have still not been clearly demonstrated. In this context, any new information on the properties of these materials is most welcome. μSR is certainly able to report on the dynamical properties: it opens a particularly appropriate time window for the measurement of correlation times, in the range 10^{-4}–10^{-10} s. Much of this range (10^{-4}–10^{-8} s) is otherwise inaccessible—it bridges the gap between AC susceptibility measurements, neutron spin echo and Mössbauer spectroscopy for instance (Uemura 1981a). Measurements of the type sketched in figure 61 have the particular advantage of avoiding any possible perturbation of the spin glass dynamics by an applied field. It may also be possible to draw some conclusions as to the nature of the spin-glass-ordered state.

Figure 61 may be compared and contrasted with figure 57. The differences originate in the basic distribution of local fields which for dilute systems is lorentzian rather than gaussian. This is true for any coupling between the host and probe spins which has an r^{-3} range dependence (e.g. dipolar and RKKY), and assuming that the probe spins also occupy the lattice at random (i.e. that there is a continuum of probe–host separations). The coupling between the muons and the host spins is usually assumed to be dipolar, and this has been confirmed explicitly by Heffner *et al* (1986) in **CuMn** and in **AgEr**. The same authors find a larger coupling in **AgMn**, however, which they attribute to an interaction of the RKKY type, i.e. an exchange coupling mediated by the conduction electrons. Considering the muon as a '*nuclear*' spin, this example is remarkable. Of course it is RKKY coupling between the host *atomic* moments that is the origin of the spin glass magnetic behaviour.

A consequence of the lorentzian field distribution is that the initial depolarisation is exponential, and notably that it has finite slope at (or very close to) the origin. Again a recovery to a third of the initial polarisation is expected if the fields are static (Kubo 1981) as in figure 61(*a*) as well as a long-term damping of this component at the onset of slow modulation, as in figure 61(*b*). In all the spin glasses investigated, slow modulation of the interstitial field is indeed seen—at temperatures well below T_g. As the muons themselves are believed to be static in the lattice, this implies a certain fluctuation of the host spins in the supposedly frozen regime. The characteristic damping of the $\frac{1}{3}$-tail to the relaxation function is seen in **CuMn** and in **AuFe**, for instance, up to about 0.5 T_g (Uemura *et al* 1980).

The stretching of the initial relaxation as the fluctuation rate increases (figure 61(*b*), curve B) is not, however, as straightforward as in figure 57(*b*). Considering the zero-field relaxation to be a superposition of oscillatory components (as depicted in figure 58(*b*)), a depolarisation rate that is finite close to the origin implies the existence of very high-frequency components, corresponding to extreme values of the local field. In normal motional narrowing, the depolarisation rate is greatly reduced when the steady accumulation of phase error for individual muons is replaced by a random walk of phase steps, *each individual step being small*. No such criterion can be satisfied if the continuum of frequencies involved extends indefinitely. (For comparison, high-frequency components are essentially absent in the case of a gaussian field distribution, whence the flat beginning of the relaxation function in figures 57(*a*) and figure 58. The requirement for motional narrowing can be quantified as $\tau_c\sigma < 1$, where for this purpose τ_c characterises the timescale on which the muon's magnetic environment fluctuates, and σ is the RMS width or root second moment of the field distribution; this latter quantity diverges for a strict lorentzian). No motional narrowing would be expected therefore for the case of a muon diffusing through a spin glass lattice, if it were to sample indefinitely high local fields by passing close to the host spins. In practice, of course, there is always a cut-off to the distribution, representing the minimum distance of approach.

The case of interest here, however, is that of static muons probing fluctuations of the local fields at fixed sites due to the host spin dynamics. Muons located some distance from the nearest spin will then certainly not experience large local fields, that is, they do not sample the whole field distribution but only some limited portion of it. In an early formulation of this problem due to Uemura (1980), small-amplitude gaussian fluctuations were assumed locally (these distributions being individually susceptible to motional narrowing) with a superposition that recreated the overall lorentzian distribution in a phenomenological fashion. A single effective correlation time τ_c for the fluctuation was also assumed, this parameter characterising the shape of the 'spin glass' relaxation function in this prescription. Its value, extracted from the fitted data for **CuMn**, **AuFe** and **AgFe**, covers nearly five decades from slow fluctuation below T_g to fast fluctuation above T_g (Uemura *et al* 1980, Heffner *et al* 1982). Data for the different materials (and different alloy concentrations) also scale as T/T_g, with $\tau_c \simeq 10^{-8}$ s at T_g

itself, so this value seemed to be a common, if not fundamental, characteristic of spin glass systems. The particualrly steep temperature dependence of the single parameter τ_c can undoubtedly be taken as a measure of how rapidly the spin dynamics is changing in the vicinity of the glass temperature. Yet the variation with temperature is smooth and monotonic, with no discontinuity of either magnitude or slope at T_g that could be taken as indicative of a phase transition. This is to be contrasted with the following, more recent, interpretation.

The portion of the total field distribution sampled by individual muons is also restricted if the surrounding spins do not reorient fully, but retain a memory of their initial direction, as in figure 62(*a*). This is the expectation of mean-field theories in which individual spins retain a time-average polarisation. The Edwards–Anderson order parameter Q (Edwards and Anderson 1976), for instance, is just the square modulus of this polarisation:

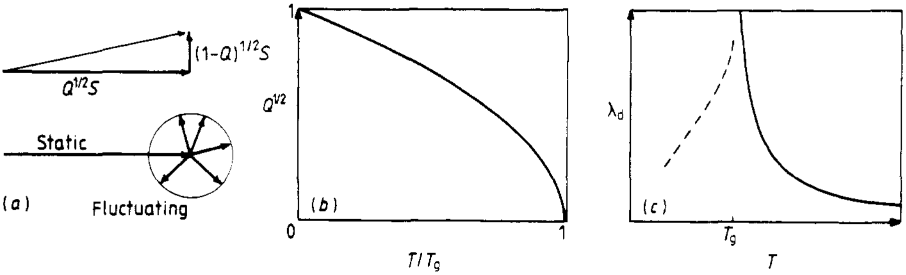

Figure 62. A spatially homogeneous model of spin glass freezing and supportive μSR results. Each individual spin (upper sketch) and local field at a muon site (lower sketch) is shown in (*a*), fluctuating within a limited range about a static component. For different spins, these 'frozen moments' are randomly oriented but their average magnitude is non-zero below T_g. The variation with temperature predicted by Kirkpatrick and Sherrington (1978) is sketched in (*b*). A distribution of static moments, roughly consistent with this behaviour, may be extracted from zero-field muon spin-relaxation function, in **AuFe** and in **CuMu** (Heffner *et al* 1982, Uemura *et al* 1984a, 1985). A dynamic depolarisation rate may also be extracted that exhibits critical behaviour in the vicinity of T_g, as in (*c*) (sketched from Uemura *et al* 1985).

$$Q = \langle S(\infty)S(0)\rangle / \langle S^2(0)\rangle \neq 0.$$

(The correlation function $\langle S(t)S(0)\rangle$ tends exponentially to this value, rather than to zero as is implicit in the single-τ_c model.) The quantity $Q^{1/2}S$ can be identified with the 'frozen moments' of Kirkpatrick and Sherrington (1978), whose predictions are sketched in figure 62(*b*). As temperature increases, the amplitude of the fluctuating component increases at the expense of the static one, which finally collapses at T_g.

Uemura *et al* (1981) find evidence for just such a coexistence of static and dynamic random fields below T_g in the form of the relaxation functions recorded in small decoupling fields. When this behaviour is incorporated explicitly in the formulation of the zero-field relaxation function (Heffner *et al* 1982, Emmerich 1982a,b, Uemura *et al* 1985) rather better fits to the experimental data are obtained. In particular the initial relaxation rate changes concomitantly with the damping of the $\frac{1}{3}$-tail (which cannot be accommodated in the older 'single-τ_c' model). In fact the initial rate in this formulation is simply a measure of the lorentzian width of the static random field distribution, and therefore of the amplitude of the frozen moments—the relaxation function 'stretches' as the static field distribution narrows. Results for **AuFe** (Heffner *et al* 1982) show a variation with temperature that is roughly consistent with figure 69(*b*), as do the original data for **AuFe** and **CuMn**, re-analysed in this model (Uemura and Yamazaki 1983, Uemura *et al* 1984, 1985). Likewise, the divergence of the dynamic depolarisation rate as T_g is approached, sketched in figure 62(*c*) for the results of Uemura *et al* (1985), may be taken as evidence of a critical slowing down of the magnetic fluctuations.

This interpretation may be contrasted with that of independent measurements in one of these systems, **CuMn**, Emmerich *et al* (1983). These measurements rely on the existence of two distinct host spin systems: the material has a dense regular array of nuclear (Cu) moments in addition to the sparse disordered array of atomic (Mn) moments. In the limit of fast fluctuation of the atomic moments, Kubo–Toyabe (figure 57(*a*)) relaxation is revealed due to the effectively static nuclear spins. In fact, in recordings of the zero-field relaxation taken to very high statistics, two components may be clearly discerned. These are attributed to spatial regions having quite different magnetic character, namely islands of spin glass order and rapid fluctuation elsewhere (figure 63). This behaviour is confirmed by the most recent experiments (Pinkvos *et al* 1984, 1986), which also demonstrate some dependence of the metallurgical history of the sample. The exchange interaction is negative for nearest-neighbour Mn pairs, positive for next nearest neighbours. The elastic interaction favours the next-nearest-neighbour configuration, so the proportion of ferromagnetically coupled spins increases with the degree of atomic short-range order.

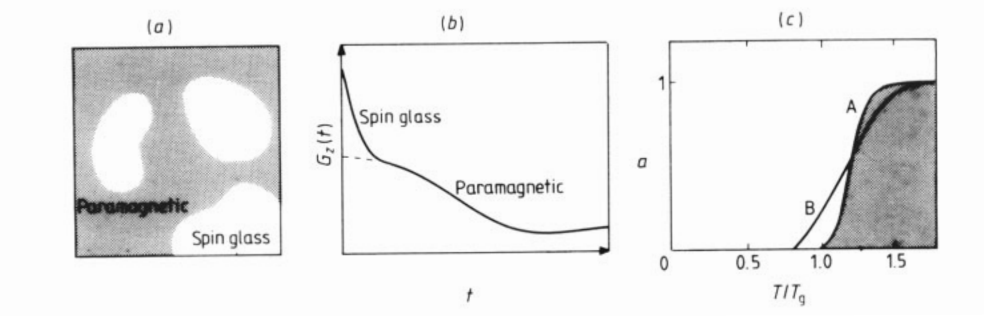

Figure 63. A spatially inhomogeneous model of spin glass freezing (*a*) and supportive μSR measurements (*b*). Islands of spin glass order, nucleating well above T_g, are illustrated in (*a*). The zero-field relaxation functions (*b*), recorded in **CuMn** *above* T_g, exhibit two components. The underlying Kubo–Toyabe function, characteristic of the regular array of static Cu nuclei, is seen for muons stopped in the paramagnetic region (the fluctuations of the atomic Mn moments being too rapid to affct this). The initial fast decay characterises the additional relaxation induced by the atomic moments for muons stopped in the islands of spin glass order. The fraction *a* of the total volume that is paramagnetic vanishes at T_g in quenched samples (A) and slightly below in slowly cooled samples (B), as in (*c*). (Sketched from Emmerich *et al* (1983) and Schenck (1985a).)

The observation of these islands of spin glass order *above* T_g, occupying an increasing proportion of the total volume as T_g is approached from above, is in direct conflict with the interpretation of figure 62 (which implies complete absence of order above T_g), and likewise with all models describing spatially homogeneous freezing! The recent **CuMn** data favour models of inhomogeneous freezing or magnetic clustering, achieving percolation at T_g. It is noteworthy that just such a model was proposed by Smith (1975) almost simultaneoulsy with the more celebrated theory of Edwards and Anderson (1975).

7.5.1. The form of the relaxation functions, and the decay of correlation functions. The form of the stretched exponentials in figure 61(*c*), as well as of the relaxation function in applied longitudinal fields is interesting. If this is written as $\exp[-(\lambda t)^{(1-n)}]$, then an exponent $n = \frac{1}{2}$ is expected in the fast-modulation limit, assuming a continuum of dipolar field strengths from different spins acting on the probe spin in a sparse or dilute system (McHenry *et al* 1972). This has been tentatively identified in the zero-field relaxation functions in **AgMn** (Heffner *et al* 1984a), and in **CuMn** (Uemura *et al* 1985). In figure 62(*c*), for instance, the results for λ_d *above* T_g (i.e. when there are no *static* random fields) were obtained by fitting the zero-field relaxation functions to the form $\exp[-(\lambda_d t)^{1/2}]$.

This 'root-exponential' form, $\exp[-(\lambda t)^{1/2}]$, has also been used by Heffner *et al* (1984a,b) to analyse the relaxation in an applied longitudinal field. This is Zeeman spin–lattice relaxation of the muons. The probability of a spin-flip transition is a measure of the spectral power in the fluctuations of the local field at the muon Larmor frequency. Its field dependence therefore maps the frequency spectrum of these fluctuations. Correlation functions for the host spins are deduced (via Fourier transform) to decay algebraically with time, i.e. as a power law, rather than exponentially (as is expected for dense spin systems) (MacLaughlin *et al* 1983). The comparison with neutron scattering data is reviewed by Heffner and MacLaughlin (1984).

7.5.2. Random magnets. Not all dilute magnetic systems show spin-glass behaviour; thus, in the dilute alloy **PdMn**, the long-range interaction Mn–Mn is ferromagnetic, but the short-range interaction, via direct overlap, is antiferromagnetic. This competition leads to spin glass behaviour for Mn concentrations above about seven atomic per cent. The admixture of antiferromagnetic couplings is insufficient at lower concentrations, and below 2% the ordered state is ferromagnetic. The comparison of μSR studies of the two regimes (Dodds *et al* 1983, Heffner *et al* 1984b) is noteworthy. No other μSR studies of random ferromagnets have been reported to date, however, and none on the more concentrated alloys where randomness is introduced by substitution of a few magnetic atoms in a regular array. This is surprising in view of the current popularity of the topic.

8. Pulsed versus continuous techniques, and muon spin *resonance*

Some seven major muon sources are currently available worldwide for μSR studies†, with various others being planned. A guide to their different muon intensities and momenta, and the relevant characteristics of the primary accelerators, is given by Grynszpan (1984). (Certain facilities have been upgraded since this compilation; those

---

† The principle facilities active in Europe at the date of writing are at CERN (European Laboratory for Particle Physics, Geneva), SIN (Swiss Institute of Nuclear Research, Villigen, near Zürich) and LNPI (Nuclear Physics Institute, Gatchina, near Leningrad); those in North America are at TRIUMF (the 'Tri-Universities Meson Facility', Vancouver) and at LAMPF (meson facility of the Los Alamos National Laboratory, New Mexico) and in Japan at KEK (National Laboratory for High Energy Physics: University of Tokyo Meson Science Laboratory, Tsukuba-gun, near Tokyo). Pioneering work was performed formerly at LBL (Lawrence Berkeley Laboratory, Berkeley, California) and at JINR (Joint Institut for Nuclear Research, Dubna, near Moscow; faciltities at Dubna are expected to be recommissioned).

at SIN (Switzerland) and TRIUMF (Canada) are now especially noteworthy for their high intensity and range of experimental facilities.) With one exception, the sources used to date (1986) are 'continuous', in the sense defined below. All the early sources were continuous, and this is reflected in the techniques of data acquisition that are most commonly used. The exception is a 'pulsed' source, which has already been operating at KEK (Japan) for a number of years, with a prodigious research output. A particularly intense new pulsed muon source dedicated primarily to condensed matter research, is now also under construction at RAL† (UK), based on the ISIS spallation neutron source.

In other spectroscopies, e.g. optical, magnetic resonance, neutron diffraction etc, the development of pulsed techniques has generally resulted in faster accumulation of data (through more efficient use of the radiation or simply increased average intensity) plus other benefits specific to each subject. With the advent of pulsed muon sources, it is appropriate now to evaluate their suitability for the various different applications of μSR, relative to continuous sources. Likewise it is appropriate to examine their potential for new science, together with any consequent changes in the style of experimentation or techniques of data acquisition that seem likely.

8.1. The limit of the data rate at continuous sources

At a continuous source, the repetition period of the primary accelerator (affectionately known as the 'machine') is short compared with the muon lifetime. This is therefore also true of any time structure in the muon intensity, which reflects that of the machine to a greater or lesser extent, depending on the manner in which the primary beam is extracted. The 'time differential' method of accumulating μSR histograms, which is adopted in the majority of experiments, generally requires that only one muon be present in the sample at a time. This was automatically the case for older machines, working at low muon intensities, but it imposes a limit on the rate at which muons should be implanted in a sample (and therefore on the rate at which data can be accumulated) even when higher intensities are available. This limit is of order $\frac{1}{10}\tau_\mu^{-1}$ for a stochastic source; the precise value generally lies between 10^4 and $10^5\ \mathrm{s}^{-1}$ depending on the nature of the experiment, as may be appreciated from figure 64.

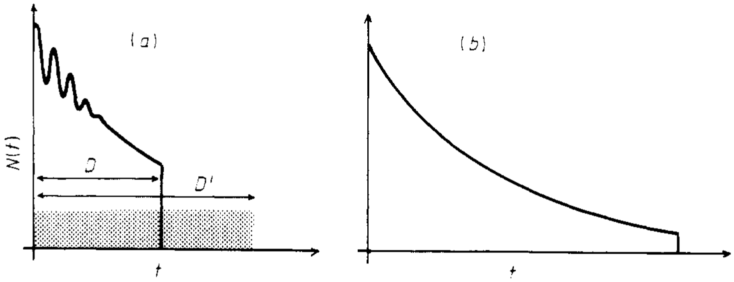

Figure 64. μSR histograms recorded for the determination of (*a*) a prominent precession frequency or rapid (transverse) relaxation function and (*b*) a slow (longitudinal) relaxation function. The data gate D (and likewise the pile-up gate D'; see the text) is necessarily longer in (*b*); here the need for good signal-to-noise ratio far into the tail of the radioactive decay curve implies a lower average data rate and longer accumulation times than in (*a*)

---

† Rutherford Appleton Laboratory (Oxfordshire; see title page). See note added in proof.

Equal weighting or counting probability must be ensured for all events within a specified 'data gate' D. Thus in the data-acquistion scheme depicted in figure 7, which is typical, events are accepted by the encoding logic if they comprise one muon start signal plus one positron stop signal, with no more of either. For instance, an event is rejected if a second muon arrives too soon, namely before a certain time interval D' has elapsed; likewise the second muon is not accepted as a new start signal under these circumstances. This device, known as a pile-up gate, largely safeguards against false muon–positron correlations for a stochastic source working close to the maximum data rate. It likewise avoids any bias in the counting probability that might favour early events, but makes inefficient use, however, of a beam with a pronounced time structure, i.e. when most muons arrive in 'bursts'.

Machines that are able to deliver muon fluxes much higher than $10^5\,s^{-1}$ cannot, therefore, be used fully in time-differential experiments of this type. Of course, it is always advantageous to have a high intensity available, for instance so that the maximum data rate can be achieved even with samples of small cross section, using tight collimation of the beam. Furthermore, the restriction on data rate does not apply to every method of data acquisition. Thus higher rates can be achieved with stroboscopic μSR (§ 3.3). This technique exploits the time structure of the muon intensity at SIN, which is especially favourable for this purpose, by tuning the μSR frequency to the neighbourhood of the machine frequency. Higher rates may also be achieved in the other experiments able to employ integral counting techniques (§§ 7.2 and 7.3). The advantage here is not necessarily proportional to raw flux however (see below).

Otherwise, for time-differential measurements, muons from continuous sources must still be implanted one-by-one; no satisfactory means of lifting this restriction has yet been demonstrated. Systems that call for muons as required, by opening and closing an intense beam in response to the data-acquisition signals themselves (or, better still, switching it between parallel experiments) are currently under consideration at SIN and at LAMPF. These should raise the data-rate limit somewhat, and likewise allow more efficient use to be made of beams with an unfavourable time structure. In principle, more than one muon may also be allowed in the sample simultaneously if these can be correctly paired with their decay positrons via trajectory reconstruction. Unfortunately, particle detectors with the necessary spatial resolution are themselves inherently slower than simple scintillation counters so no overall gain in data rate has yet been achieved by such a spectrometer (Podini and Tedeschi 1984).

8.2. *Characteristics of pulsed μSR*

A 'pulsed' source is defined here to mean one that delivers muons in discrete bursts whose duration is short, and repetition interval long, compared with the muon lifetime. Under these circumstances, the association of inividual positrons with their parent muons is neither possible nor necessary: following each burst, the arrival times of the detected positrons are measured with respect to a common start signal. In figure 65 and in the following, the term 'frame' is adopted for the cycle of implantation, data acquisition and preliminary processing. In principle a histogram may be established at each frame, and high statistics accumulated by summing the histograms from successive frames.

8.2.1. The data rate and quality of the histogram. For time-differential μSR, this mode of operation removes any fundamental restriction on data rate that is related to muon lifetime. Although the average intensity available at the KEK source is as yet barely

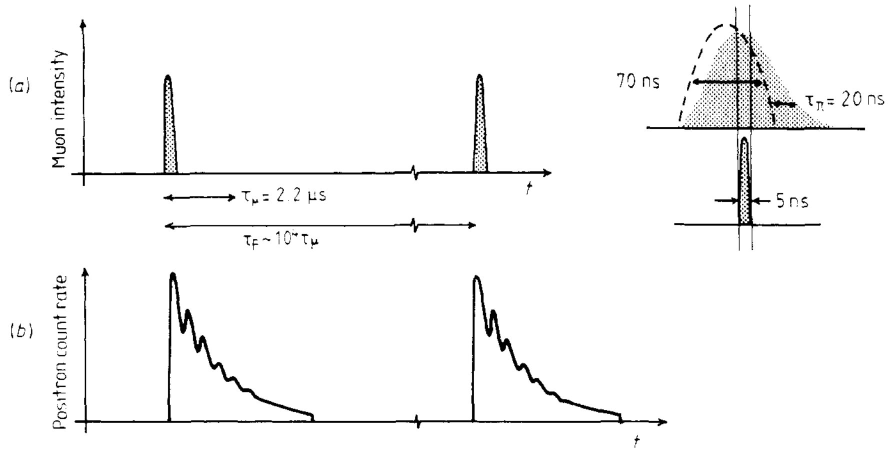

Figure 65. The delivery of muons in intense bursts with a low duty cycle at a pulsed source (*a*), allowing a complete radioactive decay curve to elapse in the time τ_F between successive bursts. (τ_F = 50 ms at KEK and 20 ms at ISIS.) The cycle of data acquisition and preliminary histogramming (*b*) is referred to as a 'frame'. Details of an individual pulse at the ISIS machine are shown at the inset to (*a*). The broken curve is the profile of the intrinsic (proton) machine pulse. Generation of surface muons lengthens this by a 20 ns tail (this is the pion lifetime); cf equation (2.1)). Selection of a narrow central 'slice' would improve the timing resolution. Compression of the pulse, better still, would achieve this without loss of intensity.

sufficient to demonstrate any advantage in this respect over the best continuous sources, substantial increases are anticipated at the ISIS source (Carne *et al* 1984, Eaton *et al* 1983). Thus the histogram of figure 3 (which comprises about 5×10^5 events—somewhat low by modern standards—and which actually took 30 minutes to record at CERN) would be accumulated in about 5 minutes at SIN or at KEK while it could represent as little as 10 s beam-time at ISIS. (The rate that can be achieved in practice is likely to be set by instrumental limits; see § 8.5.) Not least of the advantages of such high data rates are that the stability of the sample environment during the measurement time will be more easily achieved, and that detailed temperature dependences, for instance, could be recorded 'on the run', as the sample warms or cools.

Even for the 'resonant' depolarisation experiments described in § 7, which already benefit from integral counting, some improvement in sensitivity (for a given data rate) may be anticipated in the pulsed mode (Hartmann 1986). At a continuous source, integral counting implies that the polarisation is averaged over all muon lifetimes. The average is therefore weighted by the radioactive decay curve towards early events. These are of little value in seeking a resonance, however, since the depolarisation function is invariably flat at the origin. It would be possible in the pulsed mode to select a more appropriate window for the average, as in figure 66(*a*), and to improve the figure of merit of the data accordingly. More importantly, pulsed μSR can record time-differential spectra at high intensity. Thus for level crossing resonance, for instance, the additional information in the shape of the cross-relaxation function is preserved, whereas integral counting gives only the Laplace transform of this function.

The pulsed mode also eliminates a number of spectral artefacts and distortions, but can introduce some others of its own. Those illustrated in figure 67 include background and initial deadtime. Surface and non-surface beams show somewhat different features here and in the following it is assumed that positron contamination in surface beams is

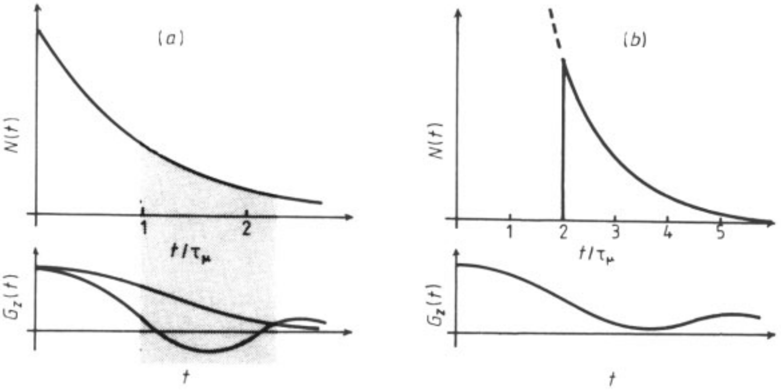

Figure 66. Possible tricks for improving the figure of merit of longitudinal-field data in the pulsed mode. In (*a*), polarisation is averaged over a lifetime interval (shaded) most appropriate to the detection of depolarisation via RF resonance or cross-relaxation. In (*b*), detection of early events is sacrificed (by suppression of the photomultiplier tube gain to avoid overload) so high intensity may be used to examine the form of the relaxation function at long times.

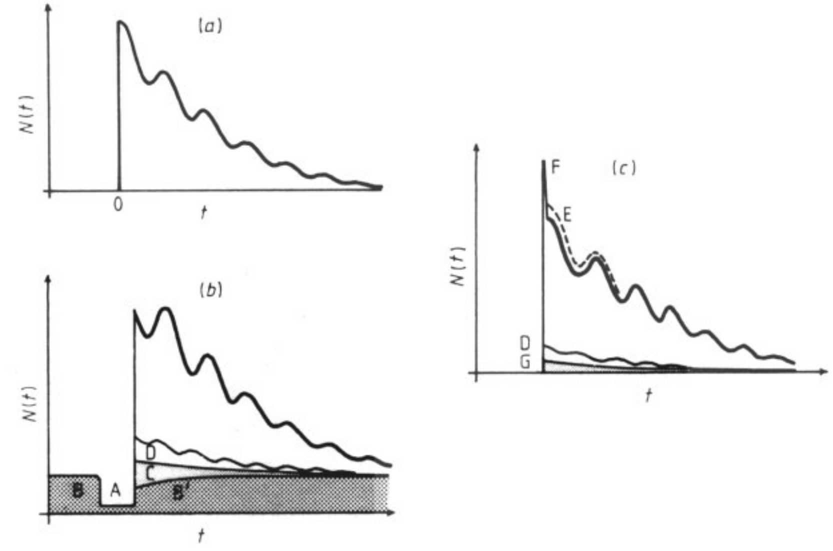

Figure 67. Instrumental artefacts in μSR histograms. An ideal histogram (*a*) would exhibit no background or distortion and allow the time-zero to be readily determined. Common artefacts are shown in (*b*): (A) anticoincidence suppression (obscuring the time-zero); (B) correlation background (often non-linear (B′) at high rates); (C) unpolarised muons (e.g. from decay of pions reaching sample); (D) oscillatory background (i.e. the precession signal of muons stopped in cryostat walls etc). A and B are absent in pulsed μSR (*c*) although counter overload can lead to underestimation of the event rate at low elapsed times (E) and in non-surface beams a substantial prompt signal (F) may be expected. A background G from the decay of muons in the production target would also be present in a surface muon beam with no mass separation. C, F and G, are eliminated in an uncontaminated (i.e. separated surface muon) beam.

entirely removed using an electrostatic separator. Background (B, B′) arises from false muon–positron correlations and is particularly troublesome (i) at short elapsed time, if it is non-linear (as may be the case when veto-circuits become overloaded at high average intensity, or through unfavourable bunching of the beam) and (ii) at long elapsed time, where it spoils the signal-to-noise ratio in the tail of the radioactive decay curve. Although the constant background (B) can be low for a particularly clean beam (e.g. at TRIUMF), for most continuous sources it precludes measurements beyond about 10 μs. For a pulsed source, since the beam-line is quiet following the particle burst, the constant or late background (B) is automatically eliminated. This is particularly advantageous for the determination of slow longitudinal relaxation functions. The importance of such clean histograms for zero-field studies especially, where the evolution of polarisation at long elapsed time is crucial to the interpretation (§§ 7.4, 7.5), may readily be appreciated. μSR studies at KEK have exploited this area accordingly (Nagamine 1984) and measurements out to 15 μs are routine (see, for instance, spectra reported by Kadono *et al* (1984) and Tanigawa *et al* (1984)). With greater intensity, the scheme of figure 66(*b*) could be envisaged, which sacrifices the initial portion of the relaxation (to avoid saturation of the particle counters) for the sake of high statistics at long elapsed time. For the ISIS design intensity, a data gate well beyond 20 μs (around 10 τ_μ) should be feasible. (A somewhat optimistic ultimate limit of 50 μs, set by the cosmic ray background, has been estimated by Bugg 1983.)

Selection of just the highest-energy positrons (by stopping those with lower energy in a degrader placed between the sample and the detectors) may also be an advantageous solution to the problem of counter overload, these having the greatest analysing power (i.e. the largest asymmetry parameter; see § 2).

For non-surface continuous beams, the anti-coincidence logic that selects correctly implanted muons obscures an initial portion (typically >30 ns) of the histogram. For a clean surface beam, this initial dead-time can be much reduced since (other than for very thin or gaseous samples) no downsteam anti-coincidence counter is necessary. In the pulsed mode there is in principle no initial dead-time, although good separation is required to avoid a prompt burst of spurious particles. The effective initial dead-time is then the pulse width itself, or the 'time-bin' width (the unit of time used in the histogramming), whichever is the greater, as explained below.

8.2.2. Time resolution. If the muon bursts were sufficiently sharp, all current μSR research could be performed in the pulse mode, and time-differential experiments would benefit simply from the potential increase in data rate. A finite duration of the pulse, however, and the corresponding uncertainty in the arrival time of individual muons with respect to the common start signal, limit the time resolution of a pulsed spectrometer. For the determination of slow longitudinal relaxation functions this is of no consequence. Such experiments benefit from the pulsed mode as stressed above, low late background generally being more important than good time resolution here. Initial fast transient components in the longitudinal relaxation function (so important for instance to the studies of Emmerich *et al* (1983); see figure 63) may well be lost, however.

For muon spin *rotation*, the pulsed mode imposes a more serious general limitation. The maximum precession frequency which may be displayed directly without excessive loss of asymmetry is of the order of the inverse pulse width. Frequency resolution and the precision of linewidth measurements are likewise inherently restricted. Thus, at KEK, the effective asymmetry is halved at about 4 MHz. Fortunately this is adequate for many studies of diamagnetic muons, i.e. for experiments at the Larmor frequency in fields up to 30 mT. Most diffusion studies in metallic systems are possible, for instance, and here the complementary measurements in zero field have proved invaluable (§ 7). It does however preclude the direct display of high precession frequencies, e.g. those encountered in radical studies or in magnetically ordered materials. Likewise it precludes high- (or zero-) field studies of muonium in solids, except via level crossing resonance, for which the pulse mode is ideally suited.

Some improvement may be envisaged by compression or 'slicing' of a muon pulse to reduce its duration (at least for a surface muon beam, which may be manipulated appropriately) as in the inset to figure 65. This is foreseen for the muon source at ISIS, reducing the original pulse width of 70 to 5 ns or less and extending the frequency range to about 100 MHz accordingly (Eaton *et al* 1983, 1984, Carne *et al* 1984). This range embraces a proportion of current hyperfine-field measurements in magnetic materials and organic radical systems but it is still well short of the capability of most spectrometers at continuous sources, which is typically 500 MHz (and can be much higher still, see §§ 4.1 and 4.2). Suitable resonance techniques will have to be developed to regain access to frequencies above 100 MHz. These are the subject of § 8.3.

8.3. Pulsed muon spin resonance

The feasibility of RF resonance experiments is greatly increased by the low duty cycle of a pulsed muon source. The RF power required to flip a muon spin within its radioactive lifetime is considerable, and leads to serious heating problems if it must be applied continuously to flip individual spins, as at a continuous muon source. At a pulsed source, the RF field need only be applied intermittently, in synchronisation with the machine; it is used far more efficiently to flip many spins simultaneously, with the average power requirement reduced by the RF duty cycle.

Resonant depolarisation by an RF field has already been demonstrated, as well as the precession of the muon polarisation about the effective field in the rotating frame. At KEK, where some of these demonstrations have been performed (see, for instance, Kitaoka *et al* 1982), apparatus working at about 500 MHz is currently under development (Nagamine 1985). In parenthesis, an important application to muonium chemistry is foreseeable here. At 500 MHz, which corresponds to the muon Larmor frequency in an applied field of 3.7 T, it is estimated that chemical shifts may be measured with sufficient precision to permit an identification of the diamagnetic fraction (Cox and Nagamine 1984). This in turn would resolve the question (still outstanding in many materials) as to whether the diamagnetic species is formed thermally or epithermally.

It is noteworthy that in most demonstrations of muon spin *resonance* performed to date, the resonance lineshape has been plotted out point by point (each point representing the accumulation of a complete histogram, which is time consuming). Also the line is power-broadened, so its intrinsic width is not readily obtained. There is therefore little to be lost in terms of information and a lot to be gained in terms of increased data rate on an intense continuous source if integral counting is used. The 'rotating-frame wiggles' are smeared out by the time-average measurement, and a broad resonant depolarisation detected. For studies where intrinsic linewidth information is important, and a pulsed source available, the following variant has been proposed (Cox 1981, Cox and Scott 1983, Carne *et al* 1984). This exploits the discontinuous muon input by emulating the 90° pulse method, familiar in NMR.

The muons are allowed to accumulate in the sample for the duration of the machine pulse (i.e. about 100 ns), before the RF field H_1 is applied. In a longitudinal magnetic field H_0 they are implanted in a stationary state and their polarisation is therefore preserved during this time. An RF pulse ($H_1 \perp H_0$ as usual) is then applied, which tips the polarisation through approximately 90° into the plane perpendicular to H_0, so the muons then begin to precess. Their precession may then be detected in a transverse telescope in the usual fashion (provided, of course, that the time resolution of the *instrumentation* is adequate).

Although the RF pulse must be short compared with the muon lifetime or with the appropriate depolarisation times, there is no other particularly stringent requirement on its rise-time, shape or homogeneity. The pulse is applied only after the arrival of the muons, so they are excited coherently as in pulsed NMR. Referring to figure 68(*a*), (*b*), it is noteworthy that even the *growth* of the transverse magnetisation during irradiation may be monitored. (In NMR experiments this is impossible to detect by induction during the transmitter pulse.) The width and form of the RF pulse determine the band width, or the portion of the spectrum that is excited. For complex spectra it should be possible to excite and display the different spectral lines individually in this manner (figure 68(*c*)). Unlike in pulsed NMR, the 'renewal' of the muons at each machine burst removes any limitations that their Zeeman relaxation rate would otherwise place on the pulse repetition frequency†.

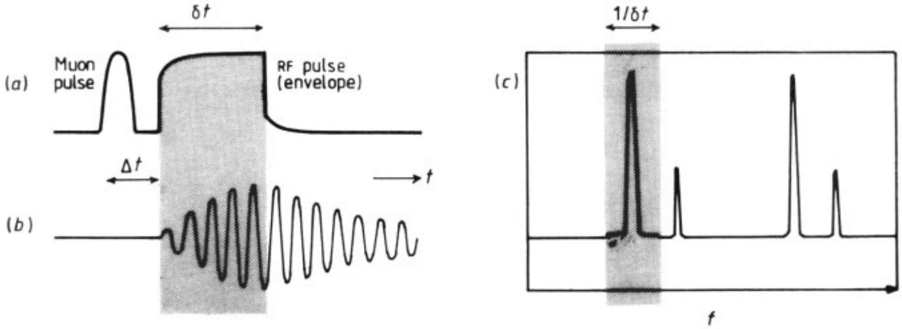

Figure 68. The proposed 90° pulse technique of muon spin resonance. The RF pulse is applied following implantation of the muons (*a*). Growth of the transverse magnetisation of the muon ensemble during irradiation, and its subsequent free precession, are illustrated in (*b*). A window is excited in the μSR frequency spectrum (*c*) centred on the RF frequency and with width equal to the inverse pulse length, allowing individual lines to be displayed. Successive RF pulses are applied with the same initial phase and provide the start signals for compilation of the μSR histogram; variation of the delay Δt allows analysis of the muon state as a function of the time elapsed from implantation.

A noteworthy application concerns the possible evolution of the μSR frequencies with the time elapsed following implantation. This may be envisaged if the muon changes its state via a relatively slow chemical reaction, or if the diffusing muon is eventually trapped, the mobile and immobile muon (or muonium) having different characteristic frequencies. In conventional transverse-field μSR the frequencies characteristic of *both* initial and final state, or reactant and product, are rarely seen; the polarisation transfer between them is insufficient if the frequency difference exceeds the conversion rate (i.e. phase coherence with respect to the start signal is lost). Since longitudinal polarisation

---

† The detection of muon spin echoes, following a subsequent 180° pulse, could likewise be envisaged although the muon lifetime itself imposes a severe limitation here.

is preserved, however, the muon state may always be analysed by *resonance* at any given time following implantation. A preliminary experiment by RF depolarisation demonstrates a shift in resonance frequency observed in MnO, for instance, and therefore a change in the preferred muon site, over an interval of several microseconds following implantation (Ishida *et al* 1984a). Applications to the study of muon trapping at defects in irradiated metals, and muonium trapping at defects or impurities in non-metals, are proposed for the ISIS facility (Seeger 1984a, Weidinger 1984b). In the scheme depicted in figure 68, suitable for poorly conducting samples, the time-dependent analysis would be performed simply by varying the delay of the 90° pulse with respect to the muon burst.

For conductive samples, muon spin resonance suffers the same skin-depth problems as NMR. Fortunately its application to many metals is not entirely excluded, provided techniques ae chosen that do not rely on a homogeneous RF field within the sample. An alternative solution, e.g. for highly conductive samples, might be high-frequency modulation (or deflection) of the beam itself, in conjunction with stroboscopic μSR. This would also be particularly advantageous for very intense continuous sources.

8.4. *Synchronous excitation*

The benefits of a low duty cycle extend to any experiment that requries a repetitive or period excitation of the sample (Manning 1978, Ishikawa 1984). Synchronisation with the machine cycle allows μSR measurements to be made efficiently in two new categories:

(i) under extreme conditions of the sample environment that cannot be sustained continuously; and

(ii) by advancing the stimulus with respect to the arrival of the muon burst, to monitor or explore the sample's response.

Apart from RF fields, intense pulsed electric or magnetic fields are obvious possibilities for experiments in the first category. Likewise excitation of the sample by laser flashes (Patterson 1980) or indeed by radiolysis from the intense muon burst itself (Mitchell 1981) could also be envisaged and these might be followed by time-domain spectroscopy. The potential for laser spectroscopy, especially with regard to elucidating the properties of muonium-substituted molecules in chemical studies, and of the muonium defect centres in solids, is manifest.

In experiments of the second category, the frame length of the existing KEK and proposed ISIS facilities may be considered as extending the timescale of transient phenomena which may be studied into the millisecond range. (This has been called 'μSR with macroscopic timing'; see Nagamine 1983.) Suppose that the μSR parameters depend on some property of the host material that responds, evolves or relaxes in time following a sudden excitation; figure 69 illustrates how measurements made as a function of the time delay between the excitation and the machine pulse may be used to display this response function. Given that the data gate is 1–10 μs, depending on the frequencies and depolarisation rates to be measured, and that machine periods are of order 10 ms (20 ms at ISIS, 50 ms at KEK) the technique is most suitable for the measurement of response times in the range 10 μs–10 ms. Somewhat slower functions could clearly also be explored, by missing out some of the machine pulses, before the benefits of synchronous data accumulation are lost.

One such proposed application is the determination of slow relaxation times, not of the muon spins, but of the *host* spins themselves (Cox 1984). Here an obvious application

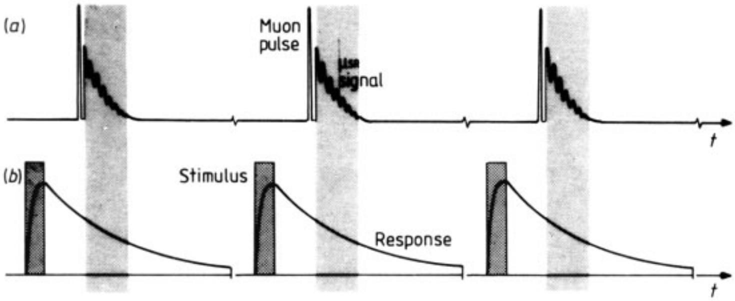

Figure 69. Pulsed μSR (*a*) and synchronous excitation of the sample (*b*) (after Cox 1984). Varying the advance Δt of the excitation with respect to the arrival of the muon burst allows the μSR spectrum to monitor the response function.

is to metallic systems, where NMR methods are disadvantaged by the skin-depth problem, and where the technique offers an opportunity to measure low Korringa constants.

8.5. Data acquisition

The essential instrumentation in any μSR spectrometer comprises:

(i) particle detection;
(ii) timing; and
(iii) data acquisition.

Whilst simpler in principle than the scheme of figure 7 (anti-coincidence, correlation and pile-up logic being eliminated), a digital scheme for pulsed μSR must be able to cope with high count rates. Each of the above component systems has its inherent limitation. The requirement is especially severe immediately following the muon burst, i.e. at the peak of the radioactive decay curve, when any error due to overload of the detectors results in a distortion of the histogram (figure 67(*c*)). The requirement may always be met by segmentation of the counters into arrays of independent smaller detectors, reducing the solid angle covered by each until the count rate in any one is manageable. (For scintillators, photomultipliers and subsequent electronics in common use, a net dead-time of up to 10 ns following an 'event' is typical, although some improvement may be foreseen here.) This method has been successfully demonstrated at KEK, where up to 32 segments are employed. Each segment has its own clock to 'time-stamp' events as they arrive. The data from these parallel channels are subsequently combined as required, for instance in two groups of sixteen for forward and backward telescopes and in four groups of eight for four transverse telescopes. Correction factors can be applied for minor initial distortions of the histograms (Nakayama *et al* 1981). Although further subdivision can always cope with the particle detection as muon intensity is increased† the overall problem is then deferred to the computer interface, where the information collected following each burst must be buffered, and transferred during the remainder

---

† Here a move from scintillators to the miniature elements of a silicon micro-strip detector might be envisaged (eliminating, into the bargain, lightguides and bulky photomultipliers). These devices are inherently fast enough and, with some development to speed up read-out electronics, could be suitable. Read-out of the similar two-dimensional arrays known as CCDs is certainly too slow to time events, but these might also be considered for integral counting, taking a long-exposure 'photograph' of all events within a single frame.

of the frame†. Phased arrays might be considered for large solid-angle coverage in transverse-field measurements, but these would greatly increase the complexity of the data processing and analysis.

An inherently simpler solution, appropriate to very high particle fluxes, is to examine the distribution of the total emitted positron charge by analogue means. This has been effectively achieved using a single large Cerenkov counter and photomultiplier tube, by displaying the waveform of the anode current (Nakayama *et al* 1981). This waveform may be subsequently digitised and analysed as required. Although less suitable than digital data acquisition for measurements far into the tail of the radioactive decay curve, such a device can display the inital signal without distortion at high data rate. It may also prove suitable for the detection of RF or level crossing muon spin resonance, in the pulsed mode.

9. Conclusion

These examples illustrate the broad range of application of implanted-muon studies, and the extent of the information that is available. There is scarcely an area of condensed-matter science where new information has not been obtained or old problems re-examined.

The muon may be used simply as a microscopic Gaussmeter, reporting on internal fields, local spin structures and spin dynamics. This it does from a new vantage point in most lattices, namely from an interstitial rather than a substitutional site. The μSR data then ideally complement those obtained by other nuclear probes, e.g. via NMR, PAC and Mössbauer spectroscopy. The muon's microsecond lifetime sets the timescale for the dynamical effects that may be studied. New time windows are opened on spin dynamics, notably on very rapid fluctuations in the hard magnets and other systems exhibiting very large exchange interactions, and very slow fluctuations in spin glasses. Magnetic materials and their phase transitions still provide the most convenient systems in which to test all that is new in statistical mechanics, so a spin-$\frac{1}{2}$ probe able to access unusual components of the correlation functions, and that may be implanted in a wide variety of materials, is invaluable. The impact of μSR studies on the spin glasses is particularly noteworthy, and similar contributions may be anticipated in other topical problems, especially perhaps in heavy-fermion systems‡.

Many examples can be found, notably in ionic magnetic insulators, where this information represents the intrinsic properties of the host. In this limit, the muon is essentially a 'passive probe'. This is also the case in certain chemical studies, where the muon is a convenient radioactive label for particular molecules, used to monitor reaction rates etc. Those who had innocently hoped that the muon could be used universally in this manner are perhaps, nonetheless, disappointed. Sceptics likewise find their suspicions justified. More often than not the muon, being a charged probe, causes too great a local disturbance to provide information on intrinsic properties. Each inves-

---

† Various unorthodox solutions to the problem of high data-acquisition rates may be envisaged. A streak-camera solution is also under consideration, in which an image from the scintillator segments is reconstructed, via a matrix of lightguides, on phosphor pixels. Like solutions employing a digitising oscilloscope, this would have a readily variable time resolution but, together with other novel proposals, has yet to be tested (Podini and De Renzi 1985).

‡ And, of course, in the new high-temperature superconductors.

tigation must be preceded by detailed consideration of the site adopted and the local electronic or chemical state. Many 'new' questions are raised.

This is surely a recommendation, however. Indeed in the majority of studies the muon is an 'active probe'—the principal participant in the phenomenon of interest. This is true of most studies in metals and semiconductors, for instance, where the μSR results have been particularly provocative. Yet our understanding of metallic systems is far from complete if the response of the electron gas to a unit 'test charge' cannot be modelled. Likewise our understanding of semiconductors is incomplete if the states of a hydrogen-like impurity cannot be explained, still less anticipated. In both systems direct measurements of electronic spin density at the muon, the principal source of information in experiments to date, has been indispensible in building up a picture of local electronic structure. In metals, the μSR results have proved a notable stimulus to the theory of charge screening. In semiconductors, a great deal more information will certainly be forthcoming, now that transverse-field spectra can be obtained in high decoupling fields, and level crossing spectrometry in longitudinal fields promises to provide more detailed maps of spin density in the vicinity of the muon. Hopefully the molecular radical models used here to interpret the existing data are not premature and may even provide a framework for future studies, experimental and theoretical.

The muon can also be a 'mobile probe'. As the lightest representative member of a whole class of light interstitials, it is invaluable in elucidating the possible mechanisms of mobility. These studies are unique in probing the infinite-dilution limit, which is inaccessible to hydrogen. In metals, the 'inertia' of the distortion field that accompanies the interstitial particle was expected to impede the tunnelling. μSR data confirm and quantify this behaviour, and establish the importance of phonon-assisted tunnelling at moderately low temperatures. However, the possible inertia of the screening charge was not anticipated; the μSR studies at very low temperature highlight this effect and reveal that the electron cloud cannot always follow the particle adiabatically. Tunnelling in the presence of thermal excitations is a difficult problem—and one that is fundamental to the understanding of quantum motion. μSR presents the opportunity to study dissipative tunnelling in three dimensions, in crystalline lattices, and possibly also in one dimension, in molecular rotation. A topical question in both subjects is how quantum tunnelling goes over to classical over-the-barrier motion at high temperature.

These are not isolated problems, posed by μSR to be solved by μSR. They have a much wider relevance. The major importance of implanted-muon studies surely lies in the new information that can be obtained via comparison of muon and proton behaviour. In aspects of chemical physics, the equivalent comparison is between muonium and hydrogen. Isotope effects are found in a variety of different properties and different circumstances. They can be normal or inverse, big or small. The role of zero-point energy for the chemically bound hydrogen isotopes is especialy amenable to study, both in its effect on hydrogen reaction or transfer rates and on the hyperfine couplings measured in hydrogen defect centres or in organic radicals. The point is that never before has such a large isotopic mass ratio, or an isotope lighter than protium itself, been available for such studies. In the kinetic studies, information on the somewhat obscure area of intermediate states in chemical reactions may also be forthcoming. In the magnetic studies, μSR data is providing a new stimulus to *ab initio* calculations of electronic structure and hyperfine interaction. Level crossing spectrometry should make a decisive contribution here too, providing a particularly complete and precise characterisation of the muonium-substituted radicals. The determination of coupling constants via level crossing resonance is in fact more precise than is common in most ESR work. This, together with the observation of novel muonic species that have no counterparts in the existing ESR literature, may stimulate more careful ESR studies on the normal or unsubstituted species. Quantitative interpretation of isotope effects represents a severe test of our understanding, and detailed theoretical models, of physical and chemical processes.

The present status of μSR spectroscopy is perhaps best compared with that of magnetic resonance some decades ago. Anticipating a continuing development of techniques appropriate to continuous muon sources, and also the development of new techniques appropriate to intense pulsed sources, the potential for new science is evident.

Acknowledgments

Much of this material was gathered on visits to μSR research groups in Europe, North America and Japan. I wish to thank each group for the hospitality shown on these occasions, for innumerable discussions and for various invitations to participate in experiments. My friends and colleagues may not wish to be held reponsible for all the opinions expressed in this review, but I would like especially to acknowledge the help of those in the CERN μSR Collaboration, who introduced me to these studies, and to those now sponsoring the new experimental facilities at RAL.

Note added in proof. Since submission of this review, construction of the intense pulsed muon source and beamline has been completed at RAL. Figure 70 shows a μSR test spectrum recorded during commissioning. The familiar histogram (*a*) (cf figure 3) is displayed on log–linear scales in (*b*) to show its quality at long elapsed time. The continuous background is extremely low, as expected (arising only from stray particles in the experimental hall). As a result, the precession signal is clearly visible out to 18 μs, and may be revealed by on-line fitting to at least 22 μs, or ten muon lifetimes! The potential for studying lower depolarisation rates than hitherto (e.g. in diffusion studies, where mobility is high or nuclear magnetism weak, or in magnetism, for more

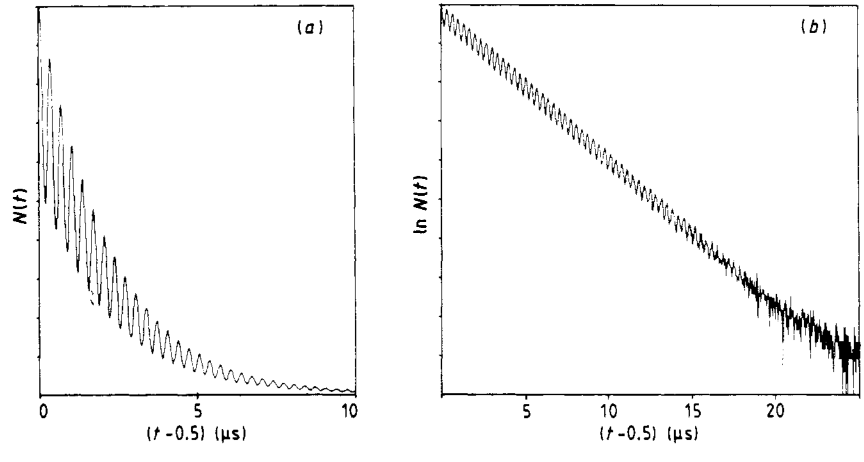

Figure 70. A test spectrum recorded with the new pulsed surface muon beam at the SERC Rutherford Appleton Laboratory. The histogram (*a*) is displayed on log–linear scales in (*b*) to reveal the μSR signal at long elapsed time. (Aluminium sample, room temperature, 22 mT, 8×10^6 recorded events).

sensitive studies of spin dynamics) is manifest. Likewise access to the behaviour of longitudinal relaxation functions at long elapsed time, so critical to the interpretation of many experiments, is greatly enhanced.

The new facilities have been sponsored by groups from France, Germany, Italy, Japan, Sweden and the United Kingdom, and by the 'Stimulation' programme of the European Community.

References

Abragam A 1961 *Principles of Nuclear Magnetism* (Oxford: OUP)

—— 1984 *C.R. Acad. Sci., Paris* **299** 95–100

Albert E, Mosland A, Rechnagel E and Weidinger A 1983 *Hyperfine Interact.* **15–16** 525

—— 1984 *Hyperfine Interact.* **17–19** 611–4

Arnold K-P, Döring K-P, Gladisch M, Haas N, Herlach D, Jacobs W, Krauth M, Liebke S, Metz H, Orth H, Schaeffer H-E and Seeger A 1984 *Hyperfine Interact.* **17–19** 219–24

Asch L, Boucher B, Chappert J, Hartmann O, Kalvius G M, Karlsson E, Litterst J, Nagamine K, Nishiyama K, Wappling R, Yamazaki T and Yaouanc A 19885 *Physica* B **130** 469–73

Asch L, Chappert J, Hartmann O, Kalvius G M, Karlsson E, Norlin L O, Wäppling R and Yaouanc A 1983 *J. Magn. Magn. Mater.* **31** 697–8

Asch L, Kalvius G M, Chappert J, Yaouanc A, Hartmann O, Karlsson E and Wäppling R 1984 *Physica* B **130** 453–68

Badertscher A, Dhawan S, Egan P O, Hughes V W, Lu D C, Ritter M W, Woodle K A, Gladisch M, Orth H, zu Putlitz G, Eckhause M, Kane J, Mariam F G and Reidy J 1984 *Phys. Rev. Lett.* **52** 914–7

Badertscher A, Egan P O, Gladisch M, Greene M, Hughes V W, Mariam F G, Lu D C, Zu Putlitz G, Ritter M W, Sanders G, Sonder P A and Werbeck R 1985 *Nucl. Instrum. Methods* A **238** 200–5

Baker M and Owen J 1983 unpublished

Barsov S G, Getalov A L, Gordeev V A, Evseev V A, Konopleva R F, Kruglov S P, Kudinov V I, Kuz'min L A, Mikirtychyants S M, Minaichev E V, Myasishcheva G G, Obukhov Y V, Savel'ev G I, Firsov V G and Shcherbakov G V 1984 *Hyperfine Interact.* **17–19** 551–5

Barth S, Gygax F N, Ott H-R, Schenck A and van der Wal A J 1985 *Int. Conf. Magnetism (San Francisco) 1985*

Baumeler H-P, Blazey K W, Choyke W J, Estle T L, Keller H, Kiefl R F, Kündig W, Meier P F, Odermatt W, Patterson B D, Rudaz S L, Schneider J W and Schwab C 1985 *SIN Newsletter No* 17, pp 69–71

Baumeler H-P, Grynszpan R I, Imazato J, Keller H, Kiefl R F, Kündig W, Nagamine K, Nishiyama K, Patterson B D and Yamazaki T 1984 *SIN Newsletter No* 17, pp 72–3

Boekema C 1984 *Hyperfine Interact.* **17–19** 305–20

Boekema C, Chan K C B, Lichti R L, Brabers V A M, Denison A B, Cooke D W, Heffner R H, Hutson R L and Schillaci M E 1986 *J. Magn. Magn. Mater.* **54–57** 353–4

Boekema C, Holzschuh E, Kündig W, Meier P F, Patterson B D, Reichart W and Ruegg K 1981a *Hyperfine Interact.* **8** 401–4

Boekema C, Lichti R L, Brabers V A M, Denison A B, Cooke D W, Heffner R H, Hutson R L, Leon M and Schillaci M E 1985 *Phys. Rev.* B **31** 1233–8

Boekema C, Ruegg K and Hofmann W P 1981b *Hyperfine Interact.* **8** 609–14

Bolton P R, Badertscher A, Egan P O, Gardner C J, Gladisch M, Hughes V W, Lu D C, Ritter M, Sander P A, Vetter J, zu Putlitz G, Eckhauser M and Kane J 1981 *Phys. Rev. Lett.* **47** 1441–4

Böni P and Shirane A 1986 *Phys. Rev.* B **33** 3012–9

Brewer J H 1981 *Hyperfine Interact.* **8** 375–80

—— 1986 private communication

Brewer J H, Beder D S and Spencer D P 1979 *Phys. Rev. Lett.* **42** 808–11

Brewer J H, Crowe K M, Gygax F N, Johnson R F, Patterson B D, Fleming D G and Schenck A 1973 *Phys. Rev. Lett.* **31** 143–6

Brewer J H, Crowe K M, Gygax F N and Schenck A 1975a *Muon Physics* vol 3, ed. V W Hughes and C S Wu (New York: Academic) pp 3–139

Brewer J H, Fleming D G, Crowe K M, Johnson R F, Patterson B D, Portis A M, Gygax F N and Schenck A 1975b *Phys. Scr.* **11** 144–8

Brewer J H, Fleming D G and Percival P W 1982 *Fourier, Hadamard and Hilbert Transforms in Chemistry* ed. A G Marshall (New York: Plenum)

Brewer J H, Fleming D G and Spencer D P 1981a *Nuclear and Electron Resonance Spectroscopies Applied to Materials Science* ed. E N Kaufmann and G K Shenoy (Amsterdam: North-Holland)

Brewer J H, Koster E, Schenck A, Schilling H and Williams D L 1981b *Hyperfine Interact.* **8** 619–22

Brewer J H, Kreitzman S R, Noakes D R, Ansaldo E J, Harshman D R and Keitel R 1986 *Phys. Rev.* B **33** 7813–6

Brewer J H and Percival P W (eds) 1981 *Proc. 2nd Int. Topical Meeting Muon Spin Rotation (Vancouver) 1980; Hyperfine Interact.* **7**

Brewer J H, Spencer D P, Fleming D G and Coope J A R 1981c *Hyperfine Interact.* **8** 405

Brice D K 1978 *Phys. Lett.* **66A** 53

Browne A M 1982 *PhD Thesis: AERE Harwell Report* TP 0973

Browne A M and Stoneham A M 1982 *J. Phys. C: Solid State Phys.* **15** 2709

Bucci C 1981 *Proc. INTERMAG 1980; Nucl. Sci. Appl.* **1** 81

Bucci C, De Renzi R, Guidi G, Podini P, Tedeschi R and Norlin L O 1981 *Hyperfine Interact.* **8** 385–8

Bucci C, Guidi G, De Munari G M, Manfredi M, Podini P, Tedeschi R, Crippa P R and Vecli A 1978 *Chem. Phys. Lett.* **57** 41

Bugg D 1983 unpublished

Burkhard P, Roduner E and Fischer H 1985 *Int. J. Chem. Kinetics* **17** 83–93

Burkhard P, Roduner E, Hochmann J and Fischer H 1984 *J. Phys. Chem.* **88** 773–7

Butz T, Chappert J, Defresne J F, Hartmann O, Karlsson E, Lindgren B, Norlin L O, Podini P and Yaouanc A 1980 *Phys. Lett.* **75A** 321–4

Camani M, Gygax F N, Klempt E, Ruegg W, Schenck A, Schulze R and Wolf H 1978 *Phys. Lett.* **77B** 326

Camani M, Gygax F N, Ruegg W, Schenck A and Schilling H 1977 *Phys. Rev. Lett.* **39** 836

Carne A, Cox S F J, Eaton G H, De Renzi R, Scott C A and Stirling G C 1984 *Hyperfine Interact.* **17–19** 945–52

Carstanjen H-D and Seeger A 1984 *Muons and Pions in Materials Research* ed. J Chappert and R I Grynszpan (Amsterdam: North-Holland) pp 293–362

Casperson D E, Crane T W, Denison A B, Egan P O, Hughes V W, Mariam F G, Orth H, Reist H W, Souder P A, Stambaugh R D, Thompson P A and zu Putlitz G 1977 *Phys. Rev. Lett.* **38** 956–9

Castro M, Keller J and Schilling H 1979 *Hyperfine Interact.* **6** 43

Catterall R 1984 unpublished

Catterall R, Cox S F J, Scott C A and Weeks G H 1985 preliminary results

Cavagnat D and Lascombe J 1982 *J. Mol. Spectrosc.* **92** 141

Celio M and Meier P F *Phys. Rev.* B **27** 1908–10

Chan K C B, Boekema C, Lichti R L, Cooke D W, Schillaci M E and Denison A B 1985 *Int. Conf. Magnetism (San Francisco) 1985*

Chappert J 1984 *Proc. Muons and Pions in Materials Research* ed. J Chappert and R I Grynszpan (Amsterdam: North-Holland) pp 35–62

Chappert J and Karlsson E 1983 *La Recherche* **14** 156–65

Chappert J, Yaouanc A, Hartmann O, Karlsson E, Norlin L-O and Niinikoski T O 1982 *Solid State Commun.* **44** 13–6

Clawson C W 1984 *Hyperfine Interact.* **17–19** 103–8

Clawson C W, Crowe K M, Kohn S E, Rosenblum S S, Huang C Y, Smith J L and Brewer J H 1982 *Physica* B **109–10** 2164–7

Claxton T A and Graham A M 1987 unpublished

Clough S 1986 private communication

Clough S, Heidemann A, Horsewill A J, Lewis J D and Paley M N J 1982 *J. Phys. C: Solid State Phys.* **15** 2495–508

Cooke D W, Heffner R H, Hutson R L, Schillaci M E, Smith J L, Daniel H and MacLaughlin D E 1985 *Bull. Am. Phys. Soc.* **30** 408

Cotts R M 1978 *Hydrogen in Metals, Springer Topics in Applied Physics* vol 1, ed. G Alefeld and J Völkl (Berlin: Springer)

Cox S F J 1981 unpublished

—— 1984 *Hyperfine Interact.* **17–19** 953–8

—— 1986 *Proc. 17th Int. Symp. Free Radicals (Granby, CO) 1985* NBS Special Publication No 716 (Washington, DC: US Government Printing Office) pp 191–205

Cox S F J, Claxton T and Symons M C R 1986 *Radiat. Phys. Chem.* **28** 107–13

Cox S F J, Hill A and De Renzi R 1982 *J. Chem. Soc. Faraday Trans.* I **78** 2975–95

Cox S F J and Nagamine K 1984 unpublished

Cox S F J, Ross D K, Witchell D, Hartmann O, Hempelmann R, Richter D and Stoneham A M 1984 *Report* RAL-84-132

Cox S F J and Scott C A 1983 unpublished

Cox S F J and Symons M C R 1986a *Radiat. Phys. Chem.* **27** 53–64

—— 1986b *Chem. Phys. Lett.* **126** 516–25

De Renzi R, Guidi G, Podini P, Tedeschi R, Bucci C and Cox S F J 1984a *Phys. Rev.* B **30** 186–96

—— 1984b *Phys. Rev.* B **30** 197–204

Denison A B, Graf H, Kündig W and Meier P F 1979 *Helv. Phys. Acta* **52** 460–517

Dodds S A, Gist G A, MacLaughlin D E, Heffner R H, Leon M, Schillaci M E, Nieuwenhuys G J and Mydosh J A 1983 *Phys. Rev.* B **28** 6209–15

Eaton G H, Carne A, Reading D H and Sandels E G 1983 *Nucl. Instrum. Methods* **214** 151–67

Eaton G H, Daum M, Frosch R and Kettle P-R 1984 *Nucl. Instrum. Methods* **219** 34–40

Eauchus R S and Symons M C R 1970 *J. Chem. Soc.* A 1336

Edwards S F and Anderson P W 1975 *J. Phys. F: Met. Phys.* **5** 965–74

—— 1976 *J. Phys. F: Met. Phys.* **6** 1927–38

Ellis D E and Lindgren B 1984 *Hyperfine Interact.* **17–19** 279–86

Emin D 1981 *Hyperfine Interact.* **8** 515–21

Emmerich K 1982a *Hyperfine Interact.* **12** 59–69

—— 1982b *PhD Thesis* Technical University of Braunschweig

Emmerich K, Gygax F N, Hintermann A, Pinkvos H, Schenck A, Schwinck Ch and Studer W 1983 *J. Magn. Magn. Mater.* **31–34** 1361–2

Emmerich K, Lippelt E, Neuhaus R, Pinkvos H, Schwink Ch, Gygax F N, Hintermann A, Schenck A, Studer W and van der Wal A J 1985 *Phys. Rev.* B **31** 7226–32

Estle T L 1981 *Hyperfine Interact.* **8** 365–70

—— 1984 *Hyperfine Interact.* **17–19** 585–8

—— 1985a *Eur. Workshop Spectroscopy of Sub-Atomic Species in Non-Metallic Solids (Paris) 1985*

—— 1985b *Hyperfine Interact.* **25** 701–8

Estle T L and Brower T 1985 private communication (from T L Estle)

Estreicher S and Meier P F 1982 *Phys. Rev.* B **25** 297–310

—— 1983 *Phys. Rev.* B **27** 642–8

—— 1984 *Hyperfine Interact.* **17–19** 327–31

Estreicher S, Ray A K, Fry J L and Marynick D C 1985 *Phys. Rev. Lett.* **55** 1976

Falicov L M and Haller E E 1985 *Solid State Commun.* **53** 1121

Feher G, Prepost R and Sachs A M 1960 *Phys. Rev. Lett.* **5** 515

Ferrell R A and Chaos F 1957 *Phys. Rev.* **107** 1322

Ferrell R A, Lee Y C and Pal K M 1960 *Phys. Rev.* **118** 317–9

Fessenden R W 1964 *J. Chem. Phys.* **61** 1570

Fleming D G, Arseneau D J, Garner D M, Senba M and Mikula R J 1984 *Hyperfine Interact.* **17–19** 655–78

Fleming D G, Garner D M, Vaz L C, Walker D C, Brewer J H and Crowe K M 1979 *Positronium and Muonium Chemistry, Advances in Chemistry Series* vol 175, ed. H J Ache (Washington, DC: American Chemical Society) pp 279–334

Fleming D G, Mikula R J and Garner D M 1982 *Phys. Rev.* A **26** 2527–44

Flik G, Bradbury J N, Cooke D W, Heffner R H, Leon M, Paciotti M A, Schillaci M E, Maier K, Rempp H, Reidy J J, Boekema C and Daniel H 1986 *Phys. Rev. Lett.* **57** 563

Flynn C P and Stoneham A M 1970 *Phys. Rev.* B **1** 3966

Ford G W and Mullin C J 1957 *Phys. Rev.* **108** 477

Fournier P G and LeRoy R J 1984 *Chem. Phys. Lett.* **110** 487

Foy M L G, Heiman N, Kossler W J and Stronach C E 1973 *Phys. Rev. Lett.* **30** 1064–7

Fry C A, Warren J B, Kiefl R F, Oram C J, Ludgate G A, Schmor P W, Olin A, Marshall G M, Erickson B and Morris G 1984 *Hyperfine Interact.* **17–19** 691–6

Fuji S 1979 *J. Phys. Soc. Japan* **46** 1833–42, 1843–51

Garner D M, Fleming D G and Brewer J H 1978 *Chem. Phys. Lett.* **55** 163–7

Garwin R L, Lederman L M and Weinrich M 1957 *Phys. Rev.* **105** 1415

Geeson D, Symons M C R, Roduner E, Fischer H and Cox S F J 1985a *Chem. Phys. Lett.* **116** 186

—— 1985b preliminary results

Goldman A and Westphal D 1983 *J. Phys. C: Solid State Phys.* **16** 1335

Graf H, Hofmann W, Kündig W, Meier P F, Patterson B D and Reichart W 1977 *Solid State Commun.* **23** 653–6

Graf H, Hofmann W, Kündig W, Meier P F, Patterson B D and Rodriguez A 1978a *Solid State Commun.* **25** 1079–81

Graf H, Holzschuh E, Recknagel E, Weidinger A and Wichert Th 1979 *Hyperfine Interact.* **6** 245

Graf H, Kündig W, Meier P F and Patterson B D 1978b *J. Appl. Phys.* **49** 1549–51

Graf H, Kündig W, Patterson B D, Reichart W, Roggwiller P, Camani M, Gygax F N, Ruegg W, Schenck A, Schilling H and Meier P F 1976 *Phys. Rev. Lett.* **37** 1644–7

Grebinnik V G, Gurevich I I, Zhukov V A, Manych A P, Meleshko E A, Muratova I A, Nikol'skii B A, Selivanov V I and Suetin V A 1975 *Sov. Phys.-JETP* **41** 777–80

Grynszpan R I 1984 *Muons and Pions in Materials Research* ed. J Chappert and R I Grynszpan (Amsterdam: North-Holland) pp 63–76

Gurevich I I, Ivanter I G, Meleshko E A, Nikolskii B A, Roganov V S, Selivanov V I, Smilga V P, Sokolov B V and Shestakov V D 1971 *Sov. Phys.-JETP* **33** 253–9

Gurevich I I, Klimov A I, Maiorov V N, Meleshko E A, Muratova I A, Nikol'skii B A, Roganov V S, Selivanov V I and Suetin V A 1974 *Sov. Phys.-JETP* **39** 178–80

Gurevich I I, Klimov A I, Maiorov V N, Meleshko E A, Nikol'skii B A, Purogov A V, Roganov V S, Selivanov V I and Suetin V A 1975 *Zh. Eskp. Teor. fiz.* – (Engl Transl. 1976 *Sov. Phys. JETP* **42** 741–2)

Gurevich I I, Mel'eshko E A, Muratova I A, Nikol'sky B A, Roganov V S, Selivanov V I and Sokolov B V 1972 *Phys. Lett.* **40A** 143–4

Gygax F N, Hintermann A, Ruegg W, Schenck A, Studer W and van der Wal A J 1984a *J. Less-Common Met.* **101** 97

—— 1984b *J. Less-Common Met.* **101** 327

Gygax F N, Hintermann A, Ruegg W, Schenck A, Studer W, van der Wal A J and Kaplan N 1984c *Hyperfine Interact.* **17–19** 177

Gygas F N, Kündig W and Meier P F (eds) 1979 *Proc. 1st Int. Topical Meeting Muon Spin Rotation (Rorschach) 1978; Hyperfine Interact.* **6**

Gygax F N, Ruegg W, Schenck A, Schilling H, Studer W and Schulze R 1980 *J. Magn. Magn. Mater.* **15–18** 1191–2

Harshman D R, Keitel R, Senba M, Kiefl R F, Ansaldo E J and Brewer J H 1984 *Phys. Lett.* **104A** 472

Hartmann O 1977a *Proc. 1st Course International School of Physics of Exotic Atoms (Erice) 1977* ed. G. Fiorentini and G Torelli (Frascati: Servizio Documentazione dei Laboratori Nazionalidi)

—— 1977b *Phys. Rev. Lett.* **39** 832–5

—— 1981 *Hyperfine Interact.* **8** 525

—— 1986 unpublished

Hartmann O, Karlsson E, Lindgren B and Wäppling R (ed.) 1986 *Hyperfine Interact.* **31, 32**

Hartmann O, Karlsson E, Norlin L-O, Niinikoski T O, Kehr K W, Richter D, Welter J M, Yaouanc A and le Hericy J 1980 *Phys. Rev. Lett.* **44** 337–40

Hartmann O, Karlsson E, Norlin L-O, Pernestal K, Borghini M and Niinikoski T O 1979 *Hyperfine Interact.* **6** 47

Hartmann O, Karlsson E, Wäppling R, Richter D, Hempelmann R, Schulze K, Patterson B D, Holzschuh E, Kündig W and Cox S F J 1983 *Phys. Rev.* B **27** 1943–6

—— *Hyperfine Interact.* **17–19** 183–90

Hartmann O, Norlin L-O, Yaouanc A, Le Hericy J, Karlsson E and Niinikoski T O 1981 *Hyperfine Interact.* **8** 533–8

Hayano R S, Uemura Y J, Imazato J, Nishida N, Nagamine K, Yamazaki T, Ishikawa Y and Yasuoka H 1980 *J. Phys. Soc. Japan* **49** 1773–83

Hayano R S, Uemura Y J, Imazato J, Nishida N, Yamazaki T and Kubo R 1979 *Phys. Rev.* B **20** 850–9

Heffner R H, Cooke D W, Hutson R L, Schillaci M E, Dodds S A, Gist G A and MacLaughlin D E 1986 *J. Magn. Magn. Mater.* **54–57** 1103–4

Heffner R H, Cooke D W, Leon M, Schillaci M E, MacLaughlin D E and Gupta L C 1984a *Hyperfine Interact.* **17–19** 463–6

Heffner R H, Leon M, Schillaci M E, Dods S A, Gist G A, MacLaughlin D E, Mydosh J A and Nieuwenhuys G J 1984b *J. Appl. Phys.* **55** 1703–5

Heffner R H, Leon M, Schillaci M E, MacLaughlin D E and Dodds S A 1982 *J. Appl. Phys.* **53** 2174–8

Heffner R H and MacLaughlin D E 1984 *Phys. Rev.* B **29** 6048–51

Heffner R H, MacLaughlin D E, Boekema C, Cooke D W, Fisk Z, Hutson R L, Lichti R L, Oostens J, Ott H-R, Schillaci M E, Smith J L and Willis J O 1985 *Int. Conf. Magnetism (San Francisco) 1985*

Hellar C and McConnell H M 1960 *J. Chem. Phys.* **32** 1535
Heller P and Benedek G B 1962 *Phys. Rev. Lett.* **8** 428–32
Heming M, Roduner E, Patterson B D, Odermatt W, Schneider J, Baumeler H-P, Keller H and Savic I M 1986 *Chem. Phys. Lett.* **128** 100–6
Hempelmann R 1984 *J. Less-Common Met.* **101** 69–96
Hempelmann R, Richter D, Hartmann O, Karlsson E and Wäppling R 1984 *J. Less-Common Met.* **104** 209–10
Herlach D 1981 *Recent Developments in Condensed Matter Physics* vol 1, ed. J T Devreese (New York: Plenum) p 93
Hill A, Allen G, Stirling G and Symons M C R 1982 *J. Chem. Soc. Faraday Trans.* I **78** 2959–73
Hill A, Symons M C R, Cox S F J, De Renzi R, Scott C A, Bucci C and Vecli A 1985 *J. Chem. Soc. Faraday Trans.* I **81** 433–48
Hintermann A, Meier P F and Patterson D B 1980 *Am. J. Phys.* **48** 956–61
Hintermann A, Stoneham A M and Harker A H 1981 *Hyperfine Interact.* **8** 475–8
Hofmann W, Kündig W, Meier P F, Paterson B D, Ruegg K, Echt O, Graf H, Recknagel E, Weidinger A and Wichert T 1978 *Phys. Lett.* **65A** 343–4
Holstein T 1959 *Ann. Phys., NY.* **8** 325, 343
Holzschuh E 1983 *Phys. Rev.* **27** 102
Holzschuh E, Denison A B, Kündig W, Meier P F and Patterson B D 1983 *Phys. Rev.* B **27** 5294–307
Holzschuh E, Graf H, Recknagel E, Weidinger A, Wichert Th and Meier P F 1979 *Phys. Rev.* B **20** 4391–6
Holzschuh E, Kündig W, Meier P F, Patterson B D, Sellschop J P F, Stemmet M C and Appel H 1982 *Phys. Rev.* B **25** 1272–86
Horvàth D and Lambrecht R M 1984 *Exotic Atoms* (Amsterdam: Elsevier)
Hughes V W and Kinoshita T 1977 *Muon Physics I: Electromagnetic Interaction* ed. V W Hughes and C S Wu (New York: Academic) pp 11–199
Hughes V W, McColm D W, Ziock K and Prepost R 1960 *Phys. Rev. Lett.* **5** 63–5
Imazato K, Nagamine K, Yamazaki T, Patterson B D, Holzschuh E and Kiefl R F 1984 *Hyperfine Interact.* **17–19** 857–64
Ishida K, Matsuzaki T, Nishiyama K and Nagamine K 1984a *Hyperfine Interact.* **17–19** 927–32
Ishida K, Matsuzaki T, Nishiyama K, Nagamine K, Miyake Y, Tabata Y and Ito Y 1984b *Hyperfine Interact.* **17–19** 933–8
Ishikawa Y 1984 *Hyperfine Interact.* **17–19** 17–34
Ivanter I G, Minaichev E V, Myasischeva G G, Obukhov Yu V, Roganov I S, Sarelev G I, Smilga V P and Firsor V G 1972 *Sov. Phys.-JETP* **35** 9
Jäckle J and Kehr K W 1983 *J. Phys. F: Met. Phys.* **13** 753
Jena P 1979 *Hyperfine Interact.* **6** 5–12
Jena P and Singwi K S 1978 *Phys. Rev.* B **17** 3518–24
Jena P, Singwi K S and Nieminen R M 1978 *Phys. Rev.* B **17** 301–7
Johnson N M, Herring C and Chadi D J 1986 *Phys. Rev. Lett.* **56** 769
Kadono R, Imazato J, Nishiyama K, Nagamine K and Yamazaki T 1984 *Hyperfine Interact.* **17–19** 109–16
Kadono R, Imazato J, Nishiyama K, Nagamine K, Yamazaki T, Richter D and Welter J-M 1985a *Phys. Lett.* **109A** 61–4
Kadono R, Imazato J, Nishiyama K, Yamazaki T, Richter D and Welter J M 1985b *Phys. Lett.* **107A** 279–82
Kagan Y and Klinger M I 1974 *J. Phys. C: Solid State Phys.* **7** 2791
Kalvius G M 1985 private communication
Kalvius G M, Litterst F J, Asch L and Chappert J 1985 *Hyperfine Interact.* **25** 709–36
Kanamori J, Yoshida H K and Terakura K 1981 *Hyperfine Interact.* **8** 573
Karlsson E 1982 *Phys. Rep.* **82** 271–338
Katayama H, Terakura K and Kanamori J 1979 *Solid State Commun.* **29** 431–4
Katayama-Yoshida H and Shindo K 1984 *Hyperfine Interact.* **17–19** 581–4
Kawasaki 1978 *Phase Transitions and Critical Phenomena* vol 5A, ed. C Comb and M S Green (New York: Academic)
Kehr K W 1978 *Hydrogen in Metals,* I, *Springer Topics in Applied Physics* vol. 28, ed. G Alefeld and J Völkl (Berlin: Springer)
—— 1984 *Hyperfine Interact.* **17–19** 63–74
Kehr K W, Richter D, Welter J M, Hartmann O, Karlssen E, Norlin L-O, Niinikoski T O and Yaouanc A 1982 *Phys. Rev.* B **26** 567

Kehr K W, Richter D, Welter J M, Hartmann O, Norlin L-O, Karlsson E, Niinikoski T O, Chappert J and Yaouanc A 1981 *Hyperfine Interact.* **8** 681

Keller J and Schenck A 1979 *Hyperfine Interact.* **6** 39

Kiefl R F 1985 private communication

—— 1986 private communication

Kiefl R F, Kreitzman S, Celio M, Keitel R, Luke G M, Brewer J H, Noakes D R, Percival P W, Matsuzaki T and Nishiyama K 1986 *Phys. Rev.* A **34** 681–4

Kiefl R F, Odermatt W, Baumeler H P, Felber J, Keller H, Kündig W, Meier P F, Patterson B D, Schneider J W, Blazey K W, Estle T L and Schwab C 1985a *Phys. Rev.* B **34** 1474–84

Kiefl R F, Patterson B D, Holschuh H and Odermatt W 1984 *Hyperfine Interact.* **17–19** 563–6

Kiefl R F, Schneider J W, Keller H, Kündig W, Odermatt W, Patterson B D, Blazey K W, Estle T and Rudaz S L 1985b *Phys. Rev.* B **32** 530

Kiefl R F, Warren J B, Marshall G M, Oram C J, Brewer J H, Judd D J and Spires L D 1979 *Hyperfine Interact.* **6** 185

Kiefl R F, Warren J B, Oram C J, Marshall G M, Brewer J H and Harshman D R 1982 *Phys. Rev.* B **26** 2432–41

Kirkpatrick K S and Sherrington D 1978 *Phys. Rev.* B **17** 4384

Kitaoka Y, Takigawa M, Yasuoka H, Ito M, Takigi S, Kuno Y, Nishiyama K, Hayano R S, Uemura Y S, Imazato J, Nakayama H, Nagamine K and Yamazaki T 1982 *Hyperfine Interact.* **12** 51

Klempt E, Schulze R, Wolf H, Camani M, Gygax F N, Ruegg W, Schenck A and Schilling H 1982 *Phys. Rev.* D **25** 652

Kondo J 1976 *Physica* B **84** 40

—— 1985 *Physica* B **125** 279–85

Kossler W J, Schone H E, Petzinger K, Hitti B, Kempton K, Seymour E F W, Styles G A, Stranach C E, Lankford W F F and Reilly J 1986 *Bull. Am. Phys. Soc.* **31** 270

Kreitzman S R, Brewer J H, Harshman D R, Keitel R, Williams D-LL, Crowe K M and Ansaldo E J 1986 *Phys. Rev. Lett.* **56** 181–4

Krusic P J, Meakin P and Jesson J P 1971 *J. Phys. Chem.* **75** 3438

Kubo R 1981 *Hyperfine Interact.* **8** 731

Kubo R and Toyabe 1967 *Magnetic Resonance and Relaxation* ed. R Blinc (Amsterdam: North-Holland) pp 810–23

Kunz 1982 *Phys. Rev.* B **26** 2070

Leggett A J 1984 *Conf. Quantum Motion (Nottingham) 1984*

Lindgren B and Ellis D E 1982 *Phys. Rev.* B **26** 636–47

—— 1984 *Hyperfine Interact.* **17–19** 279–86

Louwrier P 1986 private communication

Lovesey S 1986 *Condensed Matter Physics: Dynamic Correlations, Frontiers in Physics* vol 61 (New York: Benjamin/Cummings)

MacLaughlin D E, Gupta L C, Cooke D W, Heffner R H, Leon M and Schillaci M E 1983 *Phys. Rev. Lett.* **51** 927–30

Maier K 1984 *Hyperfine Interact.* **17–19** 3–16

Maier K and Seeger A 1983 *Proc. Int. Symp. Electronic Structure and Properties of Hydrogen in Metals* ed. P Jena (New York: Plenum)

Mainwood A and Stoneham A M 1984 *J. Phys. C: Solid State Phys.* **17** 2513–24

Manninen M 1983 *Phys. Rev.* B **27** 53

Manninen M and Meier P F 1982 *Phys. Rev.* B **26** 6690

Manninen M and Nieminen R M 1979 *J. Phys. F: Met. Phys.* **9** 1333

Manning G M 1978 *Rutherford Laboratory Meeting: Possibilities for μSR at the SNS*

Marshall G M, Warren J B, Garner D M, Clark G S, Brewer J H and Flemming D G 1978 *Phys. Lett.* **65A** 351–3

Marshall G M, Warren J B, Oram C J and Kiefl R F 1982 *Phys. Rev.* D **25** 1174–80

Martin T P 1984 *PhD Thesis* Bristol University

McHenry M R, Silbernagel B G and Wernick J H 1972 *Phys. Rev.* B **5** 2958

McKenna D and Webster B 1984 *J. Chem. Soc. Faraday Trans.* II **80** 589

—— 1985 *J. Chem. Soc. Faraday Trans.* II **81** 225–34

Meier P F 1981 *Hyperfine Interact.* **8** 591–600

—— 1984 *Muons and Pions in Materials Research* ed. J Chappert and R I Grynszpan (Amsterdam: North-Holland) pp 77–94
Meier P F, Kündig W, Patterson B D and Ruegg W 1978 *Hyperfine Interact.* **5** 311–16
Mitchell E W H 1981 unpublished
Miyake Y, Tabata Y, Ito Y, Ishida K, Matsuzaki T, Nishiyama K, Nagamine K, Crowe K M and Brewer J H 1984 *Hyperfine Interact.* **17–19** 807–14
Morija T 1962 *Prog. Theor. Phys.* **28** 371–400
Myasischeva G G, Obukhov Yu V, Roganov V S and Firsor V G 1967 *Zh. Eksp. Teor. Fiz.* (Engl. Transl. 1969 *Sov. Phys.-JETP* **29** 645)
Munger K 1980 *PhD Thesis* Zürich University
Mydosh J A 1978 *J. Magn. Magn. Mater.* **7** 237
Nagamine K 1983 unpublished
—— 1984 *University of Tokyo MSL Newsletter No* 4
—— 1985 private communication
Nagamine K, Ishida K, Matsuzaki T, Nishiyama K, Kuno Y, Yamazaki T and Shirikawa H 1984 *Phys. Rev. Lett.* **53** 1763
Nagamine K, Nishiyama K, Imazato J, Nakayama H, Yoshida M, Sakai Y, Satu H and Tominaga T 1982 *Chem. Phys. Lett.* **87** 186–91
Nagamine K and Yamazaki T 1981 *University of Tokyo MSL Newsletter No* 1
Nakayama H, Imazato J, Hayano R S, Nishiyaina K, Kuno Y, Fukuchi H, Sasaki H, Kitaoka Y, Yasuoka H, Nagamine K and Yamazaki T 1981 *University of Tokyo MSL Newsletter No* 1
Namkung M, Kossler W J, Stronach C E, Grynszpan R I and Patterson B D 1984 *Hyperfine Interact.* **17–19** 321–6
Newman K E, Brodovitch J-C and Percival P W 1985 *Chem. Phys. Lett.* **113** 347–50
Ng B W, Jean Y C, Ito Y, Suzuki T, Brewer J H, Fleming D G and Walker D C 1981 *J. Phys. Chem.* **85** 454
Nishiyama K, Nagamine K, Natsui T, Nakajima S, Ishida K, Kuno Y, Yamazato J, Nakayama H, Yamazaki T and Yagi E 1983 *J. Magn. Magn. Mater.* **31** 695–6
Oram C J, Bailey J M, Schmor P W, Fry C A, Kiefl R F, Warren J B, Marshall G M and Olin A 1984 *Phys. Rev. Lett.* **52** 910–3
Oram C J, Fry C A, Warren J B, Kiefl R F and Brewer J H 1981 *J. Phys. B: At. Mol. Phys.* **14** L789–93
Orear J, Harris G and Bierman E 1957 *Phys. Rev.* **107** 322–3
Patterson B D 1980 unpublished
—— 1984a *Muons and Pions in Materials Research* ed. J Chappert and R I Grynszpan (Amsterdam: North-Holland) pp 161–82
—— 1984b *Hyperfine Interact.* **17–19** 517–24
Patterson B D, Crowe K M, Gygax F N, Johnson R F, Portis A M and Brewer J A 1974 *Phys. Lett.* **46A** 453–4
Patterson B D and Falicov R L M 1974 *Solid State Commun.* **15** 1509–12
Patterson B D, Hintermann A, Kündig W, Meier P F, Walder F, Graf H, Recknagel E, Weidinger A and Wichert Th 1978 *Phys. Rev. Lett.* **40** 1347–50
Patterson B D, Holzchuh E, Kündig W, Meier P F, Odermatt W, Sellschop J P F and Stemmet M C 1984 *Hyperfine Interact.* **17–19** 605–10
Patterson B D, Nagamine K, Bucci C and Portis A M 1974b *Magnetism and Magnetic Materials, AIP Conf. Proc.* **24** 281
Percival P W 1979 *Radiochim. Acta* **26** 1
Percival P W, Brodovitch J E and Newman K E 1982 *Chem. Phys. Lett.* **91** 1–3
Percival P W and Fischer H 1976 *Chem. Phys.* **16** 89
Percival P W, Fischer H, Camani M, Gygax F N, Rüegg W, Schenk A, Schilling H and Graf H 1976 *Chem. Phys. Lett* **39** 333
Percival P W, Kiefl R F, Kreitzman S R, Garner D M, Cox S F J, Luke G M, Brewer J H, Nishiyama K and Venkataswaran K 1987 *Chem. Phys. Lett* **133** 465–70
Percival P W and Mogensen O E 1986 *Radiat. Phys. Chem.* **28** 85–9
Percival P W, Roduner E and Fischer H 1978 *Chem. Phys.* **32** 353–67
Perrot F and Rasolt M 1981 *Phys. Rev.* B **23** 6534
Petzinger K G 1980 *Phys. Lett.* **75A** 225–8
Petzinger K G and Wei S H 1984 *Hyperfine Interact.* **17–19** 441–6
Picraux S T and Vook F L 1978 *Phys. Rev.* B **18** 2066

Pinkvos H, Gygax F N, Lippelt E, Neuhaus R, Schenck A, Schwinck Ch and van der Wal A J 1986 *J. Magn. Magn. Mater.* **54–57** 119–20

Pinkvos H, Hintermann A, Gygax F N, Lippelt E, Neuhaus R, Schenck A, Schwinck Ch and van der Wal A J 1984 *SIN Newsletter No* 17, pp 64–6

Piper A E, Bowen T and Kendall K R 1976 *Nucl. Instrum. Methods* **135** 39

Podini P and De Renzi R 1985 unpublished

Podini P and Tedeschi R 1984 *Hyperfine Interact.* **17–19** 917–26

Poole C P and Farach H A 1985 *The Theory of Magnetic Resonance* (New York: Wiley)

Press W 1981 *Single-Particle Rotations in Molecular Crystals, Springer Tracts in Modern Physics* vol 92 (Berlin: Springer)

Ramos M J, McKenna D, Webster B C and Roduner E 1984a *J. Chem. Soc. Faraday Trans.* I **80** 255–66

—— 1984b *J. Chem. Soc. Faraday Trans.* I **80** 267–74

Reiss H 1956 *J. Chem. Phys.* **25** 681

Ricco M, Bucci C, De Renzi R, Guidi G, Podini P, Tedeschi R and Scott C A 1984 *Proc. 22nd Ampère Congr. Magnetic Resonance and Related Phenomena (Zürich) 1984* (Zürich: Zurich Univ.) ed. K A Müller, R Kind and J Roos pp 259–60

Richter D 1983 *Neutron Scattering and Muon Spin Rotation, Springer Tracts in Modern Physics* vol. 101 (Berlin: Springer) pp 85–222

Richter D, Hempelmann R, Hartmann O, Karlsson E, Norlin L-O, Cox S F J and Kutner R 1983 *J. Chem. Phys.* **79** 4564–75

Roduner E 1979 *PhD Thesis* Zürich University

—— 1980 *Exotic Atoms 1979* ed. K Crowe, J Dudes, G Florentini and G Torelli (New York: Plenum) p 379

—— 1981 *Chem. Phys. Lett.* **81** 191

—— 1984a *Hyperfine Interact.* **17–19** 785–92

—— 1984b private communication

—— 1985 *Discuss. Faraday Soc.* **78**

—— 1986a *Radiat. Phys. Chem.* **28** 75–84

—— 1986b *Prog. Reaction Kinetics* **14** 1–42

Roduner E, Brinkmann G A and Louwrier P W F 1982a *Chem. Phys.* **73** 117

Roduner E and Fischer H 1979 *Hyperfine Interact.* **6** 413–7

—— 1981 *Chem. Phys.* **54** 261

Roduner E and Münger K 1984 *Hyperfine Interact.* **17–19** 793–6

Roduner E, Percival P W, Fleming D G, Hochmann J and Fischer H 1978 *Chem. Phys. Lett.* **57** 37

Roduner E, Strub W, Burkhard P, Hochmann J, Percival P W, Fischer H, Ramos M and Webster B C 1982b *Chem. Phys.* **67** 275

Roduner E and Webster B C 1983 *J. Chem. Soc. Faraday Trans* I **79** 1939

Ruegg K, Boekema C, Hofmann W, Kündig W and Meier P F 1979 *Hyperfine Interact.* **6** 99–107

Ruegg K, Boekema C, Kündig W, Meier P F and Patterson B D 1981 *Hyperfine Interact.* **8** 547–51

Sahoo N, Mishra K C and Das T P 1985 *Phys. Rev. Lett.* **55** 1506

Sahoo N, Santosh K M, Mishra K C, Coker A, Das T P, Mitra C K, Snyder L C and Glodeann A 1983 *Phys. Rev. Lett.* **50** 913

Schenck A 1976 *Nuclear and Particle Physics at Intermediate Energies* ed. J B Warren (New York: Plenum) p 159

—— 1981 *Helv. Phys. Acta* **54** 248

—— 1982 *Helv. Phys. Acta* **54** 471

—— 1985a *Muon Spin Rotation Spectroscopy* (Bristol: Hilger)

—— 1985b unpublished

Seeger A 1978 *Hydrogen in Metals I, Topics in Applied Physics* vol 28, ed. G Alefeld and J Völkl (Berlin: Springer)

—— 1979 *High Purity Materials in Science and Technology* vol 2, ed. J Morgenthal and H Oppermann (Dresden: Zentralinstitut für Festkörperphysik und Werkstofforschung) p 253

—— 1984a unpublished

—— 1984b *Muons and Pions in Materials Research* ed. J Chappert and R I Grynszpan (Amsterdam: North-Holland) pp 251–92

—— 1984c *Hyperfine Interact.* **17–19** 75–100

Seeger A and Monachesi P 1982 *Phil. Mag.* B **46** 283–312

Shillady D D and Jena P 1984 *Hyperfine Interact.* **17–19** 247–54

Shizgal B 1979 *J. Phys. B: At. Mol. Phys.* **12** 3611

Shulman R G and Jaccarino V 1957 *Phys. Rev.* **108** 1219–31
Slifkin H 1986 unpublished
Smith D A 1975 *J. Phys. F: Met. Phys.* **5** 2148–67
Smolander 1983 *J. Phys. C: Solid State Phys.* **16** 3673
Spencer D P, Fleming D G and Brewer J H 1984 *Hyperfine Interact.* **17–19** 567–74
Stewart G R 1984 *Rev. Mod. Phys.* **56** 755
Stoneham A M 1969 *Rev. Mod. Phys.* **41** 82–108
—— 1972 *J. Phys. F: Met. Phys.* **2** 417
—— 1983 unpublished
—— 1984a *Hyperfine Interact.* **17–19** 53–62
—— 1984b unpublished
—— 1985a unpublished
—— 1985b *Theory of Defects in Solids* (Oxford: OUP)
Strub W, Roduner E and Fischer H 1984 *Proc. 22nd Ampère Congr. Magnetic Resonance and Related Phenomena (Zürich) 1984* (Zürich: Zürich Univ.) ed. K A Müller, R Kind and J Roos pp 267–8
Studer W, Gygax F N, Hintermann A, Schenck A and van der Wal A J 1984 *Phys. Rev.* B **30** 2414–8
Symons M C R 1959 *J. Chem. Soc.* 277
—— 1984 *Hyperfine Interact.* **17–19** 771–84
—— 1984b unpublished
—— 1985 unpublished
Tanigawa S, Ito K, Iwase Y, Terakado S, Nagamine K, Nishiyama K and Suzuki T 1984 *Hyperfine Interact.* **17–19** 235–40
Taqqu D 1986 *Nucl. Instrum. Methods* A **247** 288–300
Teichler H 1981 *Hyperfine Interact.* **8** 505
Teichler H and Seeger A 1981 *Phys. Lett.* **82A** 91–4
Tschalär C 1977 *SIN report* TM 30–19a
Uemura Y J 1980 *Solid State Commun.* **36** 369–72
—— 1981a *Hyperfine Interact.* **8** 739
—— 1981b *PhD Thesis* Tokyo University
Uemura Y J, Hayano R S, Imazato J, Nishida N and Yamasaki T 1979 *Solid State Commun.* **31** 731–4
Uemura Y J, Nishiyama K, Yamazaki T and Nakai R 1981 *Solid State Commun.* **39** 461–5
Uemura Y J and Yamazaki T 1983 *J. Magn. Magn. Mater.* **31–34** 1359–61
Uemura Y J, Yamazaki T, Harshman D R, Senba M and Ansaldo E J 1985 *Phys. Rev.* B **31** 546–63
Uemura Y J, Yamazaki T, Harshman D R, Senba M, Brewer J H, Ansaldo E and Keitel R 1984a *Hyperfine Interact.* **17–19** 453–6
Uemura Y J, Yamazaki T, Hayano R S, Nakai R and Hoang C Y 1980 *Phys. Rev. Lett.* **45** 583–7
Uemura Y J, Yamazaki T, Kitaoka Y, Takigawa M and Yasuoka H 1984b *Hyperfine Interact.* **17–19** 339–44
Van Vleck J H 1948 *Phys. Rev.* **74** 1168
Walker D C 1983 *Muon and Muonium Chemistry* (Cambridge: CUP)
Wang J S-Y and Kittel C 1973 *Phys. Rev.* B **7** 713
Webster B C 1985 *Ann. Rep. Chem. Soc.* C **80** at press
—— 1986 private communication
—— 1987 *New Sci.* **1550** 31–34
Wehr H, Knorr K, Gygax F N, Schenck A and Studer W 1984 *Phys. Rev.* B **29** 6381–3
Weidinger A 1984 *Hyperfine Interact.* **17–19** 153–166
—— 1984b unpublished
—— 1985 private communication
Welter J-M, Richter D, Hempelmann R, Hartmann O, Karlsson E, Norlin L O and Niinikoski T O 1984 *Hyperfine Interact.* **17–19** 117–24
Wipf H, Neumaier K, Magerl A, Heidemann A and Stirling W 1984 *J. Less-Common Met.* **101** 317
Wu C S and Hughes V W 1977 *Muon Physics I: Electromagnetic Interaction* ed. V W Hughes and C S Wu (New York: Academic) pp 2–11
Yamada K 1984 *Prog. Theor. Phys.* **72** 195–207
Yamada K, Sakurai A and Takeshinge M 1983 *Prog. Theor. Phys.* **70** 73
Yamazaki Y 1979 *Hyperfine Interact.* **6** 115–25
—— 1982 *Nucl. Instrum. Methods* **199** 133–40
—— 1984a *Muons and Pions in Materials Research* ed. J Chappert and R I Grynszpan (Amsterdam: North-Holland) pp 241–9

—— 1984b *Muons and Pions in Materials Research* ed. J Chappert and R I Grynszpan (Amsterdam: North-Holland) pp 105–17

Yamazaki T and Nagamine K (eds) 1984a *Proc. 7th Yamada Conf. Muon Spin Rotation and Associated Problems (Shimoda) 1983; Hyperfine Interact.* **17–19**

Yamazaki T and Nagamine K 1984b *University of Tokyo MSL Newsletter No* 4

Yaouanc A 1982 *Phys. Lett.* **87A** 423–5

Zax D B, Bielecki A, Zilm K W, Pines A and Weitekamp D P 1985 *J. Chem. Phys.* **83** 4877–905

Ziman J M 1964 *Principles of the Theory of Solids* (Cambridge: CUP)